LUBRICATION EFFICIENCY AND DIE DESIGN IN WIRE DRAWING

BINGSHU HUO

Doctor of Philosophy

THE UNIVERSITY OF ASTON IN BIRMINGHAM

JUNE 1997

THE UNIVERSITY OF ASTON IN BIRMINGHAM

LUBRICATION EFFICIENCY AND DIE DESIGN IN WIRE DRAWING

BINGSHU HUO

Doctor of Philosophy
JUNE 1997

SYNOPSIS

With the competitive challenge facing business today, the need to keep cost down and quality up is a matter of survival. One way in which wire manufacturers can meet this challenge is to possess a thorough understanding of deformation, friction and lubrication during the wire drawing process, and therefore to make good decisions regarding the selection and application of lubricants as well as the die design. Friction, lubrication and die design during wire drawing thus become the subject of this study.

Although theoretical and experimental investigations have been being carried out ever since the establishment of wire drawing technology, many problems remain unsolved. It is therefore necessary to conduct further research on traditional and fundamental subjects such as the mechanics of deformation, friction, lubrication and die design in wire drawing.

Drawing experiments were carried out on an existing bull-block under different cross-sectional area reductions, different speeds and different lubricants. The instrumentation to measure drawing load and drawing speed was set up and connected to the wire drawing machine, together with a data acquisition system. A die box connected to the existing die holder for using dry soap lubricant was designed and tested. The experimental results in terms of drawing stress vs percentage area reduction curves under different drawing conditions were analysed and compared. The effects on drawing stress of friction, lubrication, drawing speed and pressure die nozzle are discussed.

In order to determined the flow stress of the material during deformation, tensile tests were performed on an Instron universal test machine, using the wires drawn under different area reductions. A polynomial function is used to correlate the flow stress of the material with the plastic strain, on which a general computer program has been written to find out the coefficients of the stress-strain function.

The residual lubricant film on the steel wire after drawing was examined both radially and longitudinally using an SEM and optical microscope. The lubricant film on the drawn wire was clearly observed. Therefore, the micro-analysis by SEM provides a way of friction and lubrication assessment in wire drawing.

Finite element simulation of wire drawing process has been carried out under various initial and boundary conditions. The results obtained were analysed, in terms of stress and strain distributions within the deformation zone, with the effects of different materials and friction coefficients. The drawing stresses predicted by the theory were compared with the experiment and it was found that they were in good agreement.

Key Words: Wire drawing
Friction and lubrication
Dry soap lubricant
Die box
Finite element analysis

ACKNOWLEDGEMENTS

I would like to express my sincere thanks to my supervisor, Dr I. M. Cole, for his advice, guidance and continuous enthusiastic support given throughout the duration of the programme.

I would like to thank National-Standard Co. Ltd, International Wire and Machinery Association Education Award Committee and the Department of Mechanical and Electrical Engineering of Aston University for their financial support to the research work described in this report. I also would thank the Head of the Department, Dr J. E. T. Penny, for the permission to use the facilities of the Department.

Thanks are given to the staff at National-Standard Co. Ltd, particularly Mr N. Beard and Mr P.J. Kelly for their technical support and co-operation in the project.

Thanks are also given to Mr J. P. Jeffs for his help in instrumentation setting up, Mr A. G. Evitts and Mr D. C. Farmer for their help in using the wire drawing machine, Mr J. F. Foden for his help in using computers, and Mr R. G. Howell and J Duggins for their help in using the scanning electronic microscope.

I am grateful to Dr. S. Murphy who read through the first draft of this thesis with patience and made quite a few corrections and constructive recommendations.

Finally, I should thank Prof. M. T. Wright and Dr I. M. Cole for their efforts in establishing this research project.

To my husband Shuwen

and my son Tinger

CONTENTS

CHAPTER ONE
INTRODUCTION

CHAPTER TWO
LITERATURE REVIEW

SECTION ONE WIRE DRAWING PROCESSES AND MECHANICS

SECTION TWO FRICTION AND LUBRICATION

CHAPTER THREE

EXPERIMENTAL EQUIPMENT AND INSTRUMENTATION

CHAPTER FOUR

DRAWING PROCESS MATERIALS AND EXPERIMENTAL PROCEDURE

CHAPTER FIVE

MATERIAL CONSTITUTIVE MODELS AND STRESS-STRAIN DATA

CHAPTER SIX

EXPERIMENTAL RESULTS

CHAPTER SEVEN

OBSERVATION AND DISCUSSION

CHAPTER EIGHT

FINITE ELEMENT SIMULATION OF WIRE DRAWING PROCESS

CHAPTER NINE

CONCLUSIONS AND SUGGESTIONS FOR FUTURE WORK

APPENDICES

LIST OF FIGURES

LIST OF TABLES

NOTATION

A	surface area of the body
A_1	inlet cross sectional area of the wire
A_2	exit cross sectional area of the wire
c	specific heat of the material
c_t	thermal capacity of the material
C	constant, determined by die geometry and friction
D_1	inlet diameter of the wire
D_2	exit diameter of the wire
f	portion of the friction work converted into heat, normally f is chosen to be 0.5
$\overline{h_c}$	average unit thermal convective conductance over the convective area
J^*	externally supplied power
k	thermal conductivity of the material
L	length of the land of the die
m	friction factor
p	normal pressure
P	drawing force
P_i	externally applied stress
q_c	convection heat flow
q_r	radiant heat flow
$\dot{q}_G$	rate of energy generation per volume inside the control volume
r	reduction of area
t	time
T	temperature
T_1	surface temperature of the body
T_2	surface temperature of the ambient
U	average of the UTS of the material before and after drawing
V	volume of deformation zone
$\dot{W}_f$	power of frictional losses between the die and the wire
$\dot{W}_d$	internal power of deformation
$\dot{W}_b$	the power introduced through the back force
$\dot{W}_a$	the power introduced through the front force
x_i	co-ordinate of a reference axis system,
Y	mean yield stress of material

Y_o	initial yield stress of material
α	die semi-angle
β	portion of the work of deformation converted into heat, normally $\beta = 0.90 \sim 0.95$
$\dot{\varepsilon}_{ij}$	component of strain rate tensor
ρ	density of the material
m	emissivity of the material, for steel, $m = 0.8$
μ	coefficient of friction
σ_o	flow stress of the material being formed
σ'	constant, having stress dimensions
$\bar{\sigma}$	average generalized stress
σ_x	drawing stress
σ_{xf}	stress exerted on the wire at the exit of the die
σ_{xb}	stress exerted on the wire at the entrance of the die
σ_{sb}	Stefan-Boltzmann constant, $\sigma_{sb} = 5.67 \times 10^{-8}\ W/m^2K^4$
τ	shear stress imposed by friction
υ_i	velocity
$\lvert\Delta V\rvert$	value of velocity discontinuity over surface
δV^d	volume of the infinitesimal mass considered
δQ^d	increase in energy due to the work of deformation
δQ^f	increase in energy due to friction work at external boundary surfaces
δQ^c	change in energy due to the conduction, radiation and convection of heat into the infinitesimal volume of mass in consideration
δV	volume of the infinitesimal mass within the deforming body
$\Delta\varepsilon^p$	change in plastic strain
Δd	displacement of the surface of the material relative to the die during a time step of deformation
δA	area of the surface of the infinitesimal volume mass in contact with the die

CHAPTER ONE

INTRODUCTION

1.1 Introduction

Drawing, in its simplest form, consists of pulling material through a die under pre-determined conditions. There is evidence that wire was cold drawn through dies successfully before 1350 BC, during the ancient Egyptian civilisation [1]. Since then, wire, as we know it, has been with us for hundreds of years, showing that its versatility has withstood the test of time. Nowadays, large quantities of wires of different materials for both engineering and domestic use are finished by cold drawing [2].

Requirements of market and academic interests initiate scientific researches, which push forward engineering technology and thus promote production and application of the products. The evolution of wire drawing, as well as many other metal forming processes, follows exactly the same route.

Although theoretical and experimental investigations have been being carried out ever since the establishment of wire drawing technology, many problems still remain unsolved. Due to the difficulty of solving the plastic deformation problems in three dimensions, many investigations conducted for wire drawing were until now either analytical or empirical, both with some unrealistic assumptions [1, 2, 3, 4]. It is therefore necessary to carry out further research on traditional and fundamental subjects such as the mechanics of deformation, friction, lubrication and die design in wire drawing.

During the past decades or so technology has seen major thriving progress in many areas. Transmission Electron Microscope (TEM) and Scanning Electron Microscope (SEM) are nowadays being widely used in industry as well as academic institutions on a day-to-day basis. Modern strain gauges and computer data acquisition and control systems are readily available both for research and on-line control.

One of the most astonishing progresses in technology is probably the sophisticated numerical modelling and simulation techniques for engineering processes with the rapid development of digital computers over the last ten years [5, 6, 7, 8], which allowed the calculation of certain properties such as stress/strain conditions which previously could only be guessed. The finite-element method has been extensively used for bulk metal forming analysis and now three-dimensional finite-element simulation of wire drawing with different initial and boundary conditions is possible [9, 10].

The work described in this thesis concerns an experimental and theoretical study on the lubrication efficiency and die design in wire drawing.

This thesis consists of nine chapters. The present chapter serves as an introduction to the thesis. Chapter 2 is divided into two sections. The first section in Chapter 2 gives a review of theoretical and experimental work on wire drawing done by the previous researchers. The second section in Chapter 2 focuses on friction and lubrication in wire drawing. The concepts of different friction and lubrication mechanisms are introduced and methods of friction measurement and lubrication evaluation used by others are explained. In Chapter 3, experimental equipment and instrumentation employed in this study are detailed. The drawing process materials and experimental procedures are described in Chapter 4.

A knowledge of material flow stress data is important both for analytical and numerical analysis of wire drawing processes. In Chapter 5, material constitutive models currently available are reviewed. Tensile test results are presented. A numerical technique was developed to fit the flow stress data into a polynomial equation, which gives the best representation of flow stress and strain data.

Chapter 6 presents a complete set of the drawing experiment results in terms of drawing stress vs percentage area reduction curves, and gives the results of observations on residual lubricant film evaluation using SEM.

Chapter 7 gives detailed observation and in depth discussion on the experimental results presented in Chapter 6.

Chapter 8 is concerned with finite-element simulation of wire drawing process. A proprietary software package, ABAQUS, is introduced and used to study the characteristics of plastic deformation during wire drawing. The effect of different friction coefficients on drawing stress as well as stress and strain distribution within the deformation zone are thoroughly investigated.

Finally, conclusions and suggestions for future work are given in Chapter 9.

CHAPTER TWO

LITERATURE REVIEW

2.1 Introduction

Although evidence has shown that wire drawing dates back to ancient civilisations, theoretical studies on the mechanics of deformation during the wire drawing process did not start until early this century. Since then, theoretical and experimental investigations of wire drawing have been focused on pulling force or stress and optimum die semi-angle prediction. This chapter presents a review of theoretical and experimental work on wire drawing done by previous researchers.

This chapter is divided into two main sections. The first section gives a general review on wire drawing process and mechanics in which various drawing processes are introduced and different analytical and numerical solutions are explained.

In the second section, a specific review is carried out on friction and lubrication which are two major research areas of wire drawing. Although a considerable amount of work has been done by previous researchers, there still exist some uncertainties because of the complex nature of the problems. Therefore this section clarifies the two major research subjects according to the interest of this study.

Finally, a general summary is given at the end of this chapter based on the literature review carried out and presented.

SECTION ONE WIRE DRAWING PROCESSES AND MECHANICS

2.2 Wire Drawing Processes

The wire drawing process is performed by pulling a rod or wire through a hollow die [3], which is shown schematically in Figure 1.

The raw material for wire drawing is normally rolled rod or wire. Rolling is the most economic method of producing rods and wires. However, the dimensional accuracy and surface finish of the rolled product are not as good as those obtained by drawing.

Therefore, when these characteristics are required, drawing is generally adopted to follow rolling [2, 3].

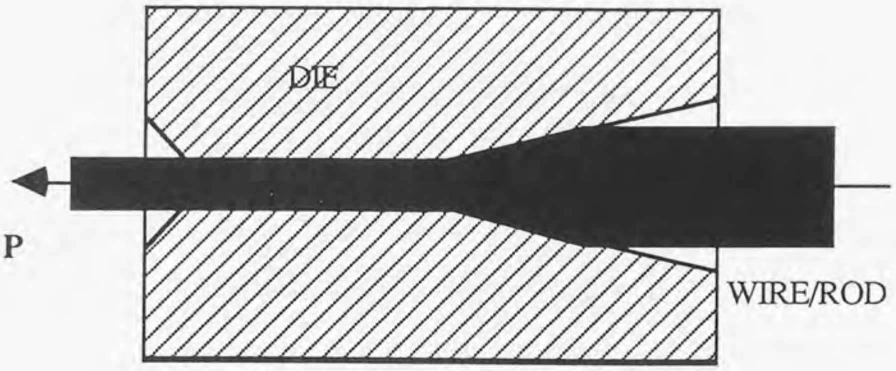

Fig. 1 Wire drawing process.

2.2.1 Conventional wire drawing

During the wire drawing process, traditionally and currently, the raw material is first cleaned of scale and/or dust by mechanical or chemical treatment. It is then coated with a suitable lubricant. After that, the end of the material is swaged in order to enter the die so it can be clamped and pulled.

The type of machinery used for wire drawing depends on the diameter of the workpiece. For large sizes, a wire drawing machine is constructed as a single block unit known as a drawbench, see Figure 2. For fine wires, a bull-block is used, see Figure 3.

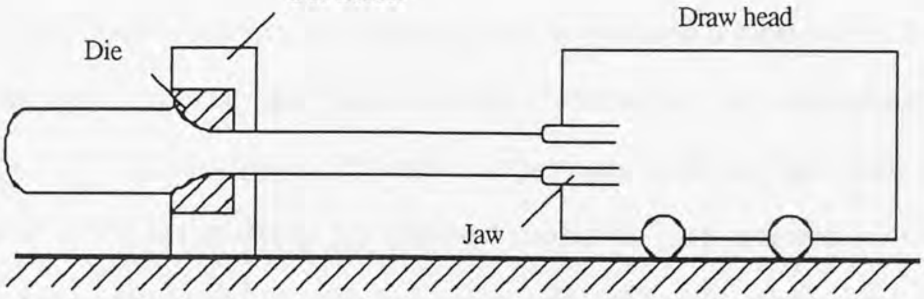

Fig. 2 Schematic drawing of a drawbench, after Dieter [11].

Since the reduction in size which can be achieved by the use of one die is limited, a series of combined drawbenches or bull-blocks is used in practice to carry out wire drawing of large deformation.

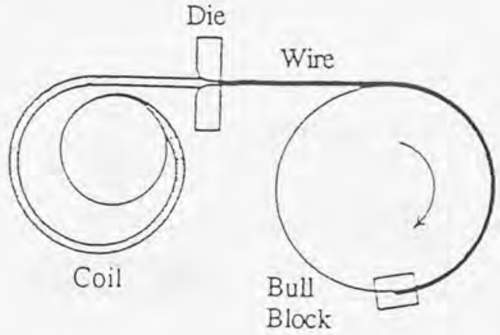

Fig. 3 Schematic drawing of a bull block, after Dieter [11].

2.2.2 New wire drawing techniques

Over the years, economic factors such as the rise in cost of raw materials, labour and power have been compelling wire manufacturers to seek new production routes in order to improve productivity and reduce cost and also to allow the expansion in the varieties of metals used and the inclusion of difficult-to-draw materials. The following introduces several notable new wire drawing techniques.

Hot drawing

Since wire drawing is normally a cold-working process, intermediate annealing is needed for large reductions in cross-section because of work hardening, so that the drawing process can be performed further. Drawing wire at elevated temperatures, however, not only avoids work hardening and hence intermediate annealing, but also reduces the pulling force. Over the last ten years, elevated temperature drawing has been extensively investigated at Aston University [4]. Figure 4 shows the high temperature wire drawing line used. It was reported that, with this equipment, mild steel, boron steel and medium carbon steel could be drawn at temperatures of up to 750 °C, considerably reducing the drawing stress and increasing the area reduction in a single die [4, 12].

Although hot drawing possesses the above advantages, it is rarely seen being used in industry. This is due to the fact that the equipment and instrumentation required are much more complicated and expensive, the process is difficult to control and the products are often subject to surface oxidisation.

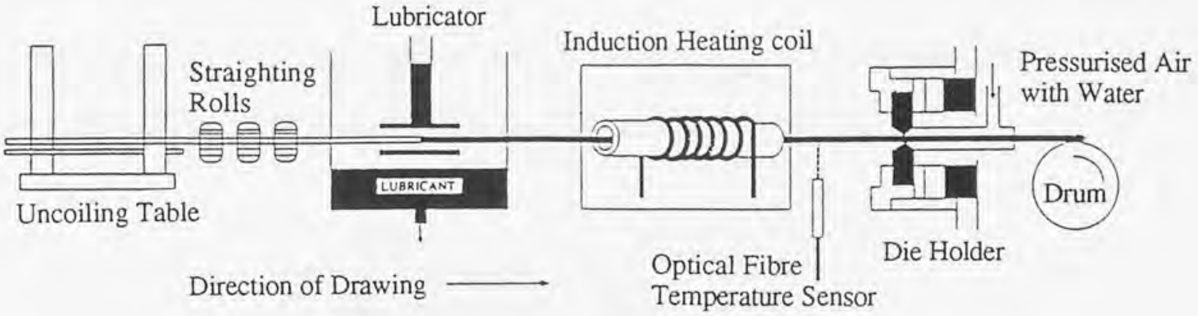

Fig. 4 High temperature wire drawing line, after Jornaz [4].

Vibration applied to wire drawing

The technique of ultrasonic vibration drawing was developed in the 1960s. It was suggested that ultrasonic vibration of a die could dramatically reduce the drawing force [13, 14]. Three reasons were given [15], namely that (a) the vibration encouraged more lubricant to enter the interface during the retraction part of the cycle, (b) the motion normal to the interface broke any adhesive junction and (c) the yield stress of the stock was reduced, either directly by heating or in some more obscure way.

Hydrostatic extrusion

The introduction of hydrostatic extrusion was the most notable advance in metal forming in the 1950s, which has some special features in relation to wire drawing [15]. There are advantages in combining hydrostatic wire extrusion and wire drawing. Very large reductions, up to 86%, can be obtained under controlled conditions in the production of stainless steel wire by this method. Even beryllium, which is normally too brittle to be drawn into wire, can be reduced by 60 percent in area to a diameter of 0.12 mm [15].

2.3 Wire Drawing Dies

When drawing wire, the required deformation is obtained by pulling the cylindrical raw material through the conical bore of a tool or die which has a smaller outlet than the size of the ingoing wire rod, and which consists of a distinctly harder material than that of the wire to be drawn. In order to obtain good deformation in a controlled manner, the drawing die must have an appropriate special profile, which in general consists of four different important parts, briefly mentioned below and shown in Figure 5 [16].

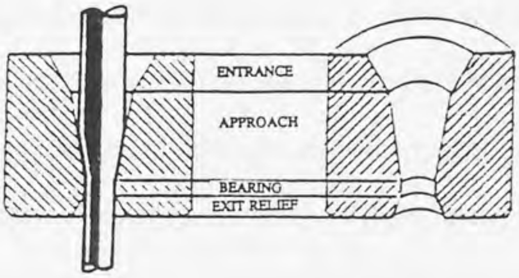

Fig. 5 Typical profile of a wire drawing die, after Eder [16].

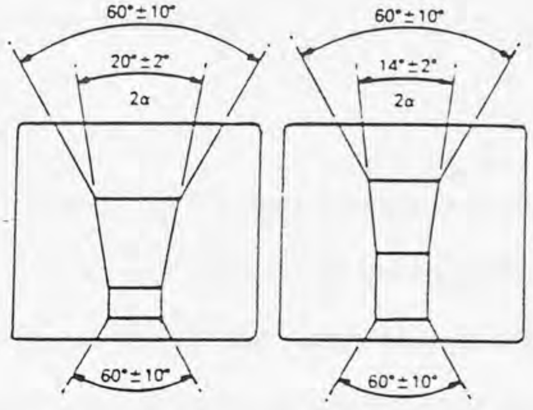

Fig. 6 Die profiles for hard (right) and soft (left) wire materials, after Eder [16].

(a) Entrance: this is used to ensure that the wire and the lubricant enter the die properly. Angles can be up to 70°.

(b) Approach: here the diameter of the incoming wire is progressively reduced. Depending on the material to be drawn, hard or soft, ferrous or non-ferrous, angles can vary from 8° to 30°.

(c) Cylindrical bearing: in this area, the diameter of the wire is stabilised to the desired final size.

(d) Exit relief: this ensures that the wire leaves the die properly. Angles - in the same way as the entrance - can be up to 70°.

The proportions of these four different regions in a die profile depend considerably on the material of the wire. As a general rule, harder materials demand a profile with smaller reduction angles and longer bearing surfaces than softer materials, see Figure 6.

In order to achieve a smooth flow of the wire through the die, and thus gain a longer life for the die, the contact surfaces must be carefully produced and then mirror polished by suitable machinery to minimise friction and heat generation during the process.

Drawing dies may be manufactured entirely of steel or, as is currently more common, contain inserts of a harder material. Mainly, there are three types of ultra-hard die tool materials available: tungsten or chromium carbide, natural single-crystal diamond and synthetic polycrystalline diamond (PCD). More recently, Syalon, which is a ceramic and consists essentially of aluminium nitride, alumina and silicon nitride, has become another alternative material for wire drawing dies.

2.4 Wire Products

Man and engineering depend on wire and wire products to a very great extent. Some examples of parts made from wire, both round and flattened, are shown in Figure 7 [17]. Innumerable wire articles are in daily use, simple obvious ones being hairpins, paper clips and key rings. In industry, the utilization of wire products is even greater. For example, in manufacturing industry, nails of different sizes, helical and coil springs, cables, chains, ropes and meshes are produced from wire in great quantity for use in many engineering fields. Wire products are simply in universal use. Man cannot live without wire and wire products.

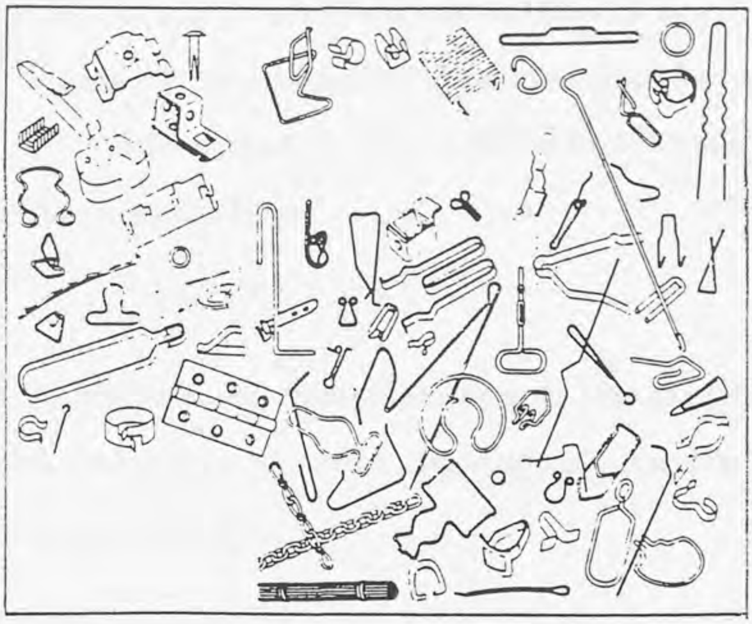

Fig. 7 Examples of parts made from round wire or flats, after Mayer et al [17].

2.5 Elementary Analysis of Wire Drawing

2.5.1 Equilibrium solution

Early theories of wire drawing are based on the equilibrium of horizontal forces acting on a segmental slice within the deformation zone. The most notable one is that proposed by Sachs in 1927 [18]. By assuming: (1) constant friction; (2) no redundant work and (3) non work-hardening material, he derived the following expression based on the Tresca yield criterion for the drawing stress:

$$\sigma_x = Y \left\{ \frac{1+B}{B} \left[1 - \left(\frac{D_2}{D_1} \right)^{2B} \right] \right\} \tag{2.1}$$

where		
	σ_x	drawing stress
	Y	average yield stress of the material
	$D_{1,2}$	diameters of the wire at inlet and exit
	B	$\mu \cot\alpha$
	μ	coefficient of friction
	α	die semi-angle

By considering the equilibrium of total horizontal forces acting on the whole area of contact between wire and die, and making the further assumption that the total redundant work done per unit volume is equal to $2/3\alpha Y$, Siebel in 1947 put forward another expression for the drawing stress [19]:

$$\sigma_x = Y\left[\left(1 + \frac{\mu}{\alpha}\right)\ln\left(\frac{A_1}{A_2}\right) + \frac{2}{3}\alpha\right] \tag{2.2}$$

where A_1 and A_2 are cross-sectional areas of the wire at the inlet and exit respectively.

Neither of the two theories is based on a rigorous analysis and their applications are therefore necessarily restricted [20]

Further developments of the Sachs and Siebel equations were carried out by other researchers, of which two examples are given in the following, while more comprehensive reviews can be found elsewhere [4, 21, 22, 23].

In 1944, Davis and Dokos [24] modified Sachs's theory to take strain-hardening into account by making the yield stress a function of the instantaneous area of the drawn wire within the die. This refinement leads to the rather cumbersome equation:

$$\sigma_x = Y_0\left(\frac{1+B}{B}\right)\left\{\left[1 - \left(\frac{D_2}{D_1}\right)^{2B}\right]\left[\left(1 - \frac{\sigma'}{Y_0 B}\right) + \frac{\sigma'}{Y_0}\ln\left(\frac{D_2}{D_1}\right)^2\right]\right\} \tag{2.3}$$

where Y_0 is the initial yield stress of the material and σ' is a constant having the dimensions of stress.

In 1961, Yang [25] derived a theoretical equation of drawing stress to include the effect of the die land which was neglected by Sachs and Siebel. Yang's equation takes the following form:

$$\sigma_x = \left\{Y_0\left(\frac{C}{1-C}\right)\left[\left(\frac{A_1}{A_2}\right)^{1-C} - 1\right] - Y_0\right\}e^{-\frac{4\mu}{D_2}L} + Y_0 \tag{2.4}$$

where L is the length of the land of the die

C is a constant, determined by the die geometry and friction, $C = \dfrac{1 + \mu \cot\alpha}{1 - \mu \cot\alpha}$

2.5.2 Semi-empirical approach

Based on certain analytical concepts and a large amount of experimental data, semi-empirical formulae have been developed and are widely used in many metal forming practices by researchers and engineers in order to approximate the deforming power required. To some extent, these formulae are convenient and economical, although without much theoretical background.

In 1955, Wistreich [22] carried out an extensive experimental and theoretical investigation of the mechanics of wire drawing. He used the so-called split die apparatus to measure the force that tends to separate the two halves of the split die concurrent with the drawing force, thus enabling the mean coefficient of friction and the mean die pressure to be calculated. After examining the validity of the previous theories of wire drawing, he derived semi-empirical formulae for the drawing forces as follows:

$$P = A_2 U \frac{(1 + \mu \cot \alpha)\, 2r}{2 - r} \qquad \text{for } \alpha < \frac{25r}{2 - r} \tag{2.5.1}$$

$$P = A_2 U \frac{(1 + \mu \cot \alpha)(1.73r + 0.035\,\alpha)}{2 - r} \qquad \text{for } \alpha > \frac{25r}{2 - r} \tag{2.5.2}$$

where P drawing force

r reduction of area

U the average of the UTS of the material before and after drawing

Later, in 1957, the experimental observations of Wistreich [22] were used by Whitton [26] in presenting another empirical expression for the calculation of drawing forces.

$$P = A_2 Y\left(1 + \frac{1}{\mu \cot \alpha}\right)\left[1 - \left(\frac{A_2}{A_1}\right)^{\mu \cot \alpha}\right] + \frac{2}{3} A_2 Y \frac{\alpha^2 (1 - r)}{r} \tag{2.6}$$

2.6 Slip-line Field Method

In the slip-line field method, a network of orthogonal lines is constructed within the deformation zone of the workpiece. The path of these lines is indicated from the directions of maximum shear stress, and the limit of the network, or field, is determined from the surface boundary conditions and the geometry of the process [27, 28]. Except for certain geometrically convenient situations, this method can be extremely laborious, particularly so because the validity of the field cannot be verified until it has been completed. However, once a valid slip-line field has been constructed, the working loads may be deduced directly from the associated stress plane.

Initially, the slip-line field method was only used to solve plane-strain problems [27, 28]. Later, this method was modified to solve axisymmetric forming processes, such as wire drawing. Due to the assumptions made and the laboriousness in applying the slip-line field method, the validity of its solution is always in doubt [22]. At present, many researchers recognise it as an aid to understanding rather than a tool to use.

2.7 Energy Method

The energy method is based on the principle of work equivalence which states that the work done by the external force in a metal forming process is equal to the deformation energy of the metal on which the force is exerted. The deformation energy can be divided into three terms: the first term is due to the homogeneous deformation; the second term is due to the friction at the boundary interfaces, and the third term is due to the redundant deformation.

The energy consumed in homogeneous and redundant deformation is determined from an assumed kinematically admissible velocity field, while the friction work done at the die/workpiece interface is calculated by means of equilibrium, either in a direct way by assuming a frictionless die pressure distribution [3], or indirectly by using the apparent strain method [29].

Siebel [30] used the energy method in solving the wire drawing problem by consideration of the total work per unit volume. He derived an expression for the homogeneous work, assuming that the die pressure is not affected by friction. He considered that the redundant work is due to shear at the boundaries of the deformation zone.

Pugh [31] applied the energy method in a simple hydrostatic extrusion of pure aluminium and an aluminium alloy. He used simple plane cross-section, conical and spherical shear surfaces for the estimation of the redundant work. It was found that the spherical shear surface gave the best estimate of the redundant work.

Avitzur [32] in 1963 used an energy method, which he called a power balance approach, in deriving an analytical expression for the required front pull for wire drawing, as well as the back push for extrusion. The power balance is expressed as follows;

$$\dot{W}_f + \dot{W}_d + \dot{W}_b - \dot{W}_a = 0 \tag{2.7}$$

where $\dot{W}_f$ power of frictional losses between the die and the wire

$\dot{W}_d$ internal power of deformation

$\dot{W}_b$ the power introduced through the back force

$\dot{W}_a$ the power introduced through the front force

According to the extremum theorem, the power computed by this method is then an upper bound of the actual power. The computed drawing stress becomes:

$$\frac{\sigma_{xf}}{Y} = \frac{\sigma_{xb}}{Y} + \frac{4}{3\sqrt{3}}\sin\alpha + 2\left[\frac{1}{\sqrt{3}\sin\alpha} + 1\right]\ln\frac{D_1}{D_2} + \frac{4}{\sqrt{3}}\frac{L}{D_2} \tag{2.8}$$

where σ_{xf} stress exerted on the wire at the exit from the die

σ_{xb} stress exerted on the wire at the entrance to the die

L length of the land of the die

Although the energy dissipated along the boundaries of velocity discontinuities has been taken into account by Avitzur in calculating the energy of deformation, he did not consider the redundant work [32].

Within the category of the energy method, limit analysis is a typical tool applied in order to study the deformation force on a workpiece during metal forming processes such as drawing and extrusion [33]. In the limit analysis approach, two approximate solutions are developed. One is the upper-bound solution, which provides a value that is known to be higher than or equal to the actual force; the other is the lower-bound solution, which provides a value that is known to be equal to or lower than the actual force; the actual force thus lies between the two solutions. Figure 8 shows curves of drawing stress against the semi-cone angle of the die, after Avitzur [33], which are from the upper and lower bound solutions and are plotted for several area reductions with corresponding measured values

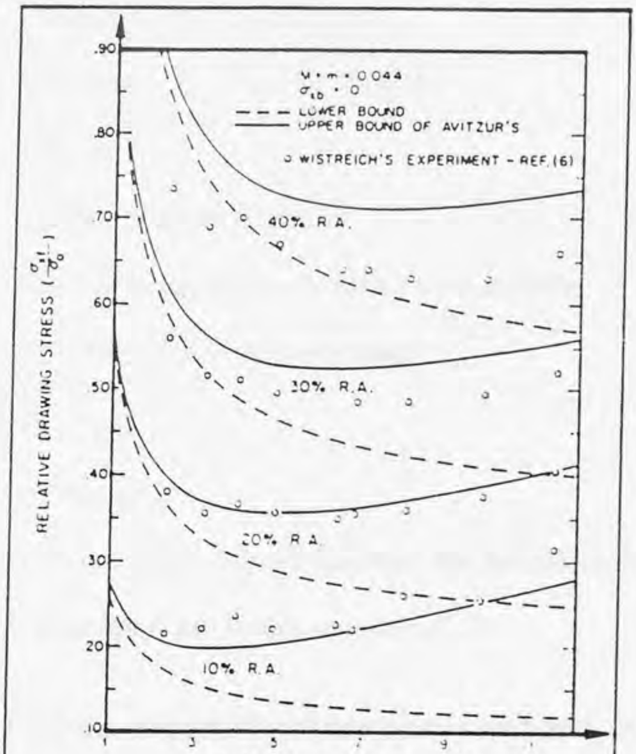

Fig. 8 Relative drawing stress against die semi-cone angle and percentage reduction in area, after Avitzur [33].

of actual stress. Figure 8 shows that, by limit analysis, an approximate solution is given with an estimate of the maximum possible error. In practice, the upper-bound solution is used more than the lower-bound solution from the point of view of the safety of metal forming facilities [2, 7, 34].

The upper-bound solution uses a balance-of-power equation with an assumed velocity field and presumes that a velocity field is optimum because it consumes less energy than other comparable fields [35]. The upper-bound theorem in its minimum-principle form leads to the following expression:

$$J^* = \frac{2}{\sqrt{3}} \sigma_0 \int_V \sqrt{\frac{1}{2} \dot{\varepsilon}_{ij} \dot{\varepsilon}_{ij}}\, dV + \int_{S_v} \tau |\Delta V|\, ds - \int_{S_t} P_i\, v_i\, ds \qquad (2.9)$$

Where:	J^*	externally supplied power
	σ_0	flow stress of the material being formed
	V	volume of deformation zone
	τ	shear stress imposed by friction
	v_i	velocity
	P_i	externally applied stress
	$\lvert\Delta V\rvert$	value of velocity discontinuity over surface
	$\dot{\varepsilon}_{ij}$	component of strain rate tensor
	$\dot{\varepsilon}_{ij} = \frac{\partial v_i}{\partial x_i}$	
	x_i	coordinate

Thus, according to the upper-bound theorem, the actual velocity field, among all the kinematically admissible ones, minimises equation (2.9).

According to Avitzur [35], the origins of limit analysis extend back to Galileo [36] and the basic theorems were further developed by Gvozdev [37], Hill [38], Prager and Hodge [39] and Drucker et al [40]. The most extensive developments and the most comprehensive application of limit analysis, however, were carried out by Avitzur [3, 33, 34, 35, 41].

The important aspect in using the upper-bound method is the selection of the velocity fields within the deformation zone, which depends very much on the characteristics of the metal process in consideration. In solving plane strain sheet drawing problems, Johnson and Mellor [42] used a velocity field simplified from the slip-line field by replacing them with appropriate straight lines. Kudo [43] introduced the concept of a unit rectangular region in plane strain problems by using three different types of velocity fields in order to find a better upper-bound solution. In solving axisymmetric problems such as wire drawing, Alexander [44] used the velocity field proposed by Johnson [28] in the upper-bound solution to represent the case of axial symmetry.

2.8 Finite Element Method

The use of numerical methods to model metal forming processes avoids the need to assume homogeneous deformation, a common feature of earlier analytical techniques. Therefore, numerical models can produce simulations representative of the real process behaviour of the workpiece and the die during forming [49, 45, 46, 47].

The finite element method is one of the most dominant numerical techniques used for modelling metal forming processes. It was first proposed by Turner et al. [48], for stress analysis in aircraft structures, using pin-jointed bars and triangular plates as the elements. Since then, the method has been developed simultaneously with the increasing use of high speed electronic digital computers and with the growing emphasis on numerical methods for engineering analysis. Now the finite element method has been applied in various fields where the exact solutions could not previously be found.

The basis of the method is the representation of a body or a structure by an assemblage of subdivisions, called finite elements, which are considered to be interconnected at joints called nodes or nodal points. For each element, the displacement of an arbitrary point is approximated by an interpolating function (or shape function) between the actual values at the nodes of the element. A virtual-work formulation can be constructed for the whole body which, in turn, determines the stiffness matrix relating nodal displacement to nodal force. For elastic deformation, the stiffness matrix is linear, but this is not the case for plastic deformation [5].

Currently, finite element treatments of metal forming processes can be divided into three types according to their basic assumptions about the behaviour of the material under consideration, namely the visco-plastic [6], the rigid-plastic [7] and the elastic-plastic [8]. The visco-plastic finite element method can be either rigid-visco-plastic or elasto-visco-plastic.

In 1979, Lee et al [49] used an elastic-plastic finite element method to analyse the stress distributions of the workpiece in extrusion. Quadrilateral finite elements were adopted in the analysis and each quadrilateral was divided by the diagonals into four constant-strain triangles. Smaller elements were chosen near the surface in order to evaluate the high shear strain gradient there more accurately. It was found that the stress fields obtained exhibited features which were consistent with the known development of extrusion defects.

In 1985, Boer and Webster [47] analysed cold drawing from round to square sections using a finite element method. In their model, only a one-quarter symmetrical section of the billet was considered, represented by 12 hexahedron-shaped elements. In the deformation zone, the elements were sized according to boundary velocities, while smaller elements were used for transition zones. Relative drawing stresses were obtained for different die semi-angles and compared with those obtained from a direct upper-bound solution. Boer and Webster did not include friction effects in their finite element model, however the disadvantage of the finite element approach in terms of time-consuming mesh generation no longer exists [50].

In 1990, Sawamiphakdi et al. [10] used a general-purpose finite element program ABAQUS to perform a parametric study in order to investigate the effects of die geometry and area reduction on the magnitude and distribution of residual stress through the wire cross-section at the die exit. Two major variables of die geometry were considered: radius and semi-angle. The parametric study indicated that the semi-angle has a significant effect on the residual stress state at the surface of the drawn wire. Small die semi-angle causes less tensile stresses at the surface and more compression stresses at the centre. A large die radius reduces the level of residual stresses, but this reduction is only marginal. Figure 9 shows the die geometry and the finite element mesh used by Sawamiphahdi et al. [10] and Figure 10 presents some of the results obtained [10].

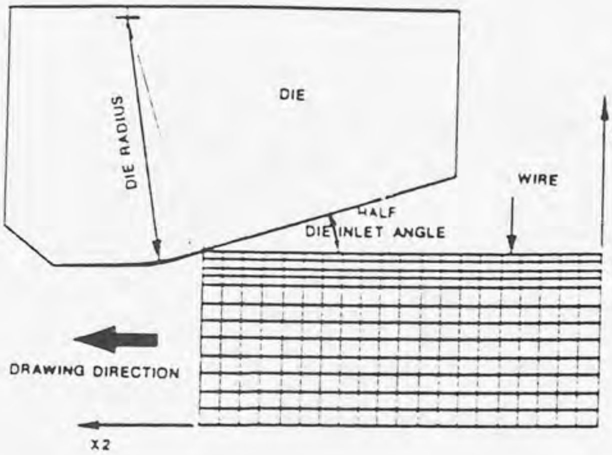

Fig. 9 Finite element models of wire drawing, after Sawamiphakdi et al [10].

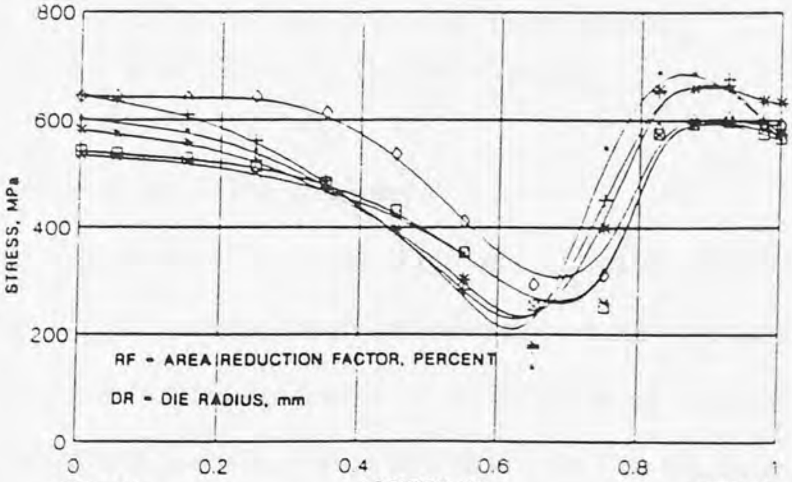

Fig. 10 Distributions of equivalent stresses in drawn wire for different area reduction factors and die radii, after Sawamiphakdi et al [10].

In 1992, Mori [51] investigated steady state deformation in the drawing of an aluminium bar with a conical die using a rigid-plastic finite element method. He considered the velocity component in the axial direction at the entry boundary as a variable because of the slight compressibility. The reduction in area R was 0.19 and the coefficient of friction μ at the die/workpiece interface was 0.1. The distributions of the hydrostatic stress in the workpiece in the bar drawing are shown in Figure 11, which shows that as the die semi-angle increases, the hydrostatic stress in the region near the centre of the bar becomes tensile.

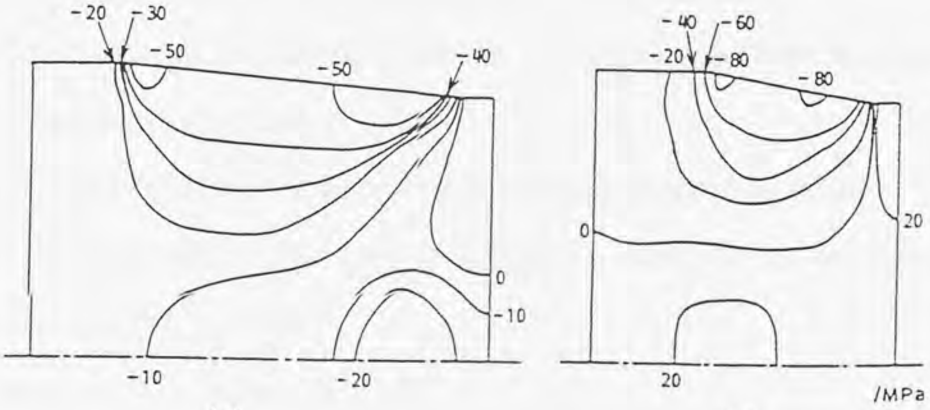

(a) (b)

Fig. 11 Distributions of hydrostatic stress in workpiece
(a) α = 5° and (b) α = 10° in bar drawing
(r = 0.19, μ = 0.1), after Mori [51].

2.9 Thermal Effects in Wire Drawing

During wire drawing, most of the work of plastic deformation and friction is converted into heat, which then causes temperature increases in both the wire and the die. The rise in temperature can cause various problems in the deformation process; for example, the mechanical properties of the wire will be affected [1, 4]. The viscosity of the lubricant is reduced and thus the lubrication condition is altered. The temperature gradients in the wire and the die will bring about thermal stresses within them, because of the non-homogeneous expansion. As a result, the life of the drawing die will decrease and the subsequent processes of drawing will become more difficult. Therefore, it is important to include thermal effects in the analysis of deformation in wire drawing.

Previous research work done on thermal effects in wire drawing are mainly analytical or experimental. A brief review is covered in reference [4], in which early experimental investigations on flow stress data of materials at elevated temperature are summarized and mathematical equations proposed by other researchers to correlate stress-strain curves at different temperatures and strain rates are presented. The temperature rise both in the drawn wire and the die during drawing is also addressed. The temperature distribution in the die is analyzed using a finite-element technique.

In calculating the temperature increase in wire drawing, Siebel and Kobitzsch [52] made the following assumptions:

(a) temperature increase due to deformation is uniform across a section

(b) temperature distribution due to friction is parabolic in the vicinity of the tool/workpiece interface

(c) no heat flow in the axial direction

(d) only 20% of the general friction heat flows into the die while the other 80% remains in the workpiece

Ranger [53] measured the temperature distribution in the die during wire drawing by combining measurements of the temperature of the outer surface of the die and of the drawing pull with electrical-analogue computations of the heat flow through the die. Figure 12 shows the temperature distribution in the die under a drawing speed of 7 m/s (1400 ft/min). Ranger compared his experimental measurement with Siebel and Kobitzsch's theory [52] and very good agreement was obtained.

As Wistreich [23] suggested, the temperature difference between the skin and the core of the wire rapidly disappears beyond the die. For the purpose of the interpass cooling requirements, therefore, merely the average temperature rise in one pass may be considered. Wistreich calculated the average temperature rise per pass from the unit pull and concluded that, in wire drawing with dry lubricant, the temperature rise per pass is about 30-40 °C for aluminium and copper, 60-80 °C for mild steel, and 100-160 °C for medium- to high-carbon steel.

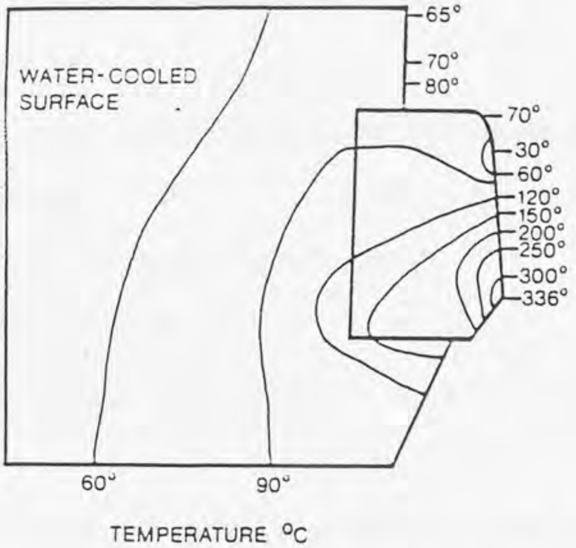

Fig. 12 Temperature distribution in the die under the drawing speed of 7 m/s, after Ranger [53].

Heat transfer theory

It is known that whenever a temperature gradient exists within a system, or when two systems at different temperatures are brought together into contact, energy (heat) is transferred. The process by which the energy transport takes place is called heat transfer. There are three basic modes of heat transfer: (1) conduction, (2) radiation and (3) convection. There are several theories of heat transfer. However, from the engineering point of view, the determination of the rate of heat transfer for a particular temperature difference is the key problem [54].

Conduction According to the Fourier's law, which assumes that the rate at which heat is transferred by conduction is proportional to the temperature gradient, the standard equation of conduction within a body can be derived [54]:

$$k \frac{\partial^2 T}{\partial x_i^2} + \dot{q}_G = \rho\, c \frac{\partial T}{\partial t} \qquad (2.10)$$

where	T	temperature, a function of co-ordinate and time
	x_i	co-ordinate of a reference axis system
	t	time
	$\dot{q}_G$	the rate of energy generation per unit volume inside the control volume
	k	thermal conductivity of the material
	ρ	density of the material
	c	specific heat of the material

Radiation The quantity of energy leaving the surface of a body as radiant heat can be calculated by the Stefan-Boltzman equation as follows:

$$q_r = A\, m\; \sigma_{sb} \left(T_1^4 - T_2^4 \right) \qquad (2.11)$$

where	q_r	radiant heat flow
	A	surface area of the radiant body
	T_1	surface temperature of the radiant body
	T_2	surface temperature of the enclosure
	σ_{sb}	Stefan-Boltzmann constant, $\sigma_{sb} = 5.67 \times 10^{-8}\ \mathrm{W/m^2K^4}$
	m	emissivity of the material, for steel, $m = 0.8$

Convection The convection mode of heat loss during metal forming consists of two mechanisms operating simultaneously: energy transfer due to molecular motion and energy transfer due to macroscopic motion of fluid parcels. Irrespective of the details of the mechanisms, the rate of heat loss by convection may be calculated from Newton's equation:

$$q_c = \overline{h_c} A (T_1 - T_2) \tag{2.12}$$

where

q_c	convection heat flow
A	surface area of the body
$\overline{h_c}$	average unit thermal convective conductance over the convective area

Calculation of temperature rise

Consider an infinitesimal volume of mass dV within a deforming body, the temperature rise during a time step of deformation can be calculated using the following equation:

$$\delta T = \frac{1}{c_t \delta V} (\delta Q^d + \delta Q^f + \delta Q^c) \tag{2.13}$$

where

c_t	the thermal capacity of the material
δV^d	the volume of the infinitesimal mass considered
δQ^d	the increase in energy due to the work of deformation
δQ^f	the increase in energy due to friction work at external boundary surfaces
δQ^c	the change in energy due to the conduction, radiation and convection of heat into the infinitesimal volume of mass in consideration

The work of deformation δQ^d The work of plastic deformation can be calculated using the following equation:

$$\delta Q^d = \beta \overline{\sigma} \Delta \varepsilon^p \delta V \tag{2.14}$$

where:

δV	the volume of the infinitesimal mass within the deforming body
$\bar{\sigma}$	the average generalized stress
$\Delta \varepsilon^p$	the change in plastic strain
β	that part of the work of deformation converted into heat, normally $\beta = 0.90 \sim 0.95$

The work of friction δQ^f The work done due to friction is given by:

$$\delta Q^f = \frac{Y}{\sqrt{3}} \, m \, f \, \Delta d \, \delta A \tag{2.15}$$

where

m	friction factor
f	that part of the friction work converted into heat, normally f is chosen to be 0.5
Δd	the displacement of the surface of the material relative to the die during a time step of deformation
δA	the area of the surface of the infinitesimal volume mass in contact with the die

The change of energy due to conduction, radiation and convection δQ^c within the infinitesimal volume of mass in the deforming body in consideration can be calculated by applying the standard heat flow expressions (2.10), (2.11) and (2.12).

With sophisticated heat transfer theory, advanced numerical techniques and powerful digital computers, thermal analysis in metal forming processes like wire drawing is now possible [4, 7, 8, 45, 51, 55, 56, 57]. Currently, there are two popular numerical techniques being used in performing the temperature predictions: the finite element method and the finite difference method.

SECTION TWO FRICTION AND LUBRICATION

Friction and lubrication are two major research areas of wire drawing. Comprehensive reviews on theories and mechanics of friction and lubrication in drawing have been presented by Loh [1], Jornaz [4] and Lim [59]. Systematic text books of friction and lubrication are also available [60].

2.10 Friction in Metal Forming

Friction is one of the most important factors in metal forming processes. Some friction is necessary in certain cases, such as in rolling, where friction helps the rolls to draw the workpiece into the roll gap and in floating-plug drawing of tube. However, in most metal forming processes, such as wire drawing, friction is no more than a drawback, which is not needed at all [61].

For example, friction can cause non-homogeneous deformation, which leads to difficulty in process control and defects on the surfaces of the products (barrelling occurring in forging, "fish tail" in blooming and surface scratching in drawing, etc). Friction results in temperature increase during forming, which again can cause serious problems, such as burning out of the lubricant or reduction in die capability. Friction also causes die wear and decreases the die life, thus increasing the cost of the products. Finally, the analysis of the metal forming process becomes more complicated with friction [62].

The following factors affect friction during metal forming [62]:

(a) the material of the die and the workpiece
(b) the topographic characteristics of the die and the workpiece surfaces
(c) the temperature of deformation
(d) the contact pressure of the die/workpiece interface
(e) the deformation speed
(f) the geometry of the die and the workpiece

(g) lubrication

Friction causes a considerable amount of energy consumption during wire drawing, but its proportion of the total work is not yet known. Moreover, die wear due to friction at the interface between the die and the drawn wire considerably reduces the die life. As a result, friction makes the drawing process complicated and the wire more expensive.

The surface topographic features of interfaces involving surfaces in relative motion are directly related to their friction characteristics [63]. Early work on friction in wire drawing with regard to this aspect are more qualitative rather than quantitative. Woodcock [64] examined the surface roughness of the wire before and after drawing. Figure 13 shows that the asperities on the surface of the wire had been polished away.

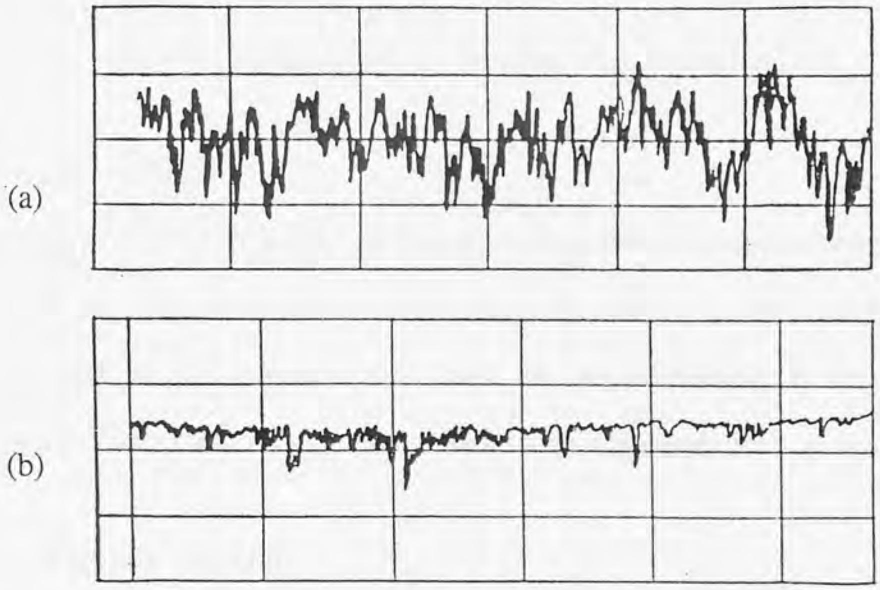

Fig. 13 Surface roughness of the wire: (a) before drawing; (b) after drawing, after Woodcock [64].

Although methods for surface roughness evaluation are available [63, 65, 66], their application to the wire drawing dies is scarce in the literature. Some useful measurements of wire surface roughness were conducted by Lancaster and Rowe [67]. They then calculated the centre line average (C.L.A.) for various asperities. However, Shaw et al [68] later discussed the wrong use of the centre line average in the assessment of surface roughness. They explained that different surface profiles can be described by the same C.L.A. number, nevertheless friction appears to increase with sharper asperities.

Wistreich [23] examined the intensity of wear along the longitudinal profile of the worn die, a typical example of such a configuration is shown in Figure 14.

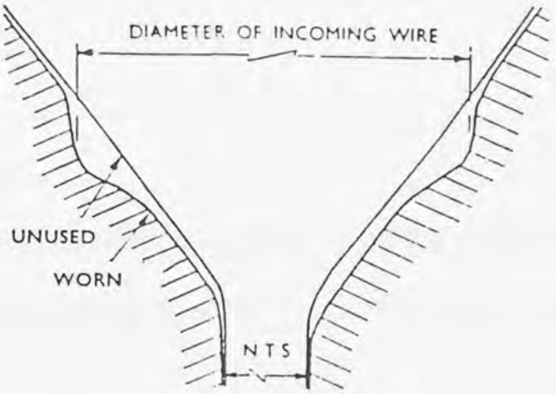

Fig. 14 Configuration of worn die, after Wistreich [23].

2.11 Friction Models

Many analyses of metal forming problems, such as the strict upper-bound solutions [35], require that the friction (or shear stress tangential to the contact surface between the workpiece and the die) is prescribed. There are several theories to describe the friction phenomenon, two of them being most notable, i. e., Coulomb friction and Tresca friction.

2.11.1 Coulomb friction

The Coulomb friction law states that the tangential stress at any point on the surface is proportional to the normal pressure between the two bodies and opposite to the direction of motion, i. e.,

$$\tau = \mu p \tag{2.16}$$

where τ is the tangential shear stress, p is the normal pressure and μ is the coefficient of friction, which is normally taken as a constant for a given die and material for simplicity.

The nature of the Coulomb friction law limits its application in some metal forming processes where large normal stresses are encountered such as rolling and forging [8]. Although it is generally accepted in wire drawing, care must be taken in choosing the friction coefficient value and different methods have been used to determine the values of the friction efficient under various drawing conditions which are to be described in Section 2.12 of this Chapter.

2.11.2 Tresca friction

In the Tresca friction law, the friction shear stress on the surface of contact between two bodies is expressed as a fraction of shear yield stress of the workpiece when plastic deformation is invoked:

$$\tau = m\,k \tag{2.17}$$

where τ is the interfacing shear stress, k is the shear yield stress of the workpiece and m is the friction factor, which takes a value between 0 and 1. When $m = 0$, zero friction is represented by equation (2.17) where the workpiece simply slides over the contact surface of the die with no restriction, and when $m = 1$, sticking friction is modelled by equation (2.17) where the movement of the workpiece material in contact with the die surface is zero relative to that surface. However, these two idealised conditions of zero and sticking friction are not met in practice, and the actual values are normally found to be in between the two limiting values.

There is little experimental data on the typical values of m. However, as Lim [59] described in his work, in tube and wire drawing theoretical predictions of drawing stress were in good agreement with experimental results when $m = 0.01$ or 0.02.

The two friction expressions are preferred by some researchers, but both of them have disadvantages. For instance, in metal forming processes such as hot forging and rolling, the normal pressures at the die/workpiece interfaces are very large, therefore Coulomb friction is not appropriate, because in such a case, the friction shear stresses calculated would be larger than the shear yield stress of the material. The problem with the Tresca friction law is that a constant friction factor is normally assumed. Thus, as shown by equation (2.17), the friction shear stress should also be constant throughout the contact surfaces, which is certainly not the case in real practice. It has been suggested that a combination of the two friction descriptions should be used in metal forming analyses, especially numerical analysis, i.e., Coulomb friction for the slipping contact and Tresca friction for the sticking contact [2, 8, 15].

Theoretically, the coefficient of friction and friction factor are affected by many factors which have been listed earlier in this section (p.42). Nevertheless, constant or average values are used for a certain metal forming problem for simplicity [3, 62].

2.12 Determination of Friction in Wire Drawing

The coefficient of friction and the friction factor can only be obtained through experiment. Since it is not feasible to carry out experiments for every drawing condition, estimations have to be made accordingly from time to time. The following methods were used by previous researchers to measure the average coefficient of friction, μ:

(a) back-pull factor method [23, 69]
(b) die rotation technique [70, 71, 72]
(c) split die technique [22, 73, 74]
(d) split rotating die technique [75, 76]
(e) redundant work estimation method [77, 78, 76, 79]

The following gives a brief review on some of these techniques.

2.12.1 Back-pull factor method

When wire is drawn without back-pull the load on the die F equals the drawing load P. When a backwards force or back-pull Q is applied on the entrance side of the die, the load on the die falls, and from the statical considerations the sum of the back-pull and the die load must equal the drawing load:

$$P = F + Q \tag{2.18}$$

It was further found experimentally that the relationship between F and Q was strictly linear, or that:

$$F = P - bQ \tag{2.19}$$

where b is the "back-pull factor" which is the slope of the F/Q curve. Hill [80] derived an expression for the back-pull factor from which the coefficient of friction μ can be deduced:

$$b = r\,(1+\mu \cot \alpha) \tag{2.20}$$

where r is the fractional reduction of area and α the die semi-angle.

2.12.2 Split die method

If the drawing die is split in half longitudinally and the force tending to separate the two halves during drawing is measured concurrently with the drawing force, then the mean coefficient of friction can be calculated directly from these measurements. By considering the equilibrium of forces acting on the die shown in Figure 3.3, Wistreich [22] derived the following equations:

$$\mu = \tan\left(\frac{P}{\pi S} - \alpha\right) \tag{2.21}$$

$$q_m = \frac{\pi S}{(A_1 - A_2)(\cot \alpha - \mu)} \tag{2.22}$$

where P is the drawing force, S the die separating force and q_m the mean die pressure.

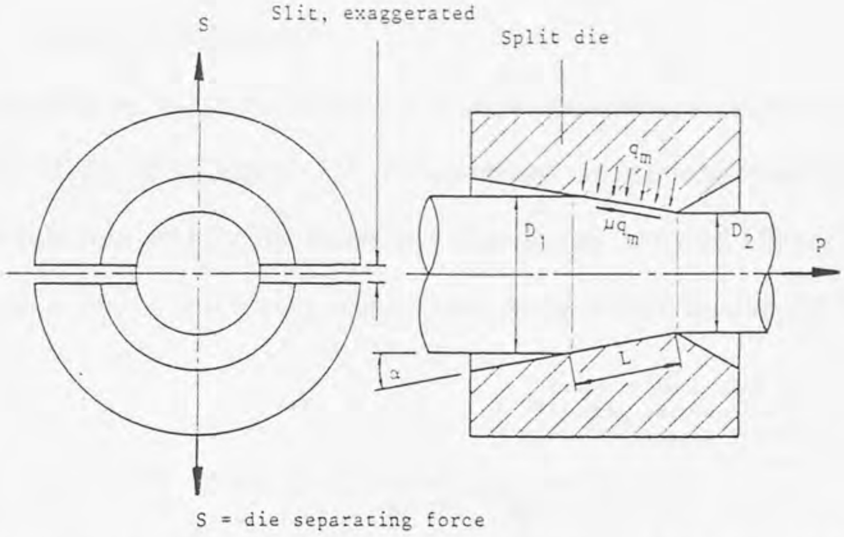

Fig. 15 Forces acting on a split die in wire drawing, after Wistreich [22]

2.12.3 Die rotation method

In the die rotation method, a torque is applied in order to rotate the die during drawing, which will result in a reduction in drawing force, provided that the magnitude of the friction factor remains unchanged. Again, according to the equilibrium of the forces acting upon the die, the following equations can be derived to calculate the mean coefficients of friction:

$$\mu_p = \frac{F}{Q} = \frac{(p - p_r)\tan\alpha}{(p_r - p\cos\phi)} \qquad (2.23)$$

$$\mu_T = \frac{F}{Q} = \frac{2T\sin\alpha}{(pD_m\sin\phi - 2T\cos\alpha)} \qquad (2.24)$$

where μ_p - mean coefficient from the consideration of reduced drawing force;

μ_T - mean coefficient from the consideration of torque;

P - drawing force without die rotation;

P_r - drawing force with die rotation;

T - torque;

Q - normal force;

D_m - mean diameter of the die within the deformation zone.

2.12.4 Split rotating die method

In order to determine the mean coefficient of friction and mean pressure in wire drawing more accurately, Basily and Sansome [75, 76] combined the split and rotating die methods and developed this split rotating die technique. The design involved "finger tipped" split dies through which the bar was drawn, while a conical die rotated around the tips.

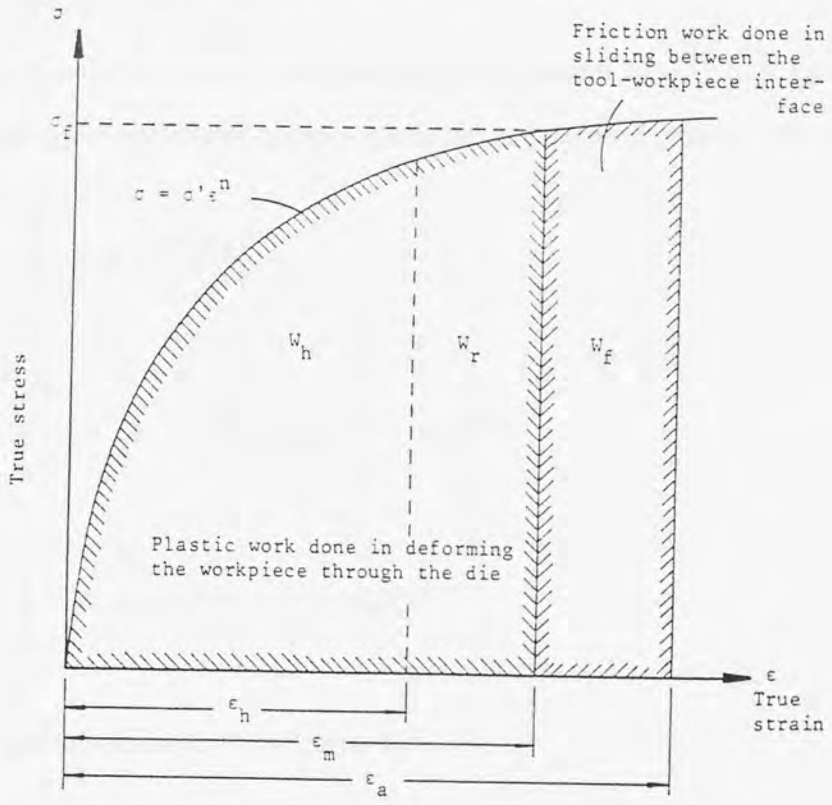

Fig. 16 Area under true stress-strain curve showing the three forms of energy expended in a drawing process, after Basily and Sansome [76]

2.12.5 Redundant work estimation method

Siebel [30] proposed that the total work done per unit volume in wire drawing W_t can be expressed as following:

$$W_t = W_h + W_f + W_r \tag{2.25}$$

where W_h - work done in homogeneous deformation;

W_f - work done against friction;

W_r - work done in redundant deformation.

By trying to determine some basic parameters in deformation Basily and Sansome [76] assumed that the true stress-stain curve illustrated in Figure 16 is parabolic and can be described by the following equation:

$$\sigma = \sigma' \, \varepsilon^{n} \tag{2.26}$$

where σ' is a strength coefficient.

Thus the three energy components in equation (2.25) can be calculated by integrating the three sections of the area under the stress-strain curve:

$$W_h = \int_{\varepsilon_0}^{\varepsilon_h} \sigma \, d\varepsilon = \frac{\sigma' (\varepsilon_h)^{n+1}}{n+1} \tag{2.27.1}$$

$$W_r = \int_{\varepsilon_h}^{\varepsilon_m} \sigma \, d\varepsilon = \frac{\sigma'}{n+1} \left[(\varepsilon_m)^{n+1} - (\varepsilon_h)^{n+1} \right] \tag{2.27.2}$$

$$W_f = \int_{\varepsilon_m}^{\varepsilon_a} \sigma \, d\varepsilon = W_t - \frac{\sigma'}{n+1} (\varepsilon_m)^{n+1} \tag{2.27.3}$$

The corresponding strains are thus given by:

homogenous strain, $\varepsilon_h = \ln \left(\frac{1}{1-r} \right)$ (2.28.1)

mean equivalent strain, $\varepsilon_m = e \left[\frac{\ln \left(\frac{\sigma_f}{\sigma'} \right)}{n} \right]$ (2.28.2)

apparent strain, $\varepsilon_a = e \left(\ln \left[(n+1) \left(\frac{W_t}{\sigma'} \right) \right] \right)$ (2.28.3)

In general the coefficients of friction in wire drawing processes are less than 0.1. According to Wistreich [16], although the coefficient of friction will vary with process conditions of wire drawing, it may be reckoned that μ is approximately 0.01 for dry drawing and 0.10 for wet drawing. The reason for μ being less for dry drawing can be explained by the fact that dry lubricants have better lubrication effect than wet lubricants under normal drawing conditions, because they have larger grain size and higher viscosity.

Experimental data on the typical values of m are scarce. According to Lim [48], a value between 0.01 and 0.02 would give good agreement between theory and experiment in terms of drawing load.

2.13 Lubrication in Metal Forming

In dry contact, no lubricant is present on the contact surfaces of the two bodies. Since, on the atomic scale, the surfaces will appear extremely rough with a large number of peaks and valleys, the sliding of unlubricated surfaces can produce severe surface interaction with high friction and surface distress. Drawing without lubrication is, therefore, not encouraged.

Proper lubrication is essential in many metal forming processes such as rod, tube and wire drawing. There are two kinds of lubrication, namely dry and wet [61].

In the dry lubrication technique, the lubricant is usually a dry soap powder, placed in a die box and picked up by the wire surface on its passage through the box. With difficult-to-draw materials, such as high-strength steels, stainless steels and high temperature alloys, the surface of the wire can be coated either with a softer material or with a conversion coating. Dry lubrication is used for steel wire larger than 0.5 mm diameter, for which a relative rough surface produced is acceptable. In the wet lubrication technique, the lubricant can be oil-based or aqueous and is applied at the die inlet, or the die is submerged in a bath. Liquids, especially water-based liquids, are most effective coolants and, as a result, are employed in order to prevent excessive temperature rise in high speed drawing. Because the lubricant layer at the die/wire surface is thinner than that in dry lubrication, a bright surface finish can more easily be imparted to the wire. The wet lubrication technique is used for steel wire less than 0.5 mm diameter.

Advantages of lubrication

The advantages of using lubrication in wire drawing are as follows [81]:

(a) reduction of the frictional resistance and thus the drawing stress
(b) reduction of the die wear and thus increase of die life
(c) cooling of the wire and avoidance of thermal breakdown of the lubricant itself
(d) prevention of adhesive metal transfer to the die and scoring the wire

Requirements of lubricants

The major requirements of a lubricant are to produce controlled frictional properties, to provide adequate cooling and to prevent metal/metal contact in the die. In addition to these, the following factors must also be included [82]:

(a) chemical stability in use, although it should break down on disposal
(b) thermal stability
(c) non-staining
(d) non-toxic, odourless and fume free
(e) ease of removal by water, heat or solvents
(f) provide a protective film
(g) provide a bright surface with no residual lubricant
(h) promote further surface treatment
(i) compatible with machinery
(j) pleasant to use, acceptable to operators
(k) viable cost

The selection of lubricants with the correct combination of the above properties is therefore not a easy task.

2.14 Lubrication Mechanisms

Although the distinctions are not always clear, it is usual to consider lubrication under separate headings: hydrodynamic friction, boundary lubrication and solid lubrication.

2.14.1 Hydrodynamic lubrication

In hydrodynamic lubrication, the two surfaces of the contacting bodies sliding over each other are separated completely by a fluid film (oil in most cases) of sufficient thickness to cover the asperities of the surfaces. The fluid film is actually formed by the relative motion of sliding which draws the lubricant fluid in between the contact surfaces. This is encouraged by a small angle between the tool and workpiece [2]. A very high pressure is generated within the lubrication film itself which keeps the two contacting bodies apart from direct contact. If a carefully designed cylindrical nozzle surrounding the wire is sealed to the die it is possible to generate enough pressure in an oil to deform the wire before it actually enters the die [2]. The shear resisting force on the contact surfaces is caused by the viscosity of the lubricant.

Since hydrodynamic lubrication relies on viscosity in order to maintain surface separation, researches have been done to investigate the viscosity characteristics of lubricants [83, 84]. It was found that fluid lubricants show exponential increases of viscosity with increasing pressure and exponential decreases with increasing temperature [85].

2.14.2 Boundary lubrication

The two surfaces of the contacting bodies are separated by a physically or chemically absorbed film of molecular proportions in which the frictional characteristics are determined by the chemical or surface properties of the lubricant and bonding solids which are of low shear strength. The objectives of the boundary lubrication is thus to reduce friction by reducing the shear strength of the junction interfaces [59].

It has been reported that fatty acids, vegetable and marine fats play a dominant role in reducing friction in boundary lubrication conditions. Metallic soaps are also good boundary lubricants, having higher melting points than the fatty acids. Long-chain organic compounds have good lubricating properties, but are less strongly bound to metal surfaces than the reaction products. Boundary lubricants are remarkably effective in wire drawing since they form very thin films which will provide low friction [2].

2.14.3 Solid lubrication

Any material of lower shear strength than that of the deforming metal can, in principle, be used as a solid lubricant in metal forming [2]. For example, thin copper coatings have been used in some industrial processes, including steel-tube sinking. Other low strength solids commonly employed in solid lubrication are graphite, molybdenum disulphide and some non-ferrous metals such as indium, tin, lead.

2.15 Promotion of Lubrication in Wire Drawing

With the current industrial demands for increased quality and productivity, it has been inevitable that ever higher finishing speed, better surface finish, longer die life and lower energy consumption are needed in wire drawing. This has created a number of problems for the lubricant engineer and die designer whose responsibility is to ensure satisfactory performance in the operation.

One problem with the increased speed is that the rate of heat generation is also increased, which ultimately affects the performance of the lubricant. The other problem is that excessive tool wear will result in frequent change of dies. The time lost in changing the die therefore becomes a large factor in determining the productivity of a high speed wire mill. Researchers have been seeking effective methods of ensuring satisfactory performance for many years, and, so far, it seems that the only practical method is to separate the die and the workpiece completely by a film of lubricant so that die wear and frictional heat are minimised. For this purpose, different hydrodynamic systems have been built in order to promote lubrication in wire drawing. The following gives a brief review.

Hydrodynamic Systems for Oil Lubrication

In order to produce hydrodynamic lubrication in wire drawing, it is necessary to supply lubricant to the entry of the die at a pressure comparable with the yield stress of the wire [86]. There are two ways of obtaining this; one being to pump high pressure oil to the die/wire interface which is a kind of hydrostatic or forced hydrodynamic lubrication, the other being pure hydrodynamic lubrication in which the oil pressure is built up by the motion of the wire.

One of the earliest designs of the hydrodynamic lubrication system was proposed by Christopherson et al [87]. This method involved the use of a tube of up to 760 mm (30 in) in length through which the wire passed before entering the die, see Figure 17. The clearance between the wire and the tube was about 50 μm (0.002 in) and a mineral oil was used as the lubricant.

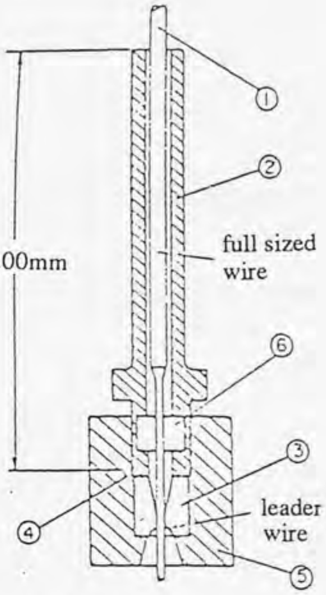

Fig. 17 The Christopherson tube for promotion of hydrodynamic lubrication wire drawing with oils, after Christopherson et al [87].

Tattersall [86] improved Christopherson's theory regarding the calculation of pressure within different zones of the hydrodynamic system. He used a simplified construction of the nozzle and die, as shown in Figure 18, to derive the following equation for calculating the hydrodynamic pressure, P_2, generated at the plane of deformation:

$$\frac{1}{\alpha} e^{-\alpha P_2} = \frac{1}{\alpha} - \left[\frac{12\mu_0 l}{h^3} \left(\frac{uh}{2} - q \right) + 6\mu_0 \left\{ \frac{u}{\alpha^2} \left(\frac{\alpha u}{2q} - \frac{\alpha}{h} \right) - \frac{q}{\alpha^3} \left(\left(\frac{\alpha u}{2q} \right)^2 - \left(\frac{\alpha}{h} \right)^2 \right) \right\} \right] \tag{2.29}$$

where h is the clearance between the wire nozzle or die surface, *l* is the length of the parallel portion of the nozzle, u is the wire speed, q is the volume rate of the lubricant flow per unit length of circumference of wire, μ_0 is the viscosity of lubricant at zero pressure or zero wire speed, and α is the die semi-angle.

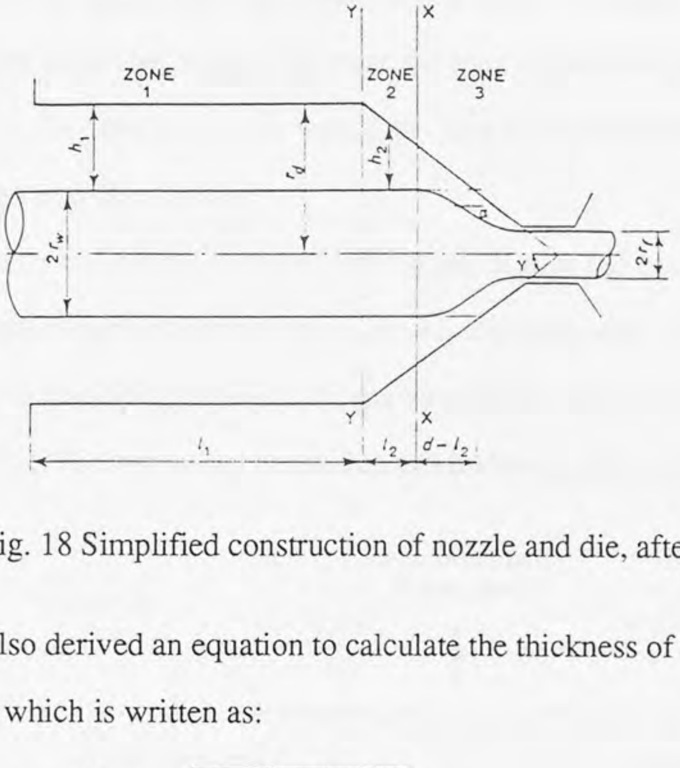

Fig. 18 Simplified construction of nozzle and die, after Tattersall [86]

He also derived an equation to calculate the thickness of the lubricant film, t, on the drawn wire, which is written as:

$$t = \frac{-\left(b - \frac{M}{u} \right) \pm \sqrt{\left(b - \frac{M}{u} \right)^2 - 4ac}}{2a} \tag{2.30}$$

where

$$a = f^2 \left[-\frac{2l}{h^3} + \frac{1}{\alpha h^2} \right] \tag{2.31.1}$$

$$b = f \left[\frac{l}{h^2} - \frac{1}{\alpha h} \right] \tag{2.31.2}$$

$$c = \frac{1}{4\alpha} \tag{2.31.3}$$

and

$$M = \frac{f}{6\mu_0\alpha}\left(1 - e^{-\alpha Y}\right) \tag{2.32}$$

here Y is the yield stress of the wire and *f* is the ratio of initial wire radius to final wire radius.

Since hydrodynamic lubrication systems require a combined effect of drawing speed, lubricant properties and geometry of the Christopherson tube, there are several limitations which prevent its industrial application in its original form [59]. For example, it may require very high speed and impractically long tubes. A series of tubes of various lengths and diameters would be required to meet the requirements of various drawing schedules. Furthermore, the lubricant film would be broken during starting and stopping at the beginning and end of each wire.

In order to overcome these difficulties, Butler [88] proposed a new method for realising hydrodynamic lubrication, as shown schematically in Figure 19. This method is independent of the lubricant viscosity, drawing speed, and process geometry. It utilises the combined effect of external pressurisation and hydrodynamic action to achieve the effect.

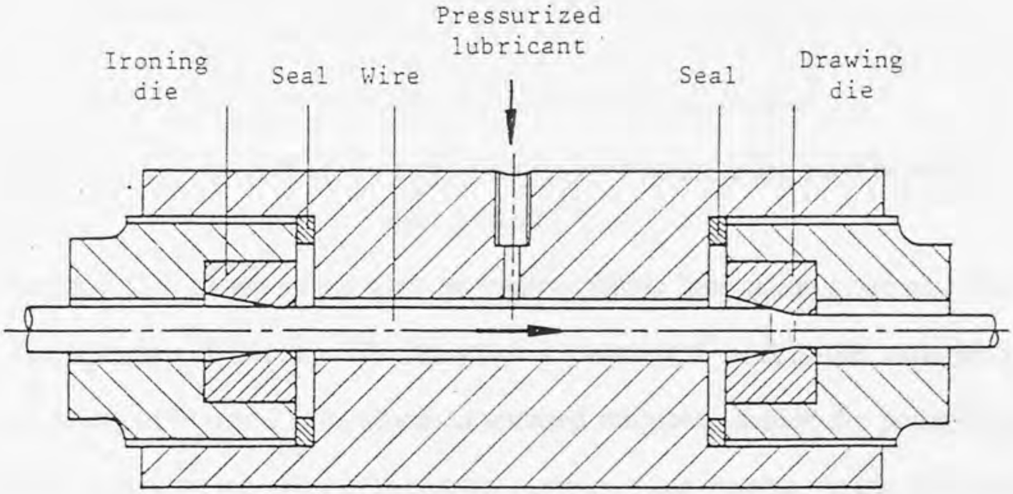

Figure 19 External pressurisation in hydrodynamic lubrication in wire drawing, after Butler [88].

Hydrodynamic Systems for Soap Lubrication

Avitzur quoted an industrial hydrodynamic lubrication system using soap as the lubricant [3], as illustrated in Figure 20. With this system, the wire passes through a bin full of soap powder first. The soap adheres to the wire surface and is therefore dragged into the small chamber through the narrow gap between the wire and an approach die in which the wire does not deform. It was assumed that, while passing through the narrow gap, frictional heating would cause the soap to liquefy. In the chamber between the two dies, the pressure is sufficiently high to cause hydrodynamic lubrication when the wire passes through the drawing die.

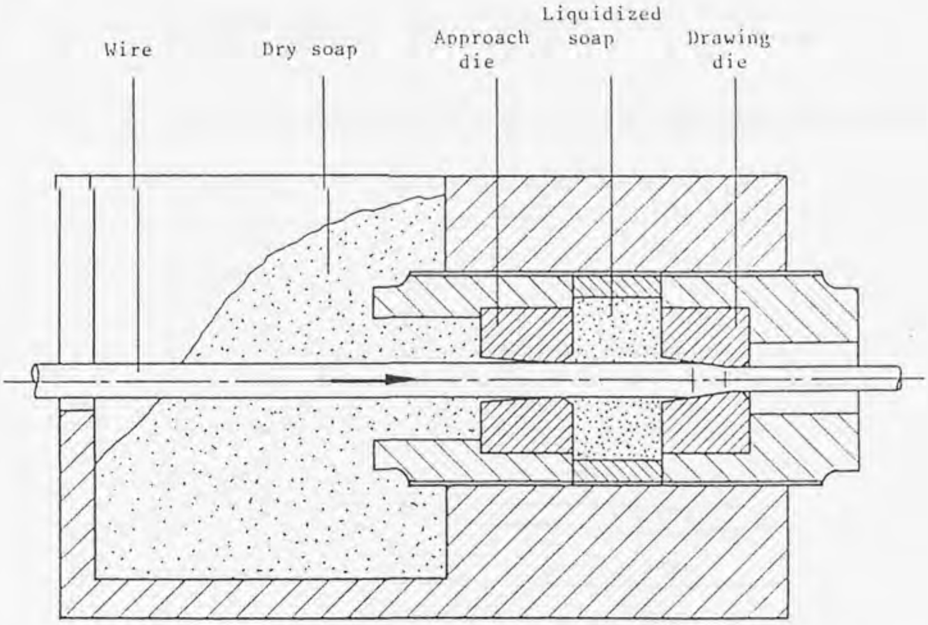

Fig. 20 An industrial hydrodynamic lubrication system using soap lubricant after Avitzur [3].

Tattersall [86] extended his work on hydrodynamic lubrication systems using oil to consider using soap lubricant. He designed a combined nozzle-die unit as shown diagrammatically in Figure 21, in which an uncased tungsten carbide die pellet fits into a recess provided for it at the end of the parallel portion of the nozzle. At the entry end, the parallel portion opens out into a conical entrance of 6 degree semi-angle and 28.6 mm (1.125 in) long. Immediately in front of the nozzle was the soap box, and lubricant was carried into the nozzle by the wire itself. Measurement of pressure developed in the nozzle was carried out by seating a 3.2 mm (0.125 in) ball-bearing on top of a 1.6 mm (0.0625in) hole which had been drilled through to the nozzle bore from the die entry end, and measuring the force to keep it there without soap leaking out.

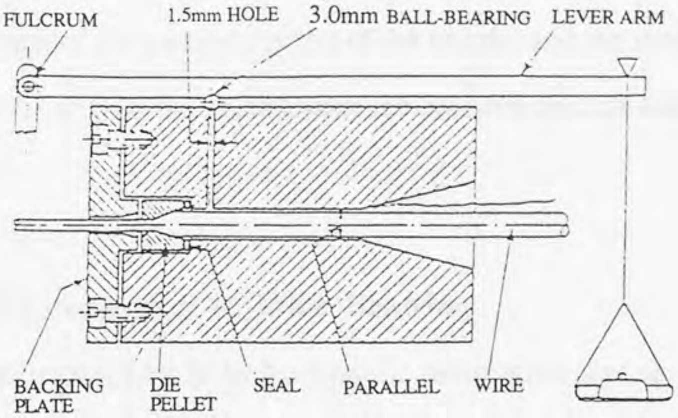

Fig. 21 A hydrodynamic lubrication system using soap lubricant with pressure measurement, after Tattersall [86].

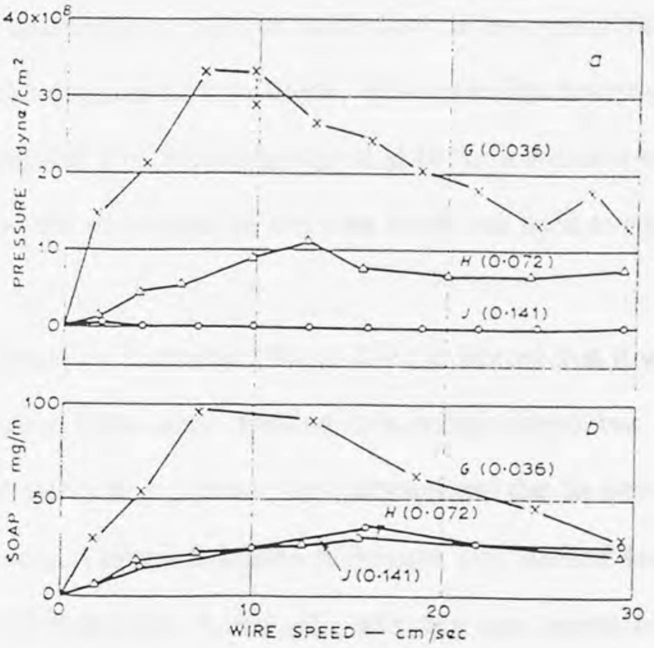

Fig. 22 The effect of drawing speed on pressure and soap throughput in hydrodynamic lubrication system using soap, after Ling et al [89]

$1\ \text{dyna/cm}^2 = 10^5\ \text{N/cm}^2$

A systematic experiment was carried out by Tattersall [86] to investigate the effects of nozzle dimensions and of the properties of the soap lubricant on the pressure developed in the nozzle and on the rate of lubricant flow. It was found that the pressure increased with speed, rose to a maximum, and then decreased to lower values, and thickness of the soap on the drawn wire also followed the same pattern, as given in Figure 22. It was also found that the greater the length of the parallel portion of the nozzle, and the smaller the clearance between the wire and the nozzle, the greater were the pressure and the lubricant throughput at a given speed.

2.16 Evaluation of Lubrication in Wire Drawing

The presence of the lubricant film in hydrodynamic lubrication was shown by Wistreich [22] and Ranger [90]. They measured the lubricant films remaining on the wire or tube after drawing, the thickness of which were 25-760 μm (1-30 μin).

In 1957, Wistreich [91] studied the physical aspects of wire drawing lubrication. He suggested that a distinction should be made for the best possible lubricant between drawing to size and drawing for surface finish. Wistreich also investigated the method of forced lubrication invented by Christopherson et al [87], in which a tube was attached to the inlet of the die and the movement of the wire itself was used to pump the lubricant to the required pressure

A report presented by Lancaster [92] in 1971 indicated that it was possible to form hydrodynamic lubrication films when drawing rods at high speed, but it also depended on the properties of the material being drawn, the lubricant and the die semi-angle.

The Christopherson tube lubrication technique was studied and further applied to tube drawing by Lim [59] in 1984. A new plug and plug attachment lubrication technique was developed, and it was found that the lubricant pressure and the film thickness varied directly with the draw speed, lubricant viscosity and the length of these devices, and inversely with the radial clearance.

Grudev et al [93] described a procedure for determining the average thickness of the lubricant layer in the deformation zone. According to their view, the lubricant thickness decreases during multi-pass dry drawing with increase in the speed and decrease in the surface roughness of the wire.

Tattersall [86], as described in the previous section, systematically investigated hydrodynamic lubrication systems both with oil and soap lubricants. He derived equations for calculation of hydrodynamic pressure and lubricant layer thickness, and compared theoretical calculations with experimental measurements; good agreement was obtained.

Recently, the scanning electronic microscope (SEM) has been used in examining the surface quality of the drawn wire. Baker and Wright [94] used it to observe the micro-surface quality of drawn wires.

2.17 General Summary

The above brief literature review shows that many attempts have been made since early this century to solve the problem of plastic flow during wire drawing using different techniques. Even so, the problem has not yet been fully solved and, of the many theories proposed, none is universally accepted and most are open to question [58]. It is therefore necessary to carry out further research in order to enrich the knowledge of the deformation mechanics of wire drawing in theory and to improve productivity and product quality in practice.

Traditional analytical methods such as equilibrium solutions, energy solutions and upper- and lower-bound solutions are useful for analysis of metal forming processes. However, they have restrictions because of the assumptions made in each case. Their applications are normally made to either plane strain or axi-symmetric deformation such as flat rolling and wire drawing. Even so, the solutions are usually implicit and complex, which have to be solved by computer programs [2, 4].

New trends in engineering show that the finite element method has become the most powerful and the most popular technique in solving metal forming problems. Commercial packages are now available in universities and academic institutions. Although there have been a few publications on process modelling using the finite element method, finite element analyses about wire drawing are scarce. Further work in this area is necessary.

One of the advantages of numerical modelling and simulation is that it can produce detailed stress and strain distributions within the deforming workpiece. Therefore, finite element analysis will be extremely useful in understanding the mechanics of wire drawing. Another advantage of numerical modelling and simulation is that it is very easy to carry out a parametric study to investigate the effect of individual parameters such as friction coefficient on drawing stress and strain distributions. As a result, experimental work can therefore be largely reduced.

In Section two of this chapter, previous work on friction and lubrication in wire drawing has been extensively reviewed. Friction and lubrication are two large and lasting research subjects in wire drawing, because of their complex nature. Since they cover a broad field, specific investigations with regard to drawing speed, area reduction, drawing die, wire material and lubricant properties are strongly recommended.

CHAPTER THREE

EXPERIMENTAL EQUIPMENT AND INSTRUMENTATION

3.1 Introduction

The experimental equipment, such as the bull-block, has been used by Winsper [14] and Dawson [95] for ultrasonic drawing, and by Loh [1], Jornaz [4] and Kumar [96] for elevated temperature drawing. For using smaller diameter dies supplied by the National-Standard Company Limited, the die holder assembly was modified and a die adapter introduced. Furthermore, a new pressure die box was designed in order to achieve hydrodynamic lubrication using dry soap lubricant. The instrumentation for data acquisition with the Tachometer and the load-cell, were reassembled, checked and re-calibrated. This chapter describes the equipment, the die of the pressure die box and instrumentation used in the present study.

3.2 Horizontal Bull-block

The bull-block used to perform the wire drawing experiments consisted of a fabricated steel frame on which a 457 mm (18 in) diameter drum was mounted, having a 457 mm (18 in) long working surface. The drum, which was carried on a carbon steel shaft, was installed horizontally, supported in heavy duty roller bearings and driven through a totally enclosed worm-gear. The bull-block was provided with a traversing table which was mounted on guides and driven by a lead screw to give 19 mm (0.75 in) traverse per revolution of the drum. The straightening rolls, the lubricator (which was not used in this research), dry lubricant container, pressure die adapter and the die holder assembly were assembled on the steel traversing table. Figure 23 shows the horizontal bull-block which was used for the work described in this thesis.

The drum shaft was driven by a 11.5 kW (15 hp) squirrel cage induction motor through a variable speed Carter gear and a four-speed box. The bull-block was designed for drawing speeds of 36, 73, 109, 146 m/min (120, 240, 360, 480 ft/min) which could be selected by means of the gear box (as described in detail by Winsper [81]. The drum speed was infinitely variable from 0.4 m/min (1.3 ft/min) up to 146 m/min (480 ft/min). This allowed drawing experiments to be performed at different drawing speeds in order to investigate the effect of drawing speed on drawing stress as well as the performance of lubricants. The bull-block operated at constant power and therefore with increasing draw speed, the die pull available decreases proportionally.

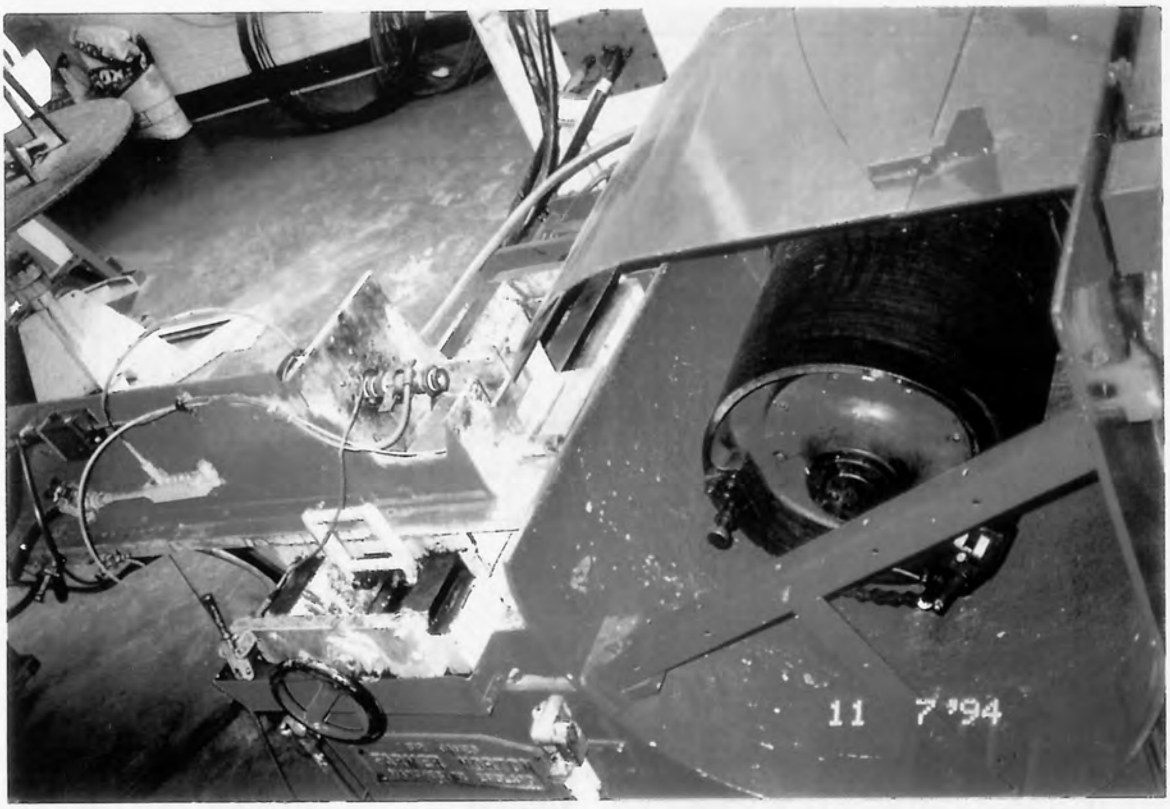

Fig. 23 Full view of the horizontal bull block.

3.3 Die Holder Assembly

3.3.1 Die holder assembly for 76 mm (3 in) diameter die

The die holder assembly was initially designed by Loh [1] in order to measure the drawing load by using a load cell. It consists of five components, namely: (a) die-holder; (b) die-holder cover; (c) die support; (d) cylindrical Sindanyo insulator; (e) load cell. The die holder assembly is schematically shown in Figure 24.

The original die-holder was for supporting the dies with 76 mm outer diameter onto the load cell, and also it has inlet and outlet holes to water-cool the die. It is mounted on an angle block by 8 screws.

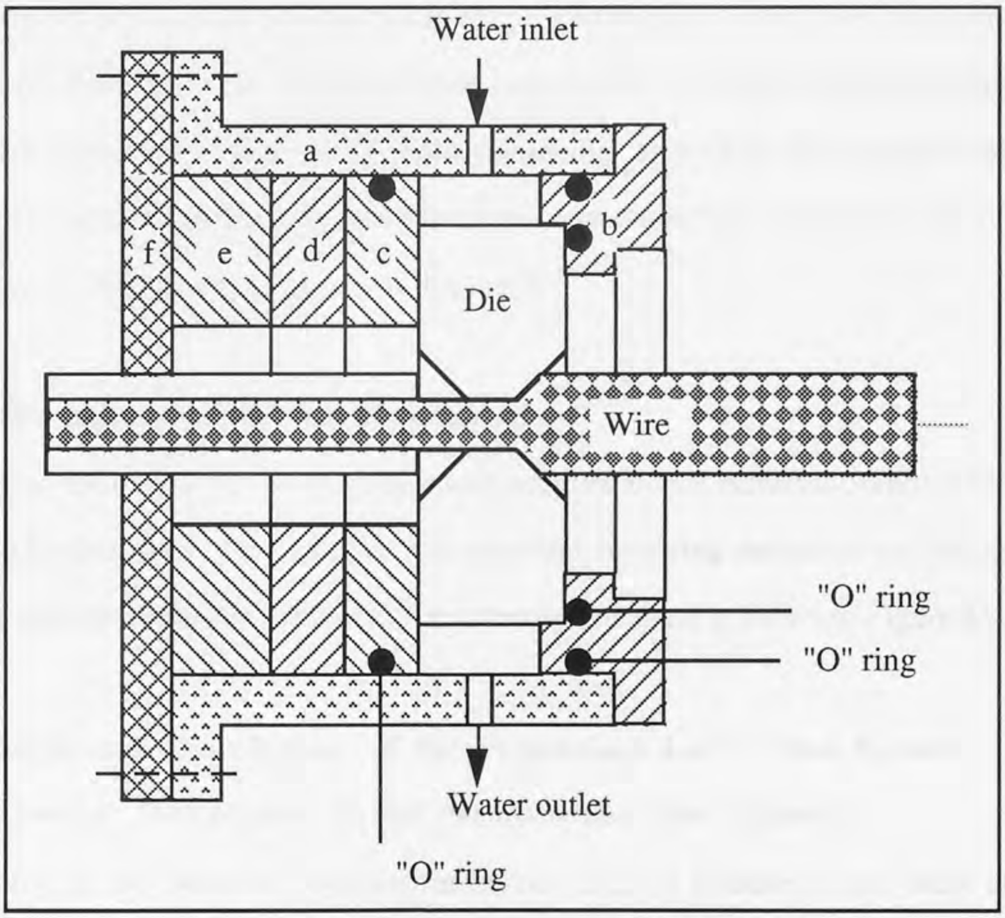

a. die holder; b. die holder cover; c. die support;
d. Sindanyo disc; e. load cell; f. angle block.

Fig. 24 Schematic diagram of the die-holder for 76 mm diameter die.

The die support has an "O" ring round its circumference to prevent the cooling water from penetrating into the load cell. A cylindrical tube was welded onto one face of the die support in order to drain away the water used for cooling the wire at exit.

The die-holder cover was screwed up to the die-holder by three screws which retain the die in position. The die-holder cover has two "O" rings to prevent leakage of water during the tests.

The load cell was placed next to the angle block. Between the angle block and the die support, a Sindanyo disc was placed to insulate the die thermally from the load cell.

This die holder assembly was designed for using 76 mm diameter dies and was only used for preliminary experiments in the present research. It has been used previously by several researchers for various drawing experiments. The preliminary experiments of this study also proved that the die holder assembly as well as the instrumentation all functioned well which gave the confidence to carry out further systematic drawing tests described in the following chapters of this thesis.

3.3.2 Die holder for 43 mm diameter die

In order to use dies of 43 mm outer diameter supplied by the National-Standard Company Limited for this study, the die holder was modified, involving the design and manufacture of a die adapter and a new die cover. The schematic diagram is shown in Figure 25.

3.4 Design and Manufacture of the Pressurised Lubrication System

3.4.1 General Description of the Pressure Die Box Assembly

According to the literature reviewed in Section 2.15 of Chapter 2, the most efficient lubrication in wire drawing is hydrodynamic lubrication, and a hydrodynamic lubrication system requires a combined effect of drawing speed, lubricant properties and geometry of the Christopherson's type of pressure tube. With all these aspects borne in mind, a hydrodynamic lubrication system using soap lubricant was designed and built for the present study regarding the evaluation of friction and lubrication in wire drawing, which is shown schematically in Figure 27. This system, called the pressure die box assembly consists of a drawing die, a die holder, a pressure die nozzle and a lubricant container. Figure 26 shows a view of the pressure die box in use.

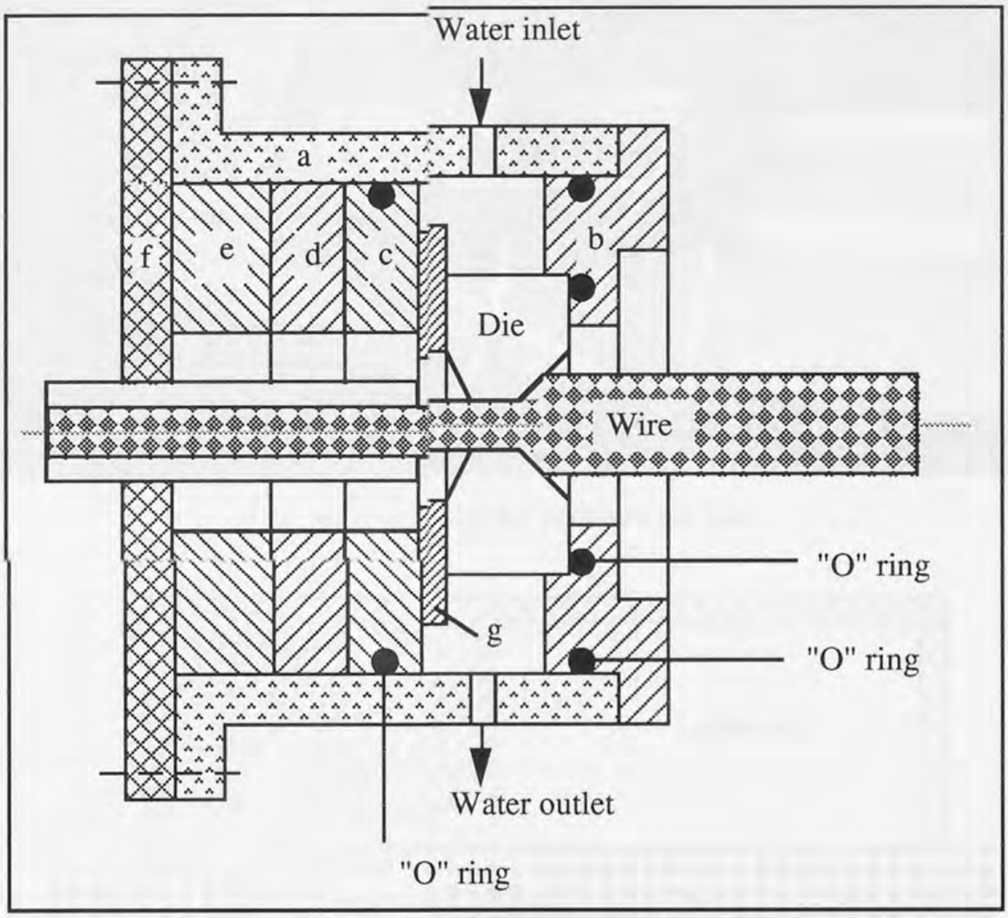

a. die holder; b. die holder cover; c. die support; e. load cell;
d. Sindanyo disc; f. angle block; g. die adapter.

Fig. 25 Schematic diagram of the die-holder for 43 mm diameter die.

The following factors were considered in the design of the whole system:

(1) Compatibility with the existing bull block and the die holder assembly;

(2) Ease of manufacture and assembly, including die, pressure die nozzle and lubricant change;

(3) Establishment of hydrodynamic lubrication.

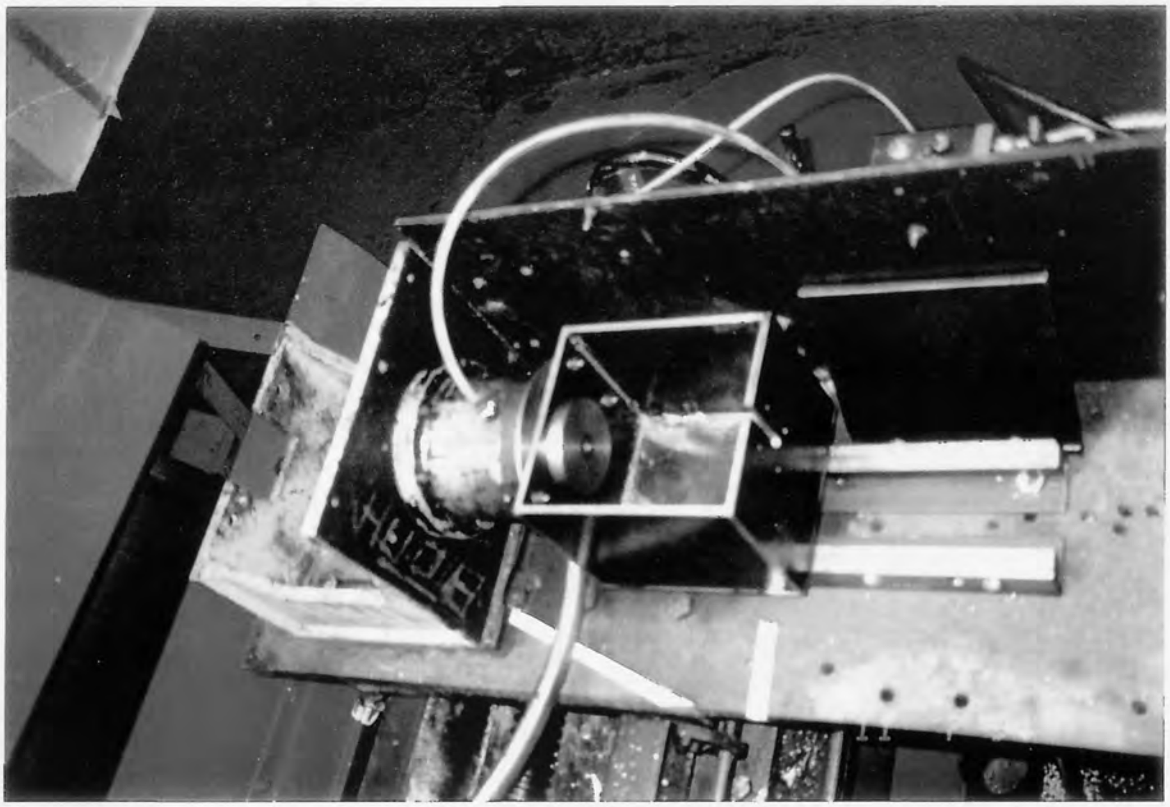

Fig. 26 A view of the pressure die box.

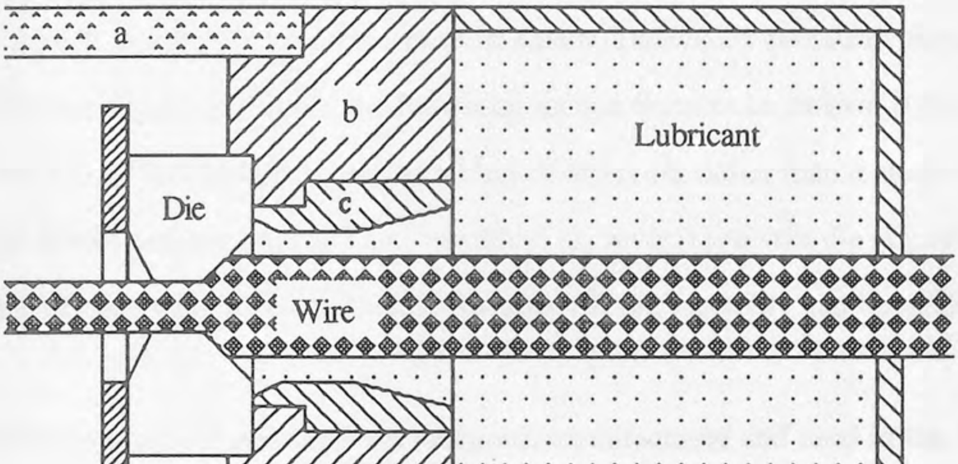

a. die holder; b. pressure die adapter; c. pressure die nozzle;
d. lubricant container.

Fig 27 A schematic view of the pressure die box assembly.

3.4.2 Consideration of the High Pressure Die Nozzle

The key component of the complete pressure die box assembly is the high pressure nozzle (item c in Figure 27), as presented in Figure 28, since it determines whether a hydrodynamic lubrication can be established.

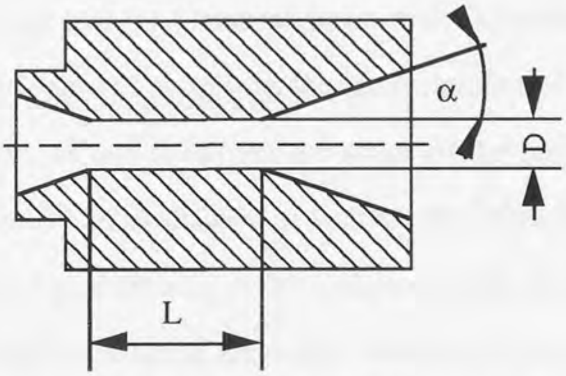

L = 20 mm; D = 6.0 mm; α = 6, 8 and 10 degrees.

Fig. 28 The high pressure die nozzle.

Although this design resembles, to some extent, Tattersall's 'pressure measurement device' [86] (see Figure 21), it has the following unique features in its own right: (1) the pressure die nozzle has been designed as a kind of insert set rather than a single chunky part, which allows easy manufacture and assembly; (2) several pressure die nozzles can be easily made at once with different internal features; (3) the assembly can be made at low cost.

Three pressure die nozzles were designed, manufactured and used in the drawing experiment of the present work. The length of the parallel part of the pressure die nozzles L was all set to be 20 mm (6 - 25 mm in Tattersall's work) and the diameter D was 6 mm, whereas the inlet semi-angle α was chosen as the variable to be 6, 8 and 10 degrees (only 6 degrees in Tattersall's work).

According to Tattersall [86], the pressure, p, at the die entry point of this pressurised lubrication system, can be calculated using the following equation:

$$p = \frac{12\mu l}{h^3}\left(\frac{uh}{2} - fut\right) \tag{4.1}$$

where l is the length of the parallel part of the pressure die nozzle, h the clearance between the pressure die nozzle and the parallel part of the pressure die nozzle, μ the viscosity of the lubricant, u the drawing speed and t the thickness of the lubricant layer.

However, the calculation as well as the measurement of the lubricant pressure, were not even attempted, as this is beyond the scope of the present study. The present study adopts a different way of evaluation of friction and lubrication, which proves that this design worked well in wire drawing as demonstrated in the following chapters.

All the engineering drawings of the design used for the production of the die holder assembly and the pressure die box can be found in Appendix B.

3.5 Instrumentation

The instrumentation for data acquisition includes a load cell and a tachometer.

3.5.1 Load cell

The load cell used to measure the drawing pull is a ring load cell which was designed for a maximum axial load of 20 kN and consists of a continuous ring of rectangular cross-section. On one side there are four integral sectoral supports equally spaced, and on the other side a similar number of equal-spaced supports placed in positions equal to half the pitch. Consequently, the ring is formed as a continuous series of circumferentially-shaped beams which strain in bending and torsion. When a compressive force is applied to the load cell, the active strain gauges, which are bonded to the ring on the face opposite to the sectoral supports, respond to a tensile bending strain. The positioning of the sectoral supports and strain gauges are shown in Figure 29. The inactive gauges are bonded to the inner and outer peripheral surfaces in the circumferential direction in line with the neutral surface. This arrangement was adopted in order to compensate for temperature variations around the ring and any distortion other than that caused by the axial thrust. The ring load cell housing was specially made to prevent the ingress of water which might cause possible damage to the strain gauges (because the drawing die is cooled with water).

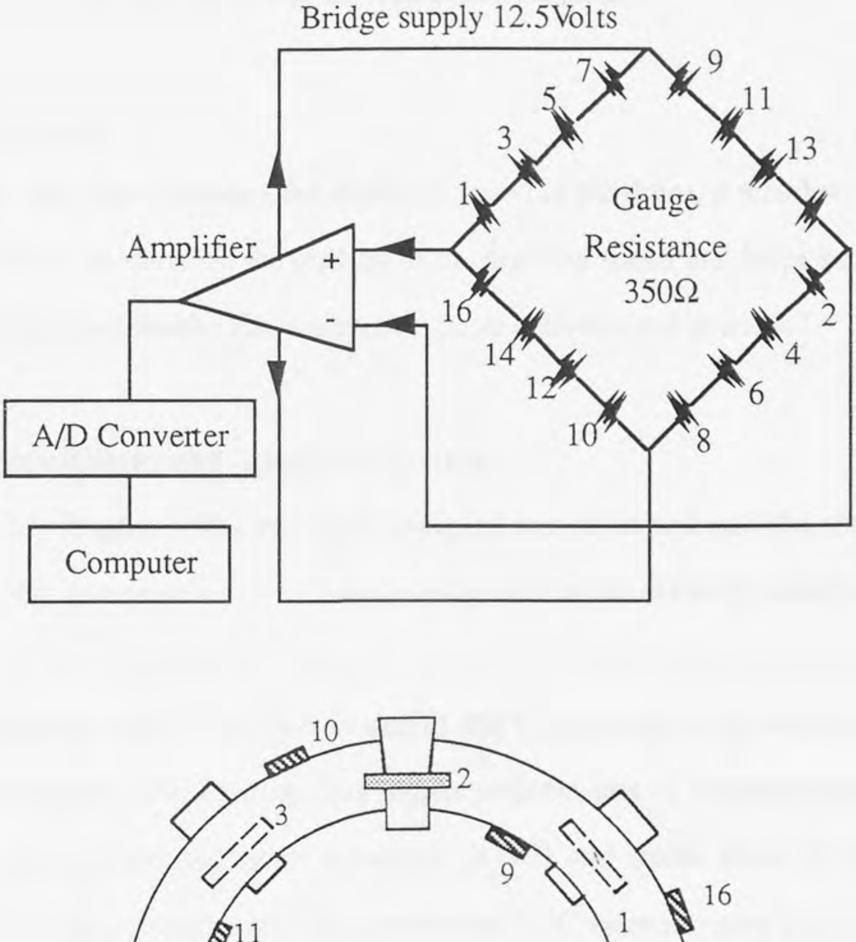

Fig. 29 Circuit diagram of the load cell.

3.5.2 The calibration of the load cell

The load cell was calibrated by compression between two platens in a 500 kN Instron Universal Testing Machine. The calibration graph is shown in Figure A.1. The loading range (0-20 kN) in the calibration was identified from the preliminary drawing tests. Figure A.1 shows that the linearity of the load cell is excellent.

3.5.3 Tachometer

A tachometer, used for measuring the rotational speed of the drum, is attached to the worm shaft of the motor which gives the reading of the drawing speed and helps set up drawing tests at different speed levels. The calibration graph is shown in Figure A.2.

3.6 Data Acquisition and Analysis System

The Picolog data logger, a Pico analogue-to-digital converter and an IBM compatible PC were used as the data acquisition and analysis system in the drawing experiments of this research.

The Picolog data logger is a powerful and flexible program which enables data logging and analysis. The Picolog data logger collects sets of measurements from the channels of an analogue to digital converter (ADC) and stores them directly on to a computer disk. It also provides tools to convert the ADC values to give parameters scaled in engineering units and to produce text and graphical reports. Its principle is shown diagrammatically in Figure 30.

The analogue-to-digital converter has eight channels. Each channel is used to measure a voltage which is a representation of a real-world parameter. In this research, two channels were used, one of which was for measuring the drawing load and the other was for measuring the drawing speed.

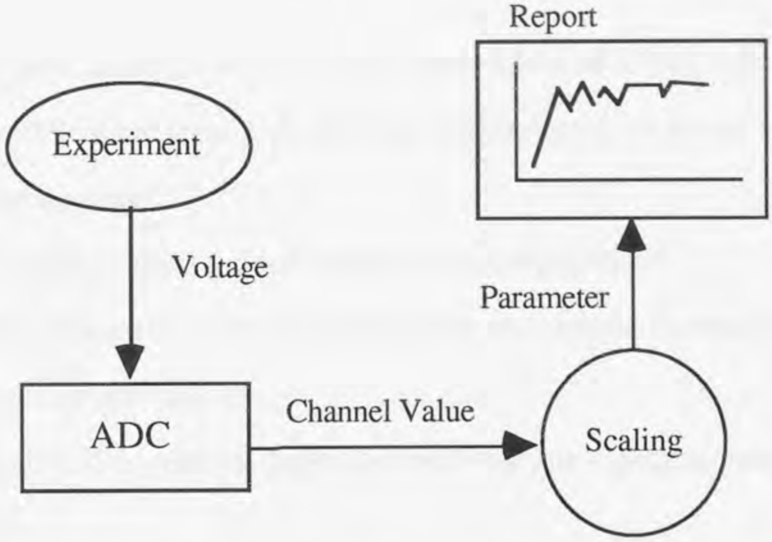

Fig. 30 Schematic layout of basic principles of Picolog data logging system.

3.7 Tensile Testing Machine

The tensile testing machine used in this research was an Instron Model 1197 Universal Testing Instrument with a maximum load capability of 500 kN. It was connected to a computer on which an operating software was installed. With this software available, the Instron could be operated and stress-strain data obtained automatically.

The tensile testing machine was used to examine the yield stress of the wire before and after drawing, thus to produce a flow stress and strain curve for the drawn materials within a strain range covering the full range of that experienced in all the drawing tests.

3.8 Scanning Electronic Microscope

The scanning electronic microscope (SEM) is widely used for the examination and analysis of the microstructure characteristics of materials in a solid form. In this study the SEM was used to investigate the residual lubricant layer on the surface of the drawn wire to evaluate the lubricant performance under a given experimental condition. The SEM examination was carried out on a Cambridge S90 SEM machine available in the Department of Mechanical and Electrical Engineering at Aston University.

The SEM examination enables morphological observations of a very fine structure and elemental analysis. There are three different ways of producing an image and these give different types of information:

(a) Secondary electron mode - shows mainly surface topography;

(b) Back-scattered electron mode - topography and non-specific chemical effects especially on smooth surfaces;

(c) Spectroscopical X-ray energy-dispersive microanalysis - specific chemical information.

The magnification ranges of the Cambridge S90 are from x15 to x20,000.

The SEM can detect elements above boron (atomic number 5) in very small amount of material (10^{-12} g) and with a detection level of 0.25%. Elements detected may be shown either as spectra or as a table of percentages. X-ray maps may also be produced to show element distributions by choosing X-ray image mode.

The SEM was used to examine and analyse the lubricant film on the surface of the drawn wire in this research.

CHAPTER FOUR

DRAWING PROCESS MATERIALS AND EXPERIMENTAL PROCEDURE

4.1 Introduction

The main objective of this research was lubrication evaluation in wire drawing. In order to obtain different conditions for lubrication and to evaluate the performance of both the lubricants and the pressure die box, two different drawing materials, five different area reductions, five drawing speeds and two lubricants were employed in the drawing tests. SEM examinations were used in order to study the residual lubricant layer on the drawn wires.

4.2 Drawing Process Materials

4.2.1 Drawing materials

The materials used in this research were: low carbon steel and medium carbon steel. The chemical compositions of the two steels are given in Table 1.

Table 1 Chemical compositions of the drawing materials (wt%).

Material	C	Si	Mn	S	P	Cr	Ni	Al
Low Carbon Steel	0.03	0.01	0.33	0.016	0.017	-	-	0.031
Medium Carbon Steel	0.37	0.022	0.69	0.022	0.014	0.03	0.01	-

4.2.2 Drawing dies

Drawing dies used in this research were supplied by National-Standard Co. Ltd. They were tungsten carbide dies with 7.5 degree die semi-angle. Figure 31 shows the general profile of the drawing dies.

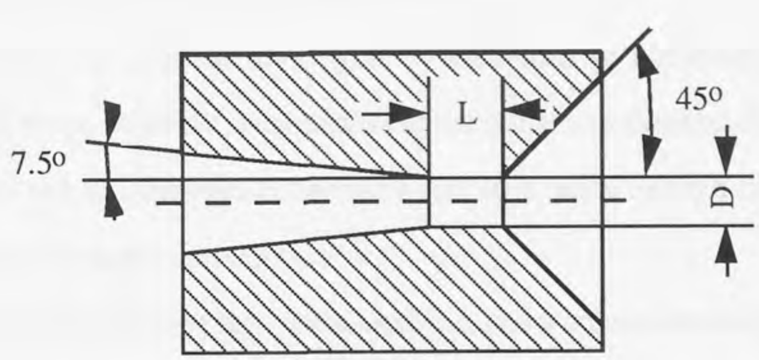

Fig. 31 Profile of drawing die from N-S.

D is the die internal diameter ranging between 4.2 mm to 5.2 mm, and L is the bearing length, L= 25%D. All the dies have an outer diameter of 43 mm.

4.2.3 Lubricants

The lubricants used in the drawing tests were two calcium-based lubricants, Condat Vicafil (TF44) and Traxit (TR 41/B), which are normally used for break-down drawing in a typical multi-pass wire drawing process.

The physical and chemical properties of TRAXIT (TR 41/B) and CONDAT VICAFIL (TF44) lubricants are as following:

TRAXIT (TR 41/B): Melting point: 210 °C
Density: 760 kg/m^3
Insoluble in water
Flash point 320 °C

CONDAT VICAFIL (TF44): Softening range: approx. 145 °C to 165 °C
Density: 700 - 800 kg/m^3
Insoluble in water
Flash range: 170 °C to 200 °C

The lubricants were fully charged into the lubricant container as supplied to submerge the pressure die nozzle before each drawing test was carried out.

4.3 Preparation of Process Materials

The initial steel wires for the drawing tests were coils of hot rolled product with a diameter of 5.5 mm. With the combination of the initial and finished diameters (4.6-5.1 mm), the area reduction ranges between 14 and 40%, wide enough for the purpose of investigation in the current research.

Before each drawing test, wires were cut into a convenient length, about 3 to 4 m, with one end swaged into a smaller diameter in order to be threaded through the conical drawing die without applying any load on the load cell. When arranging the wire on the drawing table, it was straightened by the five-roll straightener.

4.4 Drawing Tests

The drawing tests were carried out for the drawing process materials described in Section 4.2 according to the experimental design given in Table 2.

Table 2 The drawing experimental design.

Material	Lubricant	Pressure Die Nozzle Semi-angle (degree)	Area Reduction (%)	Drawing Speed (m/min)
Low Carbon Steel	CONDAT	6	17	10
	VICAFIL	8	21	20
Medium Carbon Steel		10	24	27
	TRAXIT		27	37
			30	47

Each drawing test followed the following procedures:

(1) Set up proper drawing speed by choosing different gear positions;

(2) Set the data logging software ready to capture data, such as drawing load and speed, by specifying appropriate values for required parameters;

(3) The swaged end is threaded through the five-roll straightener, pressure die

nozzle and die holder and gripped by the jaw on the drum;

(4) Balance the Wheatstone Bridge to reset the load cell reading to zero;

(5) Run the data-capturing software;

(6) Run the Bull-block and start the drawing test;

(7) Stop the Bull-block and the software when the drawing is finished;

(8) Save the logged data onto the computer hard disc for analysis.

The drawing test results are fully presented, analysed and discussed in Chapters 6 and 7.

4.5 Tensile Test

In order to obtain material flow stress and strain data, tensile tests were performed both for as received and drawn wires on the Instron tensile test machine. For each test, samples were cut to 300 mm long. A pulling speed of 5 mm/min was consistently used. The whole process of the tensile test was program-controlled through a computer. The software, a commercial programme called NENE, by which data were collected and processed, was already in use on the tensile testing machine.

The tensile test results are presented and discussed in Sections 5.4 and 5.5 of Chapter 5.

4.6 SEM Examination of Lubricant Layer

Several previous researches have attempted to examine the residual lubricant layer on the drawn wire, as reviewed in section 2.16 of Chapter 2. However none of them gave a convincing quantitative evaluation for the residual lubricant layer on drawn wire in terms of its thickness.

The best way of evaluating the performance of a hydrodynamic lubrication system or a particular lubricant, in the author's opinion, is to look for the residual lubricant layer on the drawn wire and, if there is any, quantify its thickness. Therefore, SEM examinations were carried out on samples taken from the drawn wires drawn under different conditions.

Several different ways were used to make samples for the SEM micro-structural examination. When using the usual way to make the sample, i.e. to mount sections in conductive Backelite compound, sometimes gaps appeared between the sample and the mounting compound when examined under SEM, where it is believed the residual lubricant might have been present. This is probably because:

(1) when sample is being mounted in the mounting press, the temperature of the chamber (~ 160 ^{o}C) can be higher than the melting point of the lubricant. Therefore the residual lubricant will be melted and absorbed into the melting Bakelite.

(2) Even if the lubricants are insoluble in water, they are soluble in all solvents used for the SEM sample preparing, for example, Inhibisol and polishing oil. Hence the residual lubricant might be dissolved during polishing and cleaning.

In order to overcome this and obtain a clear view of the residual lubricant layer, the following methods were also tried:

(1) The use of water as a cleaning solvent instead of organic chemical solvents in between different polishing stages during sample preparation.

(2) Cold mounting was also introduced to avoid lubricant melting when in mounting press. The so-called cold mount uses a thermosetting mixture of epoxy resin and hardener as the mounting compound, and was carried out at room temperature. The samples were examined by using a optical microscope. The magnification range for optical microscope is from x20 to x500.

(3) Gold-coating was also used to prevent charging during SEM examination, and thus get a better view of the lubricant layers.

The magnification range of the SEM used in this study is up to x 20,000. The SEM results are presented, analysed and discussed in Chapters 6 and 7.

CHAPTER FIVE

MATERIAL CONSTITUTIVE MODELS AND STRESS-STRAIN DATA

5.1 Introduction

Both analytical and numerical analysis of metal forming such as drawing, rolling, forging, etc. requires an understanding of the plastic behaviour of the particular deformation metal in terms of its flow stress, which can only be obtained by experiment [2]. There are three experimental methods which are normally employed, namely tensile test, compression test and torsion test.

Tensile Test

The tensile test is the simplest method of measuring flow stress in which the specimens are subject to a uniaxial tensile load. The specimens used are characteristically simple in form, with a central uniform region (the gauge length), of circular or rectangular cross-section. Figure 32 shows some general forms of load-extension and nominal stress-nominal strain curves [2].

The nominal stress σ' and nominal strain e are calculated using the following equations:

$$\sigma' = P / A_o \tag{5.1}$$

$$e = \Delta l / l_o \tag{5.2}$$

where P is the applied tensile load, A_o the original cross-sectional area of the specimen, Δl is the extension of gauge length and l_o is the original gauge length.

As the cross sectional area of the specimen is constantly changing, the nominal stress calculated by equation (5.1) is not really a stress. The nominal strain defined by equation (5.2) is of less basic importance than the natural or true strain experienced by the test piece at a particular time. Therefore, the true stress σ and true strain ε are used in metal forming analysis which are calculated by

$$\sigma = P / A \tag{5.3}$$

$$\varepsilon = \ln (l/l_o) \tag{5.4}$$

where A is the instantaneous cross-sectional area and l the instantaneous gauge length of the specimen.

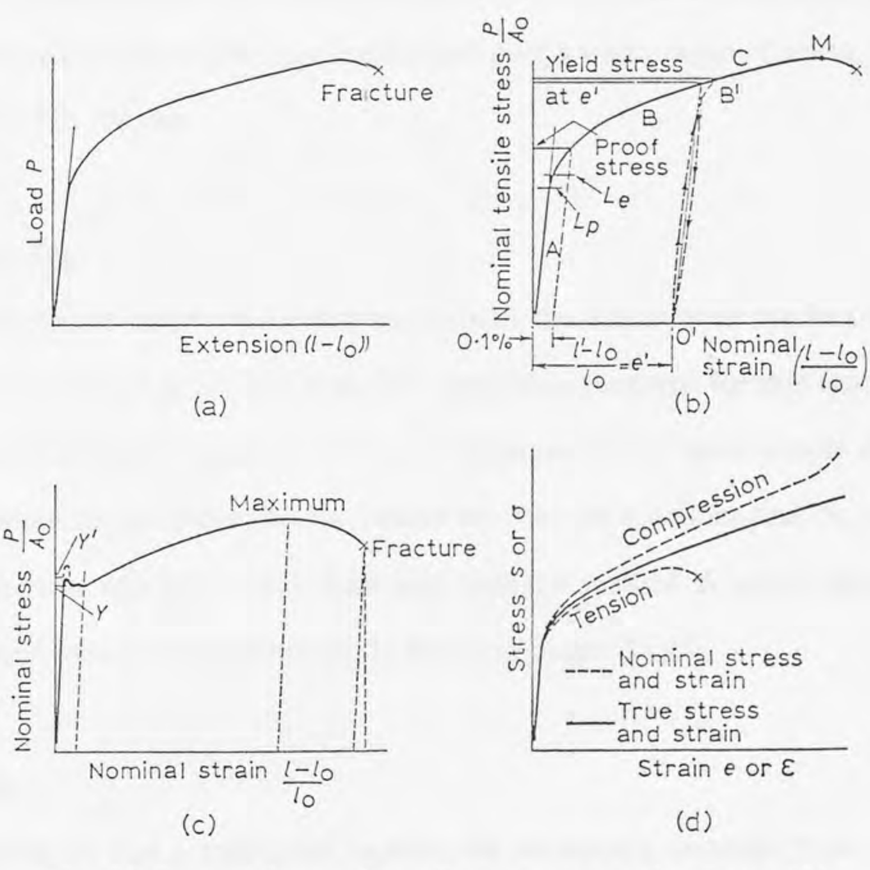

Fig. 32 General forms of tensile test curves, after Rowe [2].

(a) Load-extension curve for a ductile material such as steel.

(b) The same data replotted as nominal stress and strain curve.

(c) A nominal stress-strain curve for mild steel, showing the yield point peculiarity.

(d) Stress-strain curves for idealised compression and tension.

The true stress and strain curve (the stress and strain referred to in this thesis are true stress and strain unless otherwise stated) is in a similar form compared with the nominal stress and strain curve, see Figure 32 (d).

Although simple in its form, the tensile test has certain disadvantages [2]. It is limited to relatively small shape changes, since necking occurs to violate homogeneous deformation which is essential to the accurate calculation of true stress. Therefore other tests (compression and torsion) are consequently necessary to obtain deformation characteristics applicable to severe metal-forming operations [2, 4]. In a single tensile test, useful data can only be obtained up to a strain of 0.2 - 0.3. However multiple tests can be carried out by subjecting the specimen to different levels of plastic deformation prior to the test, in this way flow stress data can be obtained over a wider range of strain, as is seen in Section 5.4 in this chapter.

Compression Test

When specimens are subject to a compressive load, the deformation can be carried out up to a strain value of 0.7 in a single test. The specimens prepared for this type of tests are either cylindrical or tubular form. The compression test is also quite simple regarding the experimentation set-ups, nevertheless friction between the specimen and the anvils causes barrelling to occur which is a major draw back with this method. A typical stress and strain curve obtained from a compression test is shown in Figure 32 (d).

Torsion Test

Torsion testing is also a traditional method for measuring material flow stress. Solid cylindrical specimens are used and subject to rotation moment. Unlike the tensile or compression test, the specimen is deformed in a rather stable and uniform way and there is no friction between the specimen and tool involved. As a result, a test can go on up to a very high strain level [4]. It is especially good for measuring flow stress of metals at high temperatures and strain rate. Jornaz [5] used this method in his study and Figure 33 shows some of his results.

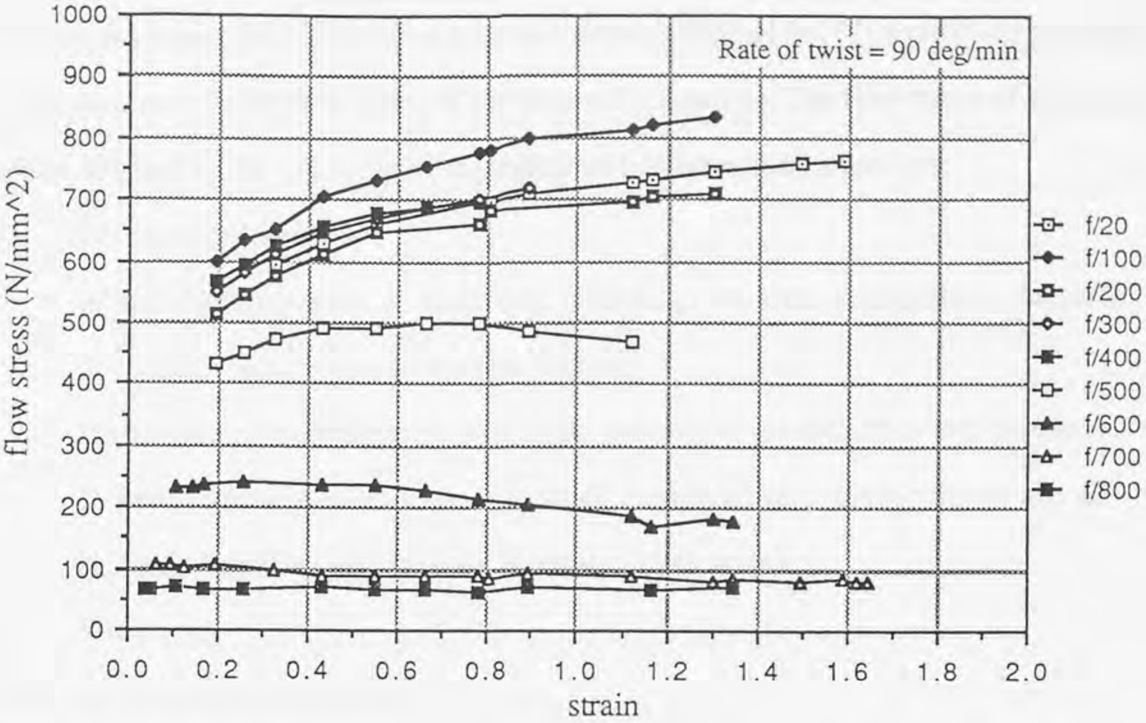

Fig. 33 Effect of temperature on the flow stress of a boron steel, after Jornaz [4]. f/20: flow stress at 20 °C; f/100: flow stress at 100 °C etc.

However there are also limitations with the torsion test: the set-up of the experimental rig is much more complicated; the analysis of experiment results is relatively difficult and the accuracy of the flow stress and strain curve is affected by stress gradient and bending of the specimen [4].

For simplicity and confidence in result analysis, the tensile test was chosen in this study to investigate the flow stress characteristics of the steels under consideration.

5.2 Factors Affecting Flow Stress of Materials

This section gives a brief overview on the factors affecting the flow stress of materials in general. Detailed documentation on this subject can be found elsewhere in the standard text books [11, 97].

It is very important to understand the flow stress of metals, because in metal forming processes the deformation load and stresses depend on: (1) workpiece geometry, (2) friction, and (3) the flow stress of the deforming material. The flow stress of material is mainly affected by the following metallurgical and deformation parameters:

(a) Chemical composition;

(b) Metallurgical structure, including phases, grain size, segregation, inclusions, dislocation density and prior strain history;

(c) Plastic strain (by definition, total strain consists of elastic strain and plastic strain. In metal forming, elastic strain is small compared with plastic strain and can be ignored. Therefore plastic strain is equal to total strain);

(d) Strain rate;

(e) Deformation temperature.

Among the above factors, (a) and (b) are metallurgical, and (c)-(e) deformational. The composition of the material and the phases contained in the material dominate its plastic flow behaviour which is clearly demonstrated in Figures 34 and 35. Figure 34 shows nominal stress-elongation curves for (a) impure iron, and (b) copper. Figure 35 gives stress-strain curves for plain carbon, HSLA and dual-phase steels.

Grain size also plays a role in affecting material flow stress. It is common knowledge that the smaller the grain size, the higher the flow stress [97].

Although Harding [103] has shown that for some metallic materials, such as aluminium, titanium and mild steel, there is a significant raising of stress-strain curve with increasing strain rate, the data presented were largely for tests carried out at strain rates of impact (up to 2000/s). There is clearly a lack of flow stress-strain data for low strain rates (less than 100/s) at which most metal forming processes, such as wire drawing and rolling, are conducted [9, 97, 103]. Meanwhile, it is a common practice, in terms of deformational parameters, that in deformation at near room temperatures such as cold drawing, the flow stress of the material is mainly considered to be a function of the plastic strain which it has undergone, and the effect of strain rate and temperature are small, hence neglected [2, 4, 7, 8, 10, 51]. Generally speaking, flow stress increases as the strain increases, as seen in Figures 32, 34 and 35.

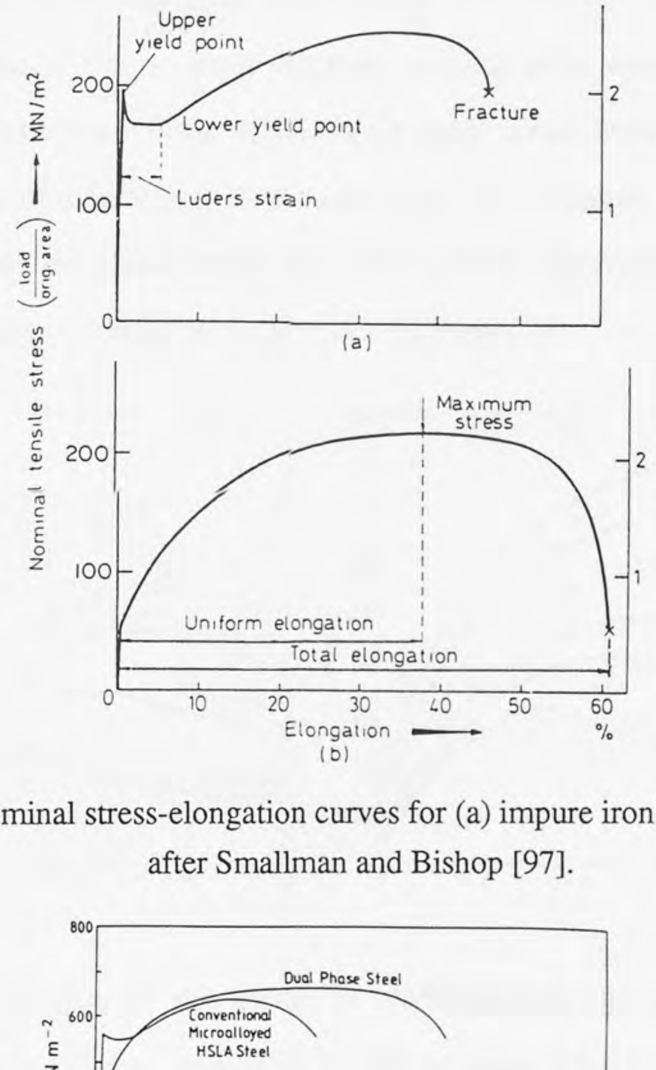

Fig. 34 Nominal stress-elongation curves for (a) impure iron, and (b) copper after Smallman and Bishop [97].

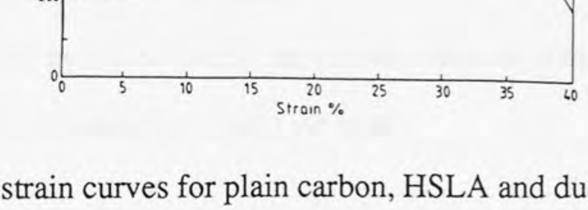

Fig. 35 Stress-strain curves for plain carbon, HSLA and dual-phase steels [97].

During deformation at high temperatures such as hot drawing however, the strain rate and temperature effects on the flow stress of materials are dominant. The flow stress usually decreases as the temperature increases and increases as the strain rate increases. Figures 33 and 36 present some experimental results by previous researchers showing the flow stress-strain curves measured at different deformation temperatures and strain rate [4, 98]. Whereas the effect of plastic strain on flow stress is more complicated, as dynamic recrystallisation, which will occur at low strain rates, causes work softening, which will compensate for work hardening. This could result in a situation where the flow stress increases at first as the plastic strain increases and then decreases as the plastic strain further increases after a certain value, as shown in Figure 36.

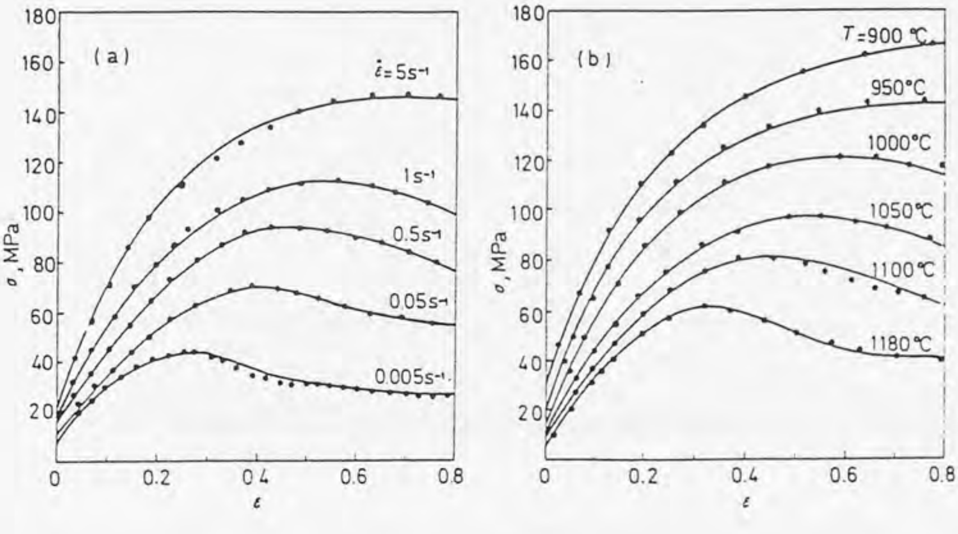

Fig. 36 Flow stress-strain curves for 14MnNb steel, after Gao et al [98]:

(a) temperature = 1050 ^{o}C and (b) strain rate = 0.5 s^{-1}.

5.3 Material Constitutive Models

It is the purpose of this section to clarify the various material constitutive models developed and used by previous researchers through the years.

According to Kobayashi et al [7], the flow stress of the material σ_f can be expressed as a function of temperature T, strain ε, strain rate $\dot{\varepsilon}$ and microstructure S:

$$\sigma_f = f\,(\,T, \varepsilon, \dot{\varepsilon}, S) \tag{5.5}$$

This is a general expression intended to cover all the factors which affect the material flow stress. In reality, however, there is no such a mathematical function available, and simplified and/or empirical material constitutive models are normally used, which only considering major factors under certain deformation states.

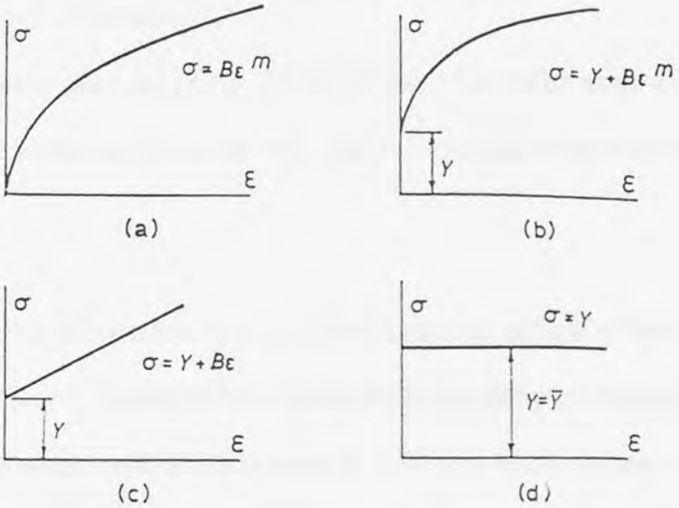

Fig. 37 Simplified forms of stress-strain curve described by Rowe [2].

Rowe [2] described four models for different types of stress-strain curve, shown diagrammatically in Figure 37. It is recognised that forms (a) and (b) in Figure 37 are reasonable and (c) and (d) are idealised.

For annealed metals with a cubic crystal structure the flow stress and strain curve can be described by a simple power law:

$$\sigma_f = B\,\varepsilon^m \tag{5.6}$$

where B and m are constants.

For metals which have already experienced some work hardening prior to deformation, the flow stress is better represented by the following equation:

$$\sigma_f = \sigma_0 (1 + A) \varepsilon^m \qquad (5.7)$$

where σ_o is the initial yield stress of the material, and A and m are constants.

Another popular relationship used to correlate flow stress and strain data is the semi-logarithmic formula:

$$\sigma_f = \sigma_0 + B \ln \varepsilon \qquad (5.8)$$

where σ_0 and B are constants.

The above equations (5.6) - (5.8) are used for deformation processes at near room temperatures, as plastic strain is the only variable and the temperature and strain rate effects are neglected.

During the forming of metals at high temperatures, the effects of temperature and strain rate have to be considered. Attempts have been made by many investigators to fit mathematical equations to the stress and strain curves at different temperatures and strain rates. Zener and Holloman [99] proposed the following type of equation to correlate the flow stress data:

$$\sigma_f = f\left[\dot{\varepsilon}, \exp\left(\frac{Q}{RT}\right)\right] \qquad (5.9)$$

where Q is the activation energy for diffusion of the metal; R the universal gas constant and T the absolute temperature. Note that σ_f is an unspecified function of strain rate and the exponential term.

Sellars and Tegart [100] recommended an equation which is particularly useful for correlating flow stress, temperature and strain rate under hot-working condition:

$$\dot{\varepsilon} = A (\sinh (\alpha \sigma))^{n'} e^{-Q/RT} \qquad (5.10)$$

where A, α and n' are experimentally-determined constants.

A more elaborate material constitutive model for deformation at elevated temperatures was first proposed by Rebelo and Kobayashi [55] and used in a finite-element program by Pillinger [101]:

$$\sigma(\varepsilon, \dot{\varepsilon}, T) = G(\varepsilon)\left(1 + A(\varepsilon)\,\dot{\varepsilon}^{B(\varepsilon)}\right) e^{f_0\left(\frac{1}{T} - \frac{1}{T_0}\right)} \qquad (5.11)$$

where f_0 ant T_0 are constants; G(ε), A(ε) and B(ε) are functions of plastic strain.

5.4 Tensile Test Results

In this study the tensile test was used to examine the flow stress and strain relationship for the two steels under consideration. The reasons being: (a) simplicity, the initial and drawn wires are all cylindrical in cross-section and very accurate in dimension, the specimens can be easily prepared and cut into length; (b) the University's Instron tensile test machine was computer-controlled and ready to use, which provides the ease of data handling; (c) confidence in result analysis, as experience had already been gained through the use of this machine and all the data would be collected and processed by computer programs so that accuracy could be assured.

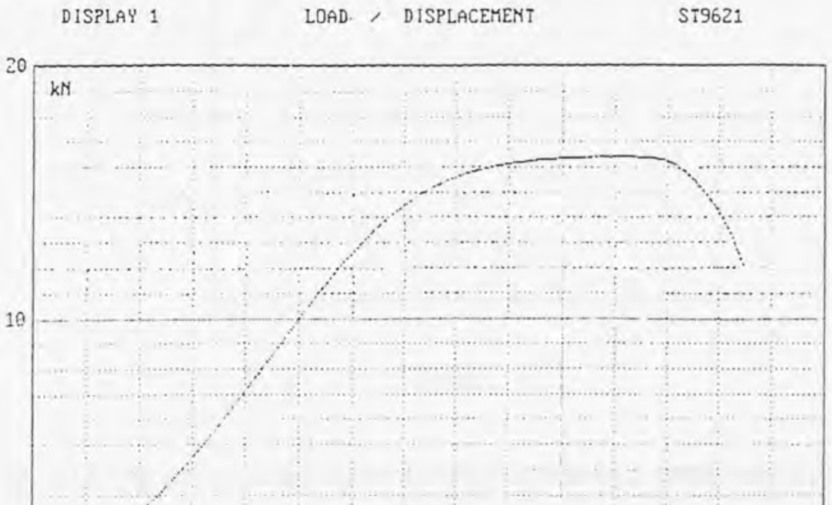

Fig. 38 Typical tensile load/elongation curve obtained from the tensile test.

The chemical compositions for drawing wires, low and medium carbon steel, are given in Table 1. Tensile tests were carried out for specimens carefully prepared using the wire both before and after drawing. Figure 38 shows a typical tensile load/elongation curve.

Since no clear yield point was seen on all the curves of the tests, $\sigma_{0.2}$ was taken as the flow stress, which is the stress calculated on the tensile test curve at an elongation of 0.2% of the gauge length. The flow stress and the natural or plastic strain were calculated, as part of the output, by the program NENE which controlled the whole loading process during the tensile test. Between 3 and 6 specimens were prepared from wires of the same deformation (drawing) history, tested and flow stresses averaged. Full tensile test results for the two steels are listed in tabular form in Appendix C. The flow stress and strain curves drawn according to these data are given in Figures 39 and 40.

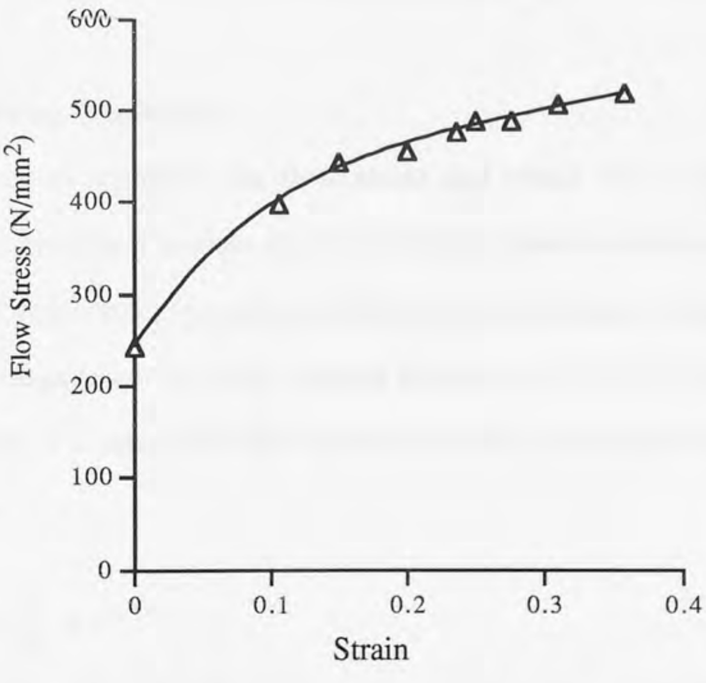

Fig. 39 Flow stress-strain curve for the low carbon steel used in the drawing experiment of this study.

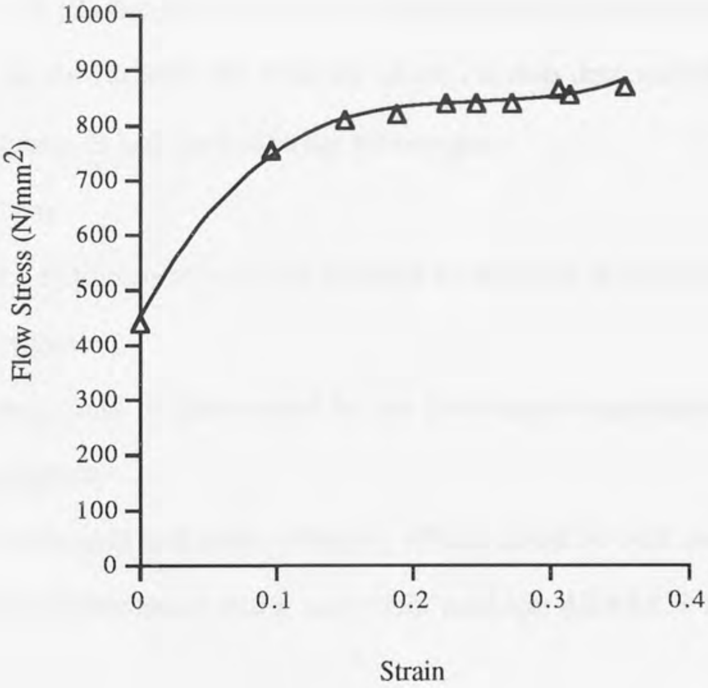

Fig. 40 Flow stress-strain curve for the medium carbon steel used in the drawing experiment of this study.

5.5 Curve Fitting Technique

It is very important to represent the flow stress and strain data to a high accuracy, especially for those numerical models, such as the finite element solution scheme, because sometimes an inappropriate representation of flow stress can cause convergency problems in the numerical computation of metal forming process [5, 8, 9, 55]. Therefore, it is the purpose of this study to correlate the flow stress-strain data from the tensile tests using the following equation:

$$\sigma_f = \sigma_0 + \sum_{i=1}^{n} a_i \varepsilon^i \qquad (5.12)$$

where σ_f is the flow stress, σ_0 and a_i are constants, ε is the plastic strain and i the index which counts from 1 to n.

In equation (5.12) the flow stress σ_f is represented as a polynomial function with the plastic strain ε as the variable, the order of which i is thus determined according to the requirement of accuracy. It had the following advantages:

(1) Simple in form;

(2) The accuracy requirement could be fulfilled by increase or decrease the order of the polynomial function;

(3) The constants could be determined by the least square regression method using a computer program;

(4) Both work hardening and strain softening effects could be well described;

(5) It was easily implemented into a numerical package ABAQUS for metal forming analysis.

A computer program was written for fitting the tensile test data into equation (5.12) based on the least square regression method for the current study, the flow chart of which is shown in Figure 41. Mathematical derivations and solving procedures as well as the program listing are given in Appendix C.

The end results for the curve fitting were as follows:

For low carbon steel:

$$\sigma_f = 242.119 + 2014.812\varepsilon - 6067.610\varepsilon^2 + 7216.161\varepsilon^3 \tag{5.13}$$

For medium carbon steel:

$$\sigma_f = 445.797 + 4558.474\varepsilon - 17872.626\varepsilon^2 + 23682.845\varepsilon^3 \tag{5.14}$$

The correlation coefficients are 0.987 for equation (5.13) and 0.991 for equation (5.14), and the standard deviations are 8.53 N/mm^2 for equation (5.13) and 7.12 N/mm^2 for equation (5.14). The curves produced by the above two equations are drawn in Figures 39 and 40. It is seen that the correlations are excellent.

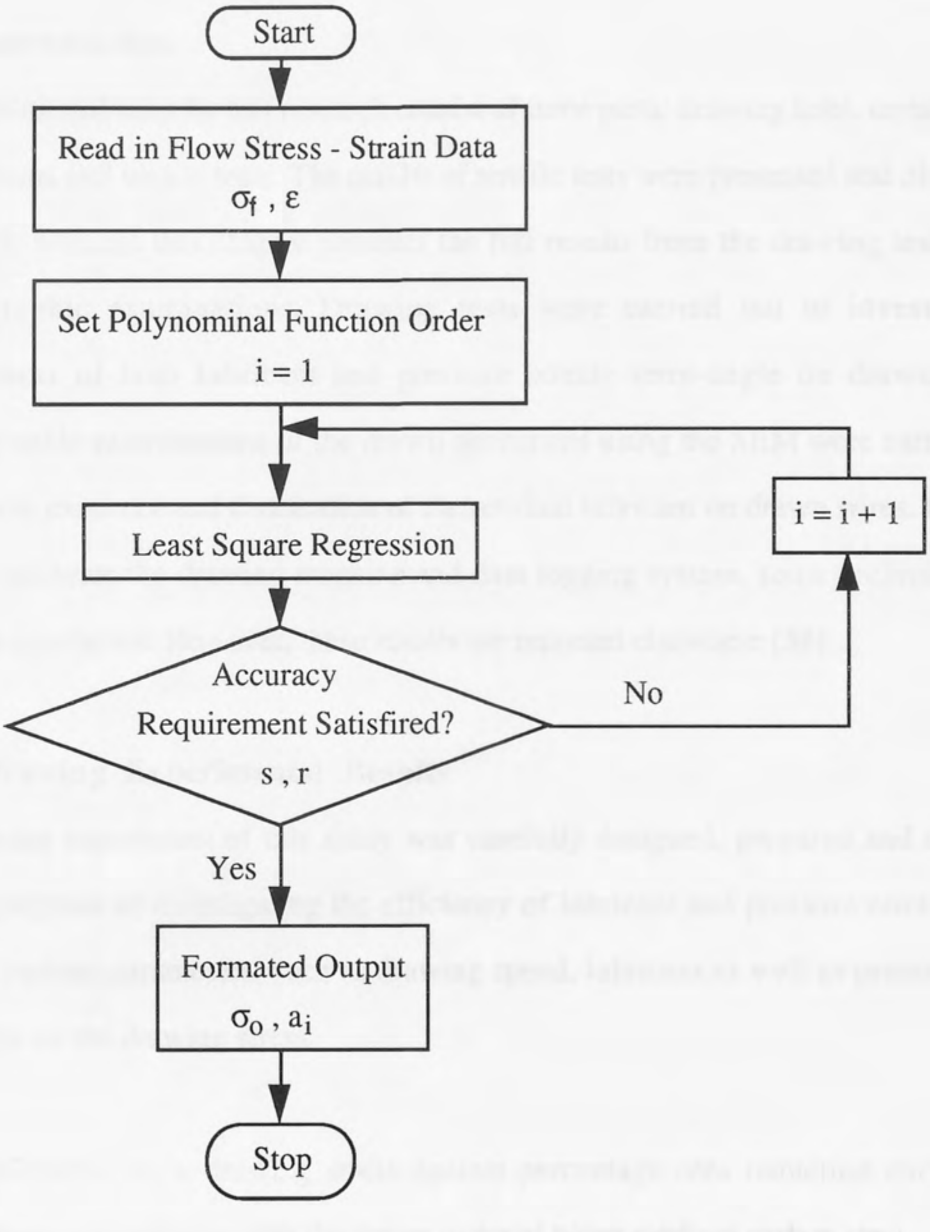

Fig. 41 Flow chart for the curve fitting program developed.

CHAPTER SIX

EXPERIMENTAL RESULTS

6.1 Introduction

The experimental tests for this research consist of three parts: drawing tests, metallographic examinations and tensile tests. The results of tensile tests were presented and discussed in Chapter 5, whereas this chapter presents the full results from the drawing tests and the metallographic examinations. Drawing tests were carried out to investigate the effectiveness of both lubricant and pressure nozzle semi-angle on drawing stress. Metallographic examinations of the drawn specimens using the SEM were carried out to evaluate the existence and distribution of the residual lubricant on drawn wires. In order to tune and calibrate the drawing machine and data logging system, some preliminary tests were also conducted. However, these results are reported elsewhere [58].

6.2 Drawing Experimental Results

The drawing experiment of this study was carefully designed, prepared and conducted with the purpose of investigating the efficiency of lubricant and pressure nozzle and the effect of various parameters, such as drawing speed, lubricant as well as pressure nozzle semi-angle on the drawing stress.

Figures 42 to 63 show drawing stress against percentage area reduction curves under various drawing conditions with the drawn material being medium carbon steel.

Figures 64 to 84 show drawing stress against percentage area reduction curves under various drawing conditions with the drawn material being low carbon steel.

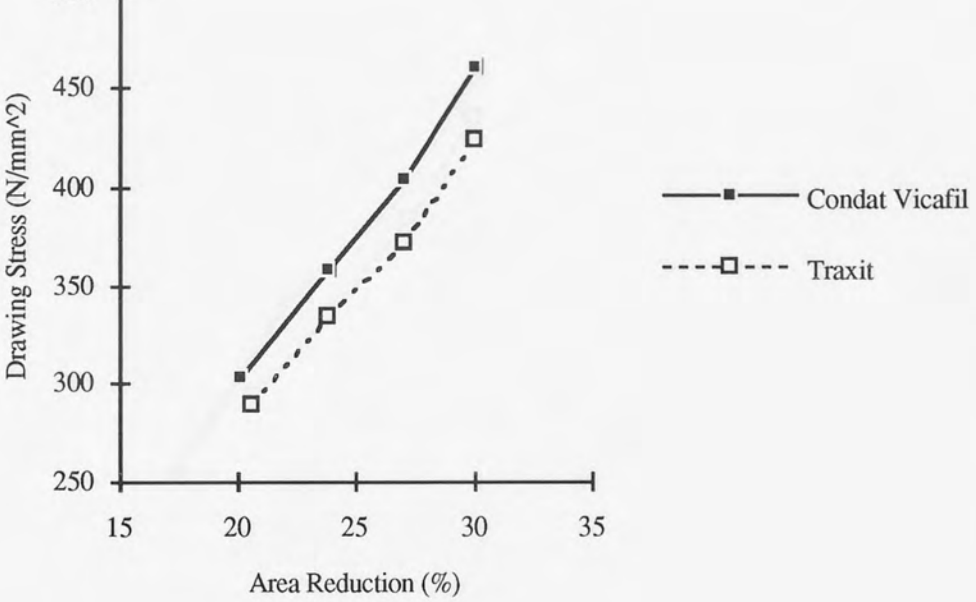

Fig. 42 Drawing stress vs percentage area reduction curves showing the effect of lubricant: Nozzle semi-angle = 6 degree; Drawing speed = 20 m/min, Medium Carbon Steel.

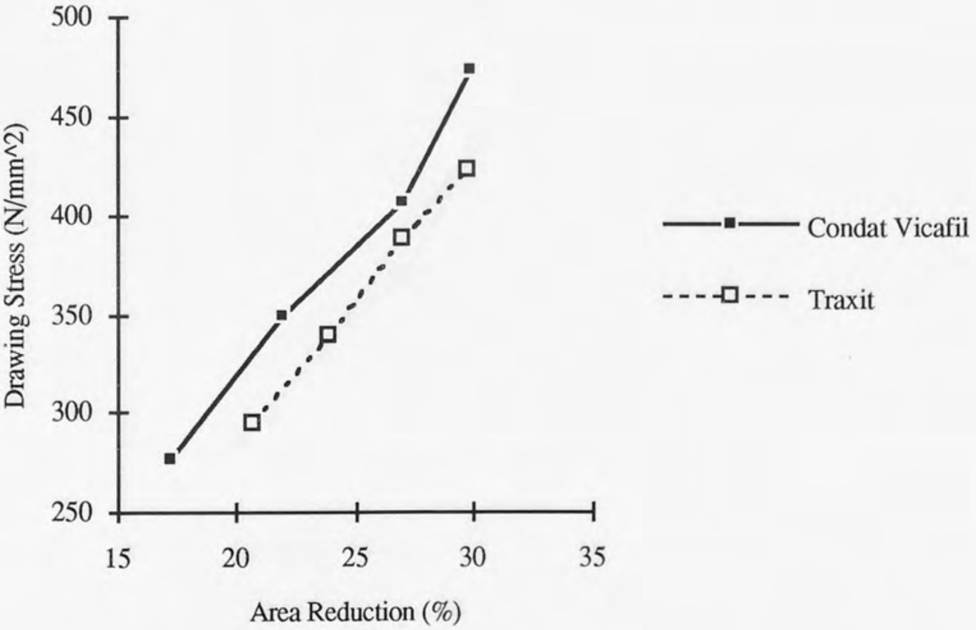

Fig. 43 Drawing stress vs percentage area reduction curves showing the effect of lubricant: Nozzle semi-angle = 6 degree; Drawing speed = 27 m/min, Medium carbon steel.

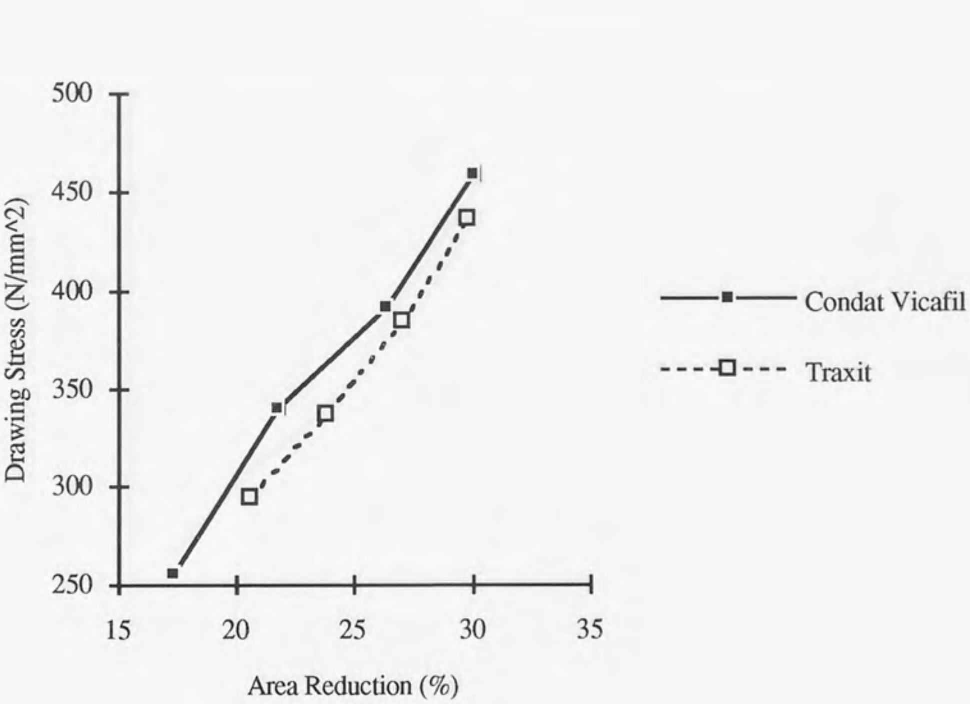

Fig. 44 Drawing stress vs percentage area reduction curves showing the effect of lubricant: Nozzle semi-angle = 6 degree; Drawing speed = 37 m/min, Medium carbon steel.

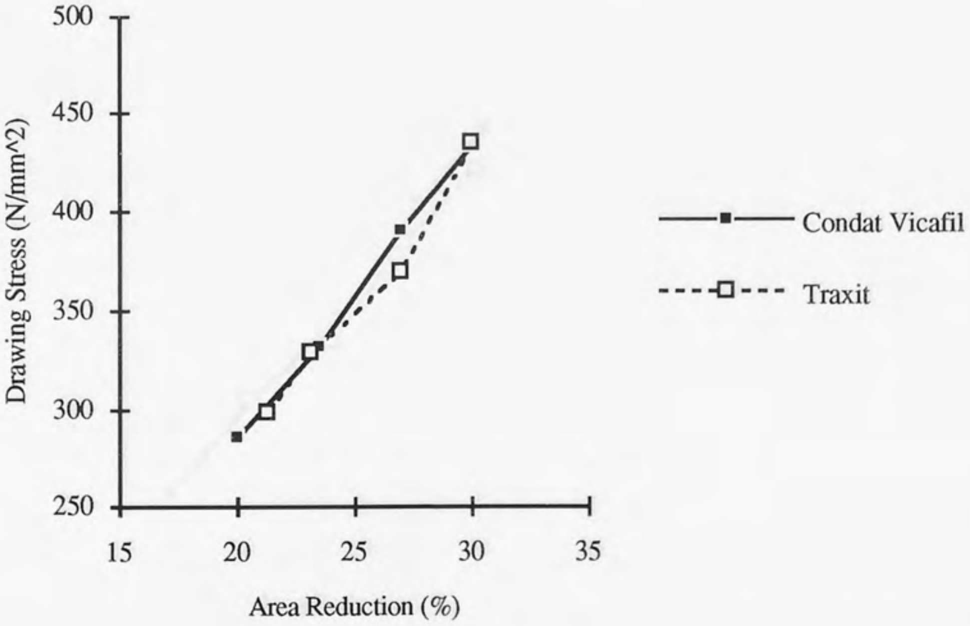

Fig. 45 Drawing stress vs percentage area reduction curves showing the effect of lubricant: Nozzle semi-angle = 6 degree; Drawing speed = 47 m/min, Medium carbon steel.

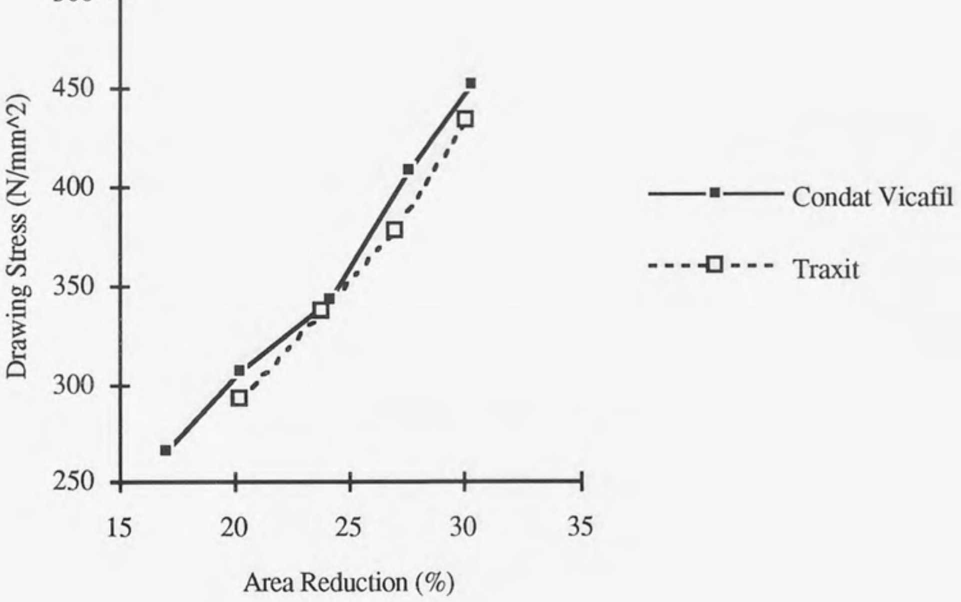

Fig. 46 Drawing stress vs percentage area reduction curves showing the effect of lubricant: Nozzle semi-angle = 8 degree; Drawing speed = 27 m/min, Medium carbon steel.

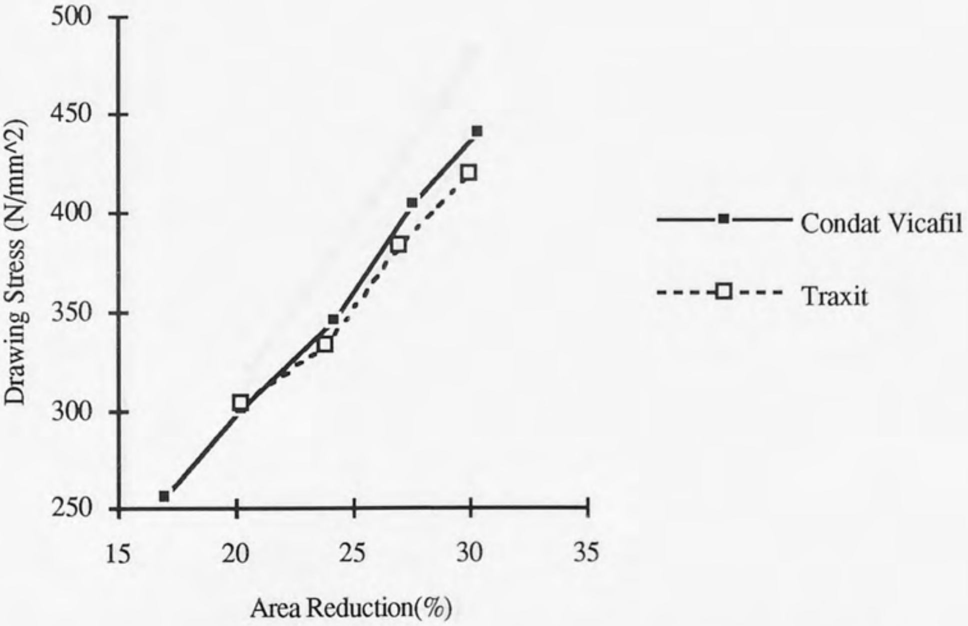

Fig. 47 Drawing stress vs percentage area reduction curves showing the effect of lubricant: Nozzle semi-angle = 8 degree; Drawing speed = 37 m/min, Medium carbon steel.

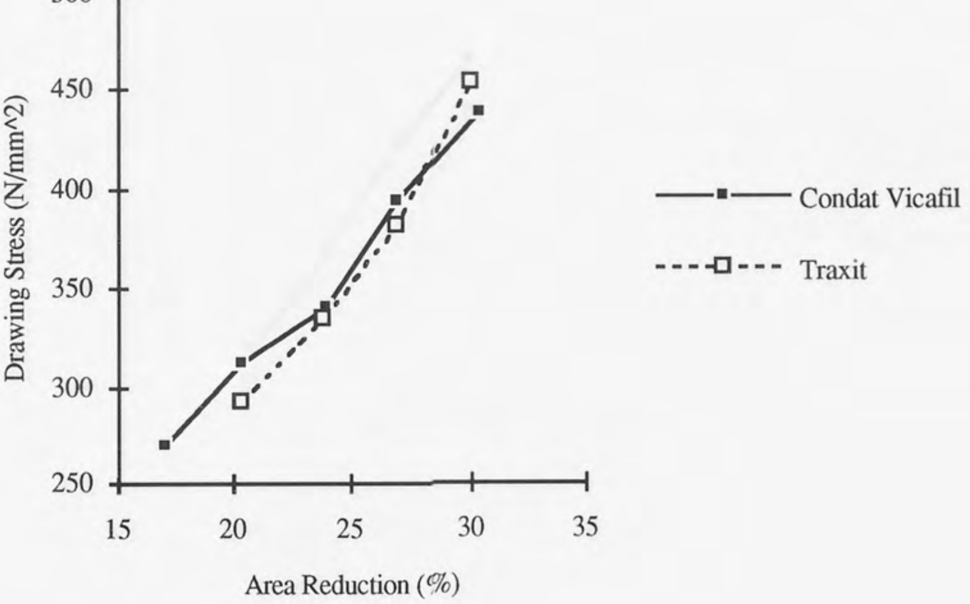

Fig. 48 Drawing stress vs percentage area reduction curves showing the effect of lubricant:
Nozzle semi-angle = 8 degree; Drawing speed = 47 m/min,
Medium carbon steel.

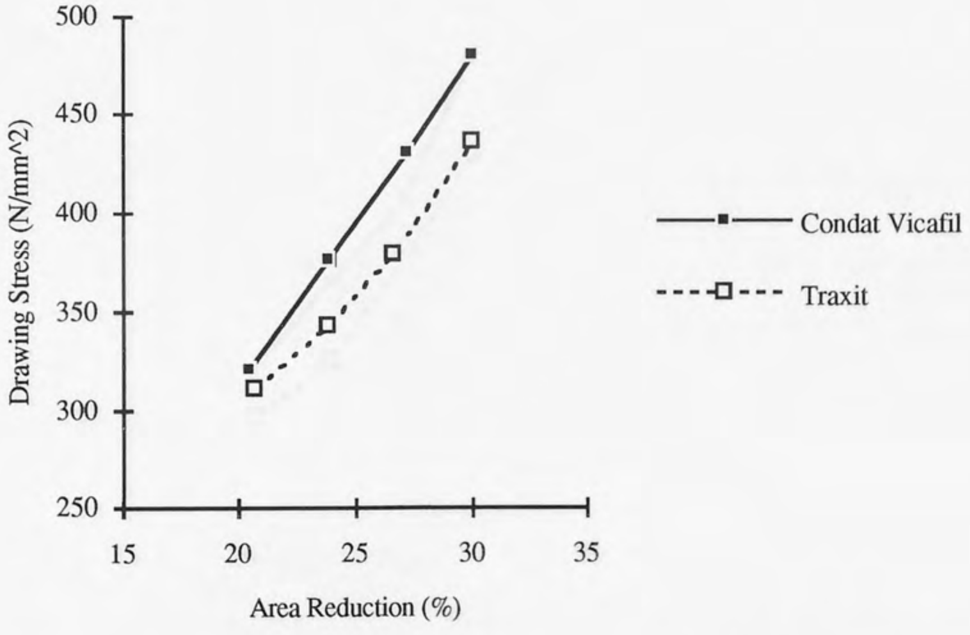

Fig. 49 Drawing stress vs percentage area reduction curves showing the effect of lubricant:
Nozzle semi-angle = 10 degree; Drawing speed = 27 m/min,
Medium carbon steel.

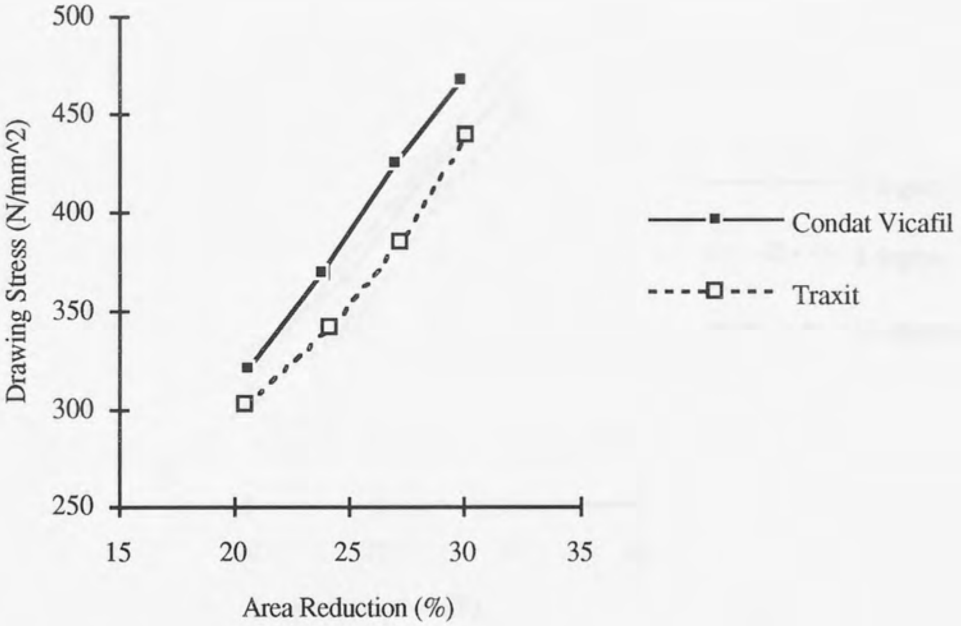

Fig. 50 Drawing stress vs percentage area reduction curves showing the effect of lubricant: Nozzle semi-angle = 10 degree; Drawing speed = 37 m/min, Medium carbon steel.

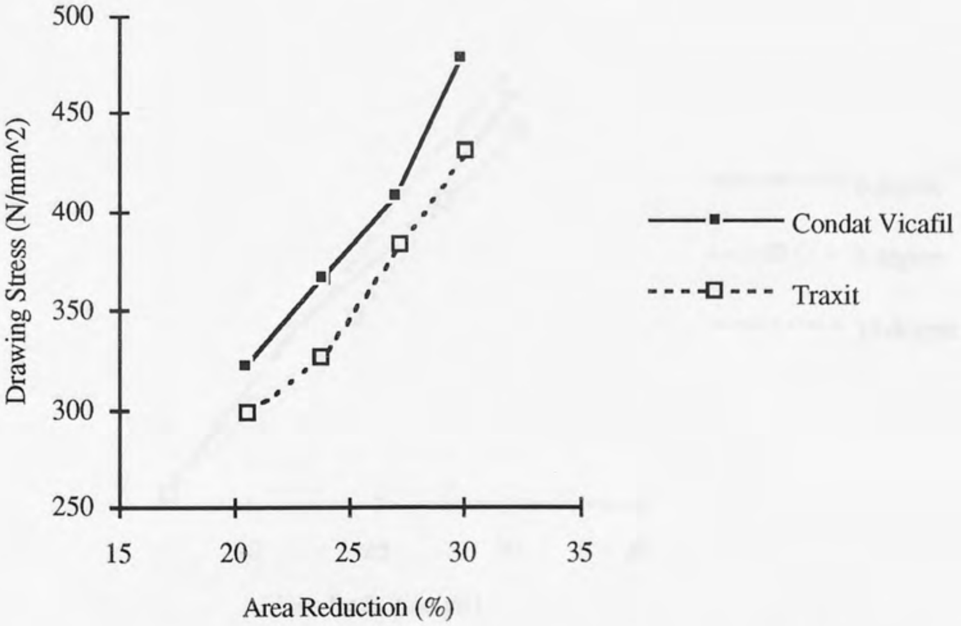

Fig. 51 Drawing stress vs percentage area reduction curves showing the effect of lubricant: Nozzle semi-angle = 10 degree; Drawing speed = 47 m/min, Medium carbon steel.

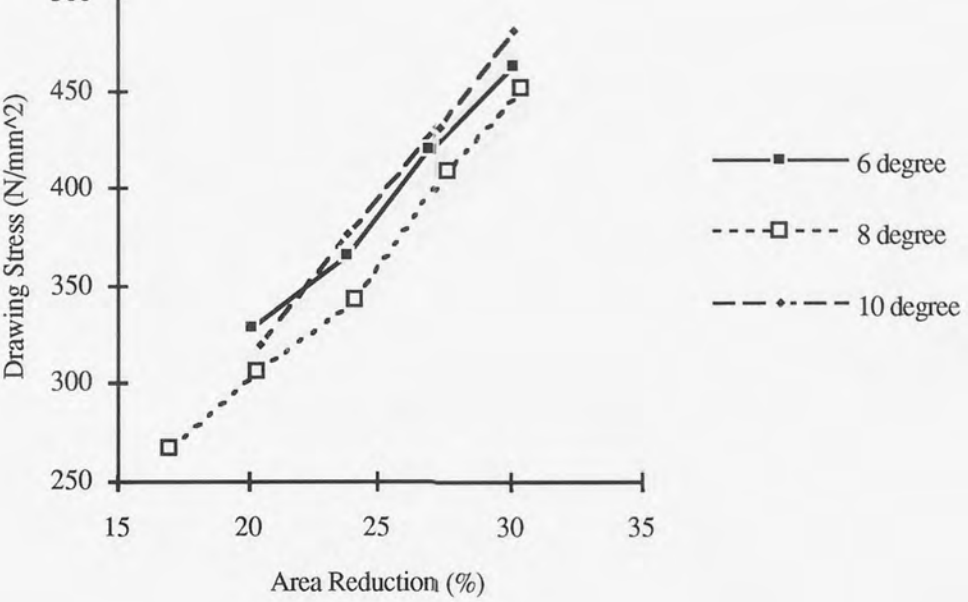

Fig. 52 Drawing stress vs percentage area reduction curves showing the effect of pressure nozzle semi-angle: Lubricant: Condat vicafil; Drawing speed = 27 m/min; Medium carbon steel.

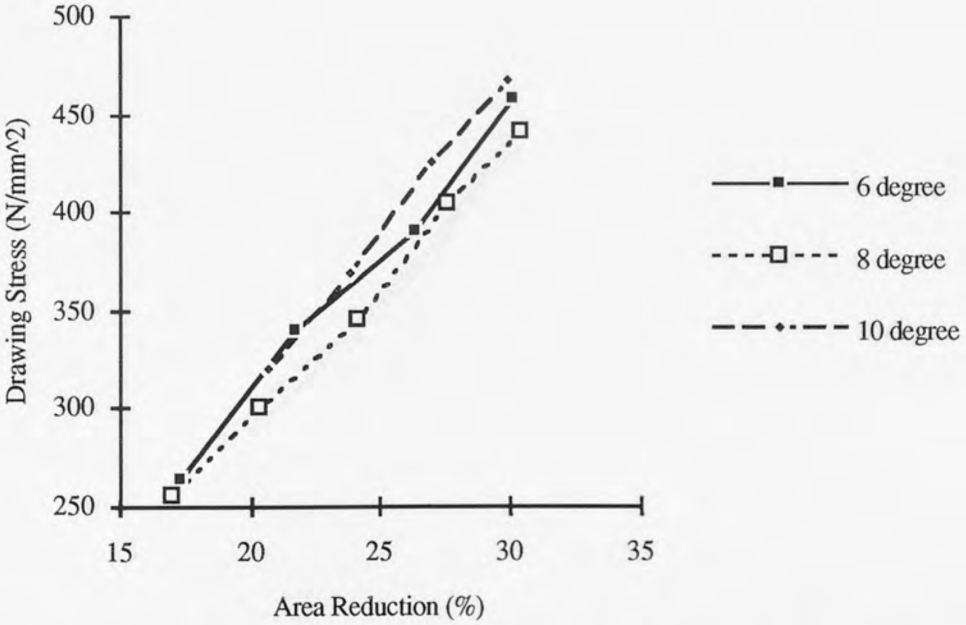

Fig. 53 Drawing stress vs percentage area reduction curves showing the effect of pressure nozzle semi-angle: Lubricant: Condat vicafil; Drawing speed = 37 m/min; Medium carbon steel.

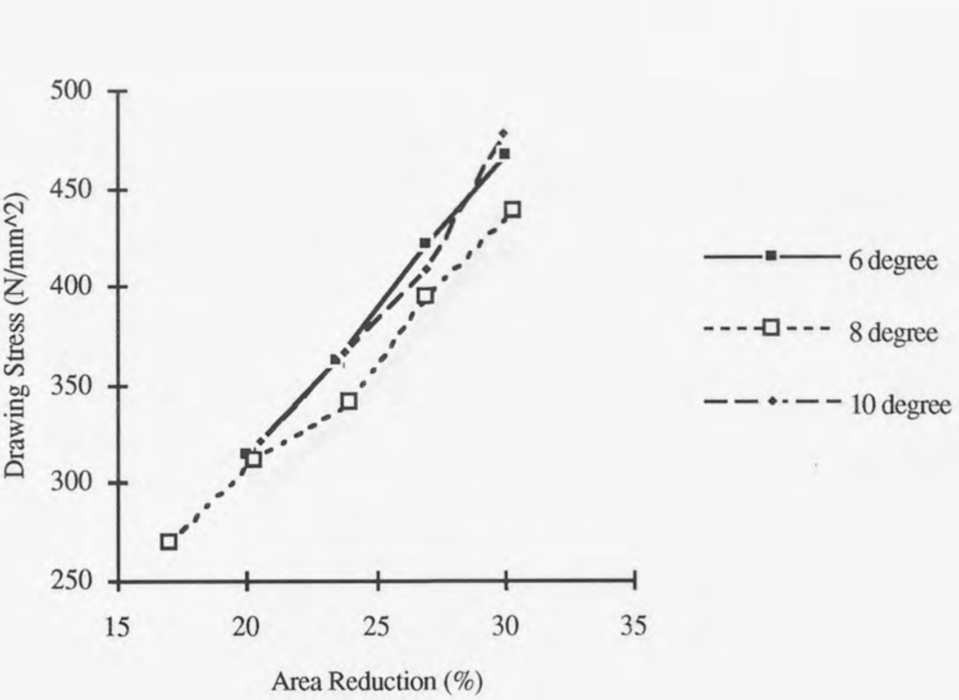

Fig. 54 Drawing stress vs percentage area reduction curves showing the effect of pressure nozzle semi-angle: Lubricant: Condat vicafil; Drawing speed = 47 m/min; Medium carbon steel.

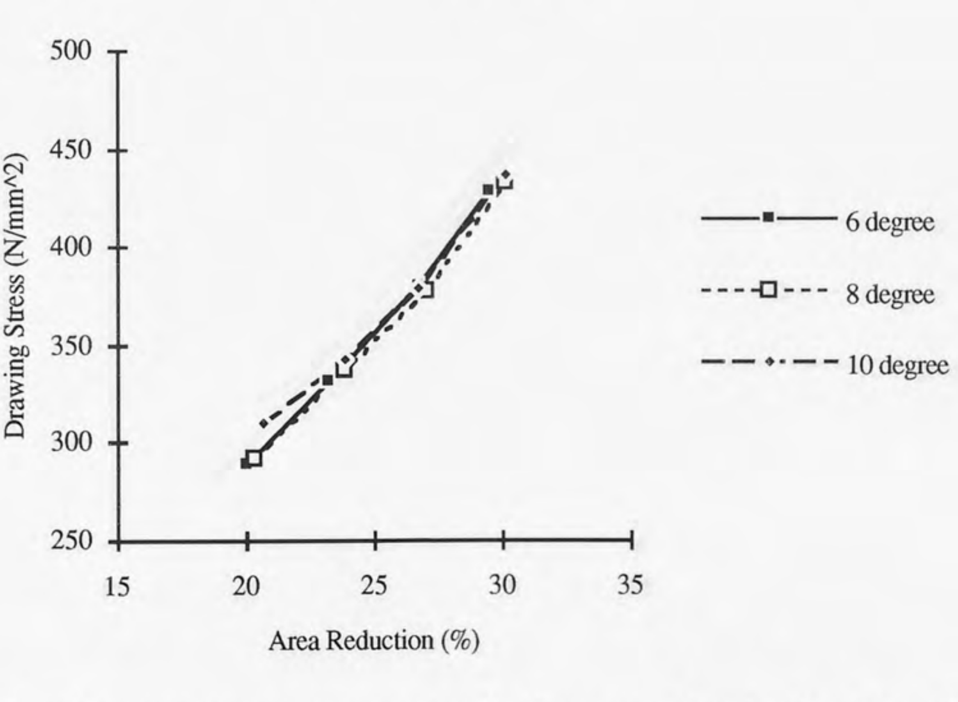

Fig. 55 Drawing stress vs percentage area reduction curves showing the effect of pressure nozzle semi-angle: Lubricant: Traxit; Drawing speed = 27 m/min; Medium carbon steel.

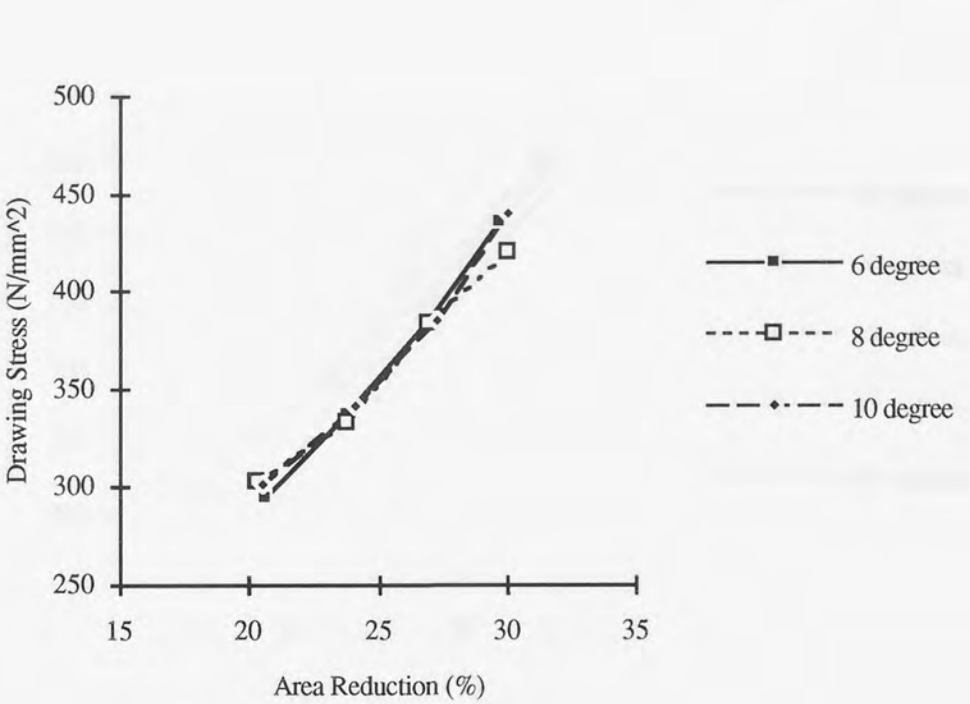

Fig. 56 Drawing stress vs percentage area reduction curves showing the effect of pressure nozzle semi-angle: Lubricant: Traxit; Drawing speed = 37 m/min; Medium carbon steel.

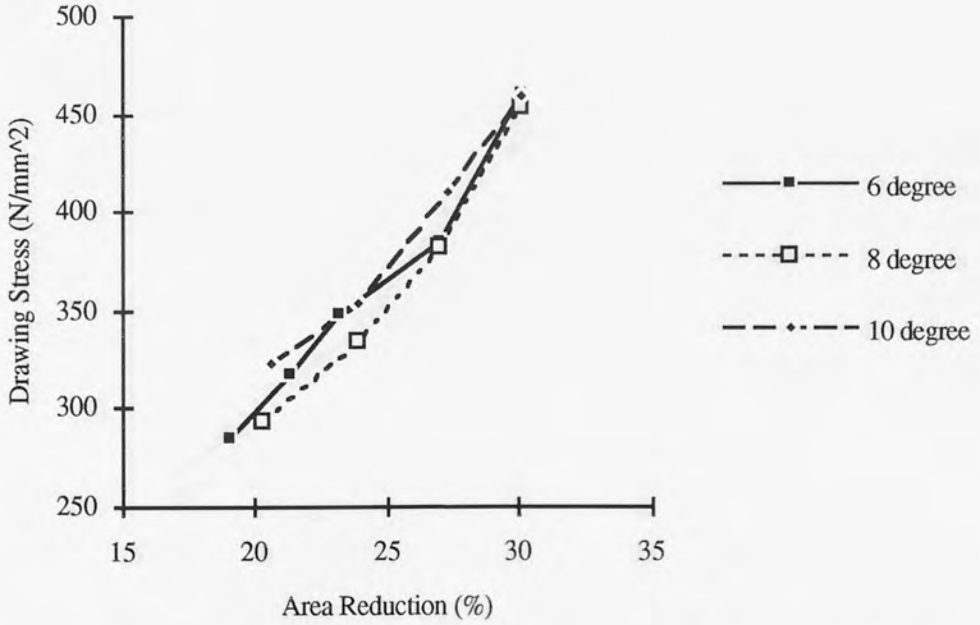

Fig. 57 Drawing stress vs percentage area reduction curves showing the effect of pressure nozzle semi-angle: Lubricant: Traxit; Drawing speed = 47 m/min; Medium carbon steel.

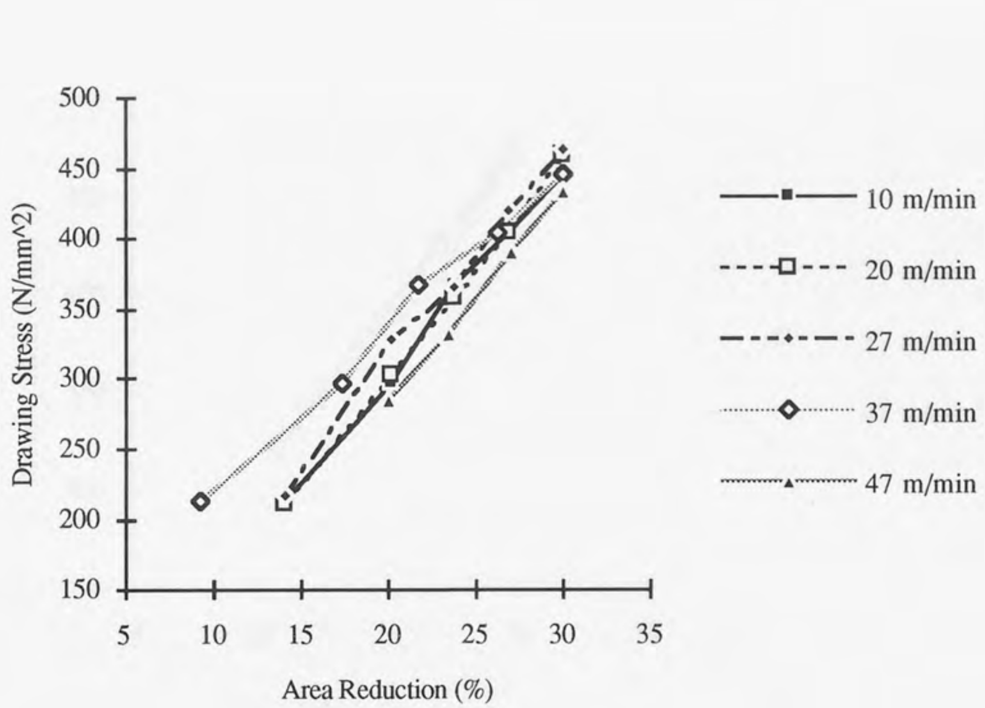

Fig. 58 Drawing stress vs percentage area reduction curves showing the effect of drawing speed: Nozzle semi-angle = 6 degree; Lubricant: Condat Vicafil; Medium Carbon Steel.

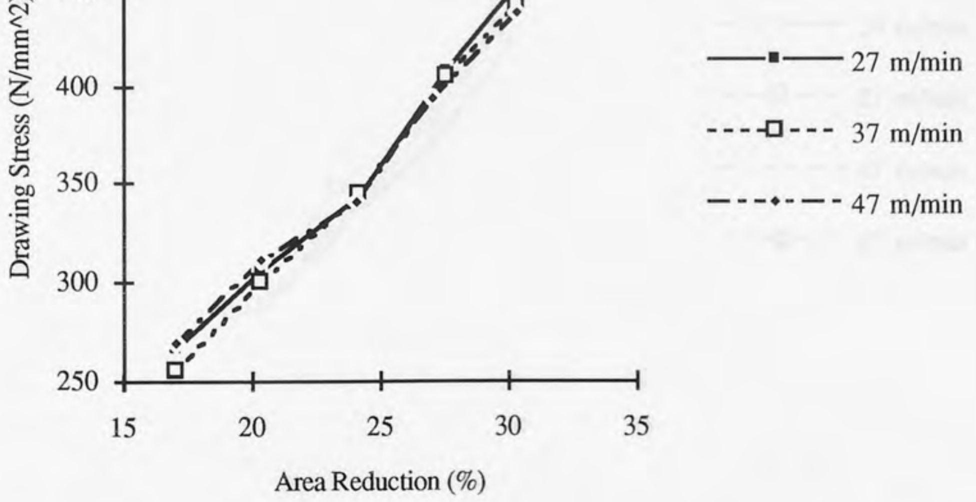

Fig. 59 Drawing stress vs percentage area reduction curves showing the effect of drawing speed: Nozzle semi-angle = 8 degree; Lubricant: Condat Vicafil; Medium Carbon Steel.

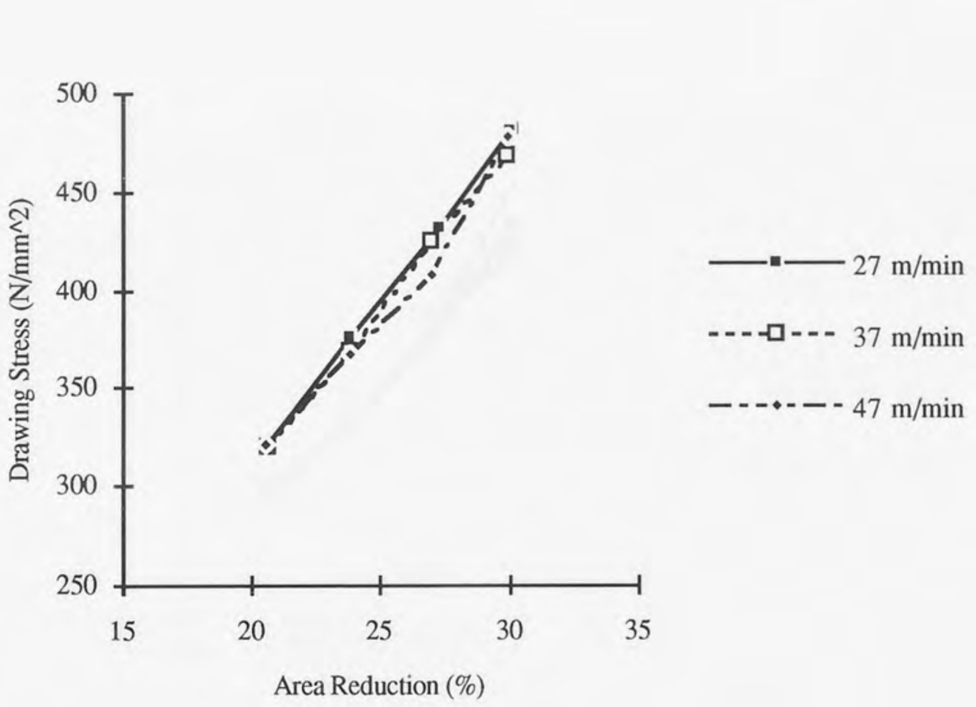

Fig. 60 Drawing stress vs percentage area reduction curves showing the effect of drawing speed: Nozzle semi-angle = 10 degree; Lubricant: Condat Vicafil; Medium Carbon Steel.

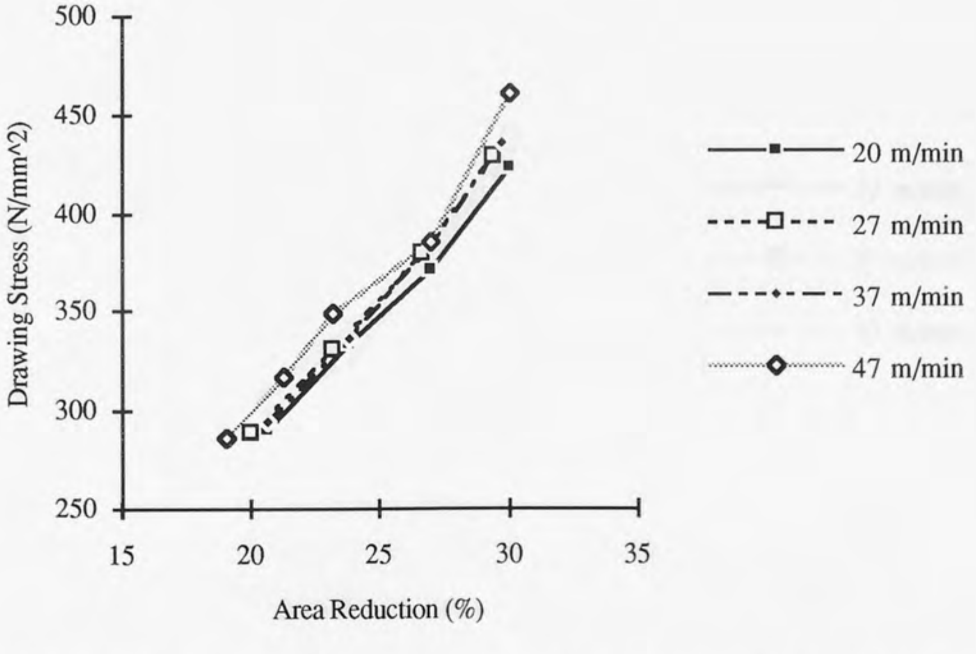

Fig. 61 Drawing stress vs percentage area reduction curves showing the effect of drawing speed: Nozzle semi-angle = 6 degree; Lubricant: Traxit; Medium Carbon Steel.

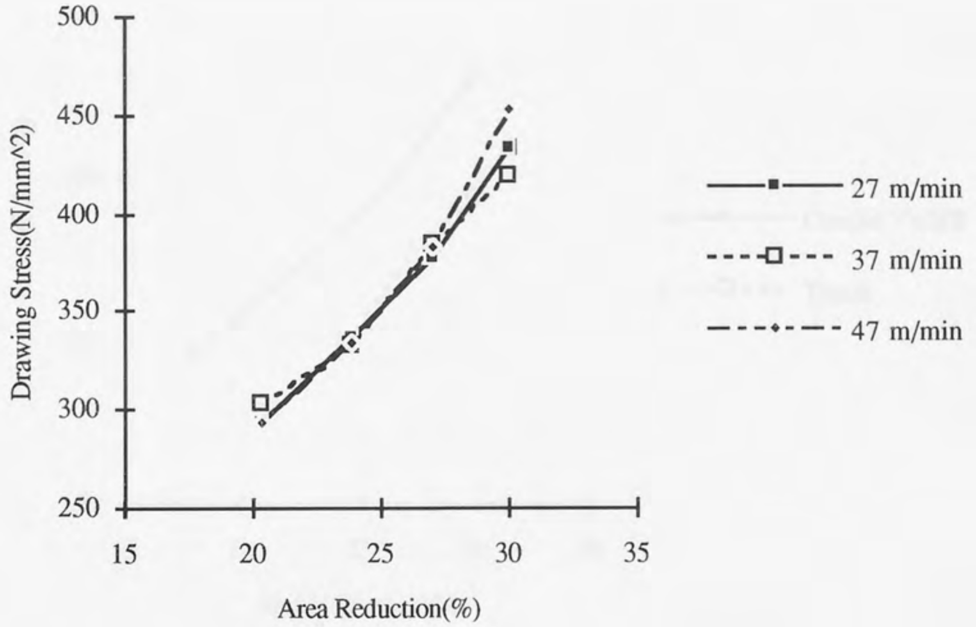

Fig. 62 Drawing stress vs percentage area reduction curves showing the effect of drawing speed: Nozzle semi-angle = 8 degree; Lubricant: Traxit; Medium Carbon Steel.

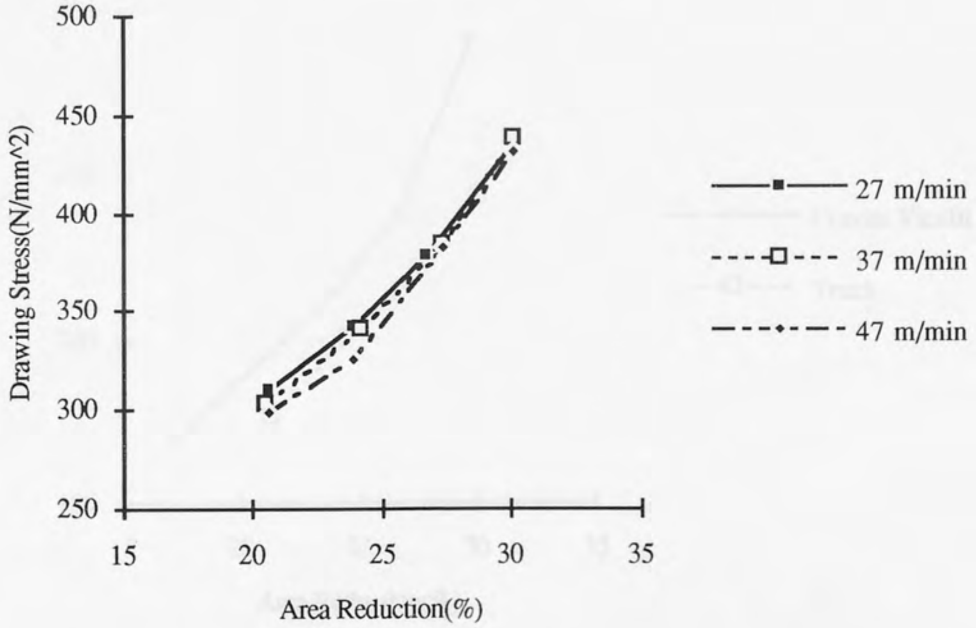

Fig. 63 Drawing stress vs percentage area reduction curves showing the effect of drawing speed: Nozzle semi-angle = 10 degree; Lubricant: Traxit; Medium carbon steel.

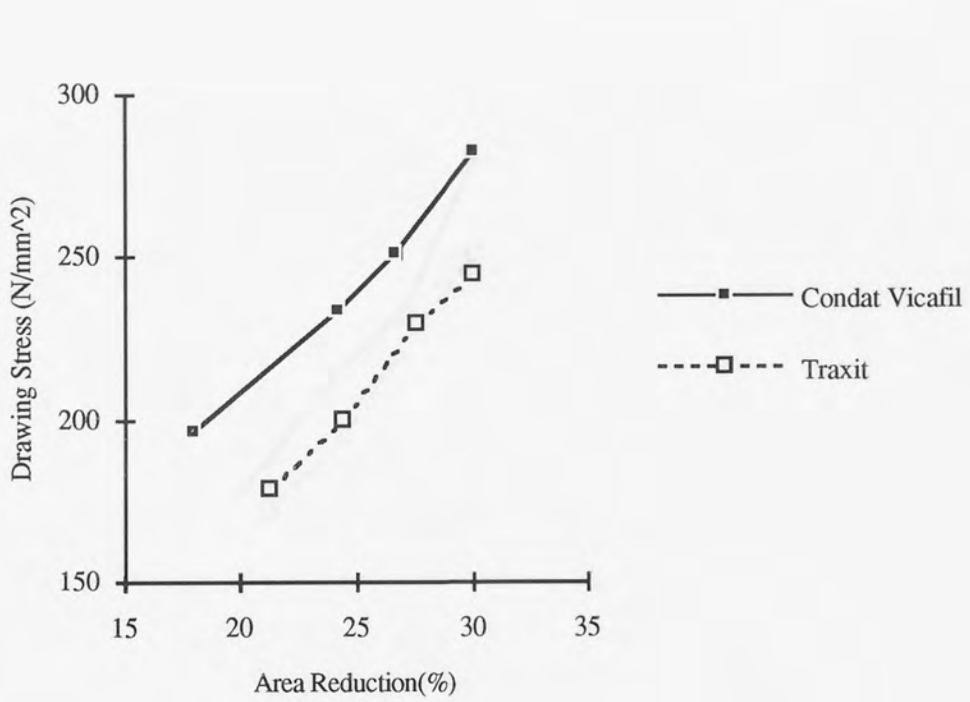

Fig. 64 Drawing stress vs percentage area reduction curves showing the effect of lubricant:
Nozzle semi-angle = 6 degree; Drawing speed = 27 m/min;
Low carbon steel.

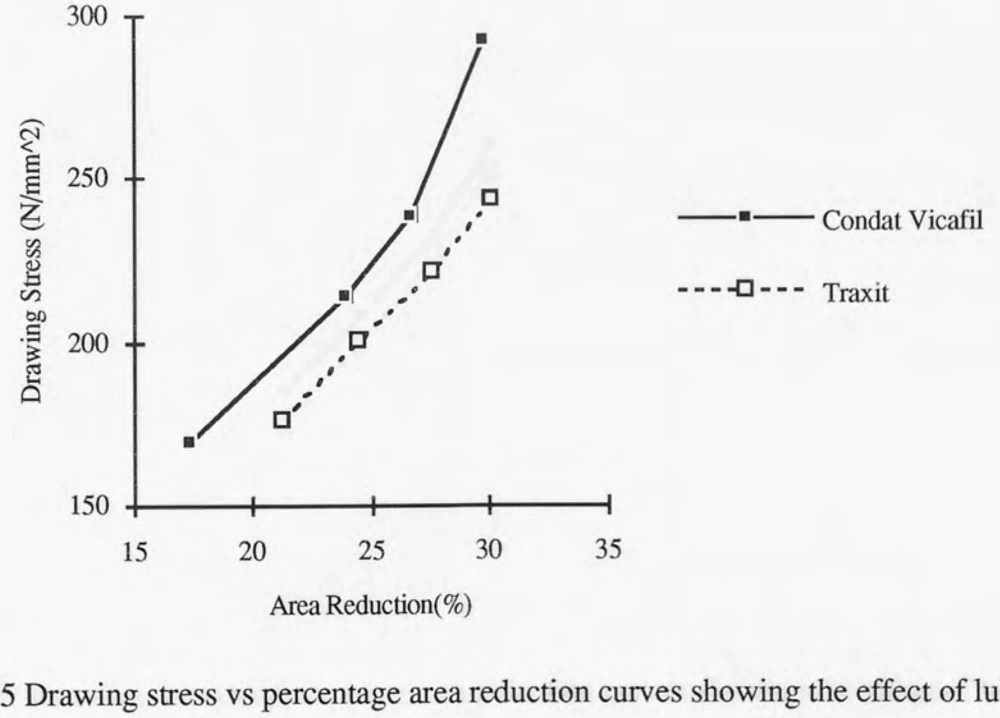

Fig. 65 Drawing stress vs percentage area reduction curves showing the effect of lubricant:
Nozzle semi-angle = 6 degree; Drawing speed = 37 m/min;
Low carbon steel.

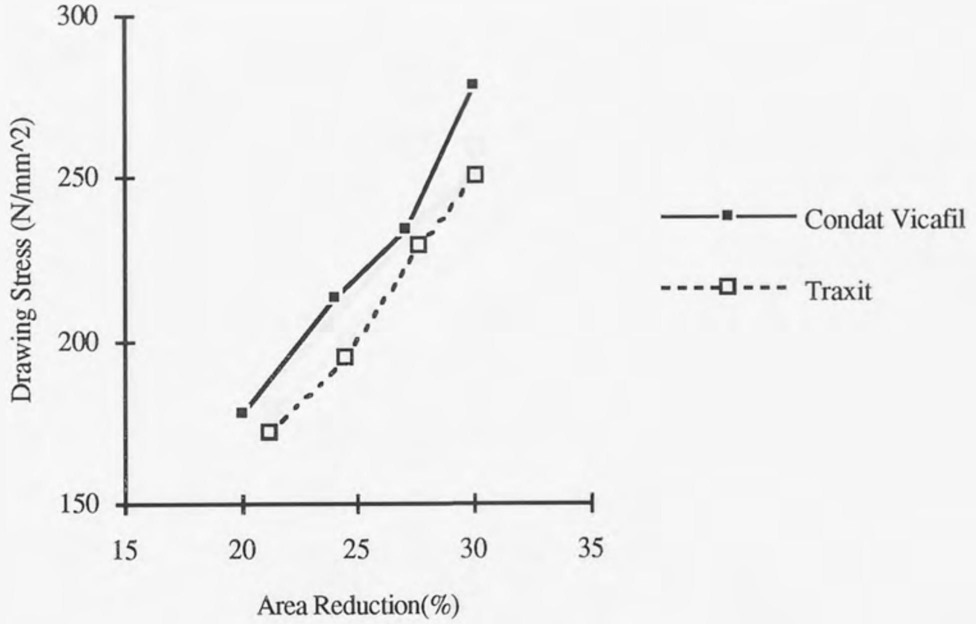

Fig. 66 Drawing stress vs percentage area reduction curves showing the effect of lubricant: Nozzle semi-angle = 6 degree; Drawing speed = 47 m/min; Low carbon steel.

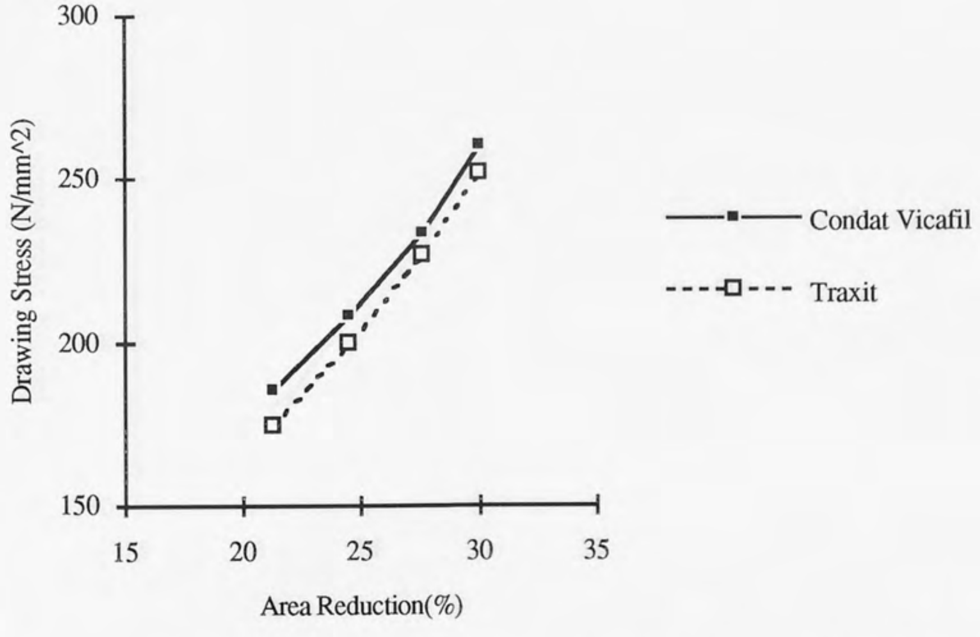

Fig. 67 Drawing stress vs percentage area reduction curves showing the effect of lubricant: Nozzle semi-angle = 8 degree; Drawing speed = 27 m/min; Low carbon steel.

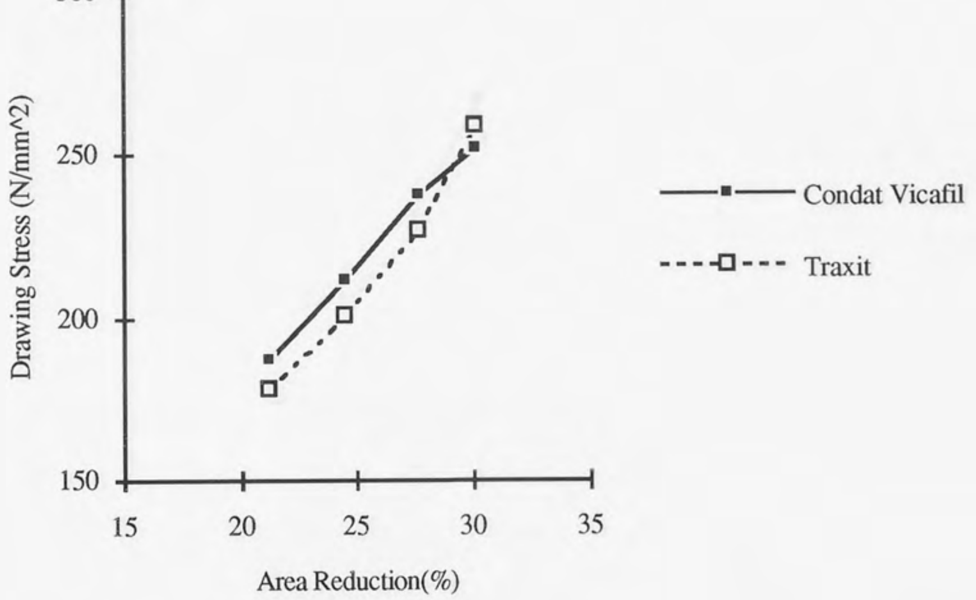

Fig. 68 Drawing stress vs percentage area reduction curves showing the effect of lubricant:
Nozzle semi-angle = 8 degree; Drawing speed = 37 m/min;
Low carbon steel.

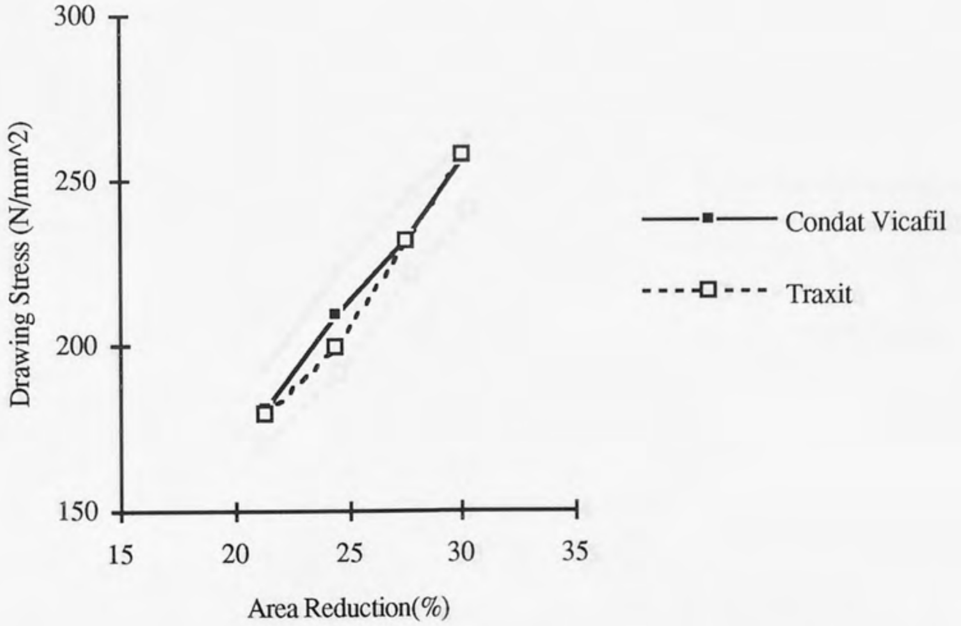

Fig. 69 Drawing stress vs percentage area reduction curves showing the effect of lubricant:
Nozzle semi-angle = 8 degree; Drawing speed = 47 m/min;
Low carbon steel.

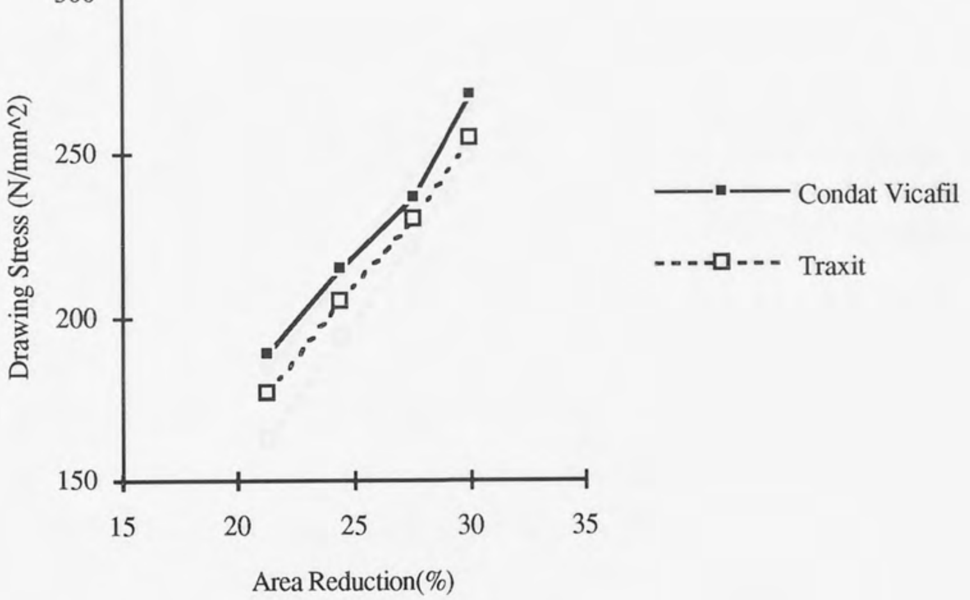

Fig. 70 Drawing stress vs percentage area reduction curves showing the effect of lubricant:
Nozzle semi-angle = 10 degree; Drawing speed = 27 m/min;
Low carbon steel.

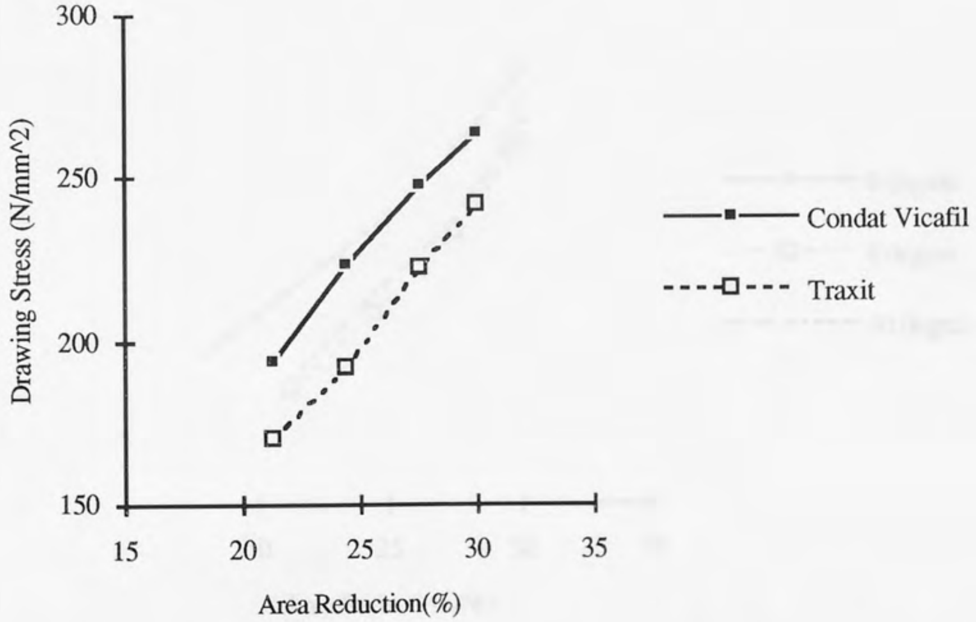

Fig. 71 Drawing stress vs percentage area reduction curves showing the effect of lubricant:
Nozzle semi-angle = 10 degree; Drawing speed = 37 m/min;
Low carbon steel.

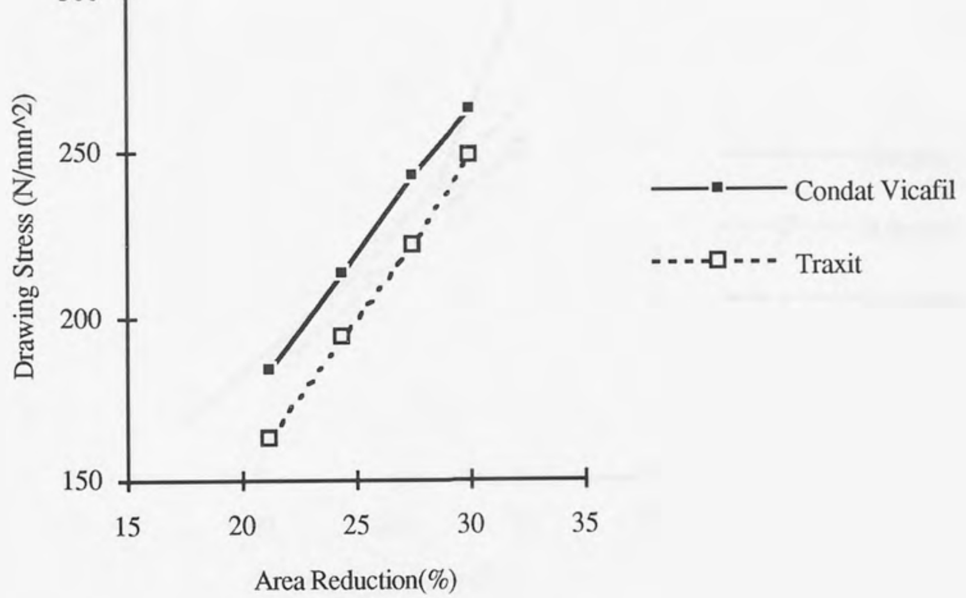

Fig. 72 Drawing stress vs percentage area reduction curves showing the effect of lubricant: Nozzle semi-angle = 10 degree; Drawing speed = 47 m/min; Low carbon steel.

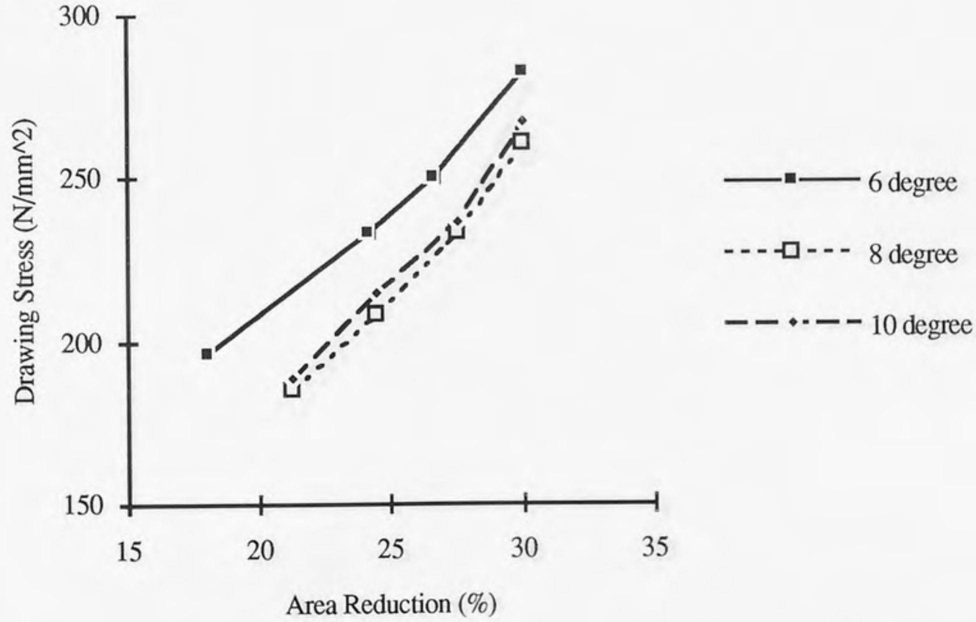

Fig. 73 Drawing stress vs percentage area reduction curves showing the effect of pressure nozzle semi-angle: Lubricant: Condat Vicafil; Drawing speed = 27 m/min; Low carbon steel.

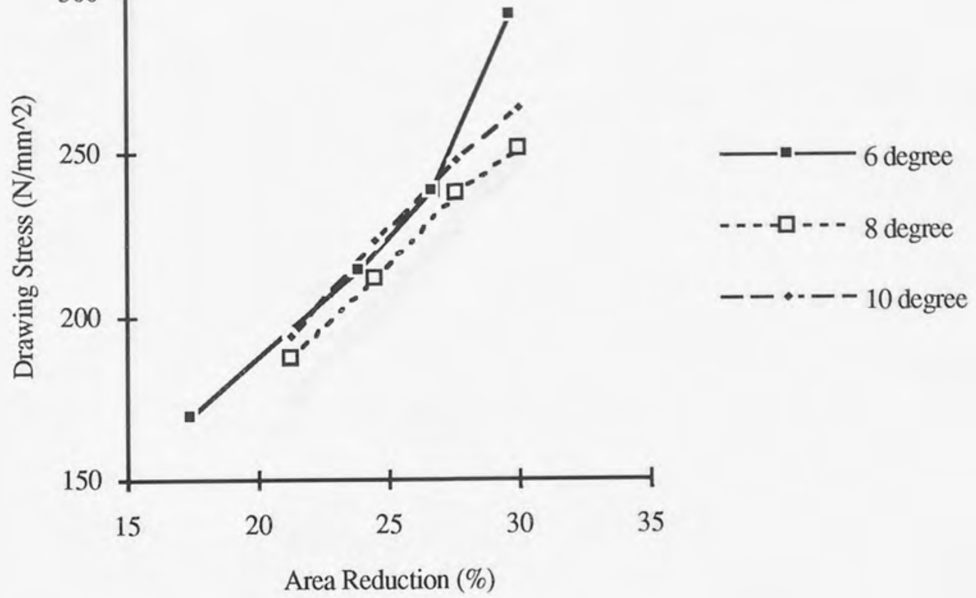

Fig. 74 Drawing stress vs percentage area reduction curves showing the effect of pressure nozzle semi-angle: Lubricant: Condat Vicafil; Drawing speed = 37 m/min; Low carbon steel.

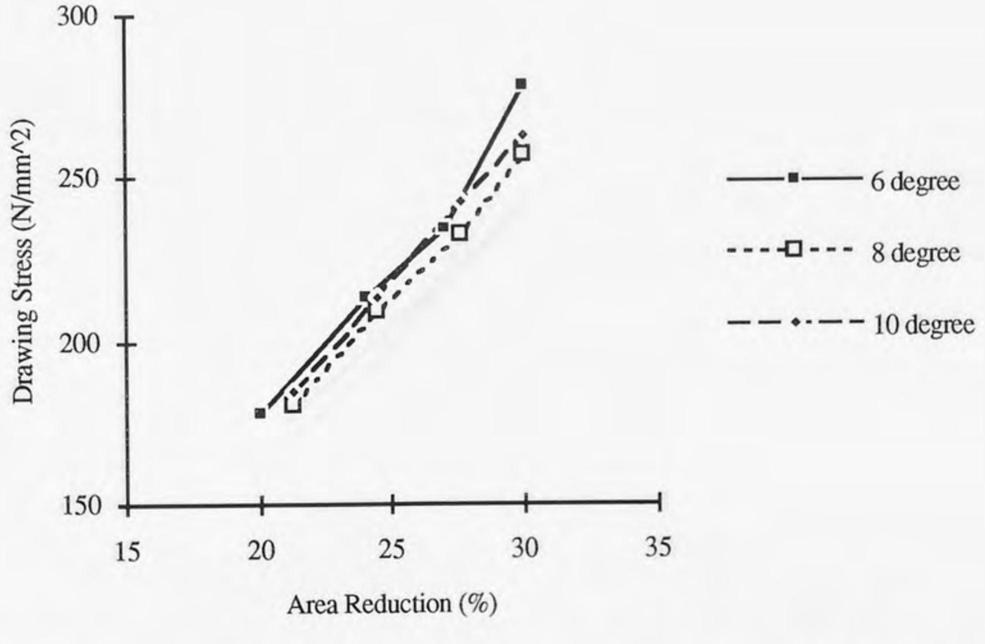

Fig. 75 Drawing stress vs percentage area reduction curves showing the effect of pressure nozzle semi-angle: Lubricant: Condat Vicafil; Drawing speed = 47 m/min; Low carbon steel.

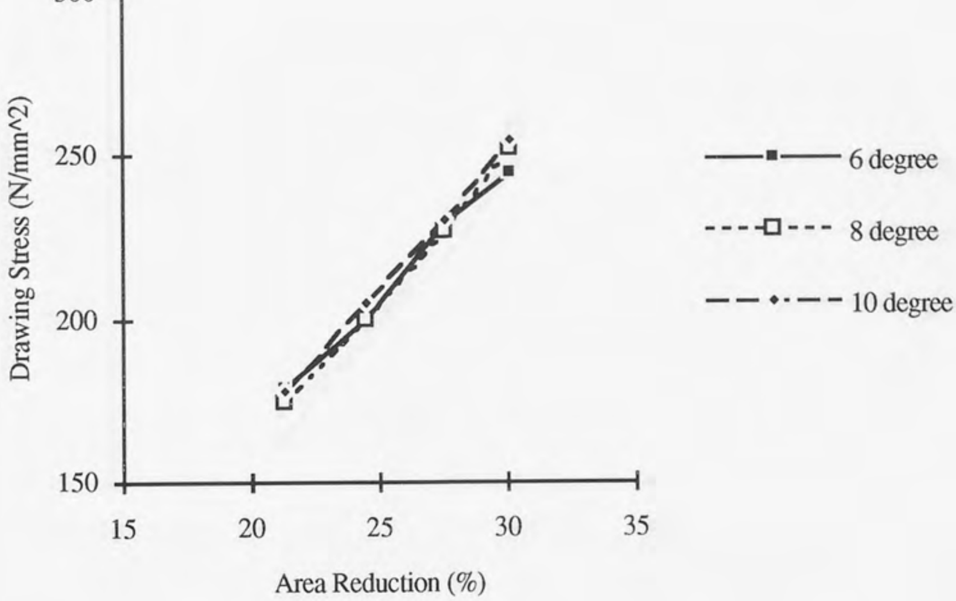

Fig. 76 Drawing stress vs percentage area reduction curves showing the effect of pressure nozzle semi-angle: Lubricant: Traxit; Drawing speed = 27 m/min; Low carbon steel.

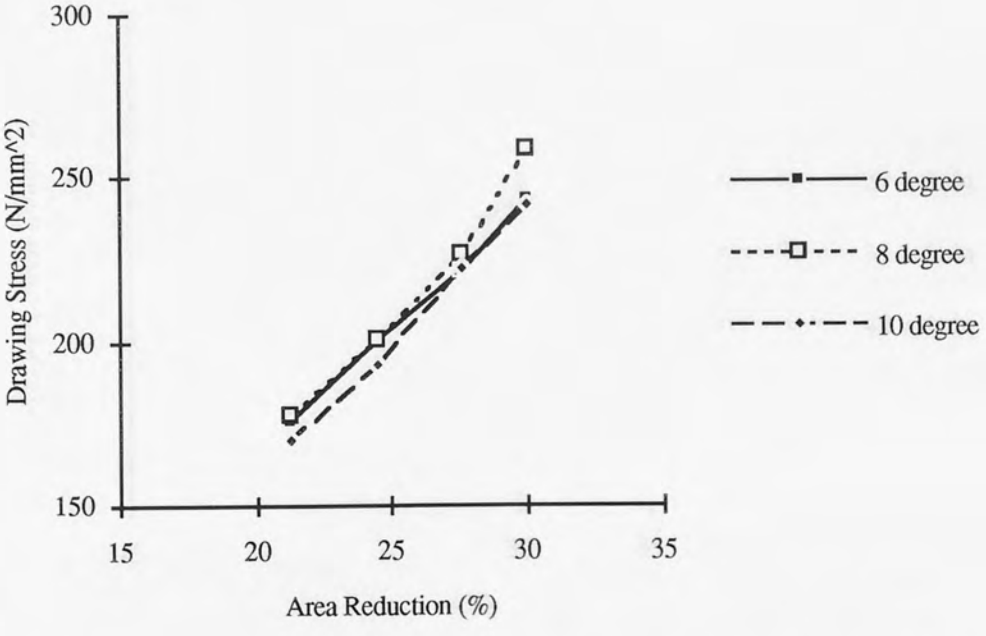

Fig. 77 Drawing stress vs percentage area reduction curves showing the effect of pressure nozzle semi-angle: Lubricant: Traxit; Drawing speed = 37 m/min; Low carbon steel.

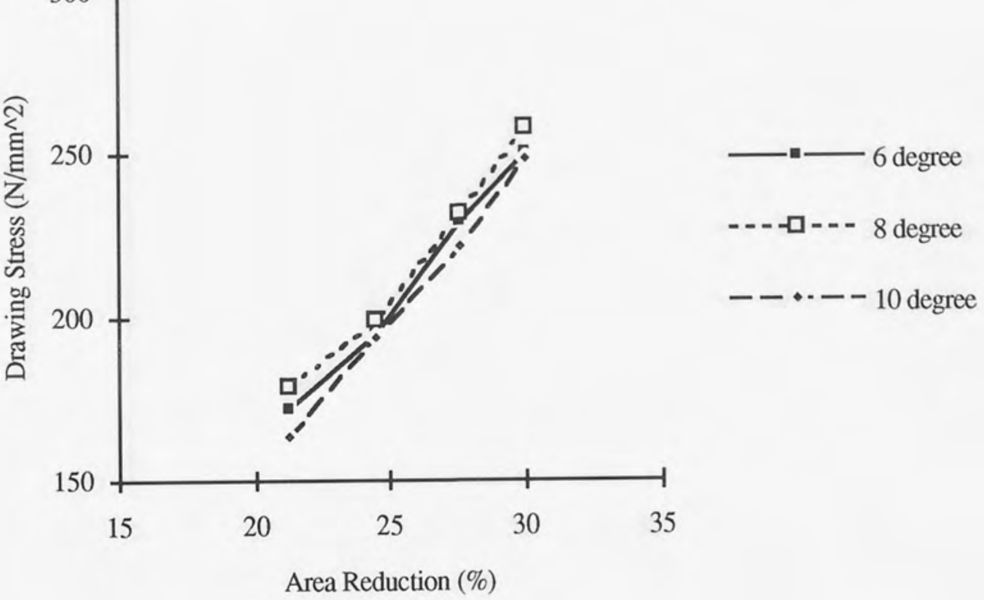

Fig. 78 Drawing stress vs percentage area reduction curves showing the effect of pressure nozzle semi-angle: Lubricant: Traxit; Drawing speed = 47 m/min; Low carbon steel.

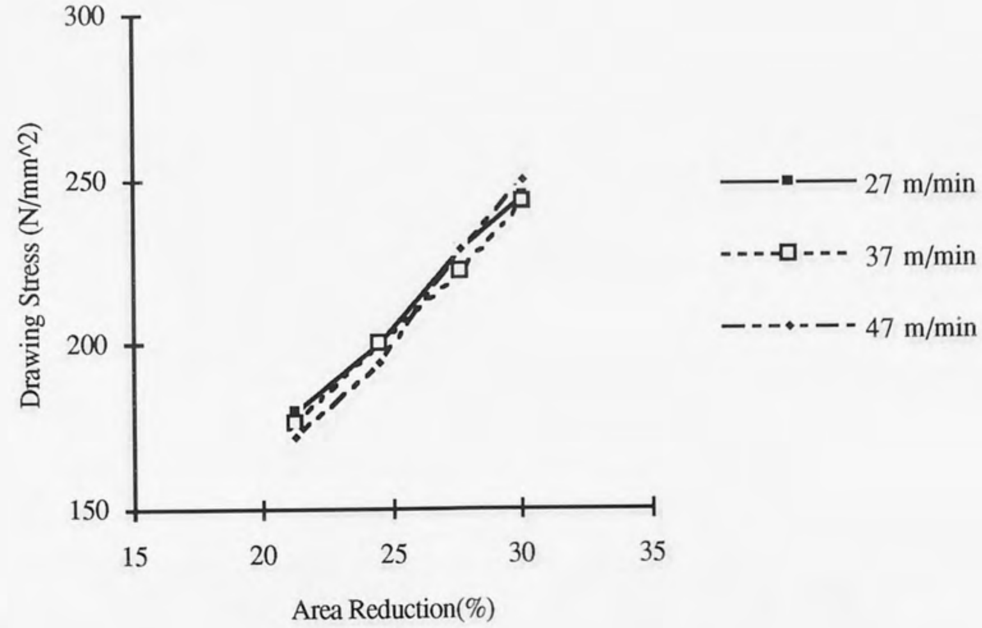

Fig. 79 Drawing stress vs percentage area reduction curves showing the effect of drawing speed: Nozzle semi-angle = 6 degree; Lubricant: Traxit; Low Carbon Steel.

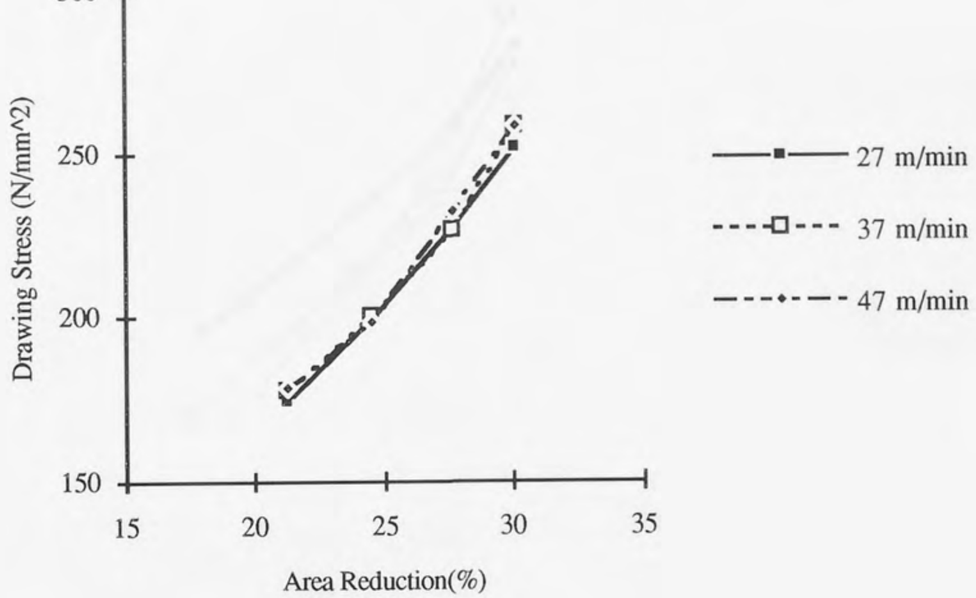

Fig. 80 Drawing stress vs percentage area reduction curves showing the effect of drawing speed: Nozzle semi-angle = 8 degree; Lubricant: Traxit; Low Carbon Steel.

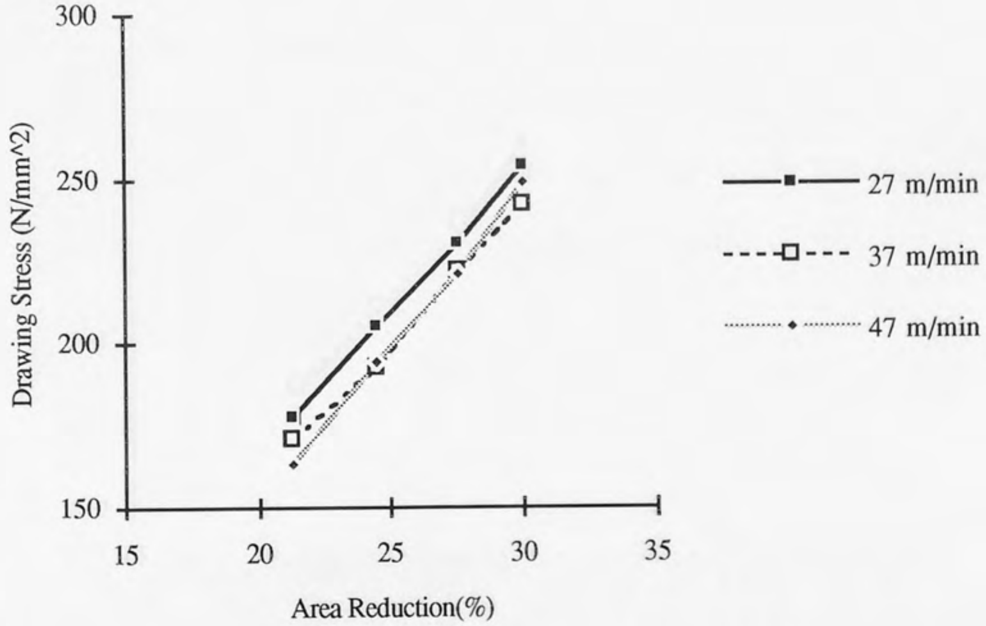

Fig. 81 Drawing stress vs percentage area reduction curves showing the effect of drawing speed: Nozzle semi-angle = 10 degree; Lubricant: Traxit; Low Carbon Steel.

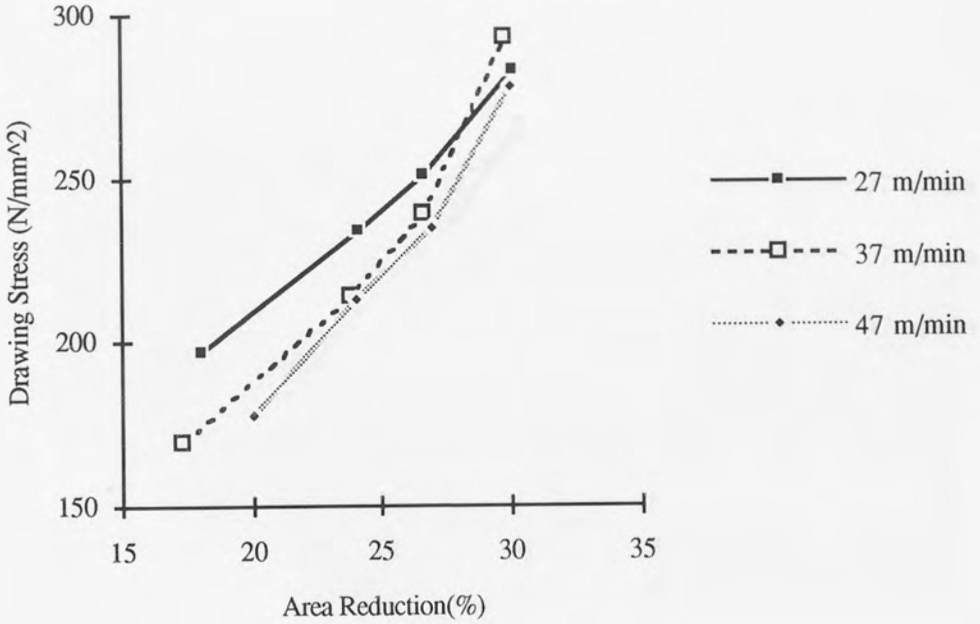

Fig. 82 Drawing stress vs percentage area reduction curves showing the effect of drawing speed: Nozzle semi-angle = 6 degree; Lubricant: Condat Vicafil; Low Carbon Steel.

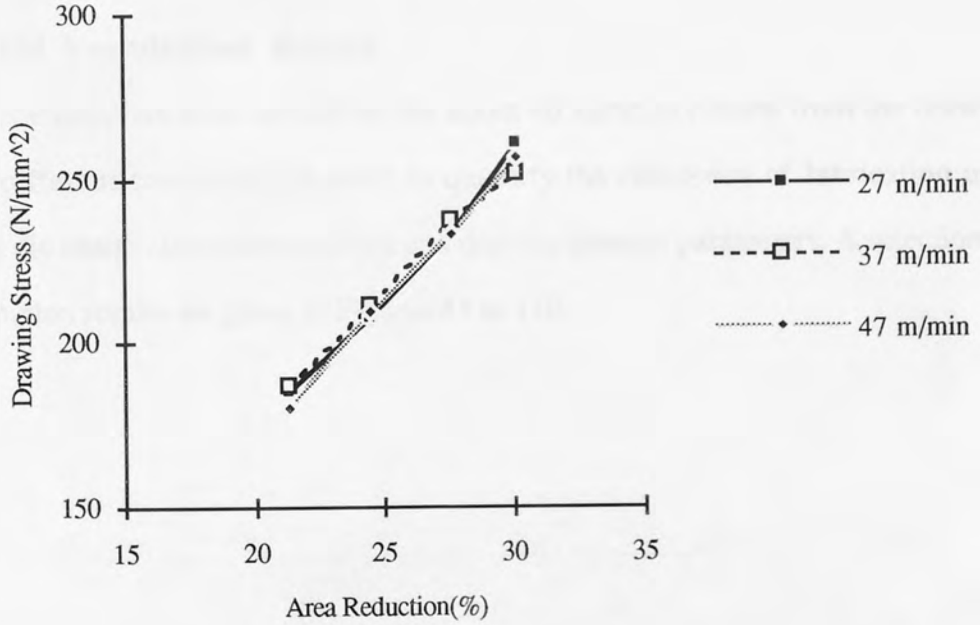

Fig. 83 Drawing stress vs percentage area reduction curves showing the effect of drawing speed: Nozzle semi-angle = 8 degree; Lubricant: Condat Vicafil; Low Carbon Steel.

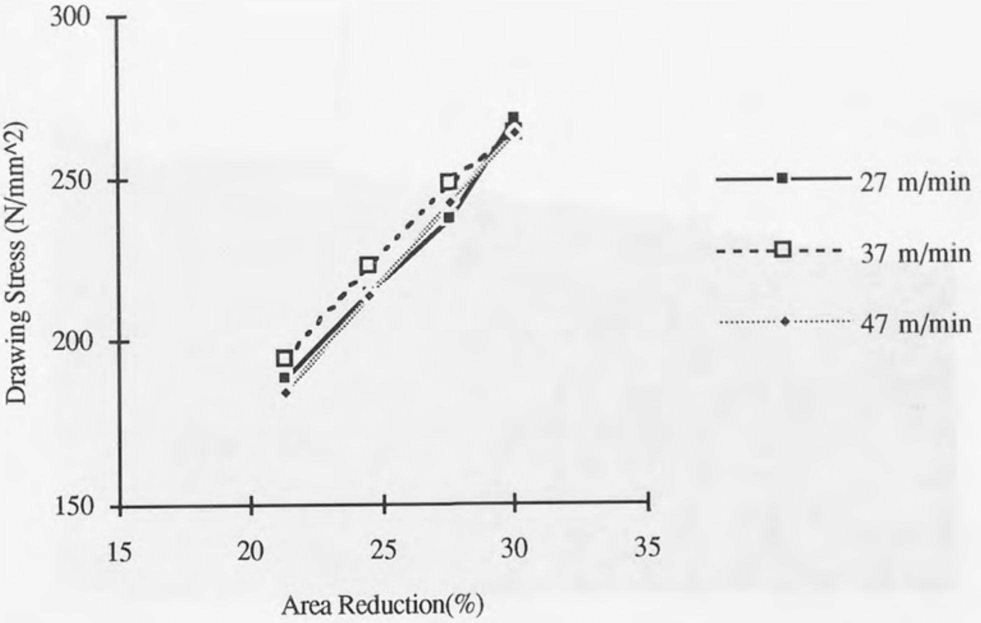

Fig. 84 Drawing stress vs percentage area reduction curves showing the effect of drawing speed: Nozzle semi-angle = 10 degree; Lubricant: Condat Vicafil; Low Carbon Steel.

6.3 SEM Examination Results

SEM examinations were carried out for about 40 samples chosen from the drawing tests under different conditions, in order to quantify the efficiency of lubrication under the current die design, lubricant selection and drawing process parameters. A selection of SEM examination results are given in Figures 85 to 110.

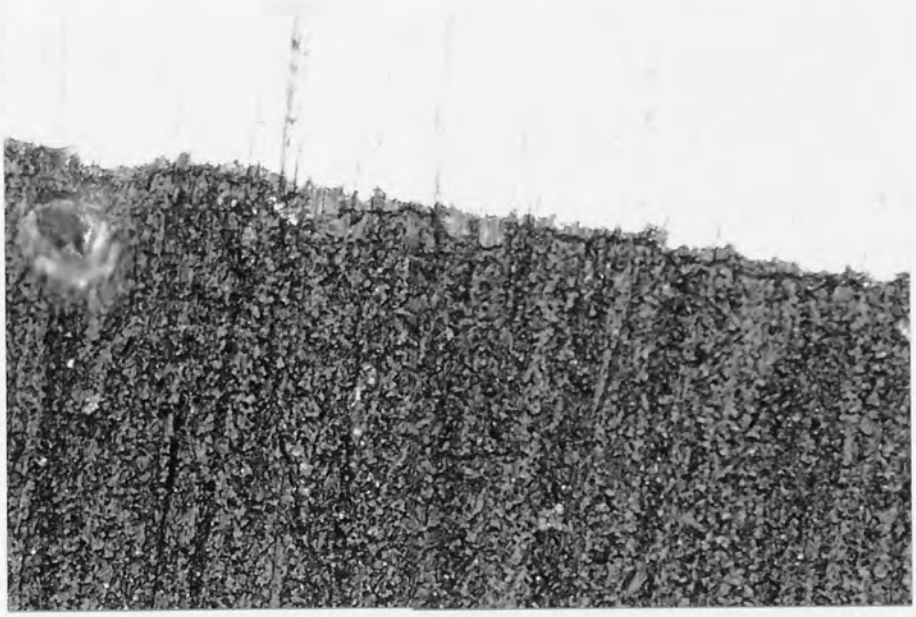

(a) Optical microscope image of an undrawn wire surface (500x)

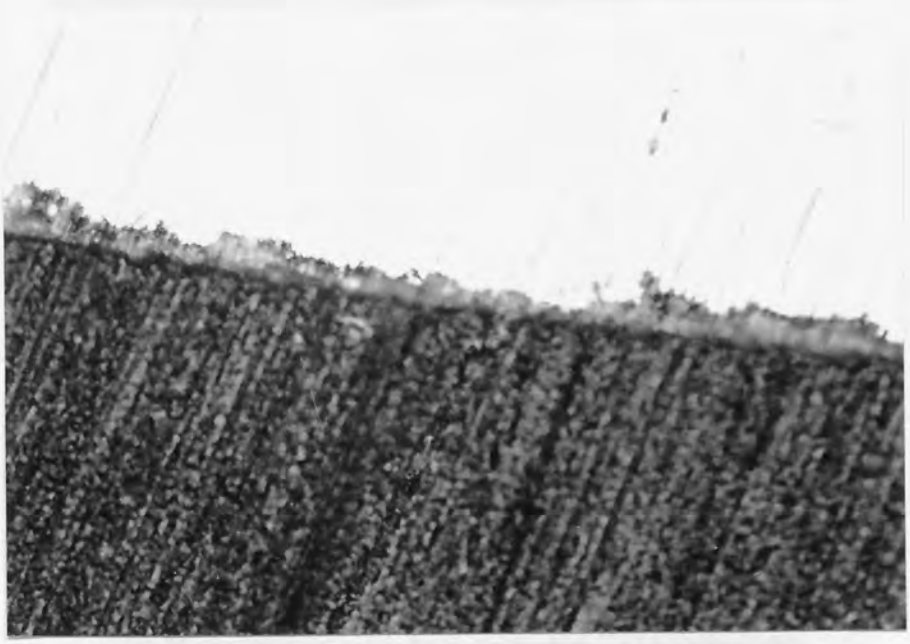

(b) Optical microscope image of a drawn wire surface (500x)

Fig. 85 Typical optical microscope images of wire surface examination for undrawn (a) and drawn (b) wires.

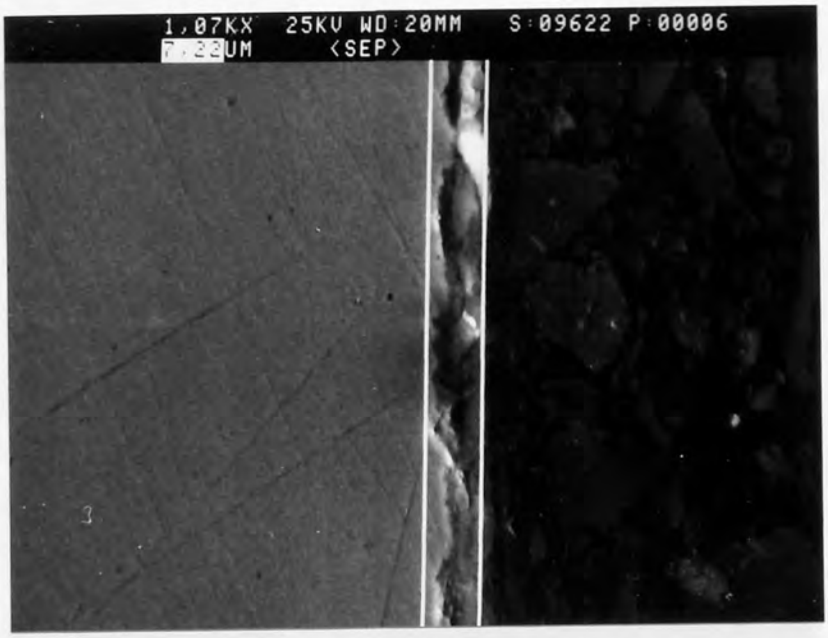

(a) Measurement under normal SEM operation mode:
Pressure nozzle semi-angle = 8 degree; Drawing speed = 47 m/min;
Area reduction = 30%; Lubricant: Traxit;
Medium carbon steel; Residual lubricant thickness = 7.2 μm.

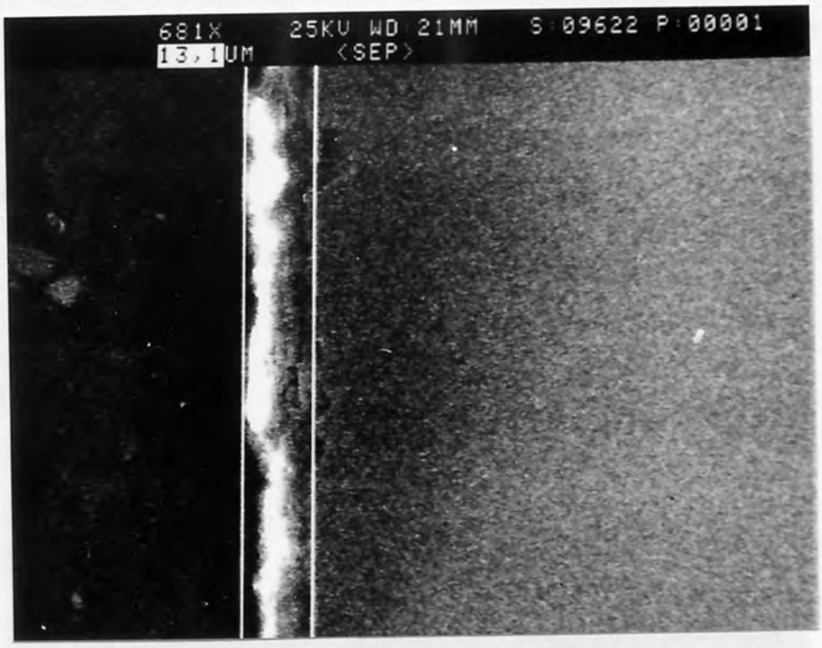

(b) Measurement with back scattered SEM technique:
Pressure nozzle semi-angle = 6 degree; Drawing speed = 30 m/min;
Area reduction = 27%; Lubricant: Condat Vicafil;
low carbon steel; Residual lubricant thickness = 13.1 μm.

Fig. 86 Measurement of residual lubricant layer using SEM.

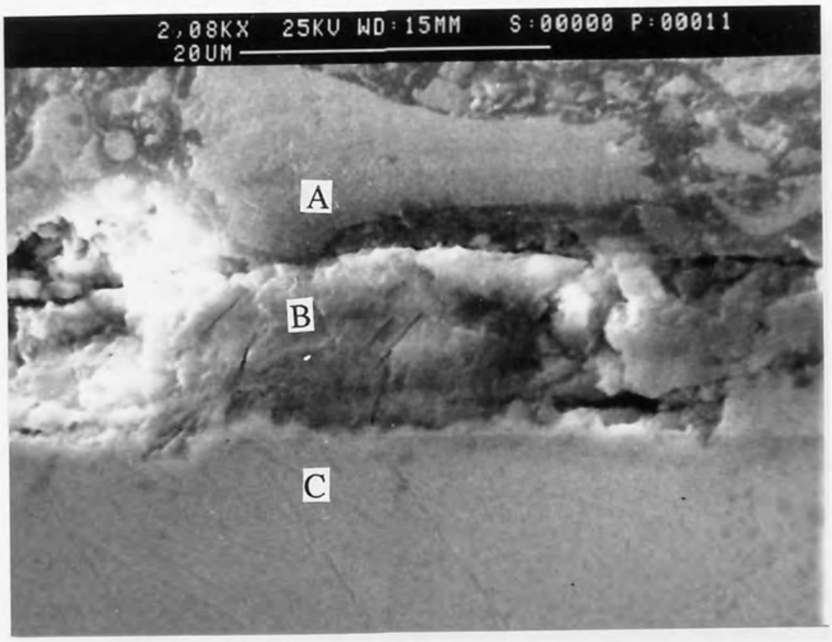

A - Mounting material; B - Residual lubricant layer and C - Wire.

Fig. 87 Typical SEM image of residual lubricant layer on a drawn wire: Pressure nozzle semi-angle = 10 degrees; Drawing speed = 37 m/min; Area reduction = 27%; Medium carbon steel; Lubricant: Traxit; Residual lubricant thickness = 11.0 µm.

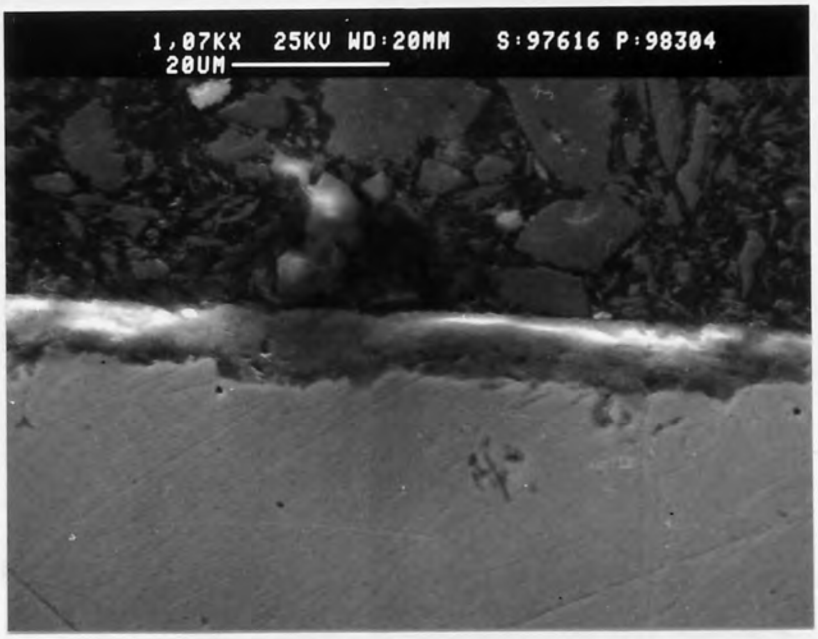

Fig. 88 SEM image of residual lubricant layer: Pressure nozzle semi-angle = 8 degrees; Drawing speed = 47 m/min; Area reduction = 30%; Lubricant: Traxit; Medium carbon steel; Residual lubricant thickness = 8.5 µm.

Fig. 89 SEM image of residual lubricant layer: Pressure nozzle semi-angle = 10 degrees; Drawing speed = 47 m/min; Area reduction = 30%; Lubricant: Traxit; Medium carbon steel; Residual lubricant thickness = 10.0 μm.

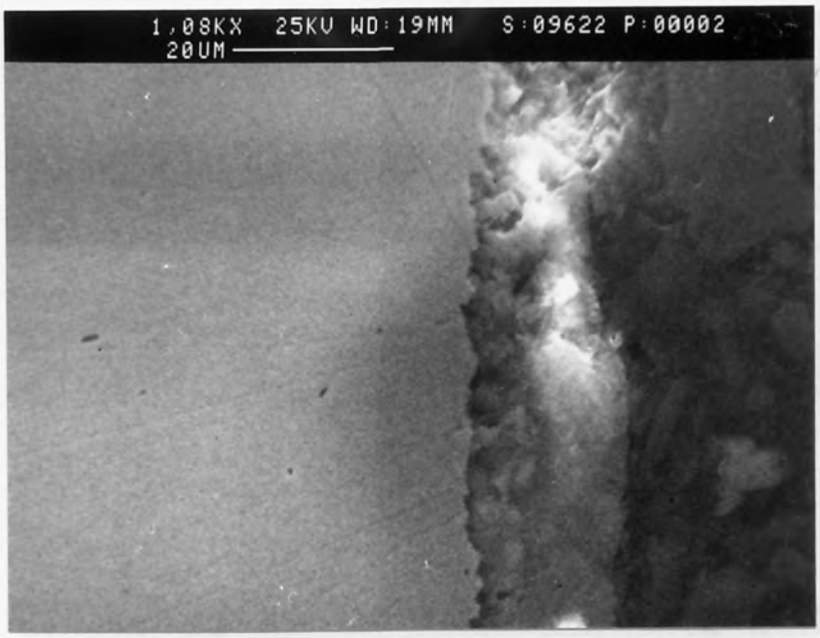

Fig. 90 SEM image of residual lubricant layer: Pressure nozzle semi-angle = 6 degrees; Drawing speed = 47 m/min; Area reduction = 21%; Lubricant: Traxit; Medium carbon steel; Residual lubricant thickness = 18.5 μm.

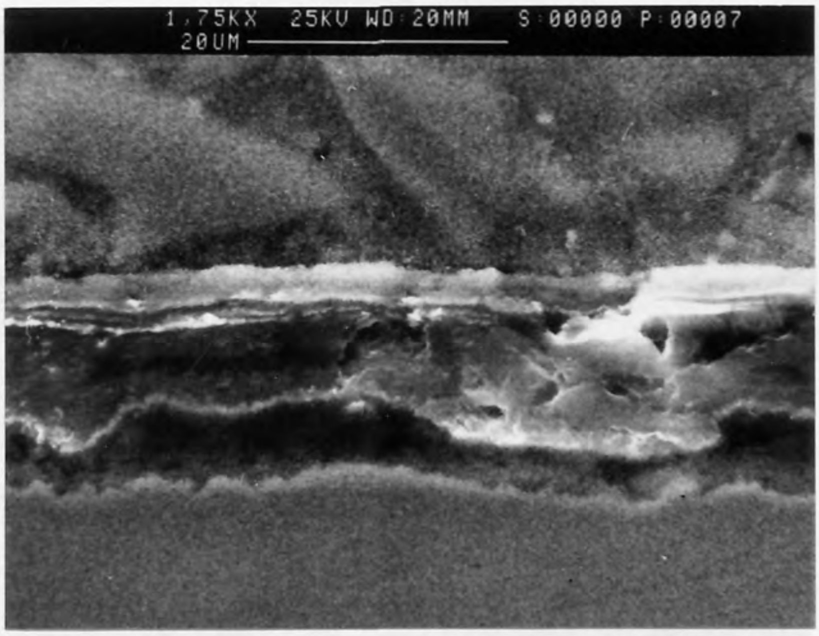

Fig. 91 SEM image of residual lubricant layer: Pressure nozzle semi-angle = 6 degrees; Drawing speed = 10 m/min; Area reduction = 20%; Lubricant: Traxit; Medium carbon steel; Residual lubricant thickness = 10.0 μm.

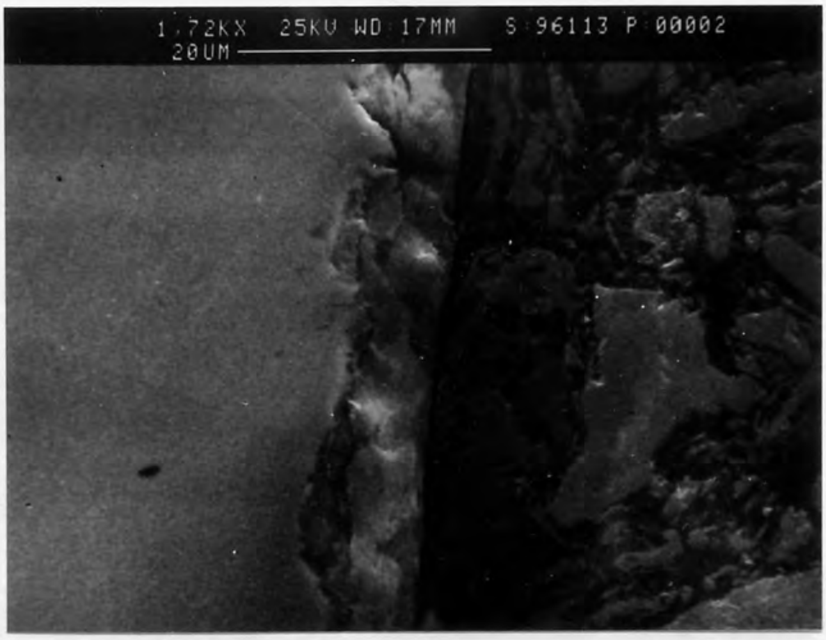

Fig. 92 SEM image of residual lubricant layer: Pressure nozzle semi-angle = 10 degrees; Drawing speed = 27 m/min; Area reduction = 27%; Lubricant: Traxit; Medium carbon steel; Residual lubricant thickness = 6.5 μm.

Fig. 93 SEM image of residual lubricant layer: Pressure nozzle semi-angle = 10 degrees; Drawing speed = 27 m/min; Area reduction = 14%; Lubricant: Traxit; Low carbon steel; Residual lubricant thickness = 4.7 µm.

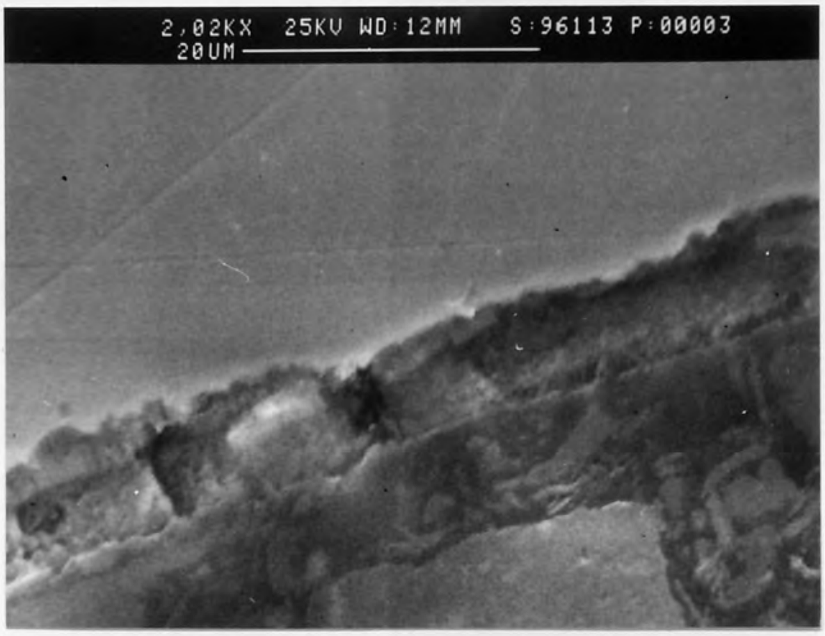

Fig. 94 SEM image of residual lubricant layer: Pressure nozzle semi-angle = 10 degrees; Drawing speed = 27 m/min; Area reduction = 27%; Lubricant: Traxit; Medium carbon steel; Residual lubricant thickness = 5.9 µm.

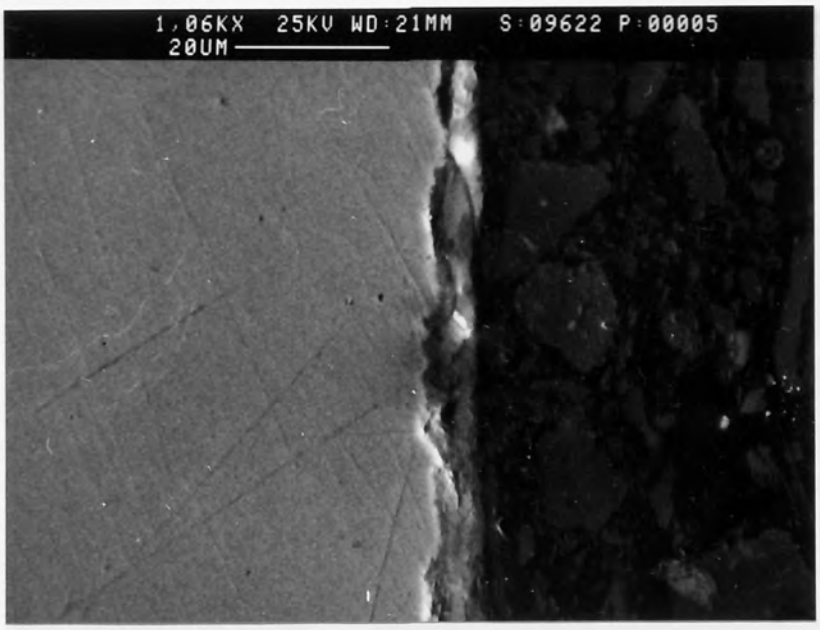

Fig. 95 SEM image of residual lubricant layer: Pressure nozzle semi-angle = 10 degrees; Drawing speed = 20 m/min; Area reduction = 27%; Lubricant: Traxit; Low carbon steel; Residual lubricant thickness = 6.1 μm.

Fig. 96 SEM image of residual lubricant layer: Pressure nozzle semi-angle = 6 degrees; Drawing speed = 47 m/min; Area reduction = 20%; Lubricant: Traxit; Medium carbon steel; Residual lubricant thickness = 5.8 μm.

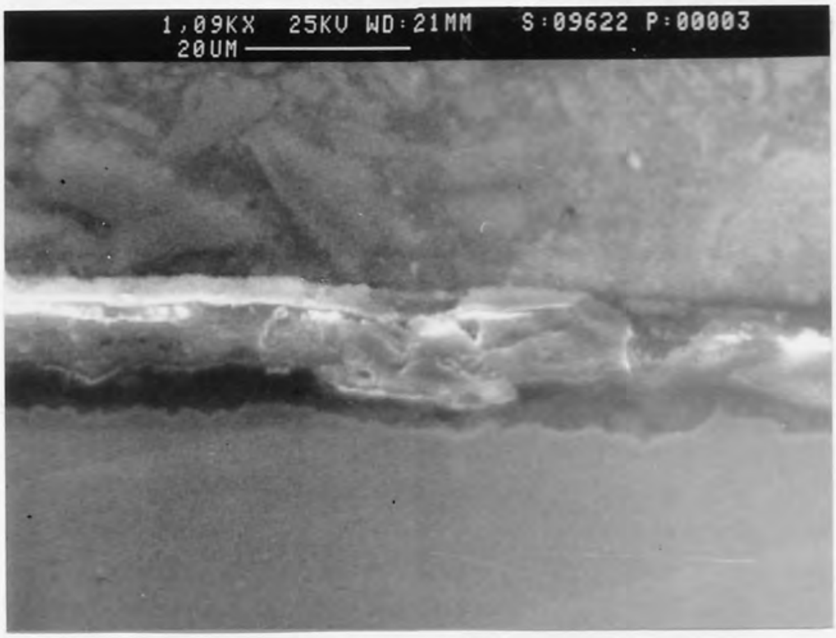

Fig. 97 SEM image of residual lubricant layer: Pressure nozzle semi-angle = 10 degrees; Drawing speed = 37 m/min; Area reduction = 30%; Lubricant: Traxit; Low carbon steel; Residual lubricant thickness = 8.8 μm.

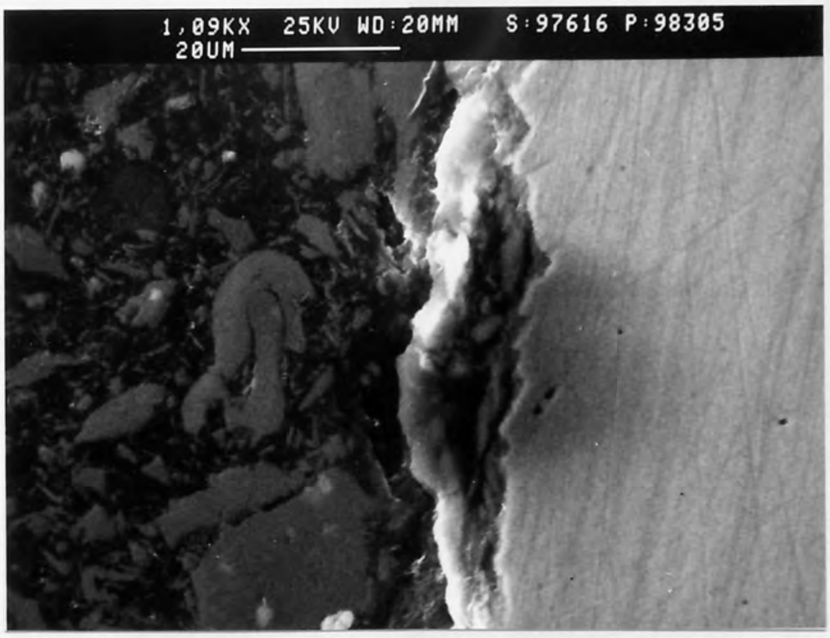

Fig. 98 SEM image of residual lubricant layer: Pressure nozzle semi-angle = 6 degrees; Drawing speed = 27 m/min; Area reduction = 21%; Lubricant: Traxit; Low carbon steel; Residual lubricant thickness = 12.5 μm.

Fig. 99 SEM image of residual lubricant layer: Pressure nozzle semi-angle = 6 degrees; Drawing speed = 20 m/min; Area reduction = 21%; Lubricant: Traxit; Medium carbon steel; Residual lubricant thickness = 9.6 μm.

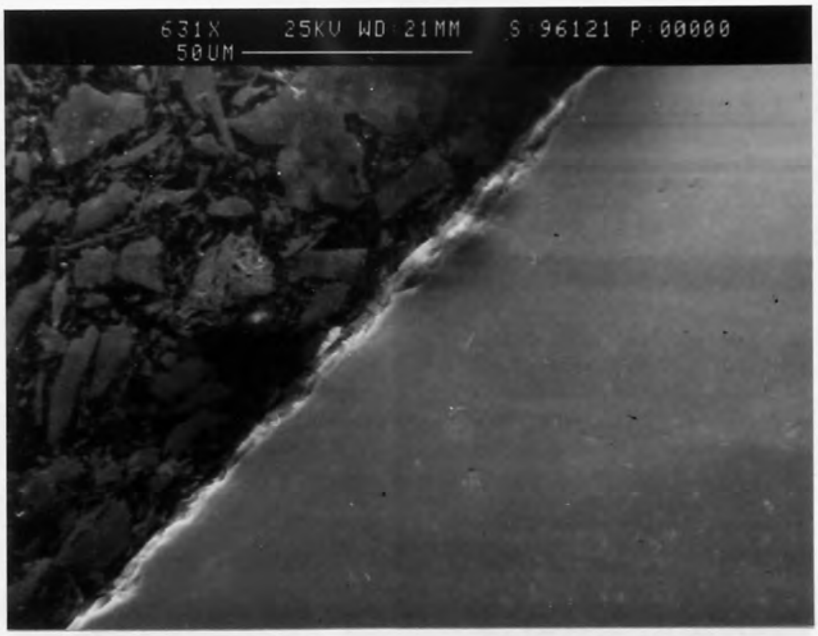

Fig. 100 SEM image of residual lubricant layer: Pressure nozzle semi-angle = 10 degrees; Drawing speed = 37 m/min; Area reduction = 30%; Lubricant: Traxit; Medium carbon steel; Residual lubricant thickness = 6.5 μm.

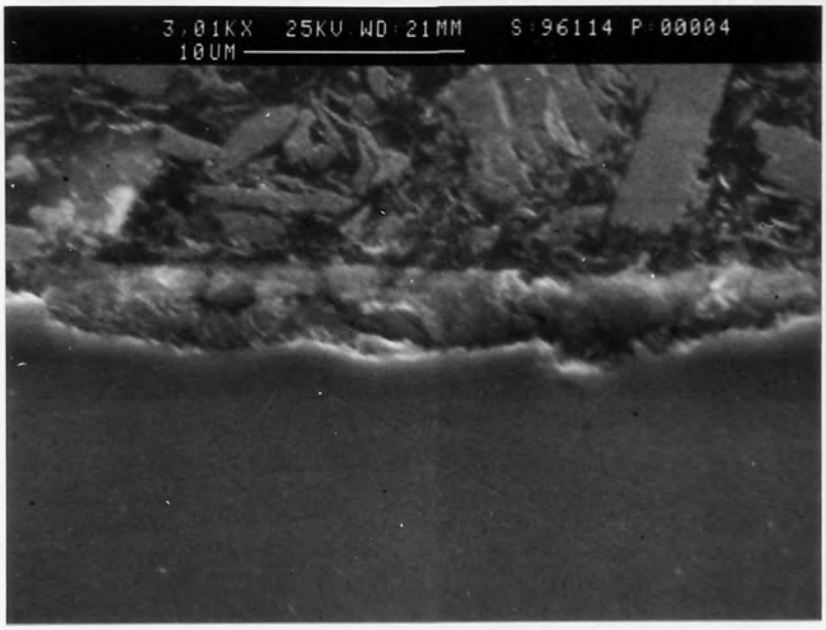

Fig. 101 SEM image of residual lubricant layer: Pressure nozzle semi-angle = 10 degrees;

Drawing speed = 27 m/min; Area reduction = 30%; Lubricant: Traxit;

Medium carbon steel; Residual lubricant thickness = 4.1 μm.

Fig. 102 SEM image of residual lubricant layer: Pressure nozzle semi-angle = 6 degrees;

Drawing speed =47 m/min; Area reduction = 24%; Lubricant: Traxit;

Medium carbon steel; Residual lubricant thickness = 7.1 μm.

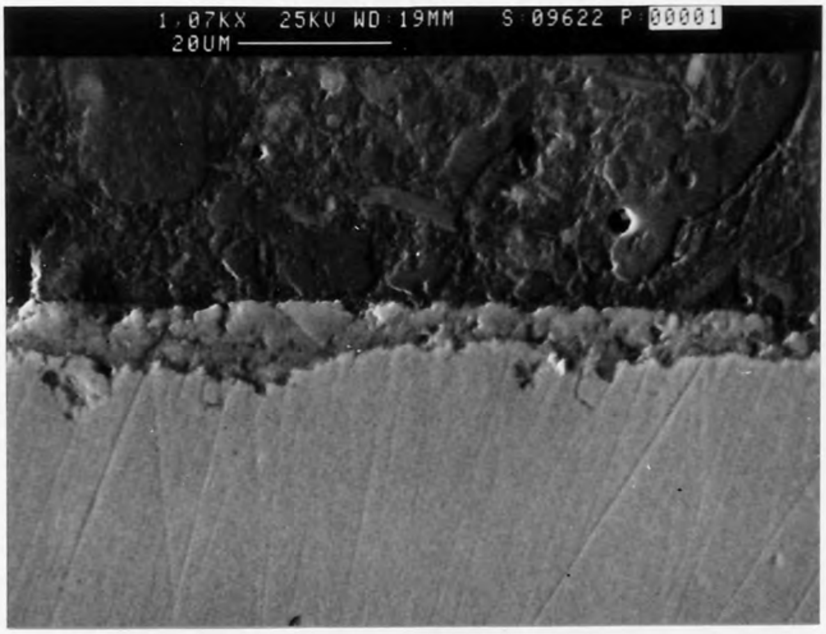

Fig. 103 SEM image of residual lubricant layer: Pressure nozzle semi-angle = 6 degrees; Drawing speed = 47 m/min; Area reduction = 21%; Lubricant: Traxit; Medium carbon steel; Residual lubricant thickness = 8.5 μm.

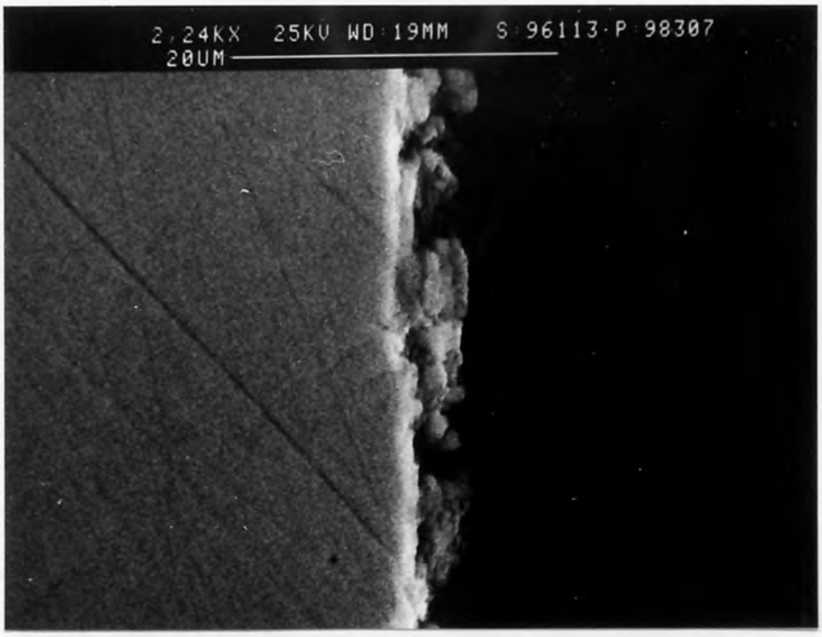

Fig. 104 SEM image of residual lubricant layer: Pressure nozzle semi-angle = 8 degrees; Drawing speed = 37 m/min; Area reduction = 30%; Lubricant: Condat Vicafil; Medium carbon steel; Residual lubricant thickness = 4.7 μm.

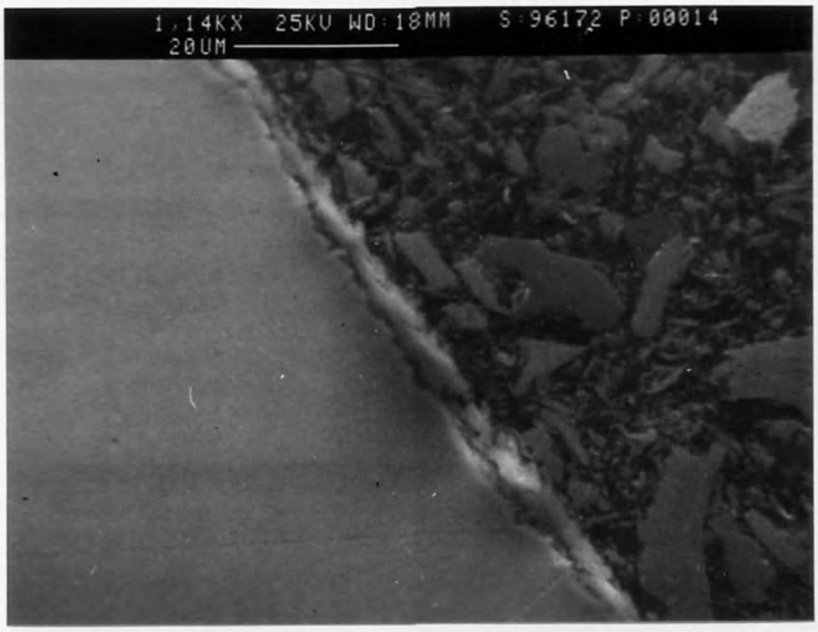

Fig. 105 SEM image of residual lubricant layer: Pressure nozzle semi-angle = 10 degrees; Drawing speed = 37 m/min; Area reduction = 24%; Lubricant: Condat Vicafil; Medium carbon steel; Residual lubricant thickness = 5.5 μm.

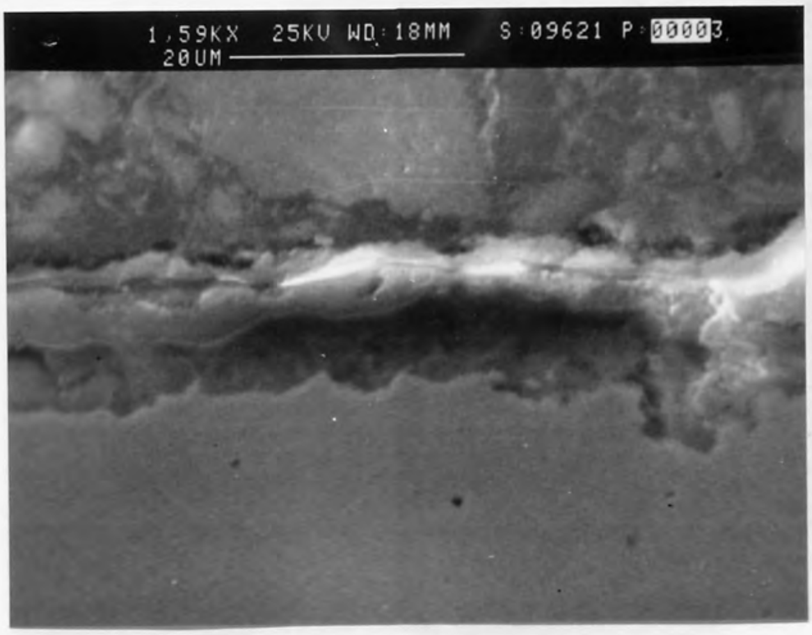

Fig. 106 SEM image of residual lubricant layer: Pressure nozzle semi-angle = 6 degrees; Drawing speed = 27 m/min; Area reduction = 21%; Lubricant: Condat Vicafil; Low carbon steel; Residual lubricant thickness = 6.7 μm.

Fig. 107 SEM image of residual lubricant layer: Pressure nozzle semi-angle = 8 degrees; Drawing speed = 27 m/min; Area reduction = 30%; Lubricant: Condat Vicafil; Low carbon steel; Residual lubricant thickness = 6.7 μm.

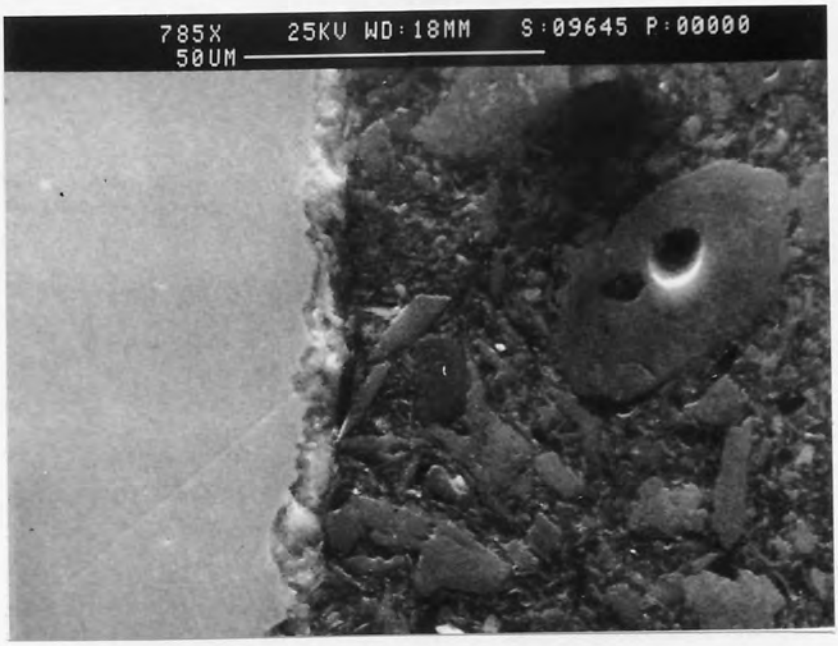

Fig. 108 SEM image of residual lubricant layer: Pressure nozzle semi-angle = 8 degrees; Drawing speed = 47 m/min; Area reduction = 30%; Lubricant: Condat Vicafil; Medium carbon steel; Residual lubricant thickness = 7.9 μm.

Fig. 109 SEM image of residual lubricant layer: Pressure nozzle semi-angle = 8 degrees; Drawing speed = 47 m/min; Area reduction = 27%; Lubricant: Condat Vicafil; Medium carbon steel; Residual lubricant thickness = 10.0 μm.

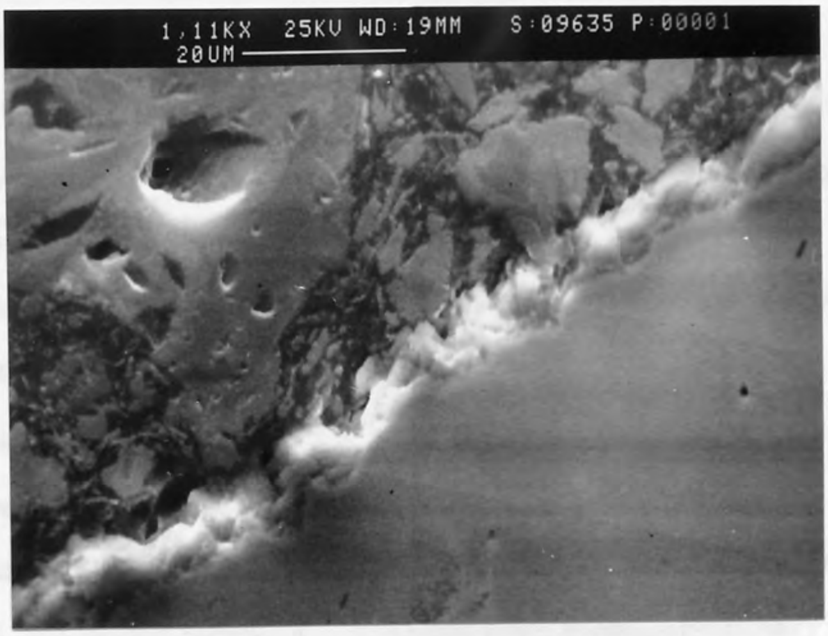

Fig. 110 SEM image of residual lubricant layer: Pressure nozzle semi-angle = 8 degrees; Drawing speed = 37 m/min; Area reduction = 30%; Lubricant: Condat Vicafil; Medium carbon steel; Residual lubricant thickness = 6.7 μm.

CHAPTER SEVEN

OBSERVATION AND DISCUSSION

7.1 Introduction

This chapter gives detailed observation and in depth discussion on the experimental results presented in the previous chapter. Since the experimental results presented in Chapter 6 mainly consist of two parts, i.e. results from the drawing experiment and results from the SEM examination, the observation and discussion of the current chapter is also divided into two parts: with the first part (Sections 7.2-7.6) concentrating on the results from the drawing experiment and the second part (Sections 7.7-7.9) dealing with the results of the SEM examination. In order to determine the flow stress and the work hardening characteristics of the drawn materials, tensile tests were also carried out and the results have been presented and discussed in Chapter 5.

7.2 General Observation of the Drawing Experiment

In the present study, a systematic drawing experiment has been carried out to investigate the efficiency of lubrication and to assist die box design, during which a large quantity of drawing tests was performed under the following conditions:

Drawing material: medium carbon steel and low carbon steel, nominal diameter = 5.5 mm
Lubricants: Condat Vicafil and Traxit
Percentage area reduction: 17, 21, 24, 27 and 30
Drawing speed: 20, 27, 37 and 47 m/min

In order to tune and validate the experimental equipment and the data acquisition systems, and thus to gain consistency in experimental results, preliminary drawing tests were carried out. However, these results are not included in this thesis.

In order to obtain experimental data of high quality and accuracy, each drawing test was carefully prepared and conducted. To allow best lubricant pick up, the lubricant chamber (box) was fully charged every time. Wires were cut in sufficient length to achieve a steady state drawing load for a reasonable period of time during drawing. The drawing load was averaged over a length of the flattest portion of the drawing load vs time curve, from which the drawing stress was calculated.

In general, all the equipment functioned well to the standard of the objectives of this study set at the very beginning of the project, and the drawing tests were stable and repeatable. Therefore, all the drawing experiments carried out were successful. The promoted lubrication mechanism (the pressure die box design) and the whole data acquisition system were also successful. Hence, there is a high degree of confidence that all the results presented and discussed in this thesis are reliable.

7.3 General Observations from the Drawing Experiment Results

All the drawing experiment results are presented in Figures 42 to 84 in Chapter 6. The raw data from which these figures were drawn are given in the Appendix D. Figures 42 to 63 are drawing stress vs percentage area reduction curves for medium carbon steel wire under various drawing conditions corresponding to tables D.1 to D.6. Figures 64 to 84 are drawing stress vs percentage area reduction curves for low carbon steel wire under various drawing conditions corresponding to Tables D.7 to D.12.

It is seen clearly from Figures 42 through 84 that the drawing stress increases with the increase of the percentage area reduction. This is well in line with the previous experimental as well as theoretical studies of wire drawing mechanics by many other researchers. In fact, the percentage area reduction is the most dominant fact affecting the drawing stress, as expressed in the equations (2.1) - (2.8) in Chapter 2 derived for drawing stress calculation.

The second dominant factor on drawing stress is certainly the drawn material, i.e. its mechanical properties, such as yield (flow) stress and the work hardening behaviour of the material in consideration; this is also clearly seen from Figures 42 to 84. The drawing stress for medium carbon steel wire ranges between 150 N/mm^2 and 500 N/mm^2, see Figure 58, for the area reductions from 10% to 30%, whereas the drawing stress for low carbon steel wire ranges between 120 N/mm^2 and 300 N/mm^2, see Figure 82, for the same percentage area reduction range. This is in good agreement with the difference in the flow stress between the two materials. As can be seen in Tables C.1 and C.2 in the Appendix C, the flow stress for medium carbon steel is between 440 and 869 N/mm^2 (Table C.2), and that for low carbon steel is only between 241 and 517 N/mm^2 (Table C.1). According to equations (2.1) - (2.8), a higher flow stress would result in a higher drawing stress.

It is also seen from Figures 42 to 84 that the drawing stress varies with the variation of other conditions or parameters, such as the lubricant, the pressure nozzle semi-angle as well as the drawing speed. This can of course be explained as an effect of friction and redundant work in addition to percentage area reduction and material properties. However, this is much more complicated and possibly involves interactive reaction effects between several of the variables during the drawing process. Further observation and discussion on the drawing experimental results are given in detail in the following sections.

7.4 Effect of Different Lubricant

The use of lubricant in wire drawing produces the following effects: an overall reduction of drawing stress, hence drawing load and power consumption; a reduction in die wear and thus increase in die life; and a good surface finish and high quality properties of drawn wire. In this section, the reduction of drawing stress is used as a criterion for evaluation of the efficiency of lubrication.

Figures 42 to 51 present the drawing stress vs percentage area reduction curves showing the effect of different lubricants on the drawing stress under different other conditions of pressure nozzle semi-angle and drawing speed for the medium carbon steel. Figures 64 through 72 present the equivalent curves for the low carbon steel.

It can be seen from Figures 42 to 51 and Figures 64 to 72 that the drawing stress was consistently lower with Traxit lubricant than with Condat Vicafil lubricant, for both medium- and low-carbon steel wire, except in Figure 48 for medium carbon steel and Figure 68 for low carbon steel where the drawing stress with Condat Vicafil lubricant was lower than that with Traxit lubricant under a larger area reduction of 30%. The maximum difference in wire drawing stress with the two lubricants is approximately 12.5%, see Figures 49 and 51, for medium carbon steel, and about 17%, see Figures 65 and 71. Therefore, it is reasonable to conclude that under the current experimental conditions, Traxit lubricant had a higher lubrication efficiency.

The lubrication efficiency is certainly related to the chemical and physical properties of a particular lubricant. However the mechanism of the interaction of these factors is difficult to explain and identify. Factors such as grain size, melting point, viscosity, etc., of the lubricant will all affect lubricant pick up, formation of the lubricant layer in the die/workpiece interface, and the establishment of hydrodynamic lubrication during wire drawing. Nevertheless, the methodology adopted in this study for qualitative as well as quantitative evaluation of lubrication efficiency by comparison of drawing stresses is viable. Therefore, under the same conditions, the drawing stress is only dependent upon friction at the workpiece/die interface. A lower drawing stress means a lower friction or better lubrication, hence higher lubrication efficiency.

7.5 Effect of Pressure Nozzle Semi-Angle

As explained in Section two, Chapter 2, the most efficient lubrication in wire drawing is hydrodynamic lubrication, and a hydrodynamic lubrication system involves the combined effects of drawing speed, lubricant properties and geometry of the Christopherson type of pressure tube or nozzle. The critical component of the pressure die box assembly designed for this study was the pressure nozzle: the length of the parallel part is 20 mm; the diameter of the parallel part is 6 mm; the inlet semi-angle was chosen as the variable to be 6, 8 and 10 degrees, see Section 3.4.2 in Chapter 3 and Appendix B.

The drawing stress vs percentage area reduction curves showing the effect of different pressure nozzle semi-angles are given in Figures 53 to 57 for the medium carbon steel and Figures 73 to 78 for the low carbon steel.

It was found that, with the Condat Vicafil lubricant the drawing stress was consistently low when the pressure nozzle semi-angle was equal to 8 degrees, under all of the current experimental conditions for both the drawn materials under consideration, see Figures 52 to 54 and Figures 73 to 75.

With Traxit lubricant, however, the measured drawing stresses were scattered within a much narrower margin with variation of the pressure nozzle semi-angle, for both the medium and low carbon steel, under various drawing conditions, see Figures 55 to 57 and Figures 76 to 78. Hence, it can be concluded that the drawing stress was less sensitive to pressure nozzle semi-angle.

7.6 Effect of Drawing Speed

The drawing stress vs percentage area reduction curves showing the effect of different drawing speeds are given in Figures 58 to 63 for the medium carbon steel and Figures 79 to 84 for the low carbon steel.

It is well understood that the effect of drawing speed on drawing stress is two fold: (1) a variation in drawing speed will some times result in a change in flow stress of the drawn material, hence the drawing stress; (2) a variation in drawing stress will change the lubrication or friction characteristics in wire drawing, hence the drawing stress will also change.

According to the previous research reported by Harding [103], strain rate or deformation speed does show a significant effect on flow stress of some metallic materials such as mild steel over a range of strain rate from quasi-static (up to 10^{-3}/s) to impact (up to 2000/s). This can obviously help explain the results plotted in Figures 58 and 61 where higher drawing speeds gave rise to higher drawing stress. Nevertheless it can be seen clearly from Figures 58 and 82 that the highest drawing speed (47 m/min) resulted in the lowest drawing stress. This seems contradicting. However, it can be explained as follows. Firstly, the nominal strain rate $\dot{\varepsilon}$ in wire drawing can be calculated by the following equation:

$$\dot{\varepsilon} = \frac{4vD_2^2}{D_1^3} tg\alpha \qquad 7.1$$

Under the experiment conditions of this study: the initial diameter of the wire $D_1 = 5.5$ mm, the finishing diameter: $D_2 = 4.6$-5.0 mm, the drawing speed v= 10-47 m/min and the die semi-angle: $\alpha = 7.5$ degrees. Hence, the nominal strain rate $\dot{\varepsilon}$ = 13-52/s, which is low and within a small range compared to that reported in reference 103. Therefore, the effect of strain rate or drawing speed on the flow stress of the drawn material, thus the drawing stress, is small, which was also demonstrated by an earlier research work carried out at Aston University [4]. Secondly, the drawing speed will certainly affect the pick up and the viscosity of the lubricant, hence the lubrication efficiency. Therefore, it is believed that the variation of drawing stress with the change of drawing speed seen in Figures 58 to 63 and Figures 79 to 84 is more due to its effect on lubrication or friction characteristics rather than due to the variation of strain rate.

By considering Figures 58 to 63 and Figures 79 to 84 it is found that although it is difficult to judge which drawing speed gives the best result in terms of best lubrication performance and minimum drawing stress, the drawing stresses are least scattered when the pressure nozzle semi-angle is equal to 8 degrees for both medium carbon and low carbon steels and for both Traxit and Condat Vicafil lubricants, compare Figures 59 and 62 with Figures 58, 60, 61 and 63, and Figures 80 and 83 with Figures 79, 81, 82 and 84.

7.7 General Observations of Lubrication Characteristics in the Experiment

During the entire drawing experiment, lubricants were applied and the lubricant box was fully charged every time. The lubrication and friction characteristics of the drawing process was closely monitored for the purpose of this study.

It was found that, apart from the properties of the two lubricants used in the experiment (Condat Vicafil and Traxit) described in Chapter 4, the Traxit lubricant came with a larger grain size than the Condat Vicafil lubricant. It was also found that the residual Condat lubricant left in the die entrance formed a shell, whereas the Traxit lubricant was in much smaller grains fully filling all the clearances within the pressurisation system, including the die entrance, and no physical bonding was seen.

It is therefore confirmed that the pressure system for using dry lubricants designed does seem to work, helping draw lubricant to feed the die/wire interface under pressure. The appearance of both lubricants near the die entrance area further confirms that the rise of pressure together with the accompanying friction from the inlet of the pressure nozzle towards the die entrance is sufficiently large to liquidise the Condat lubricant to form a shell and grind the Traxit lubricant into smaller grains.

This can also imply that the temperature within the chamber of die entrance would be higher than the melting point of the Condat lubricant (145 ^{o}C to 165 ^{o}C) so that it was liquidised, and lower than the melting point of the Traxit lubricant (210 ^{o}C) so that it stayed unbonded. However, in the deformation region, both lubricants were liquidised since residual lubricant layers formed in each case.

7.8 General Observation and Discussion of SEM Examination and Results

During this program, about 40 samples were made on which SEM examination were conducted in order to evaluate the lubricant layer on the surface of the drawn wire. Samples were cut off the drawn wires under various drawing conditions with different lubricants immediately after each drawing tests to ensure that there was no damage to the residual lubricant layer on the surface of the drawn wire.

SEM samples were prepared using conductive Backelite mounting material both with and without gold plate. Some optical samples were also prepared and examined under optical microscope. While most of the samples were examined under the SEM in order to observe and measure the residual lubricant layer on the drawn wire surface, only a selection of the images are presented in Figures 85 to 110 in Chapter 6.

Figure 85 shows typical optical microscope images of wire surface topology for and undrawn wire (Figure 85a) and a drawn wire (Figure 85b). Figure 86 shows the two SEM techniques used in measuring the thickness of the lubricant layer, i.e. under normal SEM operation mode (Figure 86a) and with back scattered method (Figure 86b). Figure 87 shows a typical residual lubricant layer observed under SEM under high magnification. Figures 88 to 103 present the SEM images of residual lubricant layer on surfaces of wire drawn with the Traxit lubricant. Figures 104 to 110 are the SEM images of residual lubricant layer on surfaces of wire drawn with the Condat Vicafil lubricant.

Generally, the residual lubricant layer on the surface of the drawn wire exists and can be clearly seen both under optical micro-structure observation and SEM examination. It has been therefore proved that the methodology adopted in this study is convincing.

7.9 Evaluation of Residual Lubricant Layer

From Figure 85 it can be clearly seen that, even under the optical microscope, there is no material between an undrawn wire and the mounting material (Figure 85a), whereas there is always a layer of extra material between a drawn wire and the mounting material (Figure 85b). This extra layer of material has been proved to be the lubricant deposited on the surface of the drawn wire, called the residual lubricant layer, by the spectrum analysis, because the main element was calcium (over 70%) and both lubricants used in this research were calcium based. A selection of the spectrum analysis graphs are given in Appendix E.

During SEM examination, once a lubricant layer was found and brought into focus, the two straight lines on the CRT were adjusted to a best fit each side of the layer, so that the distance between the two lines could be taken as the averaged thickness of it. This value was then displayed and recorded together with the magnification and scale on the

SEM image, as seen in Figure 86. This method of measurement for the thickness of the residual lubricant layer is believed to be sufficiently accurate for the purpose of this study.

According to Figures 86 to 110, the thickness of the residual lubricant layer of the Traxit lubricant on the drawn wire was between 4.1 and 18.5 μm and the thickness of the residual lubricant layer of the Condat Vicafil lubricant on the drawn wire is between 4.7 and 13.1 μm. It was the original intention of this study to use the measured thickness of the residual lubricant layer to quantify the lubrication efficiency and also to correlate it with process parameters. However, the latter was not attempted due to the small and scattering data obtained.

7.10 Summary

According to the results presented and discussed in this chapter, the following points may be noted:

(1). Under the current experimental conditions the Traxit lubricant had a higher lubrication efficiency in terms of reducing drawing stress.

(2). With the Condat Vicafil lubricant the drawing stress was consistently low when the pressure nozzle semi-angle was equal to 8 degrees under all of the current experimental conditions for both the drawn materials under consideration, however with the Traxit lubricant the drawing stress was less sensitive to pressure nozzle semi-angle.

(3). The drawing stresses were least scattered when the pressure nozzle semi-angle is equal to 8 degrees under all the current experimental conditions. It is difficult to determine the optimum drawing speed in terms of lubrication performance and minimum drawing stress.

(4). The SEM examination showed the existence of a residual lubricant layer on the surface of the drawn wire, the thickness of this was between 4.1 and 18.5 μm for Traxit lubricant, and between 4.7 and 13.1 μm for Condat Vicafil lubricant.

CHAPTER EIGHT

FINITE ELEMENT SIMULATION OF WIRE DRAWING PROCESS

8.1 Introduction

This chapter presents a finite element analysis of the wire drawing process which was carried out under various initial and boundary conditions. The finite element theory and the commercial program ABAQUS Version 5.5 used are briefly described. The results obtained were analysed in terms of stress and strain distributions within the deformation zone, with the effects of different cross-sectional area reduction and friction coefficients.

8.2 Finite Element Theory

As described in Section 2.8 of Chapter 2, there are three types of finite element methods, namely elastic-plastic, visco-plastic and rigid-plastic, which are distinguished by the material model included in the system. The rigid-plastic model ignores all elastic deformation of the workpiece; whereas the visco-plastic model simulate the plastic flow as a non-Newtonian fluid. Only the elastic-plastic model gives a realistic description of the material flow behaviour in metal forming by considering both elastic and plastic parts of the deformation, and hence was described in the following sections where appropriate. The finite element package ABAQUS used in this study is based upon elastic-plastic finite element theory.

8.2.1 Domain discretisation

In the finite element technique, the domain of a continuum is discretised into a finite number of small elements (finite element), each of which is defined and inter-connected by a certain number of nodal points (nodes). Many types of elements can be used for analysis of metal forming problems. Figure 111 shows a selection of typical finite element normally used [8].

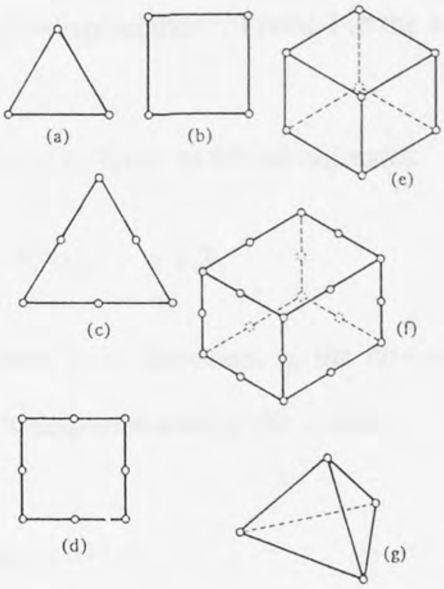

Fig. 111 A selection of typical finite element normally used in finite element analysis of metal forming processes, after Rowe et al [8].

8.2.2 Finite element expression

For each single element, the displacement at any point within it can be calculated from its nodal displacements through an interpolation function or shape function. Thus the corresponding strain is obtained

$$\varepsilon = [B]\,\mathbf{d} \tag{8.1}$$

where ε is the strain vector; $[B]$ a matrix, determined by the element type and shape function; $\mathbf{d}$ the nodal displacement vector.

For simple triangular elements

$$\varepsilon = (\ \varepsilon_{11}\ \varepsilon_{22}\ \gamma_{12}\ )^{T} \tag{8.2}$$

$$\mathbf{d} = (\ d_{11}\ d_{12}\ d_{21}\ d_{22}\ d_{31}\ d_{32}\ )^{T} \tag{8.3}$$

where ε_{ii} is the normal component of strain in x_i direction, γ_{ij} the shear component of strain in $x_i x_j$ plane and d_{Ij} the displacement of node I in the x_j direction.

Assume the shape functions to be linear to the co-ordinates

$$u_i = a_i + b_{i\,1}x_1 + b_{i\,2}x_2\,,\ i = 1,2 \tag{8.4}$$

where u_i is the displacement in x_i direction; x_i the co-ordinate; and a_i, b_{i1} and b_{i2} are constants determined by the displacements of the nodes.

Thus, the matrix [B] is given by [43]:

$$[B] = \frac{1}{2A}\begin{bmatrix} x_{22}-x_{32} & 0 & x_{32}-x_{12} & 0 & x_{12}-x_{22} & 0 \\ 0 & x_{31}-x_{21} & 0 & x_{11}-x_{31} & 0 & x_{21}-x_{11} \\ x_{31}-x_{21} & x_{22}-x_{32} & x_{11}-x_{31} & x_{32}-x_{12} & x_{21}-x_{11} & x_{12}-x_{22} \end{bmatrix} \tag{8.5}$$

where x_{Ii} is the ith co-ordinate of node I and A the area of the triangle 123 shown in Figure 112 [8].

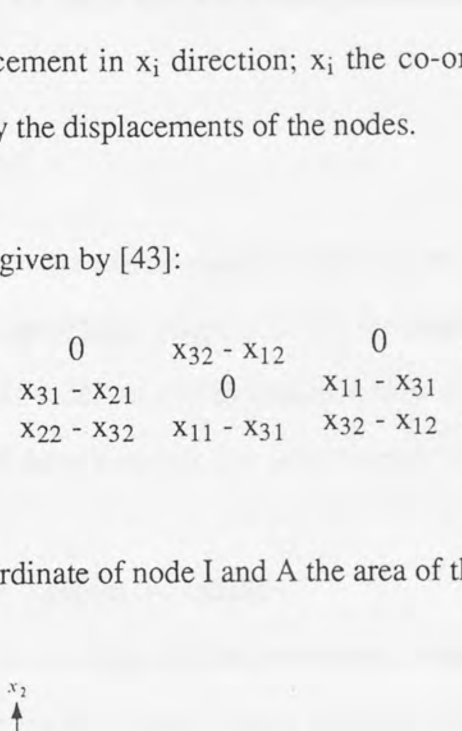

Fig. 112 Deformation of a simple triangular element, after Rowe et al [8].

The stress vector σ of an element is related with the strain vector ε by the [D] matrix

$$\sigma = [D]\,\varepsilon \tag{8.6}$$

where

$$\sigma = (\sigma_{11}\, \sigma_{22}\, \sigma_{33}\, \sigma_{12}\, \sigma_{23}\, \sigma_{13})^T \tag{8.7}$$

$$\varepsilon = (\varepsilon_{11}\, \varepsilon_{22}\, \varepsilon_{33}\, \gamma_{12}\, \gamma_{23}\, \gamma_{13})^T \tag{8.8}$$

where σ_{ij} and ε_{ij} and γ_{ij} are stress and strain components respectively. The [D] matrix can be written as

$$[D] = [D^e] - [D^p] \tag{8.9}$$

In equation (8.9), $[D^e]$ is the elastic matrix which can be easily derived from the usual isotropic stress-strain relationship, whereas $[D^p]$ is the plastic matrix which can be derived from the von Mises yield criterion and an associate flow rule (such as Prandtl-Reuss flow rule). For description of these matrices, see references 6, 7, and 8.

8.2.3 Finite element system equations

The starting point for determining the finite element system equations is to formulate an expression (functional) for the average rate of increase of potential energy using specific constitutive relations [6, 7, 8]. The calculus of variations can be used to determine the conditions such that this functional has a satisfactory value. The finite element system equations can then be written in the usual simplified form of

$$\Delta \mathbf{F} = \mathbf{K} \Delta \mathbf{u} \tag{8.10}$$

where $\Delta\mathbf{F}$ is a vector of the nodal force increments and $\Delta\mathbf{u}$ is the nodal displacement increments. **K** is the stiffness matrix, which is an assemblage of matrices that allow for deformation, material incompressibility, and rigid body rotation in the elastic-plastic finite element method [8].

The solution of equation (8.10) to give the unknowns in $\Delta\mathbf{u}$ allows the deformation of the workpiece to be determined, which in turn allows the determination of stress and strain distributions within the workpiece.

8.2.4 Solution schemes

Since in the modelling of metal forming processes both material and geometric non-linearities are involved, the solution of equation (8.10) must be performed in a series of small linear steps or increments. Some form of iterative solution procedure is required to determine the nodal displacement increment.

In the elastic-plastic finite element method there are two commonly used methods, namely (1) the initial stiffness method and (2) the secant-modulus method [8].

The advantage of the initial stiffness method is that the global stiffness matrix needs to be calculated and inverted only once, at the start of each increment, so each subsequent iteration may be performed in a fraction of the time required for a full solution of the stiffness equations. However, many iterations may be required for the convergence of the solution and occasionally the solution may not converge at all.

The secant-modulus method is actually a second-order Runge-Kutta technique in which the global stiffness matrix is evaluated using the stress and strain at the start of the increment. The equations are then solved for the set of applied forces $\Delta\mathbf{F}$ to give a first approximation to the set of incremental displacements ($\Delta\mathbf{u}^a$). These are then used to estimate the stress and strain half-way through the incremental step (σ^m, ε^m). Using these mid-increment values a new stiffness matrix is constructed and solved giving a better estimate of the incremental nodal displacement ($\Delta\mathbf{u}^c$) and the stress and strain (σ^c, ε^c) at the end of the incremental step. Although the global stiffness matrix needs to be evaluated twice for each increment in this method, additional iterations may be avoided, hence giving an overall computational saving.

8.3 Finite Element Package ABAQUS

8.3.1 General description of the program

ABAQUS is a general purpose finite element program designed specifically for advanced structural and heat transfer analysis [102], which is commercially available in the market. A wide variety of problems may be addressed with the modelling tools available within the program, including bulk metal forming processes.

The analysis types within ABAQUS are briefly described as following:

- Linear or non-linear statics
- Non-linear transient dynamics: implicit time integration
- Linear dynamics: natural frequency extraction, transient and steady state response
- Transient and steady state heat transfer
- Fracture mechanics

The analysis procedure with ABAQUS, as usual with finite element analysis, involves pre-processing, processing or finite element computation and post-processing.

One of the end results of pre-processing is an input data file, which contains all the information necessary for performing a successful ABAQUS finite element calculation. For example, in an analysis for a metal forming process, the ABAQUS input data file will include information or data on:

(1) Domain (workpiece) discretisation: nodal co-ordinates and element definition;

(2) Initial and boundary conditions: descriptions of loading, tool geometry and movement;

(3) Solver and special solution technique details;

(4) Constitutive model and mechanical property data for the materials involved;

(5) Computational parameters;

(6) Output requirements.

The input data file can be prepared using a standard text editor or interactively through a commercial finite element analysis pre/post processor like PATRAN [102]. The input is organised around intuitive keywords and their associated data. The keywords identify the option selected, and the data may be in free or fixed format. The input is read by a batch preprocessor which performs extensive input data checking. If no error is detected in the input data, the preprocessor creates the problem database and then passes control to the processing (analysis) program. Typical examples of ABAQUS input data file can be found in Appendix F.

The processing is carried out on UNIX workstations or PCs with appropriate RAM and hard disk space, during which static or dynamic problems defined in the input data file are solved and result files exported. For non-linear dynamic stress-displacement analysis, such as metal forming, ABAQUS uses direct implicit time integration and automatic time incrementation, to ensure solution stability for the largest strain possible. For solution of non-linear equations the full Newton method is used. ABAQUS is particularly efficient for large strain problems involving complex material behaviour.

In post processing, the finite element result files are analysed and useful information extracted, normally in graphical format. Within ABAQUS, an interactive graphical postprocessor is included for providing mesh plots, contour plots of results, time history plots and x-y plots.

8.3.2 Prescribing constraining and loading conditions

In metal forming analysis with ABAQUS, according to the deformation and geometry conditions certain constraining and loading can be applied correspondingly.

Nodal: Concentrated forces and moments; temperature; field variables; zero and non zero displacements, rotations, velocities or accelerations specified with arbitrary time variations.

Element: Uniform and non-uniform body forces; uniform and non-uniform pressure; hydrostatic pressures; centrifugal load, etc.

8.3.3 Modelling of tool surfaces

In most finite element analyses of metal forming processes, the forming tools are considered as rigid bodies because their elastic deformation is negligible compared to the large plastic deformation subjected by the workpiece. ABAQUS provides two ways for modelling the surfaces of rigid bodies. Firstly, simple geometric surfaces can be defined by describing the surface of their cross sections with straight and curved line segments. Secondly, rigid bodies with arbitrary geometries can be discretised and represented by a finite element surface mesh [102].

8.3.4 Interface friction

A Coulomb friction model is used in ABAQUS for all contact problems. The standard Coulomb friction model assumes that no relative motion occurs if the equivalent frictional stress, τ_{eq}, is less than the critical shear stress τ_{cr} where

$$\tau_{eq} = \sqrt{\tau_1^2 + \tau_2^2} \tag{8.11}$$

and $$\tau_{cr} = \mu p \tag{8.12}$$

where μ is the friction coefficient and p is the contact pressure.

8.4 Computational Conditions

8.4.1 Initial and boundary conditions

The geometry of the specimen in the drawing experiment is cylindrical, as shown in Figure 113. The initial length and diameter of the specimen are 30 mm and 5.5 mm respectively. Due to the axisymmetric deformation characteristics (about r=0 and z=0) of a cylindrical specimen in the drawing process, only a slice of the geometry is considered in the simulation, as seen in the shaded part of the wire in Figure 113.

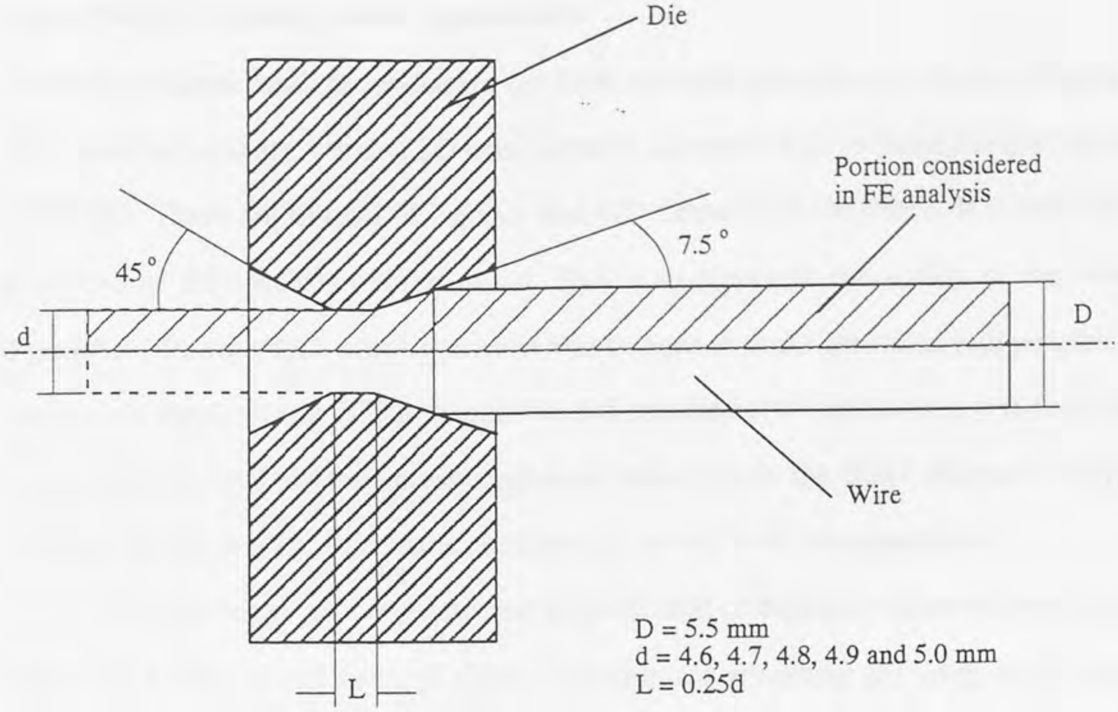

Figure 113 Geometry used in the finite element analysis of the wire drawing process using ABAQUS.

The finite element calculation conditions were chosen according to the drawing experiment carried out in this study, (Table 2 in Chapter 4) and are listed in Table 3.

Table 3 Simulation conditions.

Material	Coefficient of Friction μ	Area Reduction (%)
Low Carbon Steel Medium Carbon Steel	0.000 0.005 0.010 0.020 0.040 0.060 0.080 0.100	14 17 21 24 27 30

8.4.2 Finite element mesh generation

The finite element mesh generated for the finite element calculation is given in Figure 114. The elements used are 4 noded 2D axisymmetric elements with reduced integration points (CAX4R). There are in total 567 nodes and 480 elements in the mesh. It is seen that the front end of the mesh is necked down. This is to represent the reality of the drawing experiment during which every specimen was swaged to make the initial pull possible. The mesh is 30 mm long and 2.75 mm high (for 5.5 mm diameter initial wire). It is fixed for all the computations. Different percentage area reduction in the finite element analysis is achieved by varying the exit diameter of the die, as was so in the experiment.

The line segments describing the cross-section of the rigid die are also indicated in Figure 114, the co-ordinates of these segments are modified for each finite element analysis to achieve different cross-sectional area reductions. By using the SMOOTH parameter on the *RIGID SURFACE option in the input data file (refer to the example data file in Appendix F), the die is modelled without sharp corners and the transition region is smooth. The SMOOTH parameter was set to 0.5 mm for all the analyses.

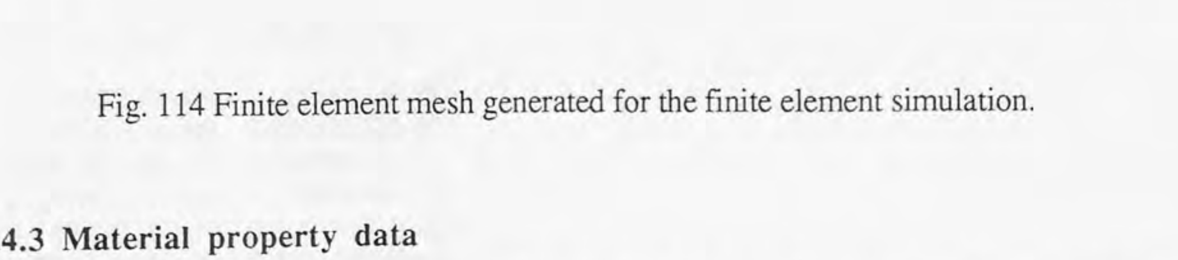

Fig. 114 Finite element mesh generated for the finite element simulation.

8.4.3 Material property data

The materials were low and medium carbon steels, the same drawn materials used in the experiment. The material properties used in the finite element computation are:

Young's modulus, E: 210 GPa

Poisson's ratio, υ: 0.35

The work hardening or the flow behaviour of the two steels are defined using equations (5.13) and (5.14) in Chapter 5. They are represented in the ABAQUS input format as following:

For the low carbon steel:

Flow Stress, Pa	Plastic Strain
0.2413480E+09,	0.0000000E-00
0.2894045E+09,	0.2500000E-01
0.3303033E+09,	0.5000000E-01
0.3647377E+09,	0.7500000E-01
0.3934014E+09,	0.1000000E+00
0.4169883E+09,	0.1250000E+00
0.4361920E+09,	0.1500000E+00
0.4517064E+09,	0.1750000E+00
0.4642251E+09,	0.2000000E+00
0.4744420E+09,	0.2250000E+00
0.4830508E+09,	0.2500000E+00
0.4907452E+09,	0.2750000E+00
0.4982189E+09,	0.3000000E+00
0.5061658E+09,	0.3250000E+00
0.5152795E+09,	0.3500001E+00
0.5262539E+09,	0.3750001E+00
0.5397827E+09,	0.4000001E+00
0.5565596E+09,	0.4250001E+00
0.5772784E+09,	0.4500001E+00
0.6026328E+09,	0.4750001E+00
0.6333165E+09,	0.5000001E+00
0.6700233E+09,	0.5250000E+00

For the medium carbon steel:

Flow Stress, Pa	Plastic Strain
0.4426120E+09,	0.0000000E-00
0.5475961E+09,	0.2500000E-01
0.6318943E+09,	0.5000000E-01
0.6978227E+09,	0.7500000E-01
0.7476971E+09,	0.1000000E+00
0.7838330E+09,	0.1250000E+00
0.8085463E+09,	0.1500000E+00
0.8241528E+09,	0.1750000E+00
0.8329679E+09,	0.2000000E+00
0.8373075E+09,	0.2250000E+00

```
0.8394873E+09, 0.2500000E+00
0.8418232E+09, 0.2750000E+00
0.8466306E+09, 0.3000000E+00
0.8562254E+09, 0.3250000E+00
0.8729232E+09, 0.3500001E+00
0.8990402E+09, 0.3750001E+00
0.9368912E+09, 0.4000001E+00
0.9887930E+09, 0.4250001E+00
0.1057061E+10, 0.4500001E+00
0.1144010E+10, 0.4750001E+00
0.1251957E+10, 0.5000001E+00
0.1383216E+10, 0.5250000E+00
```

8.4.4 Other computation parameters

The rigid die surface defined by the segments shown in Figure 114 is fixed in the computation by specifying zero displacements to the rigid surface node in all directions. Deformation is exerted onto the specimen by pulling the mesh through the die with an incremental nodal displacement applied at the front row nodes, see Figure 114. Since very large deformation will take place, the NLGEOM parameter was specified with the *STEP option. Different friction coefficients were specified under the *FRICTION option.

8.4.5 Computation procedures

The ABAQUS computation was performed in a batch mode (carried out in the background) once the input files had been carefully prepared and checked. The computation for each condition was carried out in several steps, see the sample input file in Appendix F. Small axial displacements of 5 mm were used for the first several steps in order to capture the incremental deformation characteristics of the drawing process. Larger displacements of 10 and 20 mm were used after the steady state of deformation was reached where pulling force was virtually constant, until the whole specimen was pulled through the die.

Three-dimensional initial and typical deformed meshes are shown in Figure 115. A typical die reaction force vs drawing time curve predicted by the finite element simulation is shown in Figure 116. Figure 117 gives a corresponding drawing force vs time curve recorded during experiment. It is seen from both curves that the drawing force increases first as the deformation starts and reaches a steady state for a period before it drops to zero. The general pattern and magnitude of the predicted drawing load curve (Figure 116) is in good agreement with the experiment (Figure 117). The zigzag pattern of the predicted response is caused by the discrete contact between the specimen and the die that occurs in the model, because contact is only detected at the nodes of the contact slave surface (defined by the interface element IRS21A, under the heading of *ELEMENT, refer to the ABAQUS example input data file in Appendix F). A finer mesh would provide a smoother curve.

8.5 Simulation Results and Discussions

The full finite element simulation results of the wire drawing process carried out in this research are presented and discussed in this section.

8.5.1 Incremental deformation and mesh distortion

The finite element simulation of wire drawing process was broken down into ten steps in order to show the incremental deformation procedure of the mesh. The first two steps were used just to bring the mesh in contact with the die. The real plastic deformation starts from the third step onwards. At step 10, the wire is drawn through the die completely. The initial condition is shown in Figure 114. The three-dimensional meshes at different stages of the drawing process shown in Figure 115 were created from the two-dimensional mesh using the ABAQUS post-processing function. Figure 118 shows the incremental mesh deformation through the drawing simulation in a 2D manner. Figure 119 gives a detailed view near the deformation zone for two different area reductions.

It can be seen that the deformation process during wire drawing is explicitly demonstrated by these meshes presented in Figures 115, 118 and 119. No deformation is shown in the front end of the wire, the diameter of which was deliberately reduced to simulate the swaged head in reality. It is seen from the last frame of picture in Figure 118 that a fish tail is formed at the end of the mesh. This was also seen in the experiment. Figure 119 indicates that a bigger area reduction caused larger element elongation, greater mesh distortion and longer contact area (compare Figure 119a with 119b).

8.5.2 Equivalent plastic strain distributions

The equivalent plastic strain ε_p is defined as

$$\varepsilon_p = \int \sqrt{\frac{2}{3}\, d\varepsilon_{ij}^{p} d\varepsilon_{ij}^{p}} \qquad (8.13)$$

which is the total accumulation of plastic strain during the deformation.

Figure 120 presents the equivalent plastic strain distributions predicted by the finite element calculation for the drawing of the medium carbon steel wire under two percentage area reductions (17% and 30%) and two friction conditions ($\mu = 0.01$ and $\mu = 0.06$).

It can be seen from Figure 120 that the plastic deformation in the wire starts as the material being gradually drawn into the conical mould. The plastic strain increases as the wire receives further area reduction from the die towards the die exit. Shortly after the material comes into the parallel part of the die the plastic strain reaches its maximum value and its distribution pattern remains unchanged further down the drawing line.

Comparing these contours it is easy to identify that under smaller area reduction the maximum equivalent plastic strain exists in the sub-surface area of the drawn wire, refer to Figures 120a and 120c, and under larger area reduction the maximum equivalent plastic strain is found in the surface area of the drawn wire, refer to Figures 120b and 120d. It is also seen that the plastic deformation is much more uniform in the wire under larger area reduction than that under smaller area reduction. With smaller area reduction, the plastic deformation zone extends outside the contact area, Figures 120a and 120c. However, with larger area reduction the non-plastic deformation zone extends inside the contact area, Figures 120b and 120d.

Also from Figure 120 it can be stated that friction has little effect on the general distribution of the plastic strain, nevertheless it increases the maximum value of plastic strain (compare the scales in Figures 120a and 120c, and 120b and 120d).

8.5.3 Mises equivalent stress distributions

The Mises equivalent stress σ_{eq} is defined as

$$\sigma_{eq} = \sqrt{\frac{3}{2}\sigma_{ij}^{'}\sigma_{ij}^{'}} \qquad (8.14)$$

When σ_{eq} reaches the value of material flow stress (or yield stress) plastic deformation begins.

Figure 121 presents the equivalent stress distributions predicted by the finite element calculation for the drawing of the medium carbon steel wire under two percentage area reductions (17% and 30%) and two friction conditions ($\mu = 0.01$ and $\mu = 0.06$).

It is seen from Figure 121 that the von Mises equivalent stress contours extend into the area outside the contact region, which indicates that elastic deformation of the material starts even before the wire makes the contact with the die. The value of equivalent stress increases as the area reduction increases (compare Figure 121a with Figure 121b). The increase of friction does not change the equivalent stress distribution pattern when area reduction is small (compare Figure 121a with Figure 121c), whereas it does when area reduction is large (compare Figure 121b with Figure 121d).

8.5.4 Equivalent pressure stress distributions

The equivalent pressure stress σ_p is defined as

$$\sigma_p = -\frac{1}{3}\sigma_{ii} \qquad (8.15)$$

Hence a positive value indicates the material is subject to compression and a negative one indicates the material is subject to tension.

Figure 122 presents the equivalent pressure stress distributions predicted by the finite element calculation for the drawing of the medium carbon steel wire under two percentage area reductions (17% and 30%) and two friction conditions ($\mu = 0.01$ and $\mu = 0.06$).

It is seen from Figure 122 that the equivalent pressure stress contours also extend outside the contact regions between the wire and the die. This is in good correspondence with the von Mises equivalent stress distributions shown in Figure 121.

It is important to note that the maximum value of the equivalent pressure stress decreases both with the increase of area reduction, compare Figure 122a with 122b and Figure 122c with 122d, and with the increase of friction coefficient, compare Figure 122a with 122c and Figure 122b with 122d.

With smaller area reduction, there is only one maximum equivalent pressure stress area in compression directly underneath the contact surface at the conical part of the die, see Figures 122a and 122c. However, with larger area reduction, there are three distinctive maximum equivalent pressure stress areas, see Figures 122b and 122d, two of them being directly underneath the contact surface at the conical part of the die and one of them being in the centre of the wire near the die exit.

8.5.5 Drawing stresses and comparison with experiment

A systematic finite element analysis of wire drawing process was carried out for the conditions listed in Table 3 in Section 8.4.1 of this chapter, i.e. for two materials, 5 percentage area reductions and 8 friction conditions. The full results of drawing stresses predicted by the finite element calculation are given in Table 4 for the medium carbon steel material and Table 5 for the low carbon steel material. The corresponding drawing stress vs percentage area reduction curves are plotted in Figures 123 and 124 respectively.

It can be clearly seen from Figures 123 and 124 that the drawing stress increases as the percentage area reduction increases. An increase in friction coefficient also results in an increase in drawing stress. Under the same area reduction and the same coefficient of friction, the drawing stress is higher for the medium carbon steel wire than that for the low carbon steel wire.

In general, the drawing stress vs percentage area reduction curves obtained from the finite element calculation are in good agreement with those obtained from the experiment, compare Figures 123 and 124 with Figures 42 to 84 in Chapter 7 and Tables 4 and 5 with Tables D.1 to D.12 in Appendix D. However, by closer examination and comparison of these curves and data of both theory and experiment, the drawing stresses predicted by the finite element analysis best coincide with the experiment when the coefficient of friction is between 0.06 and 0.08 for the medium carbon steel and between 0.08 and 0.10 for the low carbon steel.

Table 4 FE results of drawing stress for medium carbon steel wire drawing.

Finish Dia. (mm)	Area Re. (%)	Drawing Stress (N/mm^2)							
		μ= 0.000	μ= 0.005	μ= 0.010	μ= 0.020	μ= 0.040	μ= 0.060	μ= 0.080	μ= 0.100
5	17	168	188.2	196.6	208.8	234.3	263.5	288.2	310.1
4.9	21	214	223.8	230.2	245.5	277.2	304.0	331.2	356.9
4.8	24	245	249.0	251.4	271.2	310.1	334.7	376.8	403.4
4.7	27	272	281.7	291.0	311.0	345.4	379.7	410.8	444.7
4.6	30	314	320.9	332.6	354.8	393.7	431.5	462.5	495.3

Table 5 FE Results of drawing stress for low carbon steel wire drawing.

Finish Dia (mm)	Area Re (%)	Drawing Stress (N/mm^2)									
		μ= 0.000	μ= 0.005	μ= 0.010	μ= 0.020	μ= 0.030	μ= 0.040	μ= 0.050	μ= 0.060	μ= 0.080	μ= 0.100
5	17	100	102.9	108.8	115.2	120.0	127.2	137.6	145.1	158.7	171.3
4.9	21	119	123.2	128.3	135.8	145.9	154.7	161.6	170.0	185.4	198.5
4.8	24	135	144.1	145.9	157.6	165.7	177.3	187.4	195.9	212.9	228.5
4.7	27	153	158.3	163.9	175.7	185.0	196.0	208.7	214.7	235.7	253.7
4.6	30	177	182.2	189.4	201.0	211.2	223.1	233.8	243.5	259.3	276.8

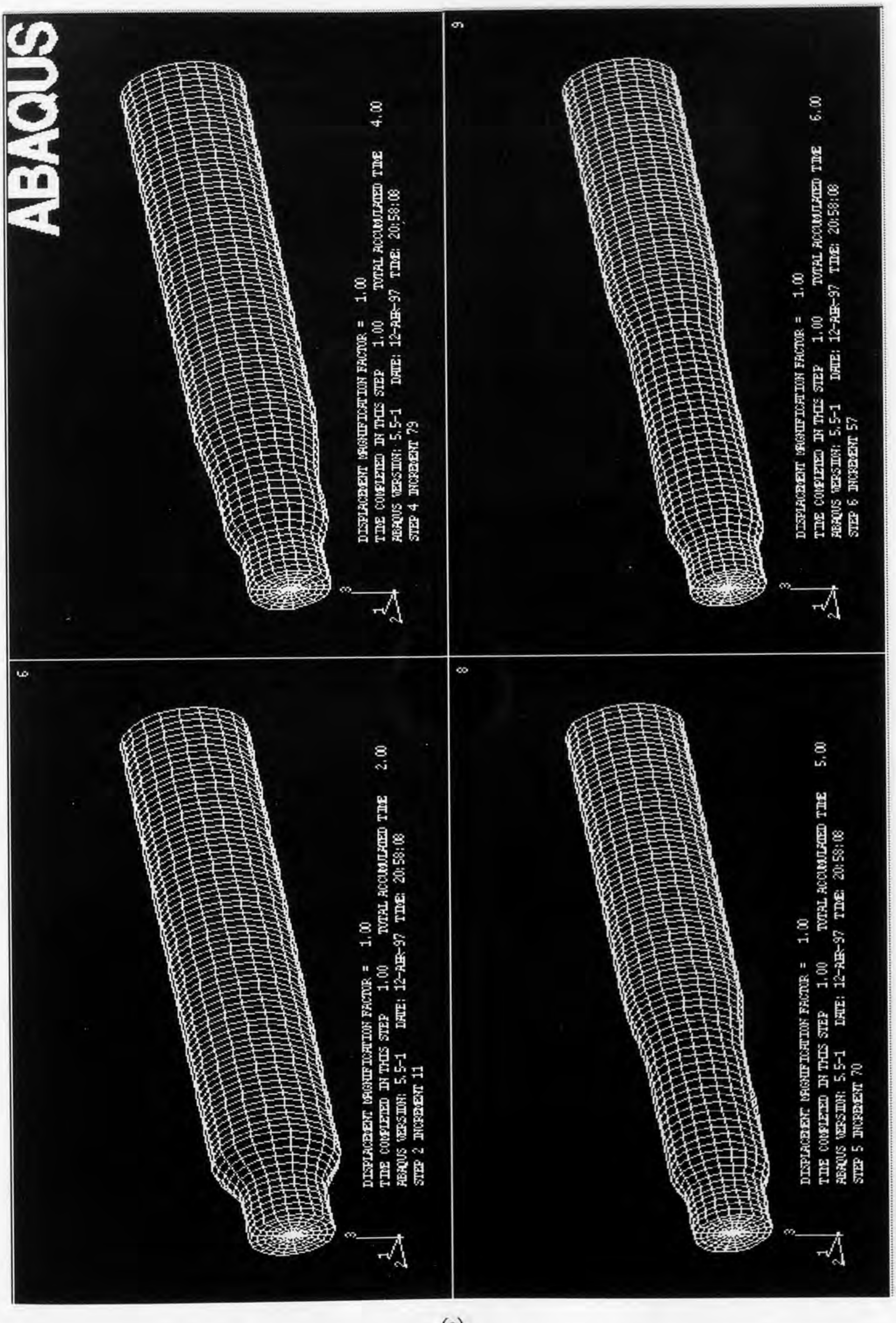

(a)

Fig. 115 Three–dimensional initial and deformed finite element meshes.

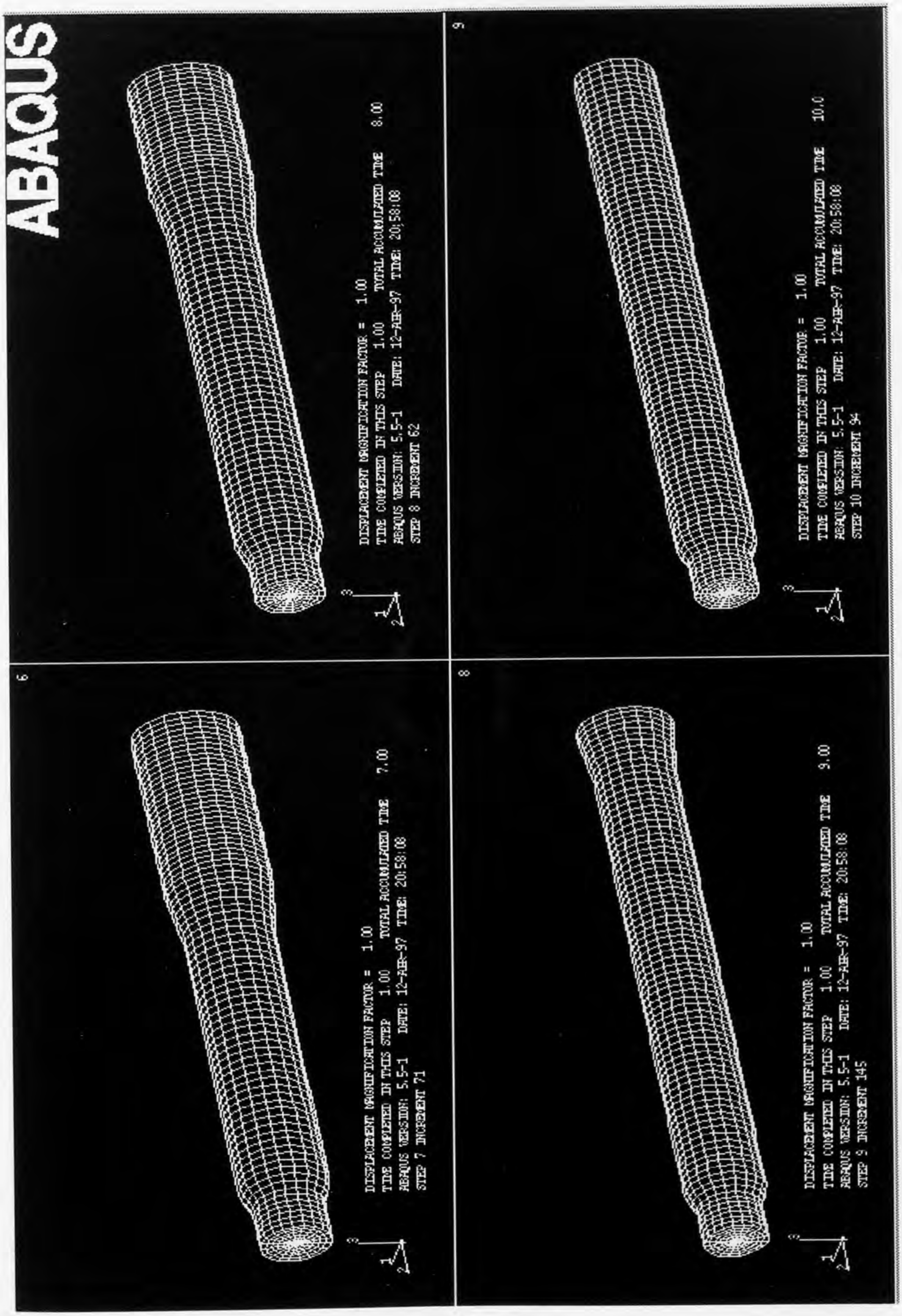

(b)

Fig. 115 Continued.

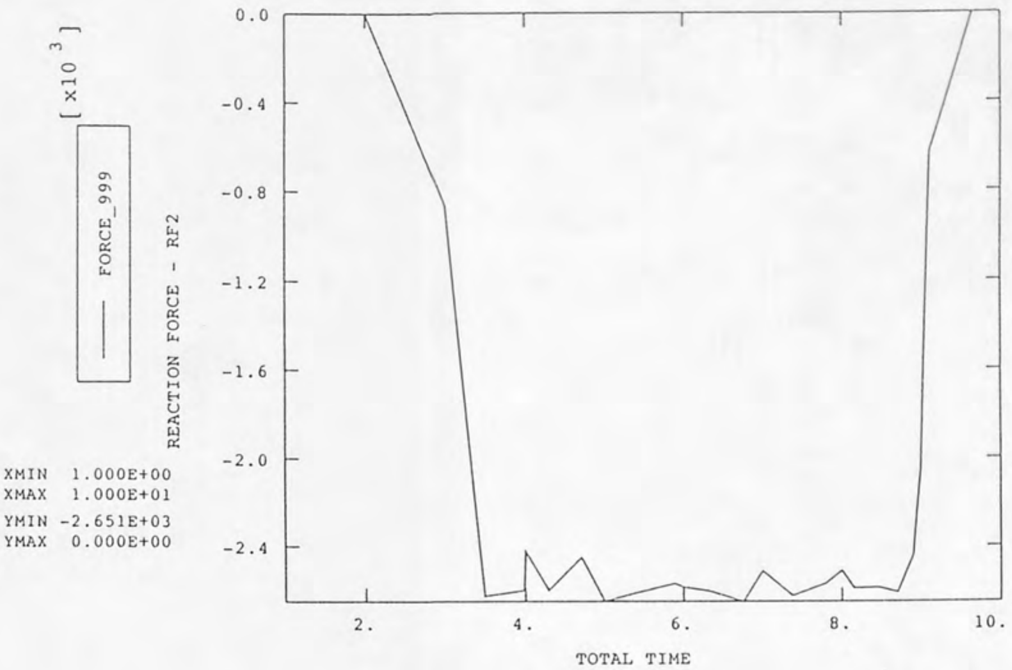

Fig. 116 Drawing load vs drawing time curve predicted by the finite element simulation: d_o = 5.5 mm, d_1 = 4.7 mm, μ = 0.01; low carbon steel.

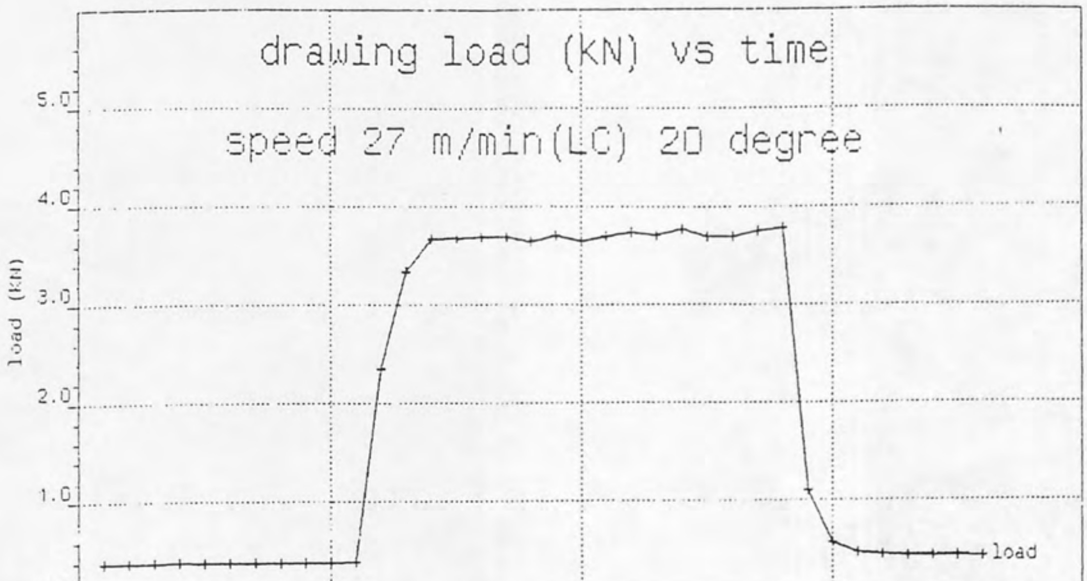

Run C:\PIC02\DR97241: collected 10:06 on 17Apr97

Fig. 117 Typical drawing load vs drawing time curve recorded in the experiment: d_o = 5.5 mm, d_1 = 4.7 mm, speed = 27 mm/min; low carbon steel ; lubricant: Traxit.

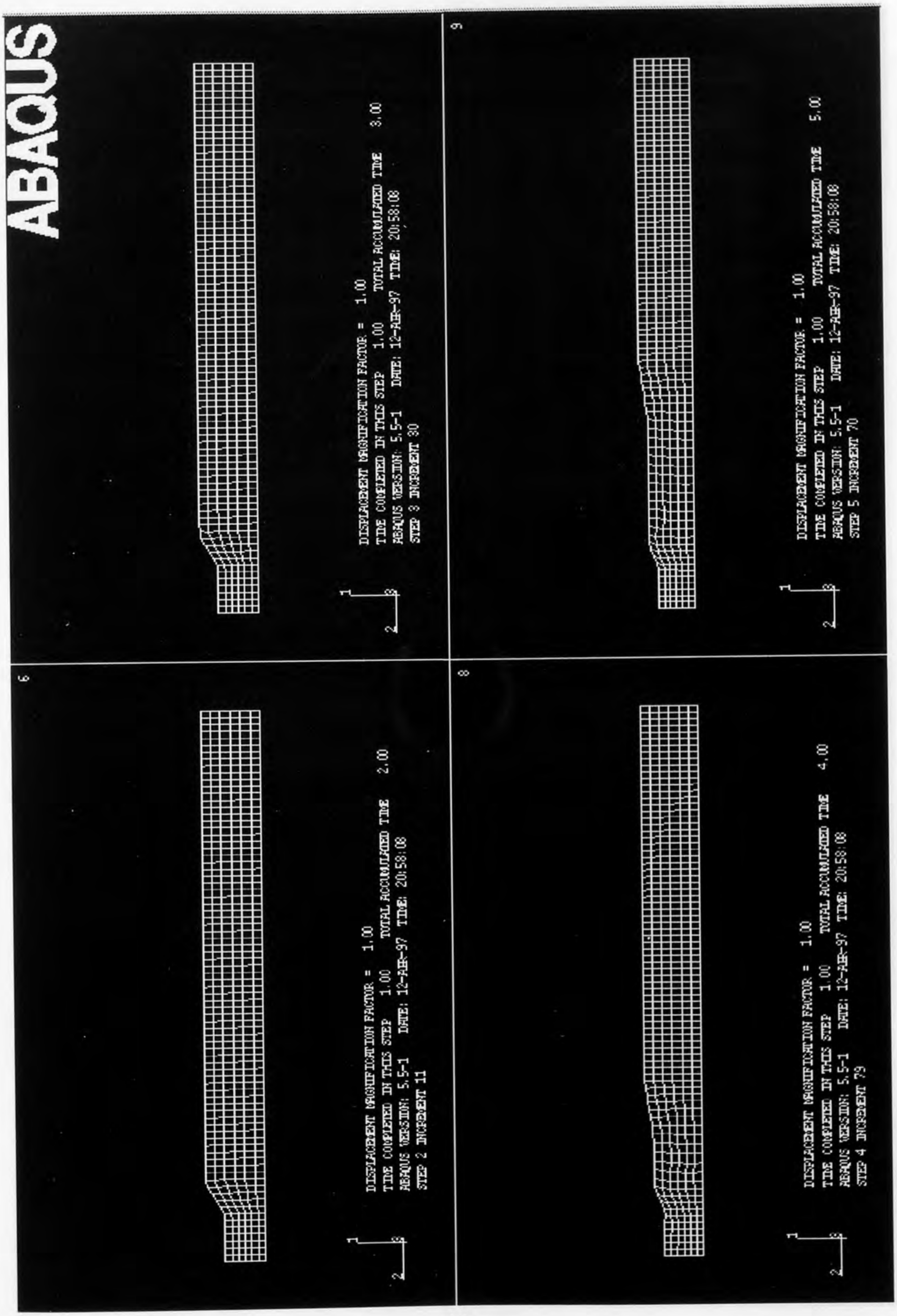

(a)

Fig. 118 Typical incremental deformation procedure of the mesh from the finite element analysis.

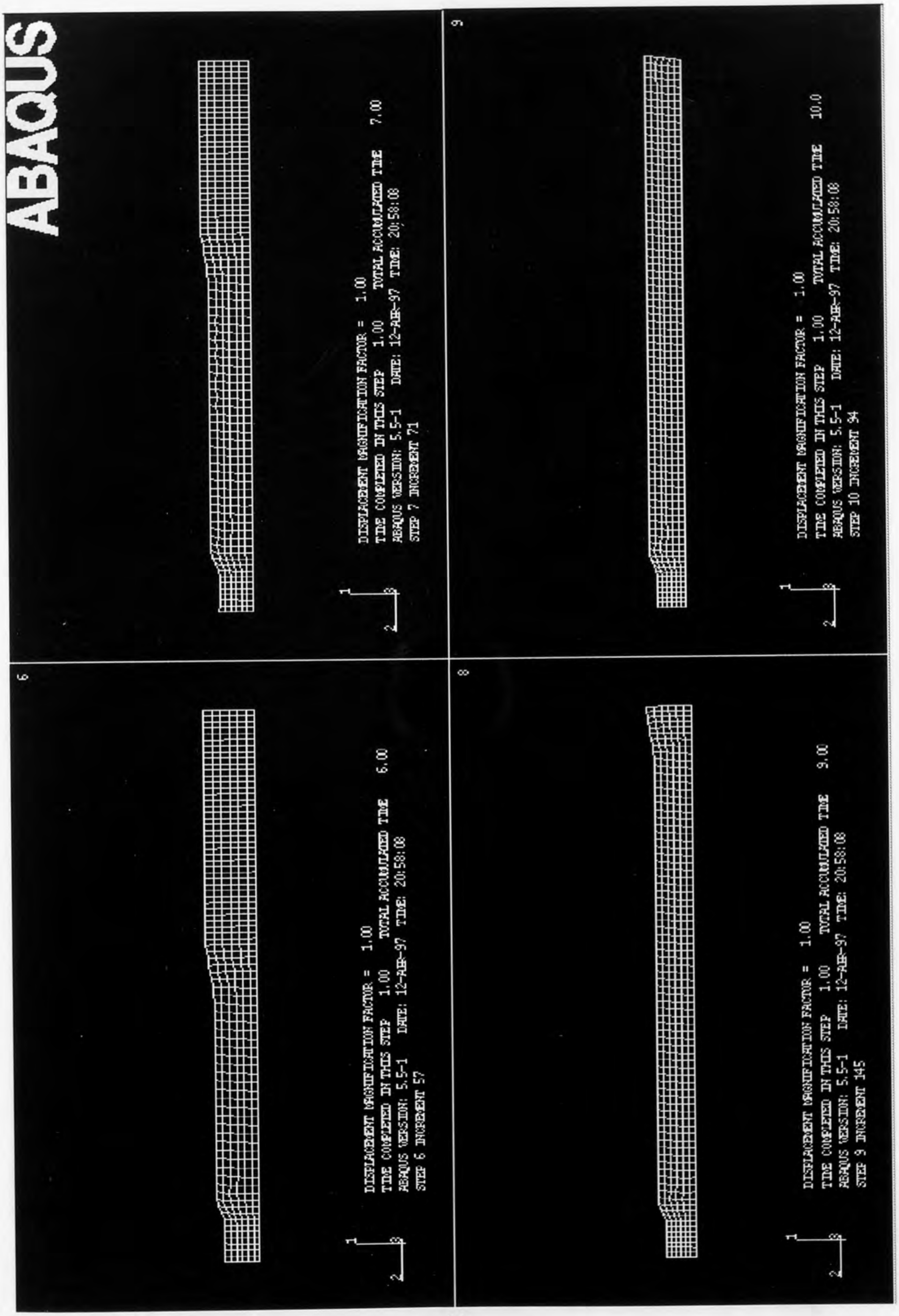

```
DISPLACEMENT MAGNIFICATION FACTOR =  1.00
TIME COMPLETED IN THIS STEP   1.00    TOTAL ACCUMULATED TIME    6.00
ABAQUS VERSION: 5.5-1    DATE: 12-AUG-97  TIME: 20:58:08
STEP 6 INCREMENT 57
```

```
DISPLACEMENT MAGNIFICATION FACTOR =  1.00
TIME COMPLETED IN THIS STEP   1.00    TOTAL ACCUMULATED TIME    7.00
ABAQUS VERSION: 5.5-1    DATE: 12-AUG-97  TIME: 20:58:08
STEP 7 INCREMENT 71
```

```
DISPLACEMENT MAGNIFICATION FACTOR =  1.00
TIME COMPLETED IN THIS STEP   1.00    TOTAL ACCUMULATED TIME    9.00
ABAQUS VERSION: 5.5-1    DATE: 12-AUG-97  TIME: 20:58:08
STEP 9 INCREMENT 145
```

```
DISPLACEMENT MAGNIFICATION FACTOR =  1.00
TIME COMPLETED IN THIS STEP   1.00    TOTAL ACCUMULATED TIME    10.0
ABAQUS VERSION: 5.5-1    DATE: 12-AUG-97  TIME: 20:58:08
STEP 10 INCREMENT 94
```

(b)

Fig. 118 Continued.

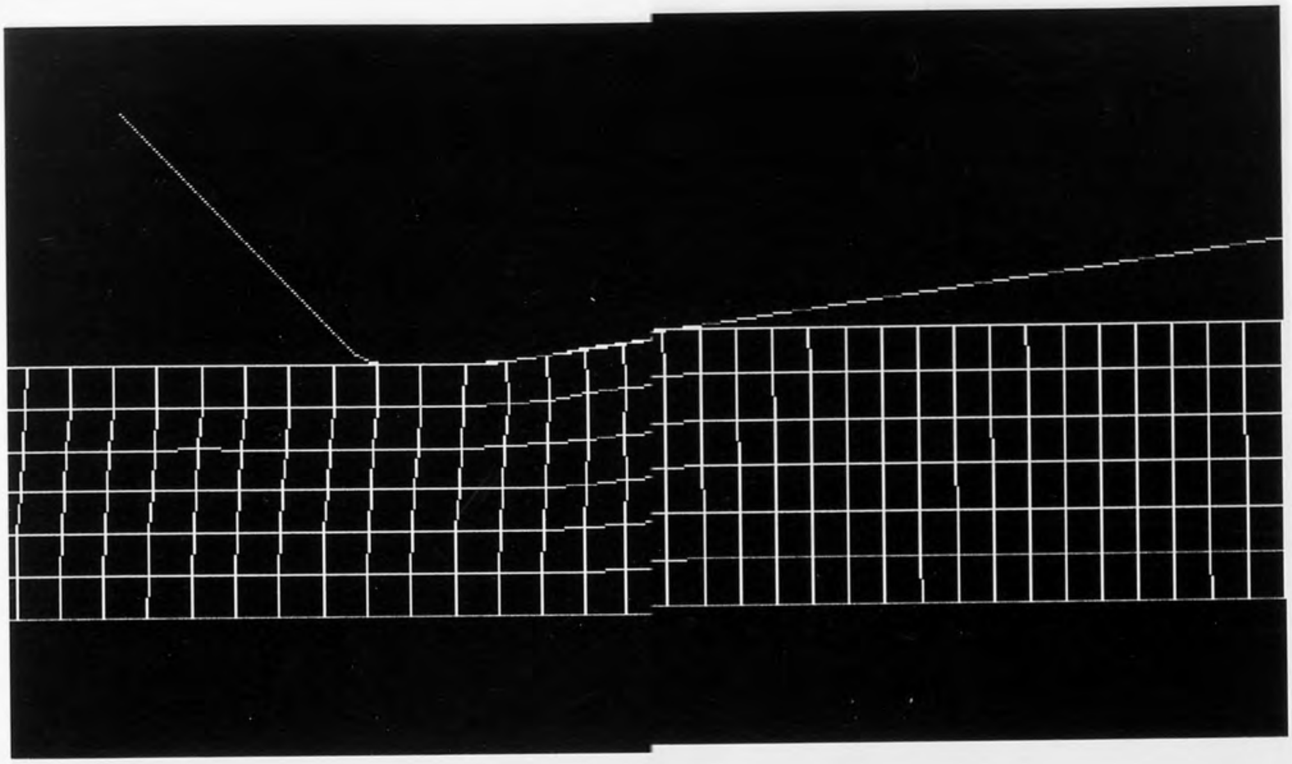

(a) D = 5.5 mm, d = 5.0 mm and $\mu = 0.01$.

(b) D = 5.5 mm, d = 4.6 mm and $\mu = 0.01$.

Fig. 119 Distorted meshes obtained from the finite element analysis of wire drawing under different percentage area reductions.

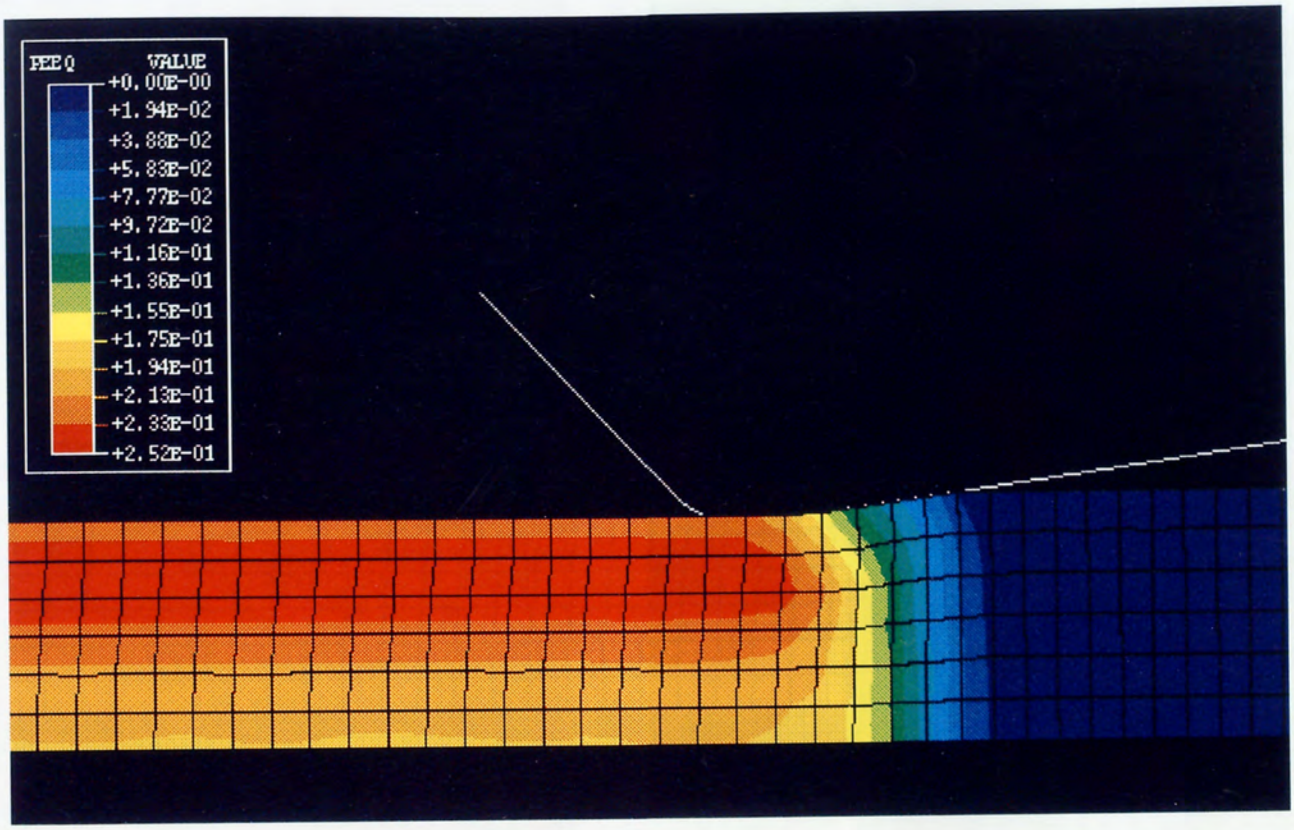

(a) D = 5.5 mm, d = 5.0 mm and $\mu = 0.01$.

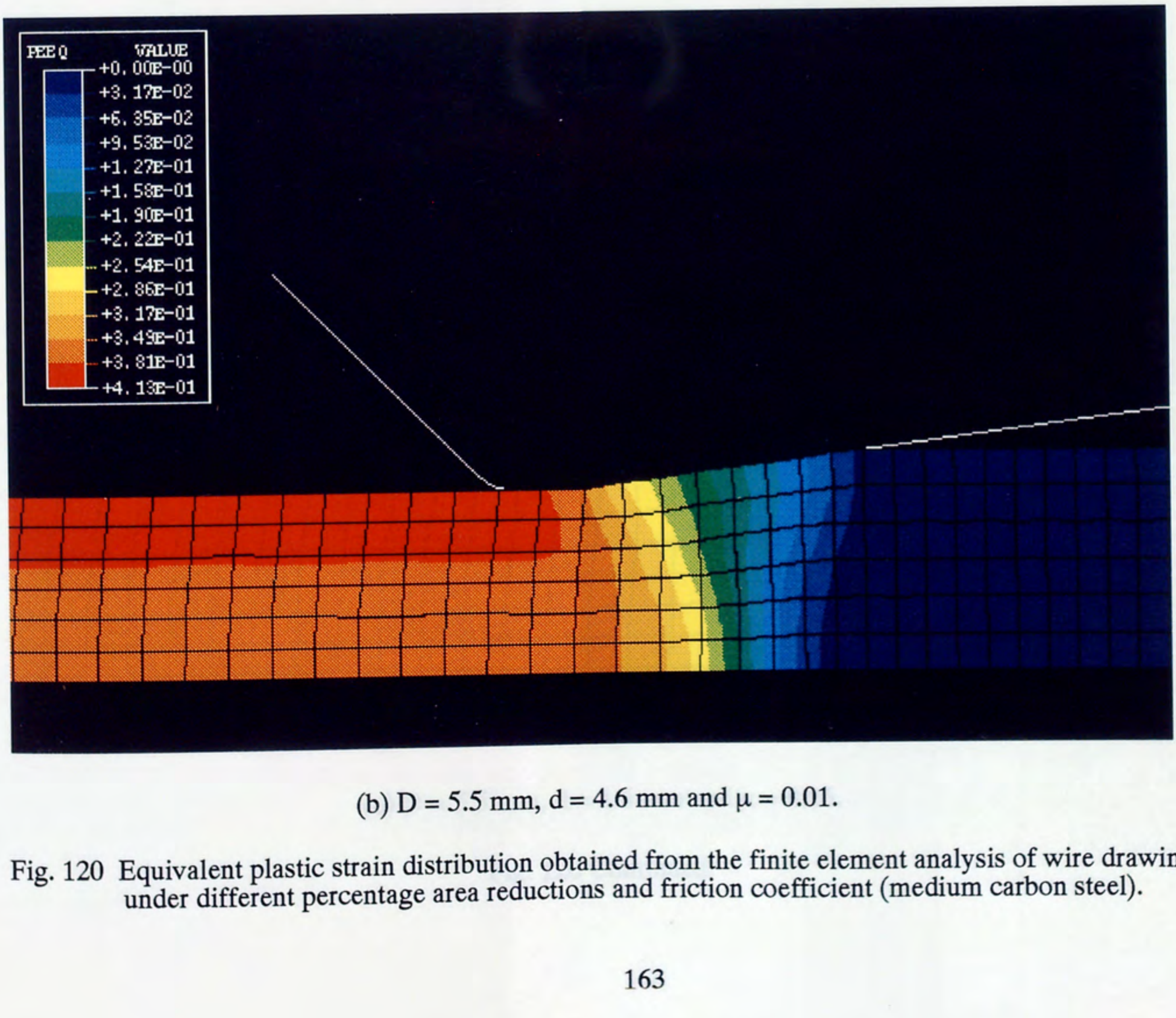

(b) D = 5.5 mm, d = 4.6 mm and $\mu = 0.01$.

Fig. 120 Equivalent plastic strain distribution obtained from the finite element analysis of wire drawing under different percentage area reductions and friction coefficient (medium carbon steel).

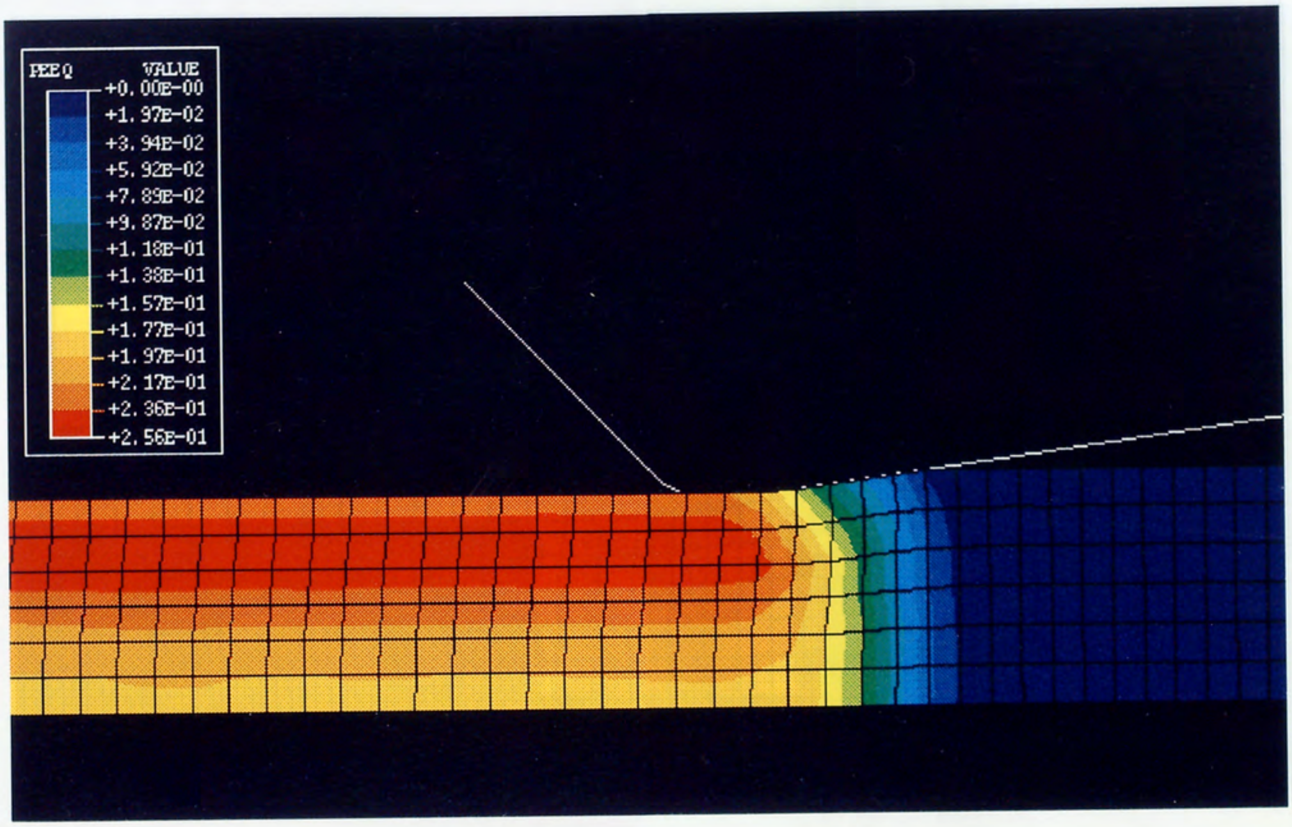

(c) D = 5.5 mm, d = 5.0 mm and μ = 0.06.

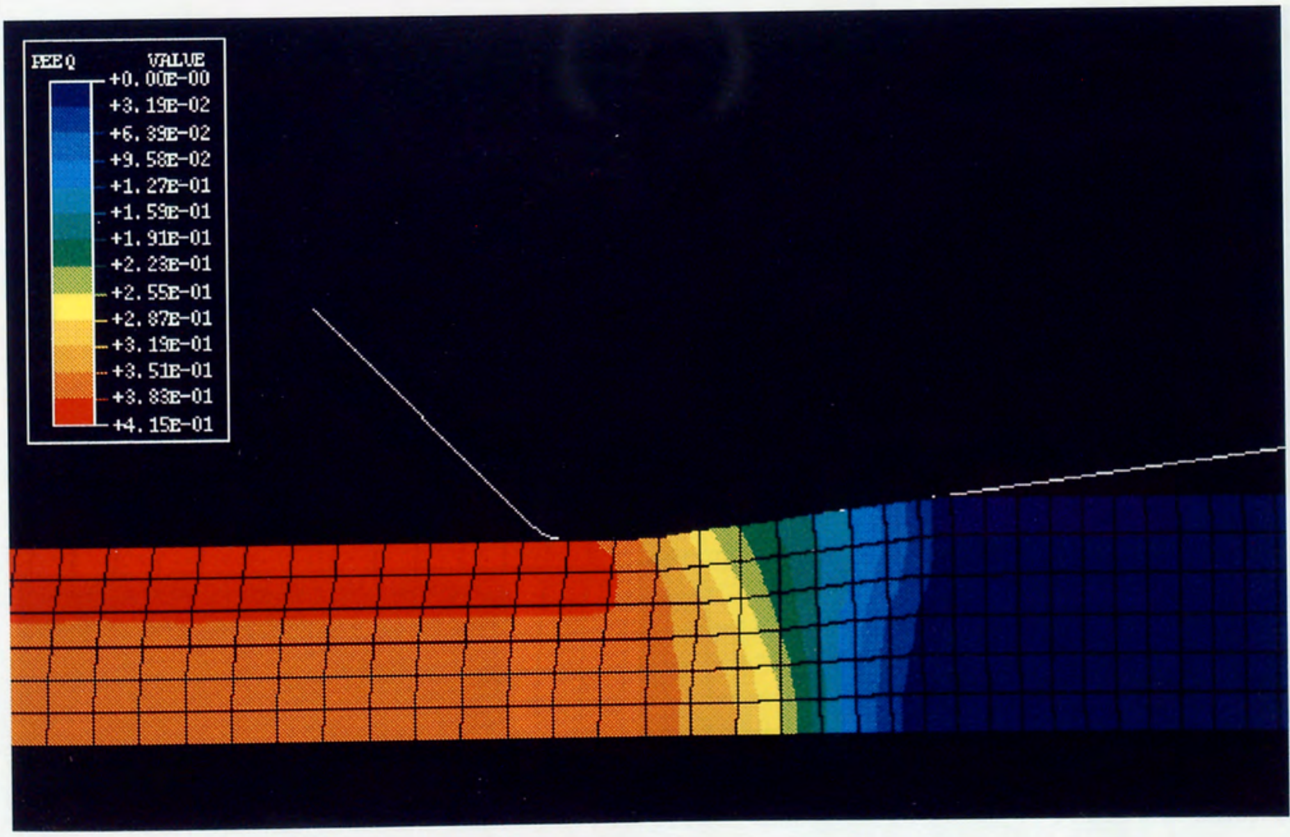

(d) D = 5.5 mm, d = 4.6 mm and μ = 0.06.

Fig. 120 Continued.

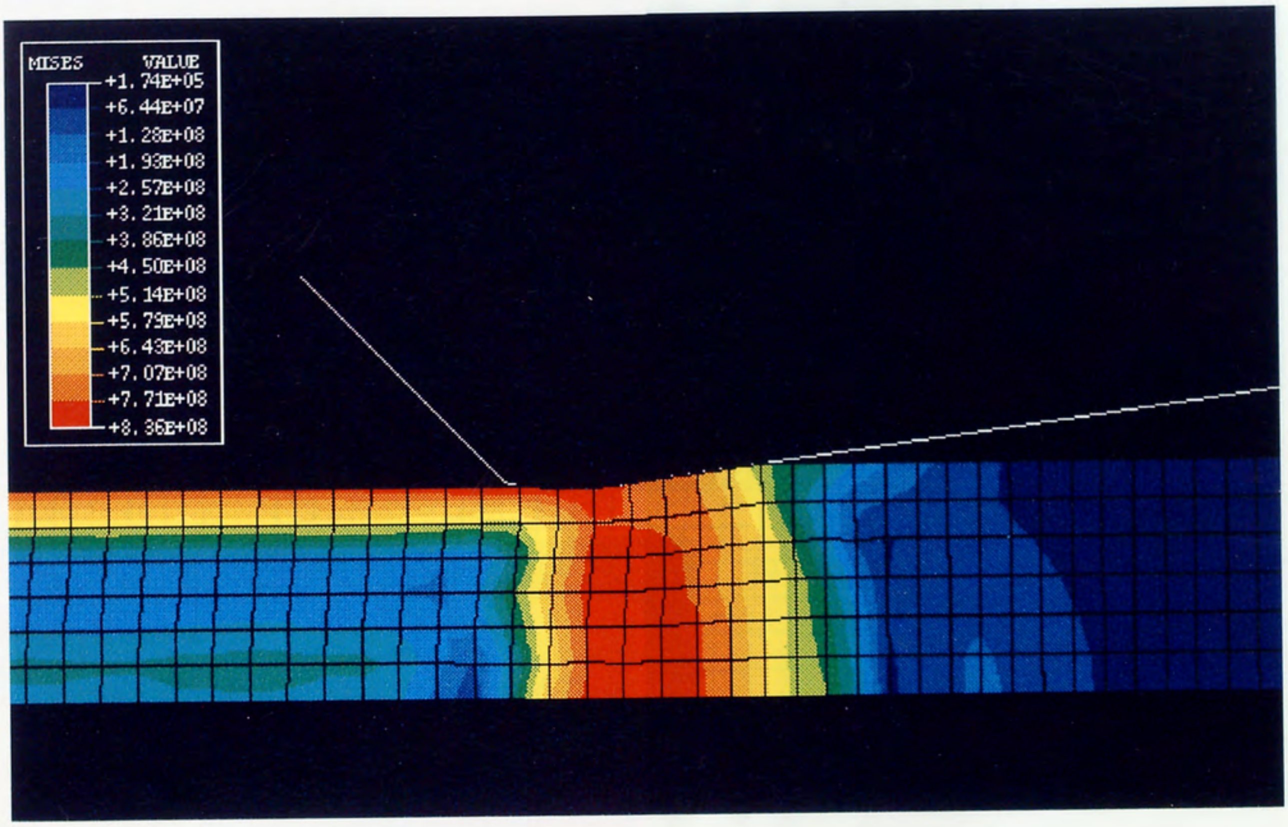

(a) D = 5.5 mm, d = 5.0 mm and $\mu = 0.01$.

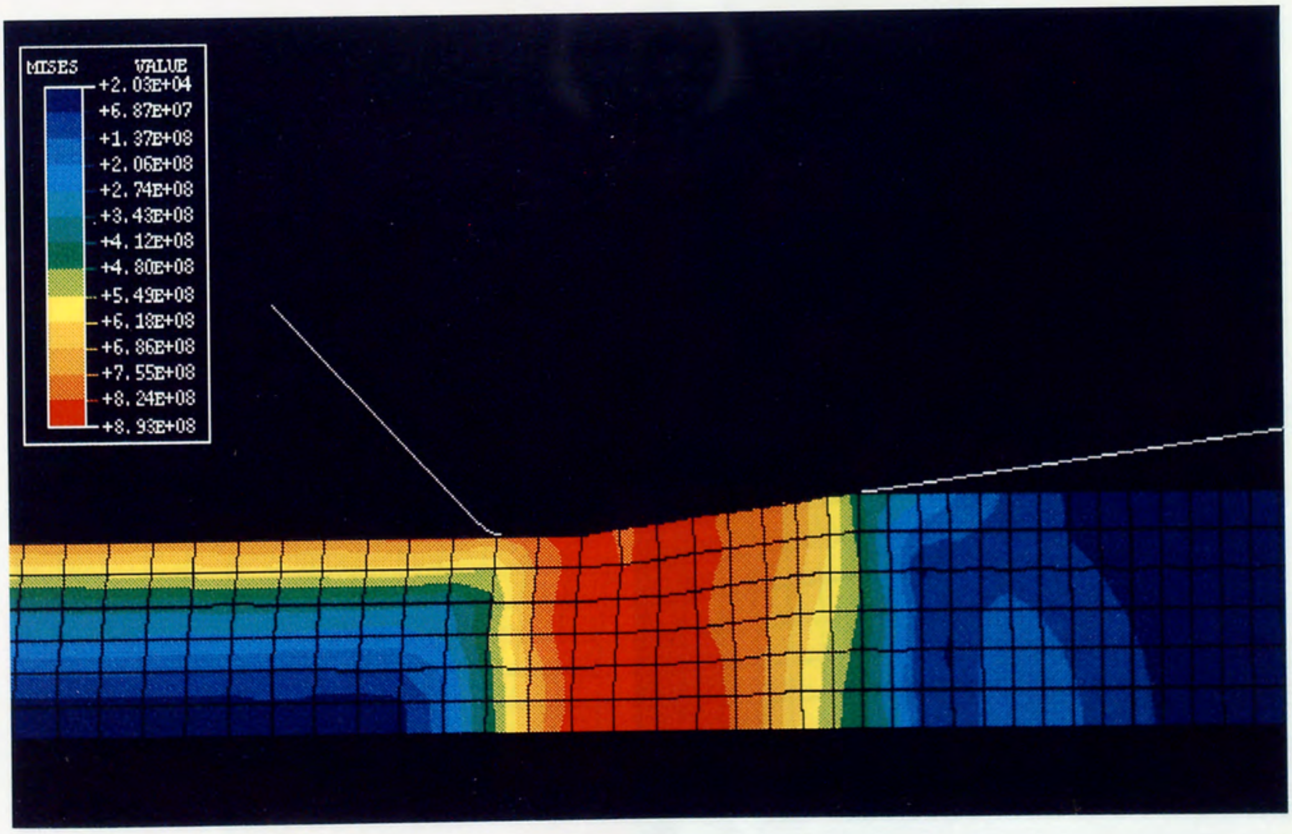

(b) D = 5.5 mm, d = 4.6 mm and $\mu = 0.01$.

Fig. 121 Mises equivalent stress distribution obtained from the finite element analysis of wire drawing under different percentage area reductions and friction coefficient (medium carbon steel).

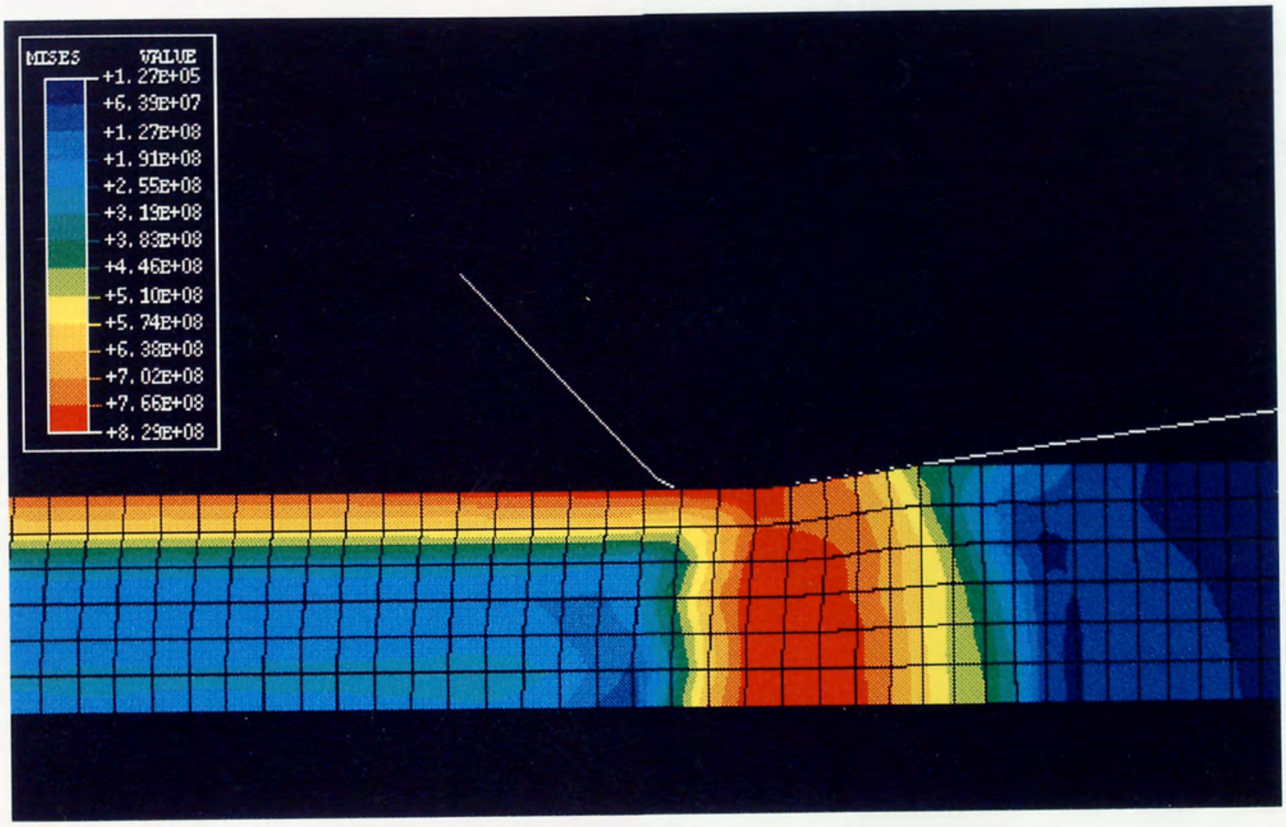

(c) D = 5.5 mm, d = 5.0 mm and μ = 0.06.

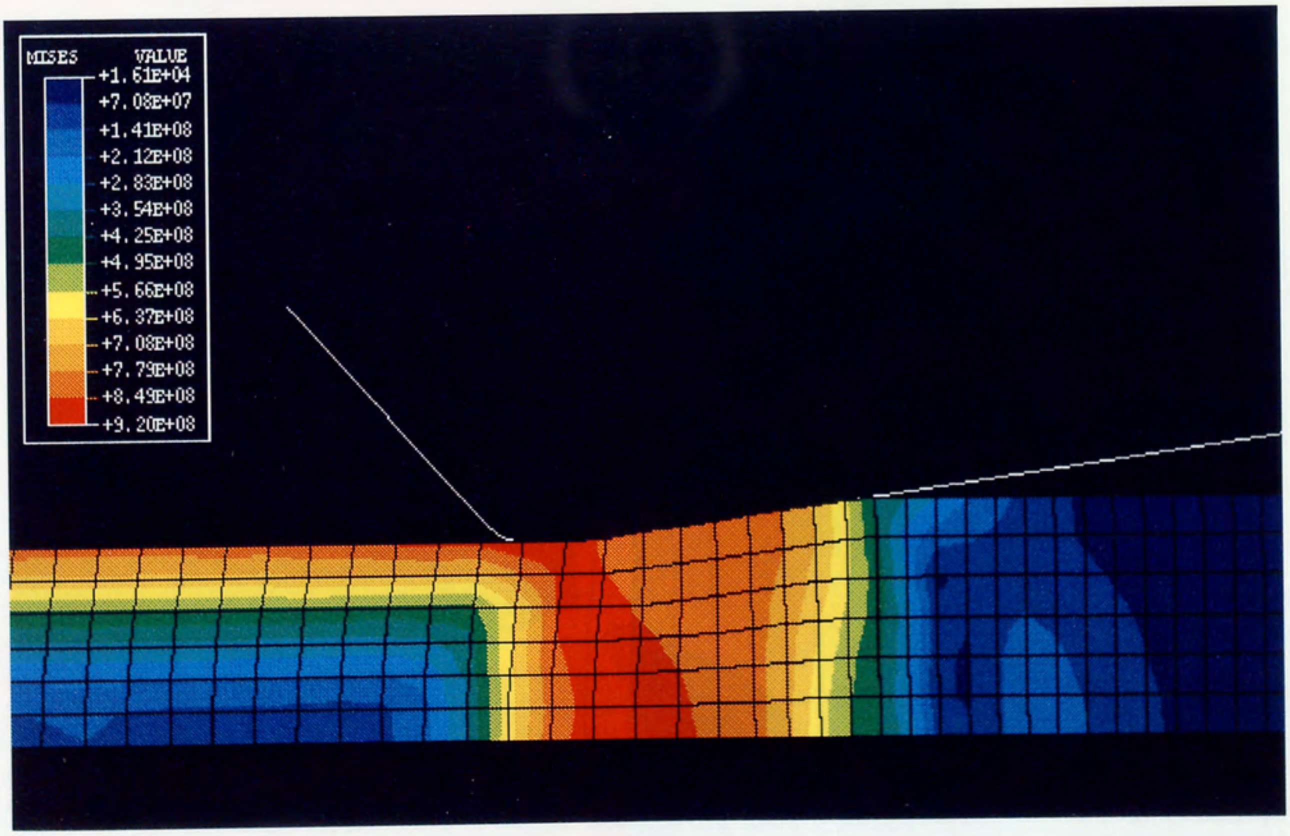

(d) D = 5.5 mm, d = 4.6 mm and μ = 0.06.

Fig. 121 Continued.

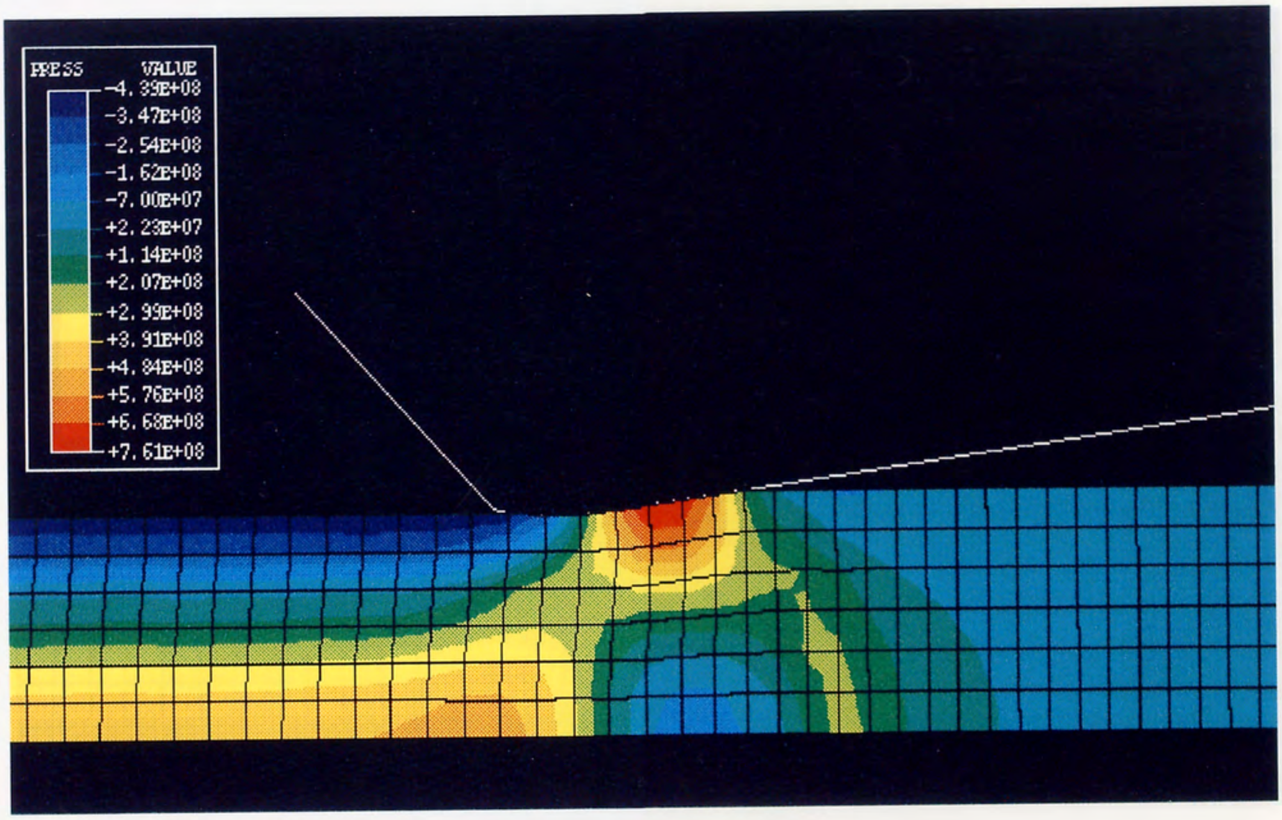

(a) D = 5.5 mm, d = 5.0 mm and μ = 0.01.

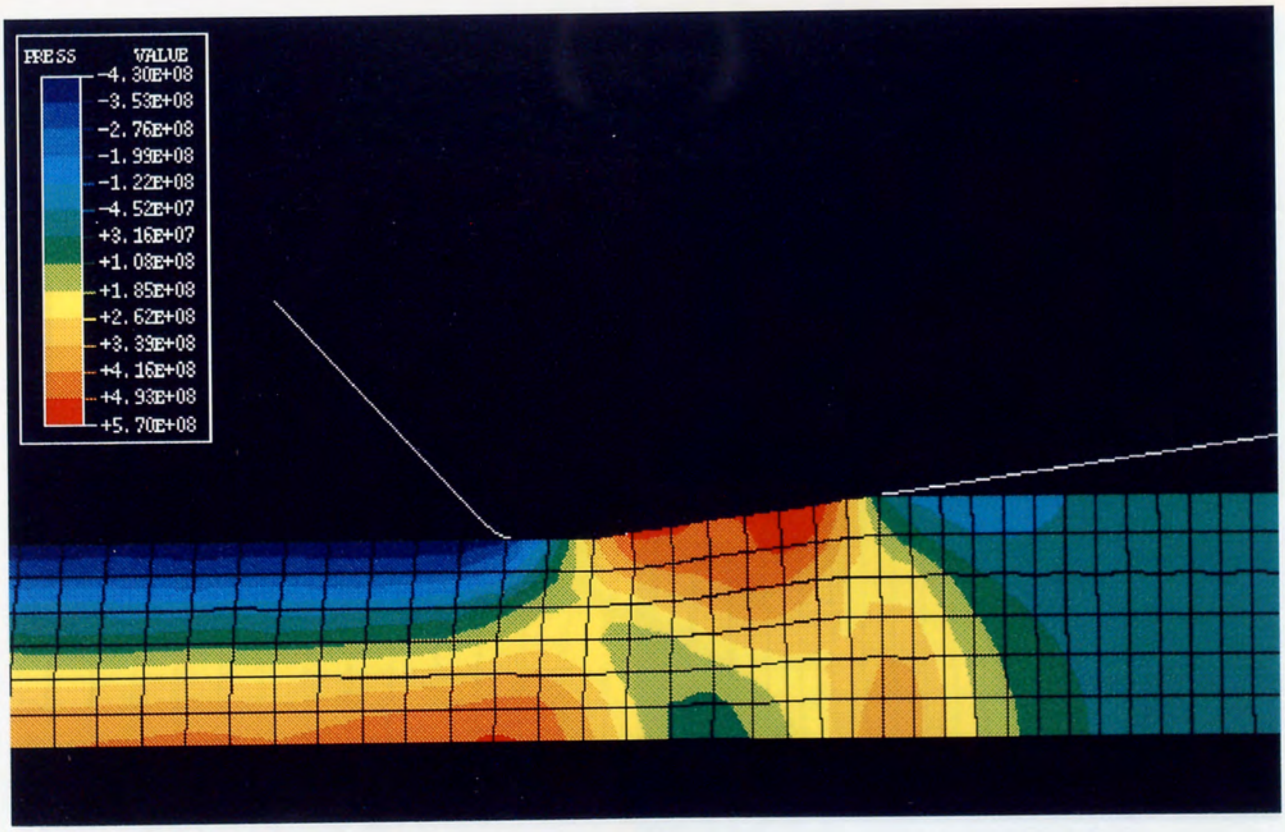

(b) D = 5.5 mm, d = 4.6 mm and μ = 0.01.

Fig. 122 Equivalent pressure stress distribution obtained from the finite element analysis of wire drawing under different percentage area reductions and friction coefficient (medium carbon steel).

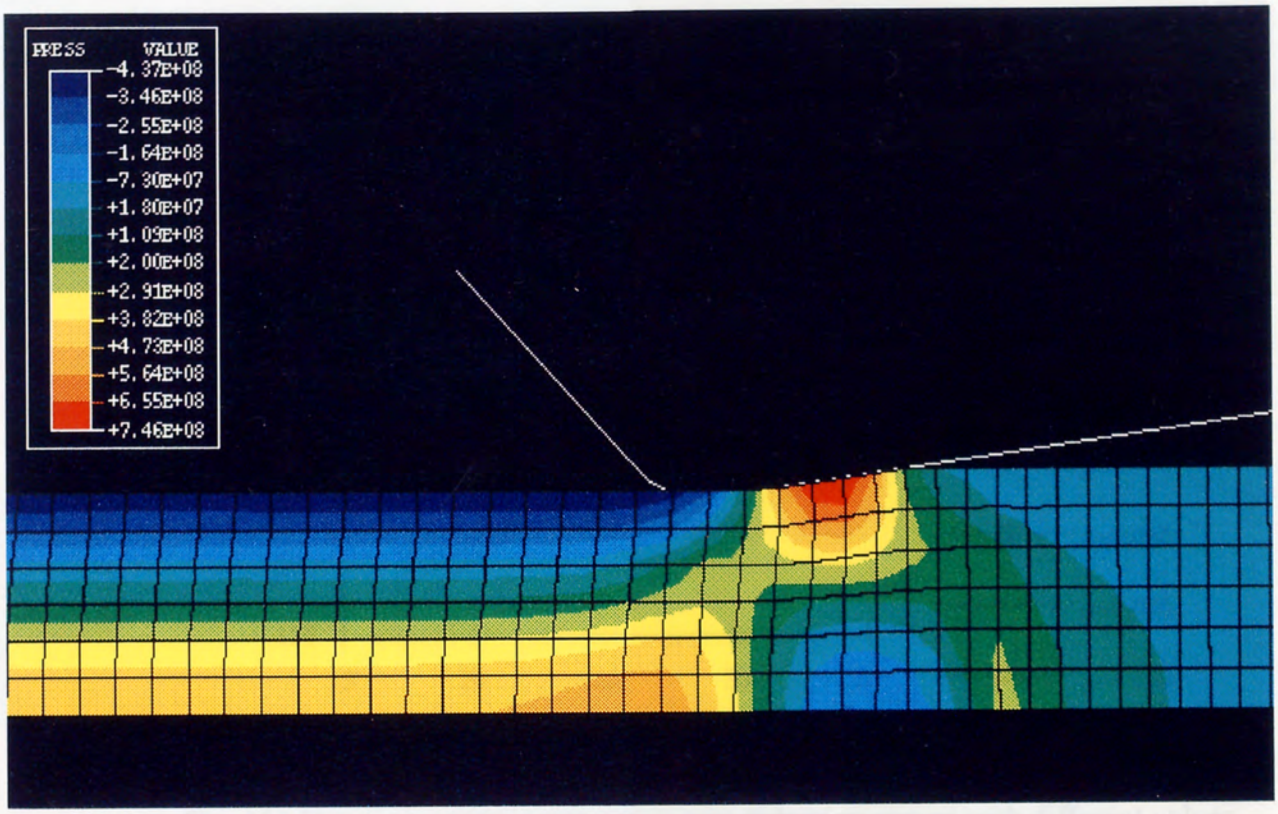

(c) D = 5.5 mm, d = 5.0 mm and μ = 0.06.

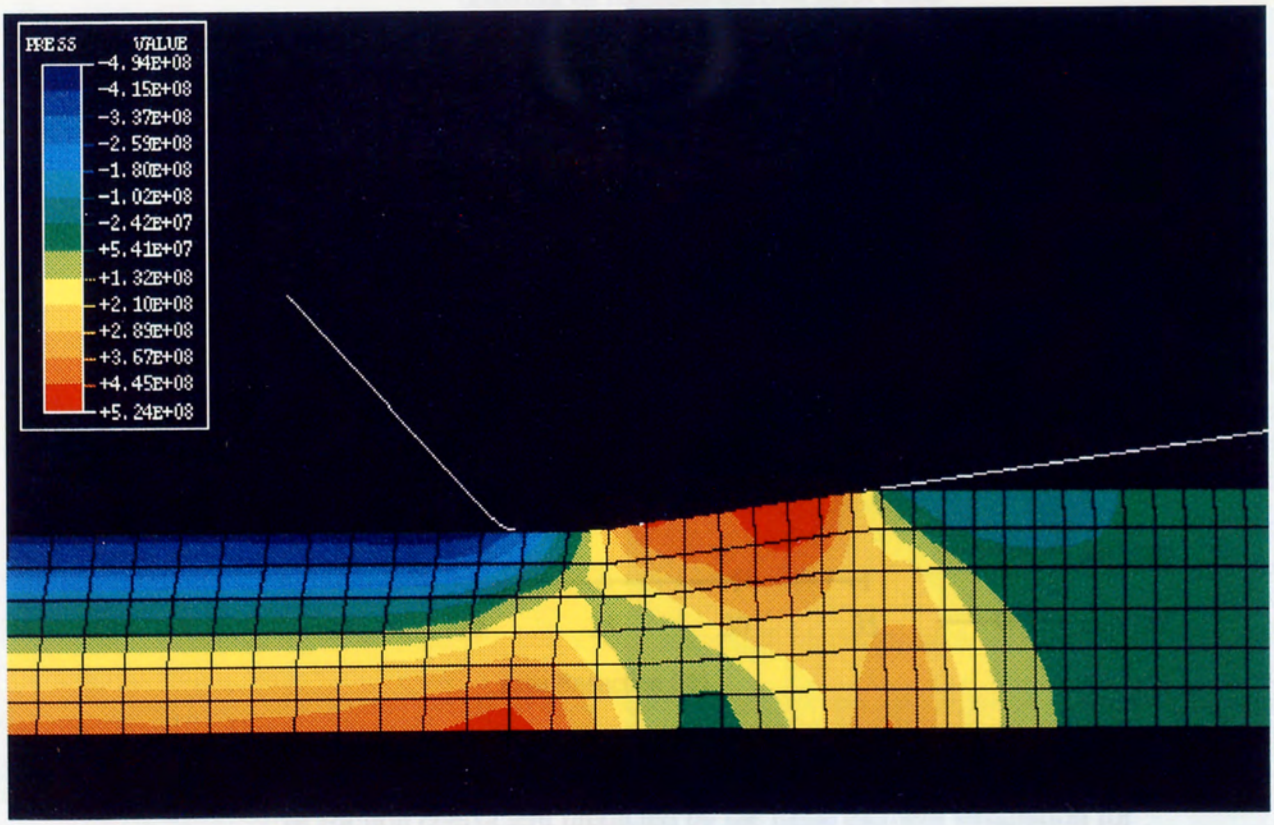

(d) D = 5.5 mm, d = 4.6 mm and μ = 0.06.

Fig. 122 Continued.

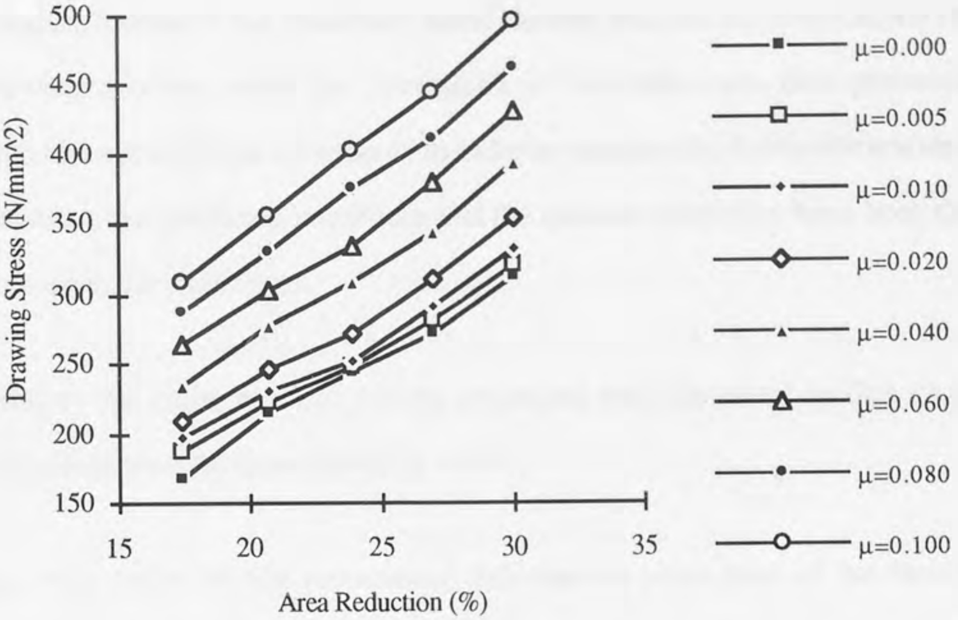

Fig. 123 Drawing stress vs percentage area reduction curves with different values of friction coefficient predicted by the finite element simulation for drawing of medium carbon steel wire.

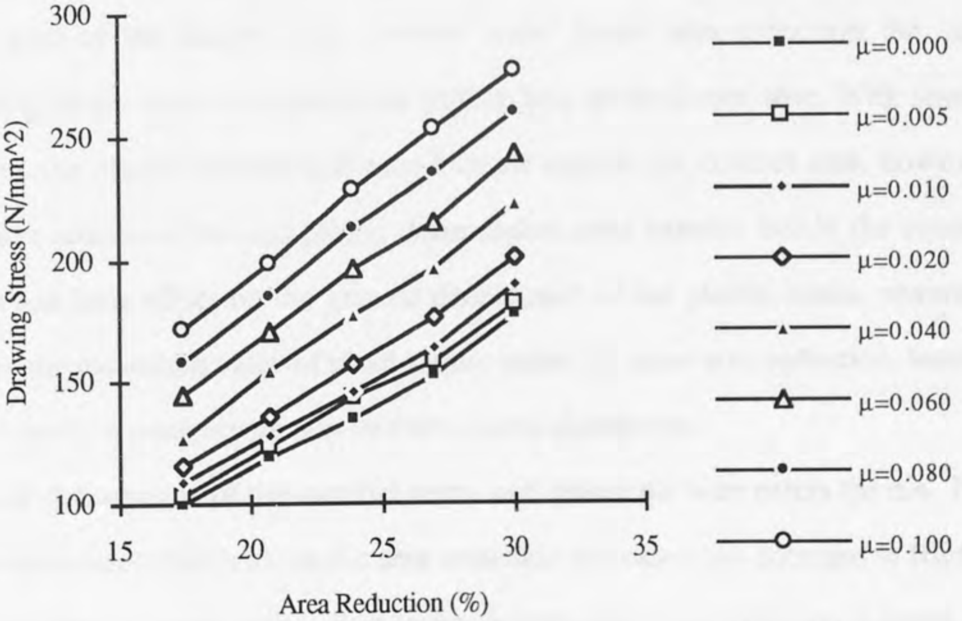

Fig. 124 Drawing stress vs percentage area reduction curves with different values of friction coefficient predicted by the finite element simulation for drawing of low carbon steel wire.

8.6 Summary

In this chapter, a detailed and systematic finite element analysis has been carried out for the wire drawing process under the conditions of two materials, five percentage area reductions and eight friction conditions. In order to compare the finite element results with the experiment, the geometric conditions and the material properties have been chosen the same as those in the experiment.

According to the finite element results presented and discussed in this chapter, the following points were deduced should be noted:

(1) It has been shown by the incremental deformation procedures of the finite element meshes in both 2D and 3D that the simulated process is very realistic and representative compared with reality. It has been shown that bigger area reduction causes larger element elongation, greater mesh distortion and longer contact area.

(2) Under smaller area reduction, the maximum equivalent plastic strain exists in the sub-surface area of the drawn wire, whereas under larger area reduction the maximum equivalent plastic strain is found in the surface area of the drawn wire. With smaller area reduction, the plastic deformation zone extends outside the contact area, however, with larger area reduction the non-plastic deformation zone extends inside the contact area. Friction has little effect on the general distribution of the plastic strain, nevertheless it increases the maximum value of plastic strain under the same area reduction, hence higher friction results in more severe non-uniform plastic distribution.

(3) Elastic deformation of the material starts well before the wire enters the die. The value of equivalent stress increases as the area reduction increases. An increase in friction does not change the equivalent stress distribution pattern when area reduction is small, whereas it does when the area reduction is large.

(4) The maximum value of the equivalent pressure stress decreases both with the increase of area reduction and with the increase of friction coefficient.

(5) The drawing stress vs percentage area reduction curves obtained from the finite element calculation are generally in good agreement with those obtained from the experiment. However, the drawing stresses predicted by the finite element analysis best coincide with the experiment when the coefficient of friction is between 0.06 and 0.08 for the medium carbon steel and between 0.08 and 0.10 for the low carbon steel.

(6) It is noticed that strain rate or drawing speed effect has not been taken into account in the finite element analysis carried out and presented in this chapter. This is based on the understanding that for metal forming conducted at room temperature and low strain rate, such as the wire drawing tests performed in this study, the strain rate effect on the flow behaviour of the deforming body is small, if any. On the other hand, the finite element analysis is also restricted by the availability of flow stress-strain data at lower strain rate. Therefore so far most publications on finite element analysis of conventional metal forming processes under room temperature have ignored strain rate as well as temperature effects.

CHAPTER NINE

CONCLUSIONS AND SUGGESTIONS FOR FUTURE WORK

9.1 Conclusions

From the research carried out in this study, the following conclusions can be drawn:

(1). The die box and the pressure die nozzle system designed and used in this study have functioned well throughout the drawing experiments conducted. Hydrodynamic lubrication with dry lubricants has been realised successfully.

(2). Under the current experimental conditions, the Traxit lubricant had a higher lubrication efficiency in terms of reducing drawing stress.

(3). With the Condat Vicafil lubricant, the drawing stress was consistently low when the pressure nozzle semi-angle was equal to 8 degrees under all of the current experimental conditions for both the drawn materials under consideration, however with the Traxit lubricant the drawing stress was less sensitive to pressure nozzle semi-angle.

(4). It was found that, although it is difficult to determine which drawing speed gives the best result in terms of best lubrication performance and minimum drawing stress, the drawing stresses are least scattered when the pressure nozzle semi-angle is equal to 8 degrees under all the current experimental conditions. The drawing stress does show variation under different drawing speeds which can be related to the strain rate effect on the flow stress of the drawn material. However, for the conditions (room temperature and low strain rate) under which the experiments were carried out, the strain rate effect on flow stress is small. Therefore, the variation of drawing stress under different drawing speeds is believed to be dominated by the effect of drawing speed on the friction and lubrication characteristics of different lubricants, which bears a more complicated nature.

(5). The SEM examination shows the existence of the residual lubricant layer on the surface of the drawn wire, the thickness of the residual lubricant layer of the Traxit lubricant on the drawn wire is between 4.1 μm and 18.5 μm and the thickness of the residual lubricant layer of the Condat Vicafil lubricant on the drawn wire is in the range of 4.7 μm and 13.1 μm.

(6). It has been shown by the incremental deformation procedures of the finite element meshes in both 2D and 3D that the simulated process is very realistic and representative. It has been shown that larger area reduction causes larger element elongation, greater mesh distortion and longer contact area.

(7). Under smaller area reduction the maximum equivalent plastic strain exists in the sub-surface area of the drawn wire, whereas under larger area reduction the maximum equivalent plastic strain is found in the surface area of the drawn wire. With smaller area reduction the plastic deformation zone extends outside the contact area. However, with larger area reduction the non-plastic deformation zone extends inside the contact area. Friction has little effect on the general distribution of the plastic strain, nevertheless it increases the maximum value of plastic strain under the same area reduction, hence higher friction results in more severe non-uniform plastic distribution.

(8). The elastic deformation of the material starts well before the wire enters the die. The value of equivalent stress increases as the area reduction increases. The increase of friction does not change the equivalent stress distribution pattern when area reduction is small, whereas it does when area reduction is large.

(9). The maximum value of the equivalent pressure stress decreases both with the increase of area reduction and with the increase of friction coefficient.

(10). The drawing stress vs percentage area reduction curves obtained from the finite element calculation were generally in good agreement with those obtained by experiment. However, the drawing stresses predicted by the finite element analysis best coincide with the experiment when the coefficient of friction is between 0.06 and 0.08 for the medium carbon steel and between 0.08 and 0.10 for the low carbon steel.

9.2 Suggestions for Future Work

It is felt that future research work continuing this study should be carried out on the following aspects:

(1). The methodology adopted in this study for friction and evaluation of lubrication efficiency should be used for evaluating the performance of other lubricants in wire drawing.

(2). Further experimental tests should be carried out using dies with different inlet semi-angles to evaluate the effect of die semi-angle on lubrication efficiency.

(3). The pressure die box assembly designed in this study is efficient and easy to manufacture, therefore further work should be done so that it can be adopted for an industrial production line.

(4). The effect of drawing speed on the efficiency of lubrication during wire drawing using dry lubricant should be investigated further.

(5). The strain rate effect on flow stress of steel should be thoroughly investigated, particularly for lower strain rate (<100/s), in order to complement the completeness of understanding of the flow behaviour under normal metal forming processes.

(6). The SEM technique should be combined with drawing experiment to further investigate the effect of different lubrication conditions on die life and the quality of the finished wire.

(7). Further finite element simulation should be carried out to look at more parameters, such as strain rate and temperature, and their interactive effects on drawing stress and residual stress in drawn wire. Ultimately, finite element analysis should be used to reduce the amount of experimental work in the research of wire drawing as well as other metal forming processes.

REFERENCES

1. Loh, N. H., 1983. The Mechanics of Drawing Wire at Elevated Temperature. PhD thesis, Aston University.
2. Rowe, G. W., 1977. Principles of Industrial Metal Working Processes. Edward Arnold, London.
3. Avitzur, B., 1968. Metal Forming: Processes and Analysis. McGraw-Hill, New York.
4. Jornaz, M. I., 1990. The Mechanics of the Drawing of Polygonal Sections from Round at Elevated Temperatures. PhD thesis, Aston University.
5. Owen, D. R. J. and Hitton, E., 1980. Finite Elements in Plasticity: Theory and Practice. Pingeridge Press. Swansea.
6. Zienkiewicz, O. C., 1977. The Finite Element Method in Engineering Science. McGraw-Hill. New York.
7. Kobayashi, S., Oh, S. I. and Altan T. 1989, Metal Forming and the Finite Element Method. Oxford University Press. New York.
8. Rowe, G. W., Sturgess, C. E. N., Hartley, P. and Pillinger, I., 1991. Finite Element Plasticity and Metal Forming Analysis. Cambrige University Press.
9. Hartley, P., Pillinger, I. and Sturgess, C. (Eds), 1992. Numerical Modelling of Material Deformation Processes: Research, Development and Applications. Springer-Verlag. London.
10. Sawamiphakdi, K., Kropp, P. K. and Lahoti, G. D., 1990. Investigation of Residual Stresses in Drawn Wire by the Finite Element Method. Journal of Engineering Materials and Technology. April, 1990, 112, 231-235.
11. Dieter, G. E., 1986. Mechanical Metallurgy. McGraw-Hill Publishing Company.
12. Jornaz, M. I. and Cole, I. M., Sept., 1990. Die Material and Lubrication in Elevated Temperature Section Drawing from Round. Proc. Int. Conf. on Developments in Forming Technology. Lisbon, Portugal.
13. Beaddle, J. D. (ed.), 1971. Metal Forming. The Macmillan Press. London.
14. Winsper, C. E., 1966. An Investigation of the Mechanics of Wire Drawing with the Super-Position of an Oscillatory Drawing Stress. PhD thesis, The Aston University in Birmingham.
15. Rowe, G. W., Dec., 1977. Wire Manufacture. Int. Metals Review. London.
16. Eder, K. G., Oct., 1986. Wire Drawing Dies and Die Working Equipment. Wire Industry.

17. Meger, Roth and Pastor, Jan., 1984. Wire, a Most Versatile Product.Wire Industry.

18. Sachs, G., 1927. Zeit, Ang. Math. Mech., 7, 235.

19. Siebel, E., 1947. Stahl u Eisen, 66-67, 171.

20. Crane, F. A. A., 1964. Mechanical Working of Metals. Introductory Monographs in Materials Science. London.

21. MacLellan, G. D. S., 1948. A Critical Survey of Wire Drawing Theory. J. Iron and Steel Inst., 158, 347-356.

22. Wistreich, J. G., 1955. Investigation of the Mechanics of Wire Drawing. Proc. Inst. Mech. Engrs., 169, 654-665.

23. Wistreich J. G., 1958. The Fundamental of Wire Drawing. Met. Rev., 3.(10), 97-142.

24. Davis, E. A. and Dokos, S. J., 1944. The Theory of Wire Drawing. J. Appl. Mech., 11, A193-198.

25. Yang, C. T., Nov. 1961. On the Mechanics of Wire Drawing. J. Engn. Ind., Trans. ASME, 523-528.

26. Whitton, P. W., 1957-58. The Calculation of Drawing Force and Die Pressure in Wire Drawing. J. Inst. of Metals, 86, 417.

27. Thomsen, E. G., Yang, C.T. and Kobayashi, S., 1965. Mechanics of Plastic Deformation in Metal Processing. New York, London, Macmillan.

28. Johnson, W., et al, 1970. Plane-Strain Slip-Line Fields: Theory and Bibliography. Edward Arnold. London.

29. Thompson, P. J., Odgen, H. O. and Butterworth, N. A., 1969. An Apparent Strain Analysis of Orthogonal Cutting. Int. J. MTDR., 9, 97-116.

30. Siebel, E., 1947. The Application to Shaping Processes of Hencky's Laws of Equilibrium. J. Iron and Steel Inst., 155, 526-534.

31. Pugh, H. D., 1964. Redundant Work and Friction in the Hydrostatic Extrusion of Pure Aluminium and an Aluminium Alloy. J. Mech. Eng. Sci., 6, 4, 362-370

32. Avitzur, B., Feb., 1963. Analysis of Wire Drawing and Extrusion through Conical Dies of Small Cone Angle. J. Engr. for Ind., 89.

33. Avitzur, B., 1989. Flow Through Dies Update -1989. Wire Industry, 4, 243-249.

34. Avitzur, B, 1983. Handbook of Metal - Forming Processes. John Wiley and Sons. New York.

35. Avitzur, B. and Talbert, J. H., 1989. Upper-bound Solution and the Balance - of - Power Approach. Plasticity and Modern Metal - Forming Technology (ed T. Z. Blazynski). Elsevier Applied Science. London.

36. Galileo, G.,1638. Dialogues Concerning Two New Sciences, Elzevired, 217.

37. Gvozdev, A. A., 1938. The Determination of the Value of the Collapse Load for Statically Indeterminate Systems Undergoing PlasticDeformation. Proc. Conf. on Plastic Deformation. Akad Nauk USSR, Moscow Leningrad. 19-33.

38. Hill, R., 1951. On the State of Stress in a Plastic - rigid Body at the Yield Point. Phil. Mag., 42, 7, 868-875.

39. Prager, W. and Hodge, P. G., 1951. Theory of Perfectly Plastic Solids. Wiley. New York.

40. Drucker, D. C., Grenberg, H. J. and Prager, W., Dec. 1951. The Safety Factor of an Elastic-Plastic Body in Plane Strain. J. Appl. Mech. Trans. ASME 73, 371-378.

41. Avitzur, B, 1980. Metal Forming: The Application of Limit Analysis. Marcel Dekker. Inc. New York.

42. Johnson, W. and Mellor, P. B., 1973. Engineering Plasticity. Chapter 13. van Nostrand. London.

43. Kudo, H.,1960. An Upper Bound Approach to Plane - Strain Forging and Extrusion - 1. J. Mech. Sci.,1, 57-83.

44. Alexander, J. M., 1959. Proc. Inst. Mech. Engrs., 173, 85-91.

45. Altan, T. and Kobayashi, S., Feb., 1968. A Numerical Method for Estimating the Temperature Distribution in Extrusion Through Conical Dies. J. of Engineering for Industry. Trans. ASME. New York.

46. Lee, C. H. and Kobayashi, S. Aug., 1973. New Solutions to Rigid-Plastic Deformation Problems using a Matrix Method. Journal of Engineering for Industry. Trans. ASME. New York, 865-873.

47. Boer, C. R. and Webster, W. D., Aug., 1985. Direct Upper-Bound Solutions and Finite Element Approach to Round-to-Square Drawing. J. of Engineering for Industry. Trans. ASME. New York, 254-260.

48. Turner, M. J., Clough, R. W., Martin, H. C. and Topp, L. T., 1956. Stiffness and defection analysis of complex structures. J. Aero. Sci., 23, 805-824.

49. Lee, E. H., Mallett, R. L. and McMeeking, R. M., 1978. Stress and Deformation Analysis of Metal Forming Processes. Metal Forming Plasticity, ed. Lippmann, H. Springer-Verlag, 177-189.

50. Henshell, R. D., 1984. PAFEC: Theory. PAFEC Limited. Strelley Hall, Nottingham, England.

51. Mori, K., 1992. Extrusion and Drawing, Numerical Modelling of Material Deformation Processes: Research, Development and Applications, ed. Hartley et al, Springer-Verlag. London, 303-317.

52. Siebel, E. and Kobitzsch, R., 1943. Temperature Increase in Material in Wire Drawing. Stahl u. Eisen, 63, 110.

53. Ranger, A. E., 1957. An Electrical Analogue for Estimating Die Temperature during Wire Drawing. J. Iron and Steel Inst., 185, 383.

54. Kreith, F. and Bohn, S. M., 1986. Principles of Heat Transfer. Fourth Edition. New York.

55. Rebelo, N. and Kobayashi, S., 1980. A Coupled Analysis of Viscoplastic Deformation and Heat Transfer-II. Int. J. of Mech. Sci., 22, 707-718.

56. Pitrzyk, M. and Lenard, J. G., 1990. The Effect of the Temperature Rise of the Roll on the Simulation of the Flat Rolling Process. J. of Materials Processing Tech., 22, 177-190.

57. Altan, T., 1970. Heat Generation and Temperature in Wire and Rod Drawing. Wire Journal, 3, 54-59.

58. Huo, B., 1993, An Experimental and Theoretical Study on Friction, Lubrication and Tool Design in Wire Drawing, First Year Report, Aston University.

59. Lim, T. B., 1984. Tool Design and Mechanics of Hydrostatic Lubrication in Tube Drawing. PhD thesis, Aston University.

60. Bowden, F. P. and Tabor, D., 1950. The Friction and Lubrication of Solids. Clarendon Press. Oxford.

61. Metals Handbook. Ninth Edition, Vol.14, 1988. Forming and Forging. Metals Park. Ohio 44073.

62. Zhao, Z. Y., 1978.Plasticity and Metal Rolling Theory. Metallurgy Press. Beijing, China (in Chinese).

63. Sherrington, I. and Smith, E. H., 1986. The significance of surface topography in engineering. Precision Engineering, 8, 2, 79-87.

64. Woodcock, D. B., 1955. Proc. Inst. Mech. Engrs., 169, 666.

65. Assessment of Surface Texture. Part 1, Methods and Instrumentation. 1988. Brtitish Standard, British Standards Institution.

66. Surface Roughness, Terminology. Part 1, Surface and Its Parameters. 1984. International Standard, International Organization for Standardization.

67. Lancaster, P. R. and Rowe, G. W., 1963-64. Experimental Study of the Influence of Lubrication upon under Approximately Plane-Strain Conditions at Low Speeds. Proc. Inst. Mech. Engrs., 178, 69-88.

68. Shaw, M. S., Stableford, W. H. and Sansome, D. H., 1970. Critical Review of Drawing with Particular Reference to Lubrication. Int. MTDR, 10, 203-212.

69. Baron, H. G. and Thompson, F. C., 1950. Friction in Wire Drawing. J. Inst Met, 78, 414-462.

70. Rothman, D.,1970. PhD thesis, Aston University.

71. Linicus, W. and Sachs, G., 1931. Mitt. Dt. Mater. Anst. Spanlose Formung der Metalle, 16, 36-67.

72. Rothman, D. and Sansome, D. H., 1970. An Investigation of Rod Drawing with Die Rotation. Inst. J. MTDR, 10, 179-192.

73. MacLellan, G. D. S., 1948. Critical Survey of Wire Industry. J. Iron and Steel Inst., 158, 654-665.

74. MacLellan, G. D. S., 1952-53. Some Friction Effects in Wire Drawing. J. Inst. Met., 81, pp. 1-13.

75. Basily,B.B., 1976.The Mechanics of Section Drawing. PhD thesis, Aston University.

76. Basily, B. B. and Sansome, D. H., 1976. Determination of the Mean Coefficient of Friction in the Drawing of Section Rods from Round Bars. Proc. 17th Int. MTDR Conf., 475-481.

77. Torzera, T. A., 1964. On Non-homogeneous Work for Wire Drawing. Trans. ASME, 57, 309-323.

78. Atkins, A. G. and Caddell, R. M., 1968. The Influence of Redundant Work when Drawing Rods through Conical Dies. Trans. ASME , 90, 411-418.

79. Thompson, P. J. and Sansome, D. H., 1976. Apparent Strain Method for Analysis of Steady State Metal Working Operations. Metals Tech., 497-502.

80. Hill, R., 1953. A note on the back-pull factor in strip-drawing, Journal of the Mechanics and Physics of Solids, 1, 142-145.

81. Rowe, G. W., April, 1978. Lubrication in the Drawing of Steel Wire. Wire Industry, 229-236.

82. Smith, B. F., April, 1976. Lubrication - Effects and Consequences in Wire Drawing. Wire Indurstry, 241-243.

83. Fuller, D., 1956. Theory and Practice of Lubrication for Engineers. John Wiley.

84. Cameron, A., 1966. Principles of Lubrication. Longman.

85. Smith, B. F. and Cooper, A., January, 1979. The Theory of Lubrication. Wire Journal, 76-81.

86. Tattersall, G. H.,1961, Hydrodynamic lubrication in wire drawing. Journal Mechanical Engineering Science, 3, No4,378-393.

87. Christopherson, D. G., Naylor, H. and Wells, J., 1954. J. Inst. Petrol, 40, 295.

88. Butler, L. H., 1965, A method for continuous wire drawing aided by externally generated hydrostatic oil pressure, J. Inst. Metals, 93, 123-125.

89. Ling, F. F., Whitely, R. L., Ku, P. M. and Peterson, M. B. (eds), 1966, Friction and Lubrication in Metal Processing,The American Society of Mechanical Engineers, New York.

90. Ranger, A. E. and Wistreich, J. G., 1954. J. Inst. Petrol, 40, 308.

91. Wistreich, J. G., 1957. Lubrication in Wire Drawing. The Inst. of Mech. Engr. Proc. Conf. Lubrication and Wear. London, 505-511.

92. Lancaster, P. R., April, 1972. A Study of Lubrication in the High Speed Drawing Process. Wire Indurstry.

93. Grudev, A. P., Dolzhanskii, A. M., Borodavkin, I. T. and Sigalov Y. B., 1984, Study of Thickness of Lubricant Layer during Drawing. Steel in the USSR, 14, 386-387.

94. Baker, G. and Wright, R. N., 1990. Surface Evaluation of Copper Wire. Proc 60th Annual Convention and 1990 Division Meetings, USA, 146-149.

95. Dawson, G. R.,1972. A Study of the Application of Low Frequency Oscillations to Multi-Tool Drawing. PhD thesis, Aston University.

96. Kumar, V., Crane, L. W. and Cole I. M., Feb. 1989. The Hot Drawing of Non-ferrous Metals. Wire Industry, 56, 662, 124-125.

97 Smallman, R. E. and Bishop, R. J., 1995, Metals and Materials Science, process, application, Butterworth-Heinemann, Oxford.

98 Gao, W. L., Bai, G. R., Zhou, Z. M., Luan, G. F. and Long, C. M., 1992, Hot deformation behaviour of Nb-bearing low carbon steel and prediction of flow stress for metals during plastic deformation, ACTA Metallurgica Sinica, 28, No.8, A352-358.

99. Zener, C. and Holloman, J. H., 1944, J. Appl. Phys., 15, 22-32.

100. Sellars, C. M. and Tegart, W. J. Mcg., 1966, Mem. Sci. Rev., 63, 731.

101. Pillinger, I., 1988, EPFEP3 Program User's Manual, The University of Birmingham.

102. ABAQUS/Users Manual, Version 5.4, 1994, Hibbitt, Karlsson & Sorensen, Inc., Pawtucket, USA.

103. Harding, J., 1987, The effect of High Strain Rate on Material Properties, Materials at High Strain Rates, ed. T. Z. Blazynski, Elsevier Applied Science, London, 133-186.

Appendix A

Calibration Graphs

A.1 Load Cell Calibration Graph

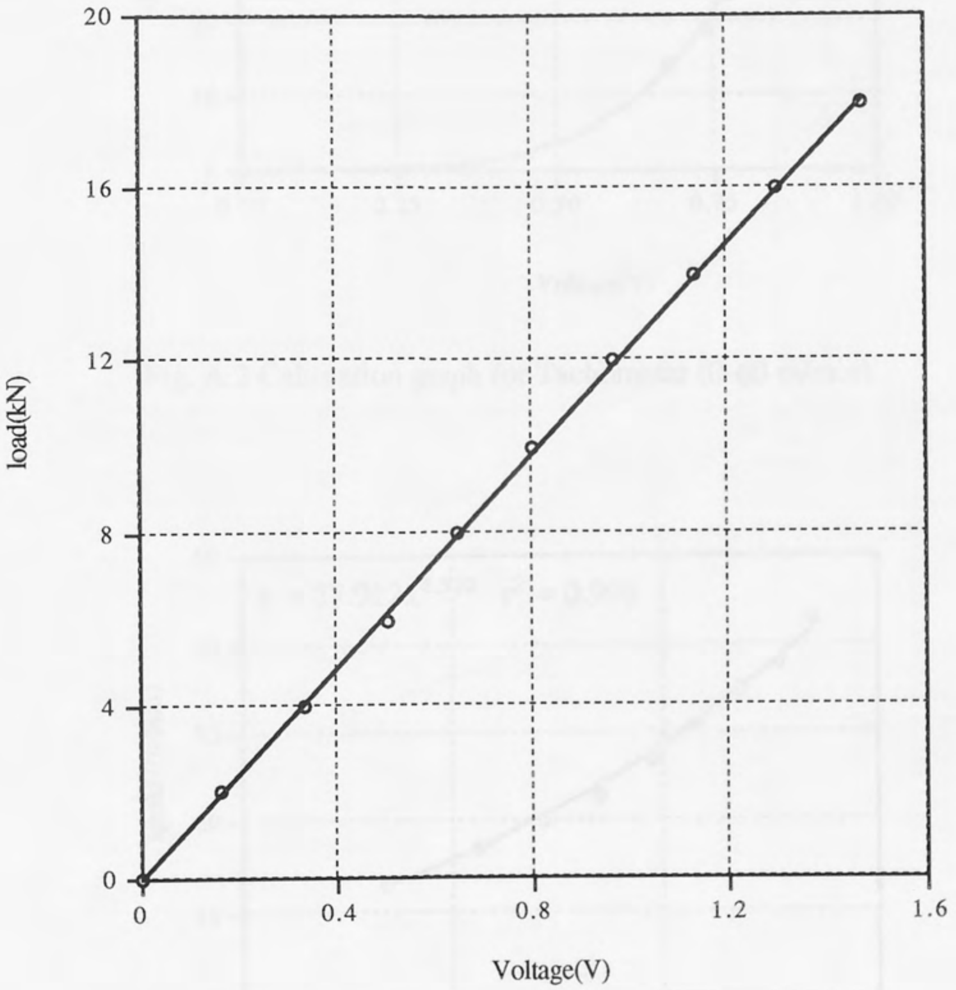

Fig. A.1 Calibration graph for load cell.

A.2 Tachometer Calibration Graphs

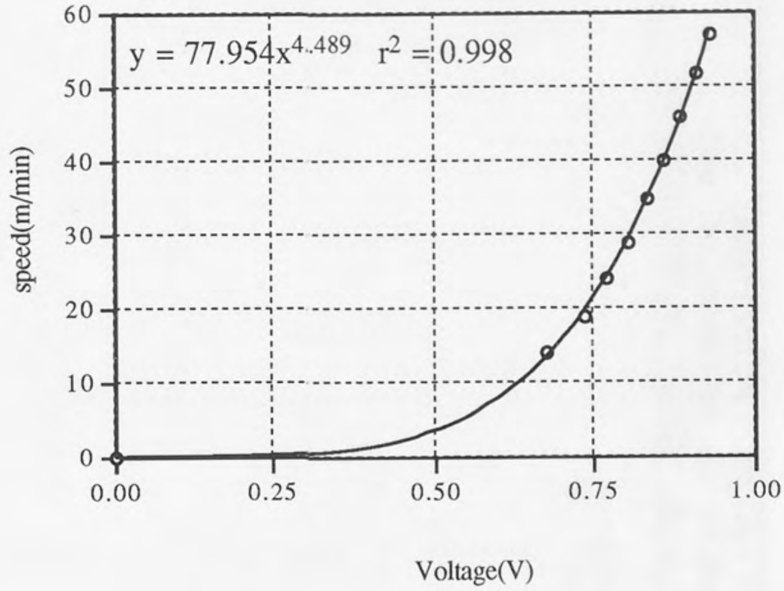

Fig. A.2 Calibration graph for Tachometer (0-60 m/min).

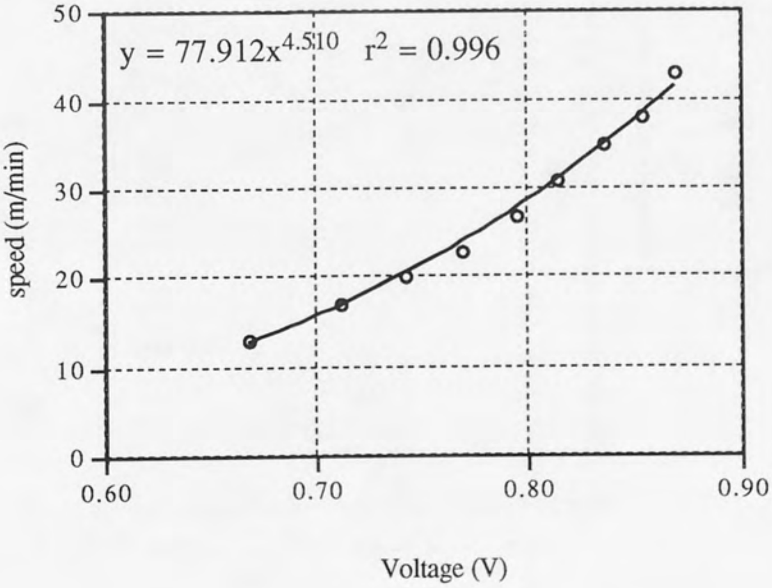

Fig. A.3 Calibration graph for Tachometer (10-50 m/min).

Appendix B Technical Drawings

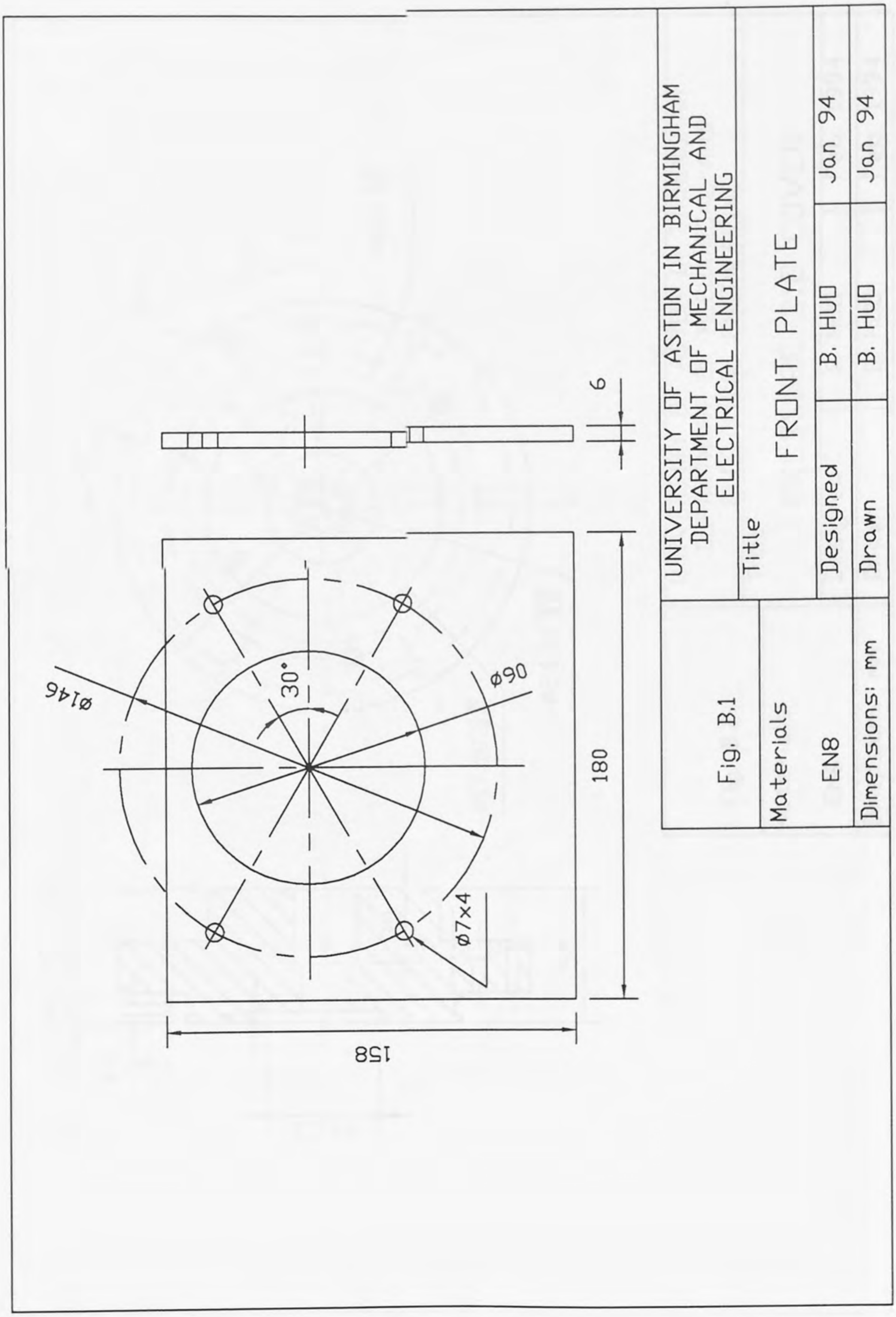

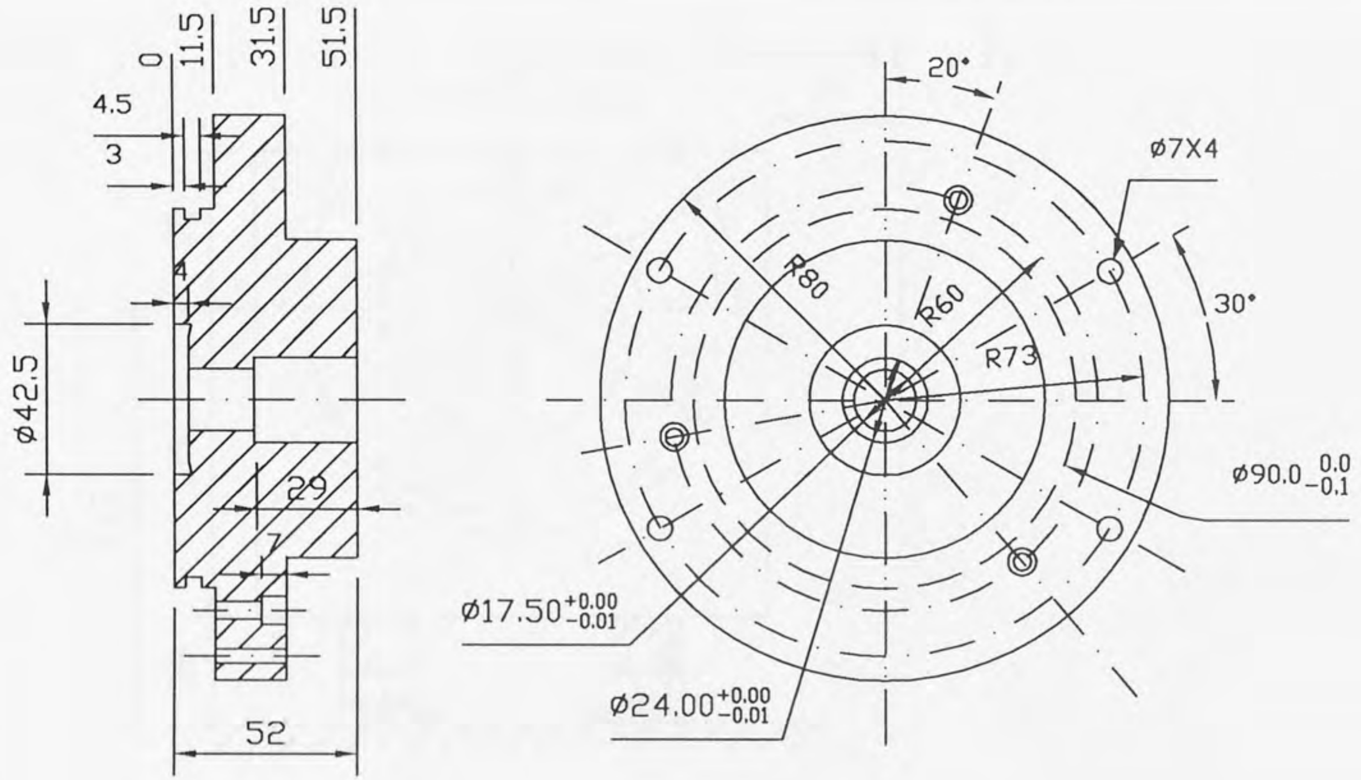

Fig. B.2	UNIVERSITY OF ASTON IN BIRMINGHAM DEPARTMENT OF MECHANICAL AND ELECTRICAL ENGINEERING		
Materials	Title PRESSURE DIE COVER		
EN8	Designed	B. HUO	Feb. 1994
Dimensions: mm	Drawn	B. HUO	Feb. 1994

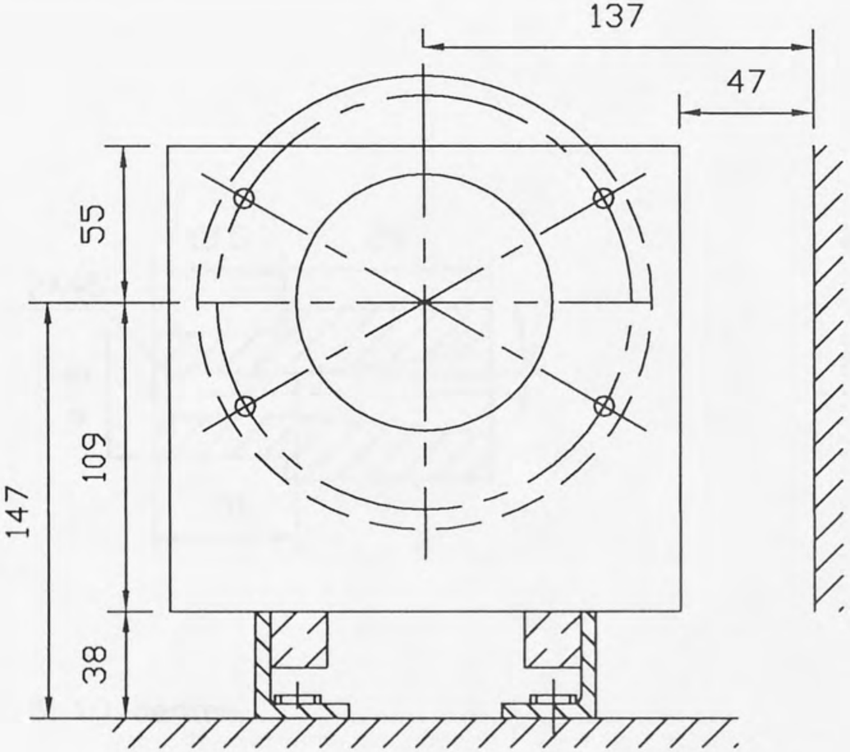

Fig. B.3	UNIVERSITY OF ASTON IN BIRMINGHAM DEPARTMENT OF MECHANICAL AND ELECTRICAL ENGINEERING		
Materials	Title DIE BOX ASSEMBLY		
	Designed	B. HUO	Feb 94
Dimensions: mm	Drawn	B. HUO	Feb 94

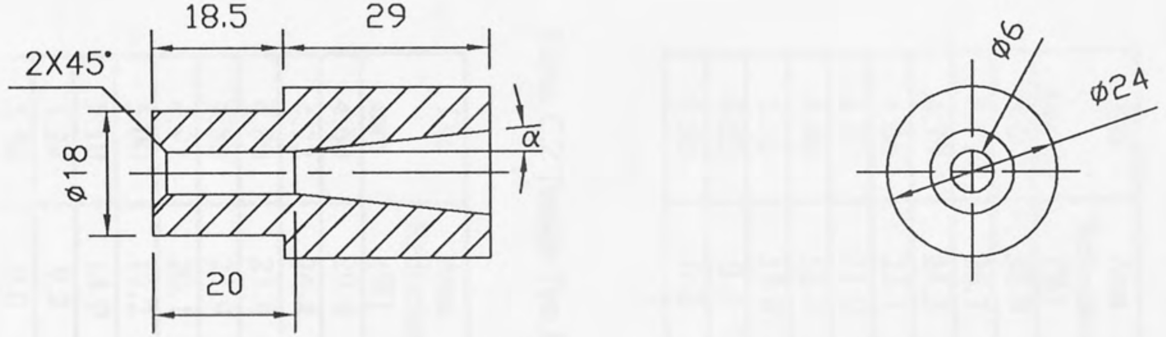

NOTE: α=6, 8, 10 degree.

Fig. B.4	UNIVERSITY OF ASTON IN BIRMINGHAM DEPARTMENT OF MECHANICAL AND ELECTRICAL ENGINEERING		
Materials Die Steel	Title NOZZLE INSERT		
	Designed	B. HUO	Feb 94
Dimensions: mm	Drawn	B. HUO	Feb 94

Appendix C

Tensile Test Data and Computer Program for Curve Fitting

C.1 Tensile Test Data

Table C.1 Tensile Test Data for Low Carbon Steel.

Dia (mm)	Area Reduction (%)	Strain	0.2% Proof Stress (N/mm^2)
4.60	30.0	0.357	516.80
4.71	26.7	0.310	504.75
4.79	24.2	0.276	487.60
4.86	22.1	0.249	488.65
4.89	21.0	0.235	476.40
4.98	18.0	0.199	456.20
5.11	13.8	0.149	441.60
5.22	9.9	0.105	397.10
5.50	0.0	0.000	241.23

Table. C.2 Tensile Test Data for Medium Carbon Steel.

Dia mm	Area Reduction (%)	Strain	Yield Stress (N/mm^2)
4.60	29.8	0.354	868.56
4.72	26.4	0.306	866.40
4.80	23.8	0.272	837.70
4.86	21.9	0.247	838.50
4.92	20.1	0.225	837.50
5.00	17.2	0.189	818.15
5.10	14.0	0.151	806.70
5.24	9.2	0.097	753.75
5.50	0.0	0.000	440.00

C.2 Basic Equations with the Least Square Regression

The polynomial function can be written in a general form:

$$\hat{y} = a_0 + a_1x + a_2x^2 + \cdots a_mx^m \tag{C.1}$$

Assuming there are n+1 sets of experimental data (x_i, y_i), where n=0, 1, ..., n, the sum of differences between the function and all the experimental data, S, is given by

$$S = \sum (y_i - \hat{y}_i)^2 \tag{C.2}$$

In the least square method, the coefficients a_i in equation (C.1) are determined by minimising equation (C.2) and solving the following set of simultaneous equations:

$$\frac{\partial S}{\partial a_j} = 0 \quad j = 0, 1, 2, ..., m \tag{C.3}$$

Equation (C.3) can be written in a matrix form:

$$\mathbf{Ga} = \mathbf{b} \tag{C.4}$$

where **a** is a vector of the unknown coefficients of the polynomial function (C.1) and

$$g_{pq} = \Sigma x_i^{pq} \quad p, q = 0, 1, 2, ... m \tag{C.5}$$

$$b_p = \Sigma y_i x_i^p \quad p = 0, 1, 2, ..., m \tag{C.6}$$

The correlation coefficient r is calculated by

$$r = \frac{\Sigma(x_i - \overline{x})(y_i - \overline{y})}{\sqrt{\Sigma(x_i - \overline{x})^2 \Sigma(y_i - \overline{y})^2}} \tag{C.7}$$

The standard deviation is calculated by

$$s = \sqrt{\frac{\Sigma(y_i - \hat{y}_i)^2}{N}} \tag{C.8}$$

C.3 Computer Program for Curve Fitting

```
c################################################################
c#                                                              #
c#  A Program Designed to Fit Material Flow Stress-Strain Data  #
c#       into a Polynomial Constitutive Function                #
c#       Using the Least Square Regression Method               #
c#                                                              #
c#                  by Bingshu Huo                              #
c#                                                              #
c#     Mechanical and Electrical Engineering Department         #
c#                  Aston  University                           #
c#                                                              #
c################################################################
      Program Curve Fitting for Material Models
c     maximum number of data points = 200
c     degree of highest polynomial = 20
      dimension x(200),y(200),xc(40),yx(20),a(20),b(20),c(20,20),
     $          d(20,20),e(20)
      open(5,file='xydata')
      open(6,file='coefficient')
      read(5,1) ll
1     format(i3)
      do 300 l=1,ll
      read (5,100) n,m
      np1=n+1
      mp1=m+1
      m2=m*2
      read (5,101) (x(i),y(i),i=1,np1)
c     form sums of powers of x(i)
      do 20 k=1,m2
      xc(k)=0.0
      do 15 i=1,np1
15     xc(k)=xc(k)+x(i)**k
20     continue
c     form sums of y(i) and x(i)
      yc=0.0
      cx=0.0
      do 22 i=1,np1
      cx=cx+x(i)
22     yc=yc+y(i)
c     form sums of products y(i)*x(i)**k
      do 30 k=1,m
      yx(k)=0.0
      do 25 i=1,np1
25     yx(k)=yx(k)+y(i)*x(i)**k
30     continue
c     generate normal matrix c using sums of powers of x(i)
      do 40 i=1,mp1
      do 35 j=1,mp1
      ipjm2=i+j-2
      if (ipjm2) 33,31,33
31     c(1,1)=float(np1)
      go to 35
33     c(i,j)=xc(ipjm2)
```

```
35     continue
40     continue
c     benerate right semi-matrix b
      b(1)=yc
      do 45 i=2,mp1
45     b(i)=yx(i-1)
c     invert normal matrix c
      call inverse (c,d,mp1)
c     form matrix product of inverse and right-side matrix
      do 55 i=1,mp1
      a(i)=0.0
      do 54 j=1,mp1
54     a(i)=a(i)+d(i,j)*b(j)
55     continue
      e(l)=e(l)+0.04*(l-1)
      write(6,*)
      write(6,111)
      write(6,110) (a(k),k=1,mp1)
100   format(3i3)
101   format(2f14.6)
110   format(1x,e14.6)
111   format('polynomial coefficients a(k)')
c     calculate satndard deviation and correlation coefficient
      sumxy=0.0
      sqxy=0.0
      ss=0.0
      do 65 k=1,np1
      yf=a(1)
      do 60 ln=2,mp1
60     yf=yf+a(ln)*x(k)**(ln-1)
       ss=ss+(y(k)-yf)**2
      sumxy=sumxy+(x(k)-cx/np1)*(y(k)-yc/np1)
65     sqxy=sqxy+((x(k)-cx/np1)**2*(y(k)-yc/np1)**2)**0.5
       s=(ss/np1)**0.5
      r=sumxy/sqxy
      write(6,*) 'the correlation coefficient r=',r
      write(6,*) 'the standard deviation      s=',s
      write(6,*)
300   continue
      stop
      end

      subroutine inverse (a,b,n)
c     matrix inversion by elimination with partial pivoting
c     original matrix=a inverse matrix=b
      dimension a(20,20),b(20,20)
      eps=0.0000001
c     construct identity martix b(i,j)=i
      do 6 i=1,n
      do 5 j=1,n
      if (i-j) 4,3,4
3      b(i,j)=1.0
      go to 5
4      b(i,j)=0.0
```

```
5    continue
6    continue
c    locate maximum magnitude a(i,k) on or below main diagonal
     del=1.0
     do 45 k=1,n
     if (k-n) 12,30,30
12    imax=k
     amax=abs (a(k,k))
     kp1=k+1
     do 20 i=kp1,n
     if (amax-abs(a(i,k))) 15,20,20
15    imax=i
     amax=abs(a(i,k))
20    continue
c    interchange rows imax and k if imax not eaqual to k
     if (imax-k) 25,30,25
25    do 29 j=1,n
     atmp=a(imax,j)
     a(imax,j)=a(k,j)
     a(k,j)=atmp
     btmp=b(imax,j)
     b(imax,j)=b(k,j)
29    b(k,j)=btmp
     del=-del
30    continue
c    test for singular matrix
     if (abs(a(k,k))-eps) 93,93,35
35    del=a(k,k)*del
c    divide pivot row by its main diagonal element
     div=a(k,k)
     do 38 j=1,n
     a(k,j)=a(k,j)/div
38    b(k,j)=b(k,j)/div
c    replace each row by linear combination with pivot row
     do 43 i=1,n
     amult=a(i,k)
     if (i-k) 39,43,39
39    do 42 j=1,n
     a(i,j)=a(i,j)-amult*a(k,j)
42    b(i,j)=b(i,j)-amult*b(k,j)
43    continue
45    continue
c     write(6,120)
c      write(6,110) ((b(i,j),i=1,n),j=1,n)
c     write(6,121)
c     write(6,110) del
99    return
93    write(6,113) k
     go to 99
110   format(2x,e15.8)
113   format(25h singular matrix for k = ,i2)
120   format(20h elements of inverse)
121   format(21h value of determinant)
     end
```

Appendix D

Drawing Test Data

Table D.1

Material: medium carbon steel

Lubricant: CONDAT VICAFIL

Pressure Nozzle Semi-angle: 6 degree

Dia out (mm)	Area reduction (%)	Speed (m/min)	Load (kN)	Yield stress (N/mm^2)	Drawing stress (N/mm^2)
5.10	14.0	19.8	4.288	834.40	209.91
4.92	20.1	19.8	5.750	842.00	303.06
4.80	23.8	19.8	6.479	836.10	358.04
4.70	27.0	19.8	7.000	829.90	403.47
4.60	30.0	19.8	7.625	806.40	458.81
5.10	14.0	23.6	4.438	823.65	217.25
4.92	20.1	23.6	6.230	853.50	328.36
4.80	23.8	23.6	6.616	834.70	365.61
4.70	27.0	23.6	7.296	838.50	420.53
4.60	30.0	23.6	7.690	830.00	462.72
5.24	9.2	30.5	3.536	869.20	163.97
5.00	17.2	30.5	5.452	850.00	277.22
4.86	21.9	30.5	6.468	843.50	348.66
4.70	27.0	30.5	7.048	851.80	406.24
4.61	29.8	30.5	7.900	866.40	473.92
5.24	9.2	38.1	3.300	877.00	153.02
5.00	17.4	38.1	5.040	880.50	256.69
4.87	21.8	38.1	6.307	859.50	339.29
4.72	26.4	38.1	6.840	868.30	390.91
4.60	30.0	38.1	7.600	857.50	457.31
4.92	20.0	47.24	5.439	850.60	286.09
4.81	23.5	47.24	6.038	835.35	332.29
4.70	27.0	47.24	6.773	866.70	390.39
4.61	29.7	47.24	7.245	850.40	434.06

Table D.2

Material: medium carbon steel

Lubricant: TRAXIT

Pressure Nozzle Semi-angle: 6 degree

Dia out (mm)	Area reduction (%)	Speed (m/min)	Load (kN)	Yield stress (N/mm^2)	Drawing stress (N/mm^2)
5.02	17.0	19.8	3.062	800.73	155.32
4.92	20.0	19.8	3.259	817.40	171.42
4.82	23.8	19.8	3.191	818.20	176.34
4.69	27.3	19.8	3.786	834.40	219.15
4.60	30.0	19.8	3.887	866.20	233.89
4.92	20.0	28.97	5.509	817.40	289.77
4.82	23.8	28.97	6.044	818.20	331.24
4.71	27.0	28.97	6.631	829.25	380.58
4.62	30.0	28.97	7.182	846.80	428.42
4.95	19.0	34.8	3.878	812.20	201.52
4.88	21.3	34.8	4.343	814.30	232.20
4.82	23.2	34.8	4.693	821.60	257.20
4.71	27.0	34.8	5.046	829.25	290.85
4.62	30.0	34.8	5.705	846.80	343.28
4.95	19.0	47.24	4.800	801.10	249.43
4.88	21.3	47.24	5.945	818.00	317.85
4.82	23.2	47.24	6.368	834.60	349.00
4.70	27.0	47.24	6.689	839.90	385.55
4.60	30.0	47.24	7.653	857.80	460.50

Table D.3

Material: medium carbon steel

Lubricant: CONDAT VICAFIL

Pressure Nozzle Semi-angle: 8 degree

Dia out (mm)	Area reduction (%)	Speed (m/min)	Load (kN)	Drawing stress (N/mm2)
5.01	17.0	26.65	5.254	266.52
4.91	20.3	26.65	5.802	306.43
4.79	24.2	26.65	6.187	343.34
4.68	27.6	26.65	7.025	408.38
4.59	30.4	26.65	7.469	451.39
5.01	17.0	38.1	5.361	271.95
4.91	20.3	38.1	5.789	305.74
4.79	24.2	38.1	6.224	345.39
4.68	27.6	38.1	6.967	405.01
4.59	30.4	38.1	7.300	441.17
5.01	17.0	47.24	5.326	270.17
4.91	20.3	47.24	5.902	311.71
4.69	27.3	47.24	6.813	394.37
4.79	24.2	47.24	6.140	340.73
4.59	30.4	47.24	7.241	437.61

Table D.4

Material: medium carbon steel

Lubricant: TRAXIT

Pressure Nozzle Semi-angle: 8 degree

Dia out (mm)	Area reduction (%)	Speed (m/min)	Load (kN)	Drawing stress (N/mm2)
4.91	20.30	26.65	5.543	377.59
4.80	23.83	26.65	6.100	333.23
4.70	26.98	26.65	6.551	293.12
4.60	30.05	26.65	7.200	453.10
4.91	20.30	38.1	6.000	337.10
4.80	23.83	38.1	6.030	316.88
4.70	26.98	38.1	6.660	419.40
4.60	30.05	38.1	6.970	382.15
4.91	20.30	47.24	5.550	292.75
4.80	23.83	47.24	6.050	433.24
4.70	26.98	47.24	6.630	383.87
4.60	30.05	47.24	7.530	334.34

Table D.5

Material: medium carbon steel

Lubricant: CONDAT VICAFIL

Pressure Nozzle Semi-angle: 10 degree

Dia out mm	Area reduction (%)	speed (m/min)	Load (kN)	Drawing stress (kN/mm^2)
4.91	20.5	26.65	5.810	431.31
4.80	23.8	26.65	6.525	369.55
4.69	27.3	26.65	7.149	323.34
4.60	30.0	26.65	7.657	479.17
4.90	20.6	38.1	5.792	375.83
4.80	23.8	38.1	6.416	320.13
4.70	27.0	38.1	7.075	467.53
4.61	29.9	38.1	7.471	406.35
4.91	20.5	47.24	5.862	320.47
4.80	23.8	47.24	6.394	480.22
4.70	27.0	47.24	6.764	425.04
4.61	29.9	47.24	7.657	368.29

Table D.6

Material: medium carbon steel

Lubricant: TRAXIT

Pressure Nozzle Semi-angle: 10 degree

Dia out (mm)	Area reduction (%)	Speed (m/min)	Load (kN)	Drawing stress (N/mm^2)
4.90	20.6	26.65	5.859	310.70
4.80	23.8	26.65	6.197	342.46
4.71	26.7	26.65	6.609	379.32
4.60	30.0	26.65	7.254	436.49
4.91	20.5	38.1	5.720	302.71
4.79	24.2	38.1	6.154	341.51
4.69	27.3	38.1	6.643	384.53
4.60	30.0	38.1	7.295	438.96
4.90	20.6	47.24	5.632	298.66
4.80	23.8	47.24	5.890	325.49
4.69	27.3	47.24	6.625	383.49
4.60	30.0	47.24	7.167	431.25

Table D.7

Material: low carbon steel

Lubricant: CONDAT VICAFIL

Pressure Nozzle Semi-angle: 6 degree

Dia out (mm)	Area reduction (%)	Speed (m/min)	Load (kN)	Yield stress (N/mm^2)	Drawing stress (N/mm^2)
5.11	13.8	19.80	1.907	537.50	93.17
4.89	21.0	19.80	1.564	501.50	83.28
4.79	24.2	19.80	1.818	516.80	100.89
4.70	27.0	19.80	1.763	509.75	101.62
4.59	30.4	19.80	1.955	520.50	118.15
5.22	9.9	23.60	1.907	488.65	89.11
4.98	18.0	23.60	2.044	495.65	104.94
4.79	24.2	23.60	2.559	487.60	142.01
4.71	26.7	23.60	2.593	476.85	148.82
4.60	30.0	23.60	2.867	477.55	172.51
5.20	10.6	30.48	0.760	467.35	35.79
5.01	17.0	30.48	2.180	476.40	110.58
4.85	22.2	30.48	2.420	456.20	130.99
4.70	27.0	30.48	2.641	443.40	152.22
4.59	30.4	30.48	3.032	438.15	183.24
5.22	9.9	38.10	0.954	515.05	44.58
5.00	17.4	38.10	1.592	502.50	81.08
4.80	23.8	38.10	2.326	504.75	128.54
4.71	26.7	38.10	2.497	497.65	143.31
4.61	29.7	38.10	3.114	478.00	186.56
4.92	20.0	47.24	3.378	500.50	177.68
4.80	23.8	47.24	3.860	491.40	213.31
4.70	27.0	47.24	4.070	485.75	234.59
4.60	30.0	47.24	4.615	482.35	277.69

Table D.8

Material: low carbon steel

Lubricant: TRAXIT

Pressure Nozzle Semi-angle: 6 degree

Dia out (mm)	Area reduction (%)	Speed (m/min)	Load (kN)	Drawing stress (N/mm^2)
4.88	21.27	23.6	3.349	179.06
4.78	24.47	23.6	3.589	199.99
4.68	27.60	23.6	3.942	229.16
4.60	30.05	23.6	3.962	238.40
4.88	21.27	38.1	3.295	176.17
4.78	24.47	38.1	3.600	200.61
4.68	27.60	38.1	3.817	221.89
4.60	30.05	38.1	4.045	243.40
4.88	21.27	47.24	3.220	172.16
4.78	24.47	47.24	3.491	194.54
4.68	27.60	47.24	3.943	229.22
4.60	30.05	47.24	4.154	249.96

Table D.9

Material: low carbon steel

Lubricant: Traxit

Pressure Nozzle Semi-angle: 8 degree

Dia out (mm)	Area reduction (%)	Speed (m/min)	load (kN)	Drawing stress (N/mm^2)
4.88	21.27	26.65	3.265	174.56
4.78	24.47	26.65	3.682	205.18
4.68	27.60	26.65	3.905	227.01
4.60	30.05	26.65	4.285	257.84
4.88	21.27	38.1	3.379	180.66
4.78	24.47	38.1	3.649	203.34
4.68	27.60	38.1	3.923	228.05
4.60	30.05	38.1	4.239	255.07
4.88	21.27	47.24	3.346	178.89
4.78	24.47	47.24	3.571	198.99
4.68	27.60	47.24	3.990	231.95
4.60	30.05	47.24	4.285	257.84

Table D.10

Material: low carbon steel

Lubricant: Condat

Pressure Nozzle Semi-angle: 8 degree

Dia out (mm)	Area reduction (%)	Speed (m/min)	Load (kN)	Drawing stress (N/mm^2)
4.88	21.27	26.65	3.471	185.58
4.78	24.47	26.65	3.733	208.02
4.68	27.60	26.65	4.109	238.87
4.60	30.05	26.65	4.427	266.38
4.88	21.27	38.1	3.499	187.07
4.78	24.47	38.1	3.790	211.20
4.68	27.60	38.1	4.087	237.59
4.60	30.05	38.1	4.180	251.52
4.88	21.27	47.24	3.439	183.87
4.78	24.47	47.24	3.756	209.31
4.68	27.60	47.24	4.004	232.76
4.60	30.05	47.24	4.369	262.89

Table D.11

Material: low carbon steel

Lubricant: Traxit

Pressure Nozzle Semi-angle: 10 degree

Dia out (mm)	Area reduction (%)	Speed (m/min)	Load (kN)	Drawing stress (N/mm^2)
4.88	21.27	26.65	3.071	164.19
4.78	24.47	26.65	3.682	205.18
4.68	27.60	26.65	3.963	230.38
4.60	30.05	26.65	4.228	254.41
4.88	21.27	38.1	3.193	170.71
4.78	24.47	38.1	3.457	192.64
4.68	27.60	38.1	3.821	222.12
4.60	30.05	38.1	4.021	241.95
4.88	21.27	47.24	3.053	163.23
4.78	24.47	47.24	3.486	194.26
4.68	27.60	47.24	3.808	221.37
4.60	30.05	47.24	4.136	248.87

Table D.12

Material: low carbon steel

Lubricant: Condat

Pressure Nozzle Semi-angle: 10 degree

Dia out (mm)	Area reduction (%)	Speed (m/min)	Load (kN)	Drawing stress (N/mm^2)
4.88	21.27	26.65	3.531	188.79
4.78	24.47	26.65	3.854	214.77
4.68	27.60	26.65	4.078	237.06
4.60	30.05	26.65	4.446	267.53
4.88	21.27	38.1	3.630	194.08
4.78	24.47	38.1	4.004	223.13
4.68	27.60	38.1	4.267	248.05
4.60	30.05	38.1	4.378	263.43
4.88	21.27	47.24	3.448	184.35
4.78	24.47	47.24	3.830	213.43
4.68	27.60	47.24	4.169	242.35
4.60	30.05	47.24	4.371	263.01

Appendix E Spectrum Analysis Results

```
MEM1: SAMPLE2 97
WINDOW  START        END  WIDTH        GROSS          NET     EFF.    %AGE
LABEL     keV        keV  CHANS     INTEGRAL     INTEGRAL   FACTOR   TOTAL
--------------------------------------------------------------------------
C         .20        .34      8          448          264     3.00    4.85
O         .44        .56      7         1350          622     2.50    9.53
Na        .92       1.10     10          193            8     2.00     .10
Mg       1.16       1.36     11          368           33      .54     .11
Al       1.40       1.60     11          427            9      .81     .04
Si       1.68       1.84      9          486           41      .68     .17
P        1.92       2.12     11          917          290     1.33    2.36
S        2.20       2.42     12          968          278      .45     .77
Cl       2.54       2.72     10          655           70      .48     .20
K        3.18       3.42     13          685           16      .81     .08
Ca       3.52       3.82     16        22911        20607      .62   77.94
Ti       4.32       4.62     16          471           15      .56     .05
Cr       5.26       5.58     17          387           -4      .62    -.02
Mn       5.78       6.02     13          300           40      .75     .18
Fe       6.24       6.54     16          868          436      .85    2.26
Ni       7.30       7.58     15          283          -10     1.19    -.07
Cu       7.94       8.12     10          181           -4     1.37    -.03
Zn       8.50       8.82     17          416          144     1.67    1.47
```

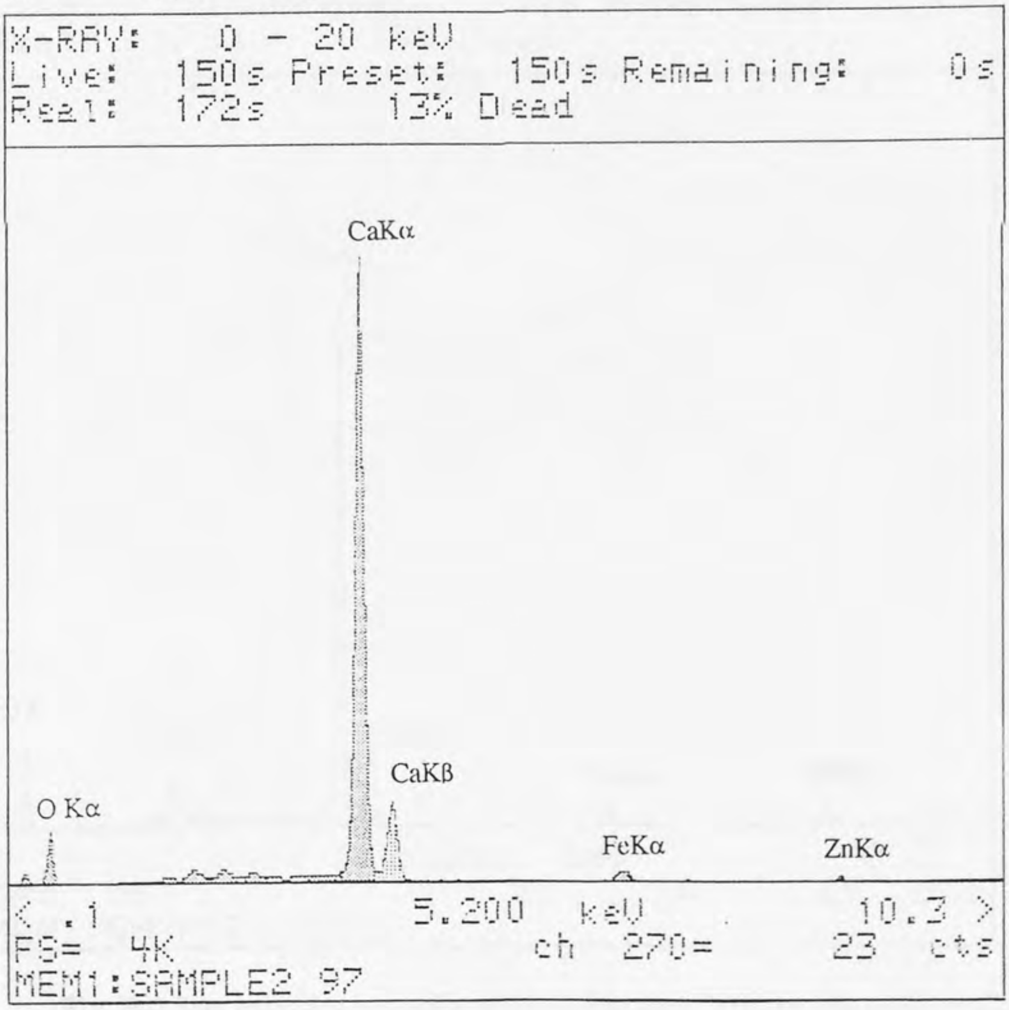

```
X-RAY:    0 - 20 keV
Live:   150s Preset:   150s Remaining:      0s
Real:   172s        13% Dead
```

```
< .1              5.200  keV          10.3 >
FS=  4K               ch  270=         23  cts
MEM1:SAMPLE2 97
```

Fig. E.1 Spectrum analysis of a residual lubricant layer on the surface of a wire drawn using Condat Vicafil lubricant.

```
MEM1: SAMPLE2 97
WINDOW  START      END  WIDTH      GROSS          NET    EFF.   %AGE
LABEL     keV      keV  CHANS   INTEGRAL     INTEGRAL  FACTOR  TOTAL
--------------------------------------------------------------------
C         .20      .34      8        636          352    3.00   5.77
O         .44      .56      7       2267          958    2.50  13.09
Na        .92     1.10     10        446          161    2.00   1.76
Mg       1.16     1.36     11        469           62     .54    .18
Al       1.40     1.60     11        508           13     .81    .06
Si       1.68     1.84      9        653           50     .68    .19
P        1.92     2.12     11       2172         1237    1.33   8.98
S        2.20     2.42     12       1086          300     .45    .74
Cl       2.54     2.72     10        755          125     .49    .33
K        3.18     3.42     13        728          -13     .81   -.06
Ca       3.52     3.82     16      19338        17274     .62  58.29
Ti       4.32     4.62     16        586           58     .56    .18
Cr       5.26     5.58     17        439          -29     .62   -.10
Mn       5.78     6.02     13        361            4     .75    .01
Fe       6.24     6.54     16       1172          724     .85   3.36
Ni       7.30     7.58     15        260          -25    1.19   -.16
Cu       7.94     8.12     10        218            3    1.37    .02
Zn       8.50     8.82     17       1257          807    1.67   7.36
```

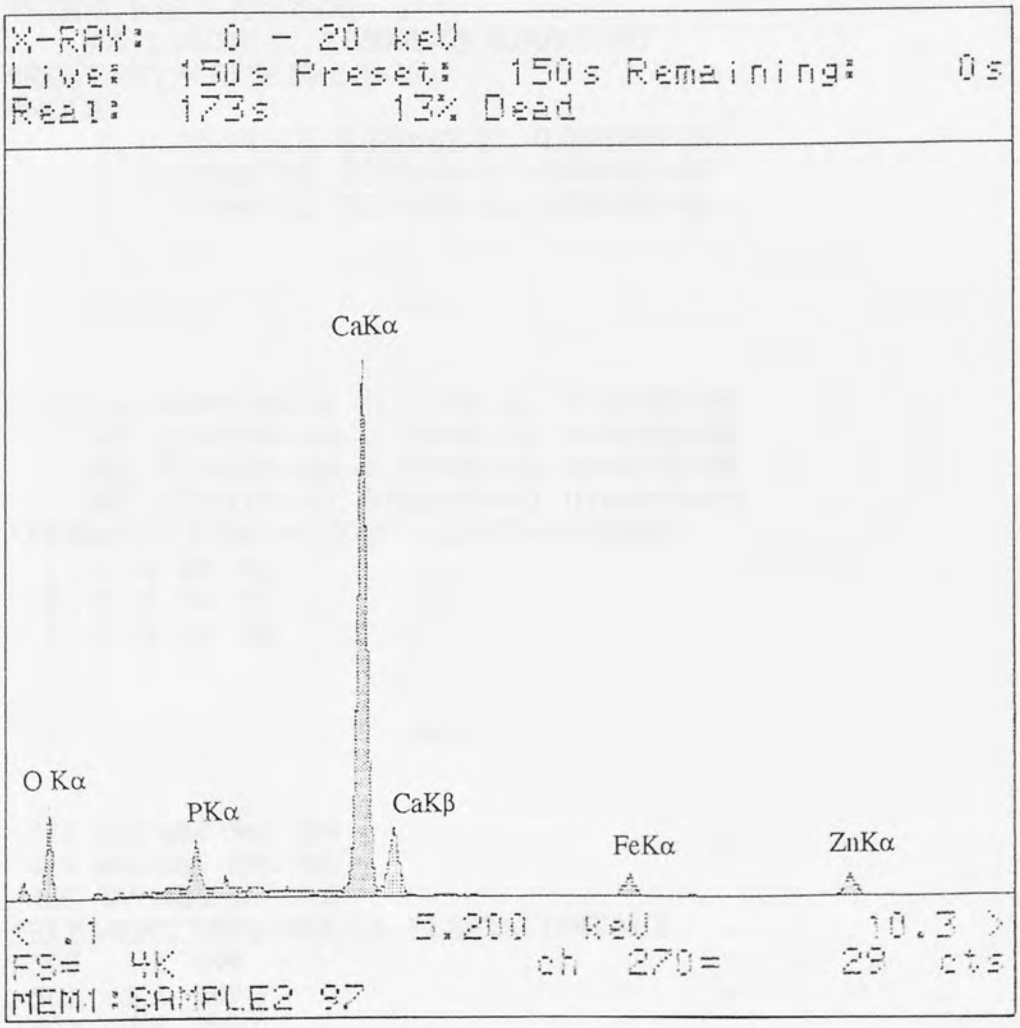

```
X-RAY:    0 - 20 keV
Live:   150s Preset:   150s Remaining:     0s
Real:   173s        13% Dead
```

Fig. E.2 Spectrum analysis of a residual lubricant layer on the surface of a wire drawn using Traxit lubricant.

Appendix F Example Input File of ABAQUS Analysis

```
**################################################################
**#                                                              #
**#       Finite Element Analysis of a Wire Drawing Process      #
**#        -- An Example Problem Simulated Using ABAQUS          #
**#                                                              #
**#                     by Bingshu Huo                           #
**#                                                              #
**#       Mechanical and Electrical Engineering Department       #
**#                   Aston  University                          #
**#                                                              #
**################################################################
*HEADING
FINITE ELEMENT ANALYSIS OF WIRE DRAWING PROCESS
*NODE, NSET=RSNODE
     999, 2.0000E-02, 7.0000E-03, 0.0000E+00
*RESTART,WRITE,FREQ=30
*NODE
       1,  0.27500E-02, -0.30000E-01,  0.00000E+00
       2,  0.27500E-02, -0.29624E-01,  0.00000E+00
       3,  0.27500E-02, -0.29248E-01,  0.00000E+00
                          .
                          .
                        omit
                          .
                          .
     564,  0.00000E+00, -0.11250E-02,  0.00000E+00
     565,  0.00000E+00, -0.75004E-03,  0.00000E+00
     566,  0.00000E+00, -0.37502E-03,  0.00000E+00
     567,  0.00000E+00,  0.00000E+00,  0.00000E+00
*ELEMENT,TYPE=CAX4R    ,ELSET=E0000001
  1   1   2  83  82
  2   2   3  84  83
  3   3   4  85  84
                          .
                          .
                        omit
                          .
                          .
 478 483 484 565 564
 479 484 485 566 565
 480 485 486 567 566
*ELEMENT,TYPE=IRS21A, ELSET=CONTACT
 500,    1,2,  999
 501,    2,3,  999
 502,    3,4,  999
           .
           .
         omit
           .
           .
```

```
 578,  78,79, 999
 579,  79,80, 999
 560,  80,81, 999
*RIGID SURFACE,ELSET=CONTACT,TYPE=SEGMENT, SMOOTH=0.0005
START,5.0e-03,-12.0e-03
LINE,2.3e-03,8.5087e-03
LINE,2.3e-03,9.6585e-03
LINE,5.0e-03,12.3585e-03
*SOLID SECTION,ELSET=E0000001,MATERIAL=M0000001
 1.000E+03   3
*MATERIAL,NAME=M0000001
*ELASTIC,TYPE=ISOTROPIC
2.1E11,0.35
*PLASTIC,HARD=ISO
  0.2413480E+09,  0.0000000E-00
  0.2894045E+09,  0.2500000E-01
  0.3303033E+09,  0.5000000E-01
  0.3647377E+09,  0.7500000E-01
  0.3934014E+09,  0.1000000E+00
  0.4169883E+09,  0.1250000E+00
  0.4361920E+09,  0.1500000E+00
  0.4517064E+09,  0.1750000E+00
  0.4642251E+09,  0.2000000E+00
  0.4744420E+09,  0.2250000E+00
  0.4830508E+09,  0.2500000E+00
  0.4907452E+09,  0.2750000E+00
  0.4982189E+09,  0.3000000E+00
  0.5061658E+09,  0.3250000E+00
  0.5152795E+09,  0.3500001E+00
  0.5262539E+09,  0.3750001E+00
  0.5397827E+09,  0.4000001E+00
  0.5565596E+09,  0.4250001E+00
  0.5772784E+09,  0.4500001E+00
  0.6026328E+09,  0.4750001E+00
  0.6333165E+09,  0.5000001E+00
  0.6700233E+09,  0.5250000E+00
*INTERFACE,ELSET=CONTACT
*FRICTION
0.00
*BOUNDARY
        81,2,,0.0000E+00
       162,2,,0.0000E+00
       243,2,,0.0000E+00
       324,2,,0.0000E+00
       405,2,,0.0000E+00
       486,2,,0.0000E+00
       567,2,,0.0000E+00
        81,1,,0.0000E+00
       162,1,,0.0000E+00
       243,1,,0.0000E+00
       324,1,,0.0000E+00
       405,1,,0.0000E+00
       486,1,,0.0000E+00
       567,1,,0.0000E+00
```

```
*BOUNDARY
     999,1,,
     999,2,,
     999,6,,
*STEP,INC=200,AMPLITUDE=RAMP,NLGEOM,MONOTONIC=YES
*STATIC
.01,1.,1.E-6
*PRINT,CONTACT=YES
*EL PRINT, ELSET=E0000001,FREQUENCY=100
S,MISES
E,PEEQ
*EL PRINT,ELSET=CONTACT,FREQUENCY=50
S,E
*NODE PRINT, FREQUENCY=25
U,RF,NT,RFL
*NODE FILE,NSET=RSNODE
RF
*PLOT,FREQUENCY=25
*DISPLACED
U,1.
*PLOT, FREQUENCY=25
*DETAIL,ELSET=E0000001
*CONTOUR
PEEQ
*CONTOUR
NT11
*END STEP
*STEP,INC=400,AMPLITUDE=RAMP,NLGEOM,MONOTONIC=YES
*STATIC
.01,1.,1.E-6
*BOUNDARY
       81,2,,5.0000E-03
      162,2,,5.0000E-03
      243,2,,5.0000E-03
      324,2,,5.0000E-03
      405,2,,5.0000E-03
      486,2,,5.0000E-03
      567,2,,5.0000E-03
*END STEP
*STEP,INC=600,AMPLITUDE=RAMP,NLGEOM,MONOTONIC=YES
*STATIC
.01,1.,1.E-6
*BOUNDARY
       81,2,,10.0000E-03
      162,2,,10.0000E-03
      243,2,,10.0000E-03
      324,2,,10.0000E-03
      405,2,,10.0000E-03
      486,2,,10.0000E-03
      567,2,,10.0000E-03
*END STEP
*STEP,INC=600,AMPLITUDE=RAMP,NLGEOM,MONOTONIC=YES
*STATIC
.01,1.,1.E-6
```

```
*BOUNDARY
        81,2,,15.0000E-03
       162,2,,15.0000E-03
       243,2,,15.0000E-03
       324,2,,15.0000E-03
       405,2,,15.0000E-03
       486,2,,15.0000E-03
       567,2,,15.0000E-03
*END STEP
*STEP,INC=800,AMPLITUDE=RAMP,NLGEOM,MONOTONIC=YES
*STATIC
.01,1.,1.E-6
*BOUNDARY
        81,2,,20.0000E-03
       162,2,,20.0000E-03
       243,2,,20.0000E-03
       324,2,,20.0000E-03
       405,2,,20.0000E-03
       486,2,,20.0000E-03
       567,2,,20.0000E-03
*END STEP
*STEP,INC=1000,AMPLITUDE=RAMP,NLGEOM,MONOTONIC=YES
*STATIC
.01,1.,1.E-6
*BOUNDARY
        81,2,,25.0000E-03
       162,2,,25.0000E-03
       243,2,,25.0000E-03
       324,2,,25.0000E-03
       405,2,,25.0000E-03
       486,2,,25.0000E-03
       567,2,,25.0000E-03
*END STEP
*STEP,INC=1200,AMPLITUDE=RAMP,NLGEOM,MONOTONIC=YES
*STATIC
.01,1.,1.E-6
*BOUNDARY
        81,2,,30.0000E-03
       162,2,,30.0000E-03
       243,2,,30.0000E-03
       324,2,,30.0000E-03
       405,2,,30.0000E-03
       486,2,,30.0000E-03
       567,2,,30.0000E-03
*END STEP
*STEP,INC=1400,AMPLITUDE=RAMP,NLGEOM,MONOTONIC=YES
*STATIC
.01,1.,1.E-6
*BOUNDARY
        81,2,,35.0000E-03
       162,2,,35.0000E-03
       243,2,,35.0000E-03
       324,2,,35.0000E-03
       405,2,,35.0000E-03
```

```
       486,2,,35.0000E-03
       567,2,,35.0000E-03
*END STEP
*STEP,INC=1600,AMPLITUDE=RAMP,NLGEOM,MONOTONIC=YES
*STATIC
.01,1.,1.E-6
*BOUNDARY
        81,2,,45.0000E-03
       162,2,,45.0000E-03
       243,2,,45.0000E-03
       324,2,,45.0000E-03
       405,2,,45.0000E-03
       486,2,,45.0000E-03
       567,2,,45.0000E-03
*END STEP
*STEP,INC=1800,AMPLITUDE=RAMP,NLGEOM,MONOTONIC=YES
*STATIC
.01,1.,1.E-6
*BOUNDARY
        81,2,,65.0000E-03
       162,2,,65.0000E-03
       243,2,,65.0000E-03
       324,2,,65.0000E-03
       405,2,,65.0000E-03
       486,2,,65.0000E-03
       567,2,,65.0000E-03
*END STEP
```